

**DISPLACEMENT-BASED SEISMIC DESIGN
OF SHEAR WALL BUILDINGS**

by

Freddy Eduardo Pina Burgos

B.Eng.(Civil Engineering)
Universidad de Santiago de Chile, 2000

A thesis submitted to
The Faculty of Graduate Studies and Research
in partial fulfillment of the requirements
for the degree of

Master of Applied Science

in
Engineering *

**Department of Civil and Environmental Engineering
Carleton University, Ottawa, Canada
May, 2006**

*The Master of Applied Science in Civil Engineering is a joint program with the University of Ottawa, administered by the Ottawa-Carleton Institute for Civil Engineering

© Copyright, Freddy Eduardo Pina, 2006



Library and
Archives Canada

Bibliothèque et
Archives Canada

Published Heritage
Branch

Direction du
Patrimoine de l'édition

395 Wellington Street
Ottawa ON K1A 0N4
Canada

395, rue Wellington
Ottawa ON K1A 0N4
Canada

Your file *Votre référence*
ISBN: 978-0-494-18331-1
Our file *Notre référence*
ISBN: 978-0-494-18331-1

NOTICE:

The author has granted a non-exclusive license allowing Library and Archives Canada to reproduce, publish, archive, preserve, conserve, communicate to the public by telecommunication or on the Internet, loan, distribute and sell theses worldwide, for commercial or non-commercial purposes, in microform, paper, electronic and/or any other formats.

The author retains copyright ownership and moral rights in this thesis. Neither the thesis nor substantial extracts from it may be printed or otherwise reproduced without the author's permission.

AVIS:

L'auteur a accordé une licence non exclusive permettant à la Bibliothèque et Archives Canada de reproduire, publier, archiver, sauvegarder, conserver, transmettre au public par télécommunication ou par l'Internet, prêter, distribuer et vendre des thèses partout dans le monde, à des fins commerciales ou autres, sur support microforme, papier, électronique et/ou autres formats.

L'auteur conserve la propriété du droit d'auteur et des droits moraux qui protègent cette thèse. Ni la thèse ni des extraits substantiels de celle-ci ne doivent être imprimés ou autrement reproduits sans son autorisation.

In compliance with the Canadian Privacy Act some supporting forms may have been removed from this thesis.

Conformément à la loi canadienne sur la protection de la vie privée, quelques formulaires secondaires ont été enlevés de cette thèse.

While these forms may be included in the document page count, their removal does not represent any loss of content from the thesis.

Bien que ces formulaires aient inclus dans la pagination, il n'y aura aucun contenu manquant.


Canada

Abstract

A displacement-based method of seismic design (DBSD) is presented with particular reference to the design of reinforced concrete shear wall buildings. For preliminary design, approximate estimates of the yield and ultimate displacements are obtained, the former from simple empirical relations, and the latter to satisfy the following criteria: (1) satisfy code-specified drift limits, (2) ensure stability under P-Delta effects, and (3) keep the ductility demand within ductility capacity. For a multi-storey building the structure is converted to an equivalent single-degree-of-freedom (SDOF) system using an assumed deformation shape that is representative of the first mode. The required base shear strength of the SDOF system is determined from the inelastic demand spectrum corresponding to the ductility demand, which is the ratio of ultimate to yield displacement. The base shear is distributed across the height using an assumed pattern, such as the one given by the National Building Code of Canada, and the structure is designed for the moments produced by the estimated shears. A modal analysis of the structure provides the first mode shape and a pushover analysis for the force distribution based on this mode gives new estimates of yield and ultimate displacements. The design process is now repeated until the base shear strength converges. The moment resistance and displacements obtained from first mode assumption are expected to be reasonable estimates of the demand. However, the shear strength demand is substantially contributed from higher modes. A full modal pushover analysis is therefore carried out to find more accurate estimates of the shear demand. An evaluation of DBSD is performed through

nonlinear response history analyses for a series of spectrum compatible ground motions especially selected for this study. The suggested DBSD procedure is observed to provide a safe and somewhat conservative approach to design of shear structures.

To my wife...Claudia

With infinite love

Acknowledgement

I would like to express my deepest gratitude to my supervisor, Professor Jagmohan Humar. It was the most enjoyable and inspiring experience that I have ever had working with a great mentor. Professor Humar is not only a patient and a wise person as well as researcher of international repute, he is also a wonderful person and a source of inspiration and encouragement. I am absolutely certain that Professor Humar will remain forever in my mind as an excellent teacher, a comprehensive researcher and a great human being.

My research greatly benefited from the constant supply of technical literature and the constructive comments and guidance that I received from Mr. Mohammad Ghorbanie. I am absolutely convinced that Mohammad will succeed in every project he undertakes. I wish him all the best in his future academic and/or professional activities.

Special thanks are due to Professors David Lau and Abhijit Sarkar for the patience they demonstrated and the guidance they provided me during my first year at Carleton University.

I am also thankful to my employer, the University of Santiago of Chile (USACH), who gave me the opportunity to study in a multi-cultural country, such as Canada, and at a prestigious institution, such as Carleton University. My sincere thanks for the financial and logistic support that the USACH gave me during my studies at Carleton.

I also offer my thanks to several friends who made myself and wife welcome in Canada through their support in our social and academic activities. Among them I would like to particularly thank: Gerardo, Marta, Viet Anh, Kate, Ryan, Rheza and Hasan for being such wonderful people and for sharing their precious time with us.

Special thanks are due to one of the most wonderful person I have ever met in my life, Nicolás Londoño. I wish him all the best in his life. I think that there are some people for whom we do not have enough words to express our gratitude. This type of person is Nicolás. “Gracias por todo Nico”.

I would like to thanks to my adopted family in Ottawa. Thanks to my cousins: Pablo, Claudio, Marco and Krystina. My deepest gratitude to my aunt Gloria Cossio and my dear uncle Roberto Quiroz. I thank them for their continuous help and gestures of love and friendship. I will be ever grateful for all of their physical and emotional support.

I wish to take this opportunity to express my deepest appreciation to my parents and sisters for their unconditional love, patience, support and for demonstrating all the virtues that one can find in a “perfect” family. I owe my life to them and I hope to be able sometimes to reciprocate for all of that they have given me.

There is not enough paper in the world to express in written words my thanks to Claudia; my love, my beautiful girl, my wonderful wife, an excellent partner, and everything positive that I can imagine. I could write millions of theses to express my feelings and gratitude to her.

Table of Contents

| | |
|---|-------------|
| Abstract..... | ii |
| Acknowledgement..... | v |
| Table of Contents | vii |
| List of Tables | xi |
| List of Figures..... | xiii |
| Symbols | xxi |
| Acronyms and Abbreviations | xxix |
| | |
| 1 Introduction..... | 1 |
| 1.1. Introduction..... | 1 |
| 1.2. Performance-based seismic design | 4 |
| 1.3. Review of displacement-based seismic design methods | 7 |
| 1.3.1. Assessment procedures | 8 |
| 1.3.2. Displacement-check procedures | 9 |
| 1.3.3. Direct procedure based on equivalent linear systems | 10 |
| 1.3.4. Direct procedure based on inelastic spectrum | 12 |
| 1.4. Review of pushover and multi-modal analysis procedures | 13 |
| 1.5. Review of design considerations on shear walls..... | 16 |
| 1.6. Objectives of the study..... | 18 |
| 1.7. Scope of the study..... | 19 |
| 1.8. Thesis layout | 20 |

| | | |
|----------|--|-----------|
| 2 | Selection of Seismic Ground Motion Time Histories for Vancouver City..... | 24 |
| 2.1. | Introduction..... | 24 |
| 2.2. | Background..... | 25 |
| 2.3. | Seismicity of Vancouver..... | 30 |
| 2.4. | Selection of seismic regions and data..... | 32 |
| 2.5. | Scaling method..... | 34 |
| 2.6. | Final selection criteria..... | 37 |
| 2.7. | Comments..... | 40 |
| 3 | Displacement-based Seismic Design..... | 54 |
| 3.1. | Introduction..... | 54 |
| 3.2. | Conceptual basis and implementation of DBSD..... | 55 |
| 3.3. | Yield displacement..... | 56 |
| 3.4. | Ultimate inter-storey drift and roof displacement..... | 57 |
| 3.4.1. | Drift limits to achieve near-collapse performance goal..... | 59 |
| 3.4.2. | Local ductility capacity limit..... | 59 |
| 3.4.3. | Limit to preclude instability caused by P- Δ effect..... | 60 |
| 3.5. | Equivalent SDOF system..... | 61 |
| 3.6. | Inelastic demand spectrum..... | 62 |
| 3.7. | P-delta effect in inelastic systems..... | 64 |
| 3.8. | Preliminary design..... | 66 |
| 3.8.1. | Stability of wall section..... | 67 |
| 3.8.2. | Base design forces and moment..... | 68 |
| 3.8.3. | Vertical concentrated reinforcement..... | 68 |
| 3.8.4. | Moment curvature relationship..... | 70 |

| | | |
|----------|---|------------|
| 3.9. | Pushover Analysis..... | 71 |
| 3.10. | Subsequent iterations in design..... | 72 |
| 3.11. | Modal pushover analysis..... | 73 |
| 3.12. | Multiple performance objectives | 75 |
| 3.12.1. | Estimated UHS corresponding to 50%/50 year probability..... | 76 |
| 3.13. | Summary | 79 |
| 4 | Application of Displacement-based Seismic Design..... | 98 |
| 4.1. | Introduction..... | 98 |
| 4.2. | Building definition..... | 99 |
| 4.2.1. | Geometry..... | 99 |
| 4.2.2. | Load definition..... | 99 |
| 4.2.3. | Material properties | 100 |
| 4.3. | DBSD of a 6-storey building | 101 |
| 4.3.1. | General Calculation | 101 |
| 4.3.2. | Gravity loads | 103 |
| 4.3.3. | DBSD..... | 106 |
| 4.4. | Summary of DBSD for 6, 12, 15, and 20-storey buildings..... | 116 |
| 4.4.1. | Total responses..... | 117 |
| 4.4.2. | Discussion on the results..... | 119 |
| 5 | Evaluation of the Displacement-based Seismic Design..... | 146 |
| 5.1. | Introduction..... | 146 |
| 5.2. | Inelastic Systems..... | 147 |
| 5.3. | Ground motions for Vancouver | 148 |
| 5.4. | Response statistics | 149 |

| | | |
|----------|--|------------|
| 5.5. | Results..... | 151 |
| 5.5.1. | Results for the 6-storey building results | 153 |
| 5.5.2. | Results for the 12-storey building..... | 155 |
| 5.5.3. | Results for the 15-storey building..... | 157 |
| 5.5.4. | Results for the 20-storey building..... | 159 |
| 5.5.5. | Summary of results for different response parameters | 161 |
| 5.6. | Comments on results..... | 164 |
| 6 | Summary, Conclusions and Recommendations | 181 |
| 6.1. | Introduction..... | 181 |
| 6.2. | Selection of ground motions | 183 |
| 6.3. | Modification of ground motions | 184 |
| 6.4. | Displacement based seismic design | 186 |
| 6.5. | Responses from displacement-based seismic design..... | 188 |
| 6.6. | Evaluation of displacement-based seismic design..... | 190 |
| 6.7. | Recommendations for future work | 191 |
| | References | 194 |
| | Appendix A. DBSD of a 12-storey building | 207 |
| | Appendix B. DBSD of a 15-storey building | 233 |
| | Appendix C. DBSD of a 20-storey building..... | 267 |

List of Tables

| | |
|--|-----|
| Table 2.1: Seismic activity measures at PGC station within the period 1996-2005 (GSC) | 42 |
| Table 2.2: Geographical and tectonic settings for different subduction regions with crustal and/or subcrustal seismicity | 43 |
| Table 2.3: Selected earthquakes from zones with seismic hazard zones similar to that of Vancouver city..... | 44 |
| Table 2.4: Median and dispersion results of ductility responses obtained from scaled records of Bin-I, Bin -II, Bin-III, and Bin-IV (adapted from Shome <i>et al.</i> 1998)..... | 45 |
| Table 2.5: Selected Records for Vancouver city..... | 46 |
| Table 4.1: Geometric parameters for the 4 shear wall buildings | 121 |
| Table 4.2: Floor dead loads and masses tributary to each wall in the 6-storey building | 121 |
| Table 4.3: Reduced live load calculations for each wall of the 6-storey building | 121 |
| Table 4.4: Gravity load combinations for each wall of the 6-storey building | 122 |
| Table 4.5: Reduced tributary live loads for calculating the P- Δ effect for each wall of the 6-storey building | 122 |

| | |
|--|-----|
| Table 4.6: Floor gravity loads tributary to each wall for calculating the P- Δ effect in the 6-storey building | 123 |
| Table 4.7: Results of moment-curvature analysis in the four iterations in the design of a 6-storey building | 123 |
| Table 4.8: First mode analysis results for the 4 design iterations on a 6-storey building | 123 |
| Table 4.9: Results from pushover analyses for the 4 design iterations on a 6-storey building | 124 |
| Table 4.10: Modal analysis results for the 4 th design iteration on a 6-storey building .. | 124 |
| Table 4.11: Results from modal pushover analysis in the 4 th design iteration on a 6-storey building | 124 |
| Table 4.12: Summary of DBSD for the 6, 12, 15 and 20-storey buildings..... | 125 |
| Table 4.13: Maximum total responses for 6, 12, 15 and 20-storey buildings | 125 |
| Table 5.1: Rayleigh damping coefficients for 6, 12, 15 and 20-storey buildings | 167 |
| Table 5.2: Final selection of 20 ground motions for the city of Vancouver | 167 |

List of Figures

| | |
|--|----|
| Figure 1.1: Recommended minimum seismic performance design objectives for buildings (adapted from SEAOC 1995)..... | 22 |
| Figure 1.2: Fundamentals of direct displacement-based seismic design (adapted from Priestley 2000) | 23 |
| Figure 2.1: Cascadia Subduction Zone. (a) 1: Crustal Earthquakes on North America plate; 2: Subcrustal Earthquakes on Juan de Fuca plate; 3: Subduction earthquakes. (b) General view (reproduced from Onur, Cassidy and Rogers 2005) | 48 |
| Figure 2.2: Deep earthquake (subcrustal) sources for Western British Columbia and Western Washington State. GEO: Georgia Strait, GSP: Georgia Strait/Puget Sound, PUG: Puget Sound (reproduced from Adams and Halchuk 2000) | 49 |
| Figure 2.3: Deaggregation results for the seismicity of Vancouver city for 2% probability of exceedance in 50 years at $S_a(1.0s)$ (reproduced from Halchuk and Adams 2004) | 50 |
| Figure 2.4: UHS for Vancouver city on site class C and 5% damping ratio(NBCC 2005) | 50 |
| Figure 2.5: Pseudo-acceleration response spectra of selected ground motions for Vancouver (Part 1)..... | 51 |

| | |
|--|----|
| Figure 2.6: Pseudo-acceleration response spectra of selected ground motions for Vancouver (Part 2)..... | 52 |
| Figure 2.7: Pseudo-acceleration response spectra of selected ground motions for Vancouver (Part 3)..... | 53 |
| Figure 3.1: Summary of capacity-diagram method: (a) Pushover curve, (b) Capacity diagram of the equivalent SDOF system, (c) Elastic demand, (d) Elastic demand diagram, (e) Determination of performance point (adapted from Chopra and Goel 1999)..... | 83 |
| Figure 3.2: Models of cantilever shear wall showing yield, plastic and ultimate displacements and drifts..... | 84 |
| Figure 3.3: Ultimate drift ratios for shear walls..... | 85 |
| Figure 3.4: Constant-ductility ($\mu = 2$) displacement response spectrum for El Centro ground motion (1940) and 5 % damping, for Model 1 (Elasto-plastic) and Model 2 (Elasto-plastic plus P- Δ effect) | 86 |
| Figure 3.5: Constant-ductility ($\mu = 2$) velocity response spectrum for El Centro ground motion (1940) and 5 % damping, for Model 1 (Elasto-plastic) and Model 2 (Elasto-plastic plus P- Δ effect) | 87 |

| | |
|--|----|
| Figure 3.6: Constant-ductility ($\mu = 2$) acceleration response spectrum for El Centro ground motion (1940) and 5 % damping, for Model 1 (Elasto-plastic) and Model 2 (Elasto-plastic plus P- Δ effect) | 88 |
| Figure 3.7: Demand and capacity diagram for the equivalent SDOF system..... | 89 |
| Figure 3.8: Moment-curvature analysis: (a) tri-linear stress-strain relationship for reinforcing steel, (b) Idealized stress-strain curve for concrete uniaxial compression, (c) moment-curvature relationship for a rectangular concrete wall (adapted from Yavari 2001) | 90 |
| Figure 3.9: Pushover analysis using first mode: (a) determination of lateral loads, (b) static analysis displacement response, (c) pushover curve. | 91 |
| Figure 3.10: Modal pushover analysis for three first modes: (a) lateral forces, (b) pushover curves..... | 92 |
| Figure 3.11: Flow chart for the preliminary part of the DBSD for shear wall buildings. | 93 |
| Figure 3.12: Iterative process of the DBSD for shear wall buildings. | 94 |
| Figure 3.13: Deaggregation of hazard for the city of Vancouver with 10% probability of exceedance in 50 years (475 years of return period). The circles shows the maximum contribution to hazard (reproduced from Adams and Halchuk 2003) | 95 |

Figure 3.14: Deaggregation of hazard for the city of Vancouver with 2% probability of exceedance in 50 years (2500 years of return period). The circles shows the maximum contribution to hazard (reproduced from Adams and Halchuk 2003) 96

Figure 3.15: Magnitude-recurrence curve for CSAR, Cascadia mountain region. (reproduced from Adams and Halchuk 2003) 97

Figure 4.1: Building plan and elevation of one cantilever shear wall..... 126

Figure 4.2: Capacity-demand diagram for the preliminary design of shear wall for the 6-storey building 127

Figure 4.3: Detail of reinforcement for the preliminary design of shear wall for the 6-storey building 128

Figure 4.4: Moment-curvature relationship for the preliminary design of shear wall for the 6-storey building 129

Figure 4.5: Pushover curves with and without P- Δ effect for the preliminary design of shear wall for the 6-storey building 130

Figure 4.6: Capacity-demand diagram for the first design iteration of the 6-storey building 131

| | |
|---|-----|
| Figure 4.7: Detail of reinforcement for the final design of shear wall for the 6-storey building | 132 |
| Figure 4.8: Moment-curvature relationship for the final design of shear wall for the 6-storey building | 133 |
| Figure 4.9: Pushover curves with and without P- Δ effect for the final design of shear wall for the 6-storey building..... | 134 |
| Figure 4.10: Capacity-demand diagram for the final design of shear wall for the 6-storey building | 135 |
| Figure 4.11: Pushover curves with and without P- Δ effect for the final design of shear wall for the 6-storey building obtained by distributing the lateral forces according to (a) the second mode shape, and (b) the third mode shape | 136 |
| Figure 4.12: Capacity-demand diagrams for the final design of shear wall for the 6-storey building obtained by distributing the lateral forces according to (a) the second mode shape, and (b) the third mode shape..... | 137 |
| Figure 4.13: (a) Inter-storey drifts ratios and (b) displacements for the 6-storey building | 138 |
| Figure 4.14: Shear forces for the 6-storey building | 139 |

| | |
|--|-----|
| Figure 4.15: (a) Inter-storey drifts ratios and (b) displacements for the 12-storey building | 140 |
| Figure 4.16: Shear forces for the 12-storey building | 141 |
| Figure 4.17: (a) Inter-storey drifts ratios and (b) displacements for the 15-storey building | 142 |
| Figure 4.18: Shear forces for the 15-storey building | 143 |
| Figure 4.19: (a) Inter-storey drifts ratios and (b) displacements for the 20-storey building | 144 |
| Figure 4.20: Shear forces for the 20-storey building | 145 |
| Figure 5.1: Histograms of the roof displacements obtained from nonlinear RHA of the 6, 12, 15, 20-storey buildings..... | 168 |
| Figure 5.2: Histograms of the maximum inter-storey drift ratios obtained from nonlinear RHA of the 6, 12, 15, 20-storey buildings..... | 169 |
| Figure 5.3: Histograms of the base shears obtained from nonlinear RHA of the 6, 12, 15, 20-storey buildings..... | 170 |
| Figure 5.4: Histograms of the base plastic rotations obtained from nonlinear RHA of the 6, 12, 15, 20-storey buildings..... | 171 |

| | |
|---|-----|
| Figure 5.5: Nonlinear RHA results and DBSD/RHA ratio for story drift ratios (top), displacements (middle), and shear forces (bottom) in the 6-storey building..... | 172 |
| Figure 5.6: Nonlinear RHA results and DBSD/RHA ratios for story drift ratios (top), displacements (middle), and shear forces (bottom) in the 12-storey building..... | 173 |
| Figure 5.7: Nonlinear RHA results and DBSD/RHA ratios for story drift ratios (top), displacements (middle), and shear forces (bottom) in the 15-storey building..... | 174 |
| Figure 5.8: Nonlinear RHA results and DBSD/RHA ratios for story drift ratios (top), displacements (middle), and shear forces (bottom) in the 20-storey building..... | 175 |
| Figure 5.9: Dispersion of story drift ratios, displacements and shear forces obtained from the nonlinear RHA for the 6, 12, 15 and 20-storey buildings..... | 176 |
| Figure 5.10: Histograms of the ratio between the roof displacements obtained from DBSD and nonlinear RHA of the 6, 12, 15, 20-storey buildings | 177 |
| Figure 5.11: Histograms of the ratio between the maximum inter-storey drift ratios obtained from DBSD and nonlinear RHA of the 6, 12, 15, 20-storey buildings..... | 178 |
| Figure 5.12: Histograms of the ratio between the base shears obtained from DBSD and nonlinear RHA of the 6, 12, 15, 20-storey buildings..... | 179 |

Figure 5.13: Histograms of the ratio between the base plastic rotation obtained from DBSD and nonlinear RHA of the 6, 12, 15, 20-storey buildings 180

Symbols

“The symbols used in this thesis are listed bellow although they are already defined in the text. Occasionally, the same symbols may be used to represent more than one parameter, but the meaning should be clear within context. For convenience to the reader, the symbols are separately presented for each of the chapters. The symbols used in Chapter 3 are used also in Chapter 5. Therefore, the symbols listed for Chapter 5 may be added to those listed for Chapter 3”

Symbols used in Chapter 1:

| | |
|-----------------|----------------------------------|
| R_y | reduction factor |
| T_n | natural period |
| μ | ductility factor |
| ϕ_{cap} | curvature capacity |
| ϕ_d | curvature demand |
| ϕ_y | yield curvature |
| ϕ_{id} | inelastic curvature demand |
| l_w | wall length |
| ε_y | reinforcement steel yield strain |
| Δ_d | design displacement |
| T_e | equivalent period |

| | |
|-------|-----------------------------------|
| K_e | equivalent stiffness |
| K_i | initial elastic stiffness |
| r | reduction factor of K_i |
| V_b | base shear |
| m_e | equivalent mass of a SDOF model |
| h_e | equivalent height of a SDOF model |
| F_y | yield force of a SDOF model |
| F_d | design force of SDOF model |

Symbols used in Chapter 2:

| | |
|---------------|---|
| $a(t)$ | ground motion time history |
| $\delta a(t)$ | adjustment time history |
| ω_i | i^{th} frequency |
| R_i | peak response value at time t_i |
| Q_i | target spectral value at frequency ω_i |
| ΔR_i | spectral misfit |
| SI_b | modified spectral intensity |
| w_i | i^{th} weight factor to compute scaling factor α_{sm} |
| α_{sm} | scaling factor proposed by Somerville <i>et al.</i> (1997) |

| | |
|---------------|--|
| PSA_t | target spectral acceleration |
| PSA_{gm} | ground motion spectral acceleration |
| T_o | fundamental period to compute SI_b |
| T_s | equivalent secant stiffness period to compute SI_b |
| R_y | reduction factor |
| n | number of records |
| δ | dispersion |
| X | factor that defines the confidence band of the median response |
| α_{sh} | scaling factor proposed by Shome <i>et al.</i> (1998) |
| ML | local magnitude |
| M_w | moment magnitude |
| M | magnitude |
| D | epicentral distance |

Symbols used in Chapter 3:

| | |
|------------|--------------------------|
| Δ_u | target roof displacement |
| Δ_y | yield roof displacement |
| μ | ductility capacity |
| θ_y | yield roof rotation |

| | |
|-----------------|---------------------------------------|
| H | height of the shear wall |
| ϕ_y | effective yield curvature |
| ε_y | yield strain of reinforcement steel |
| l_w | length of the shear wall |
| θ_u | ultimate rotation |
| θ_p | plastic rotation |
| L_p | length of the plastic hinge |
| ϕ_u | ultimate curvature |
| Δ_p | plastic roof displacement |
| θ_u | ultimate drift |
| f_y | yield strength of reinforcement steel |
| ϕ | shape vector |
| \mathbf{M} | mass matrix |
| $\mathbf{1}$ | unit vector |
| Γ | modal participation factor |
| M^* | effective modal mass |
| ϕ^r | value of ϕ at the roof |
| T_n | natural period |
| A | acceleration coordinate |

| | |
|-----------------|--|
| D | displacement coordinate |
| A_y | spectral acceleration of the inelastic spectrum |
| δ_u | ultimate displacement of the equivalent SDOF system |
| δ_y | yield displacement of the equivalent SDOF system |
| V | base shear |
| b_c | critical wall thickness |
| μ_ϕ | curvature ductility |
| c | compression zone length |
| P | axial load |
| A_d | area of the distributed reinforcement steel per unit length |
| f_c | concrete strength |
| ϕ_s | steel performance factor |
| ϕ_c | concrete performance factor |
| α_1 | ratio of average stress in rectangular compression block to f_c |
| β_1 | ratio of depth of rectangular compression block to depth to the neutral axis |
| b_w | thickness of the wall |
| M_c | concrete resistant moment |
| M_{Ad} | distributed reinforcement resistant moment |
| ϵ_{cu} | ultimate concrete strain |

| | |
|--------------------|--|
| M_P | restoring moment derived from P |
| M_{cr} | resisting moment offered by concentrated reinforcement |
| M_e | external moment |
| A_{cr} | required concentrated reinforcement |
| h_m | distance between the edge of the wall and the middle point of the concentrated reinforcement |
| ϕ_1 | first mode shape |
| s_1^* | lateral force pattern for pushover analysis using first mode |
| ϕ_i | i^{th} mode shape |
| Γ_i | modal factor obtained from the i^{th} mode |
| M_i^* | effective modal mass obtained from the i^{th} mode |
| s_i^* | lateral force pattern for pushover analysis using i^{th} mode |
| V_b | base shear coordinate of the pushover curve |
| Δ | roof displacement coordinate of the pushover curve |
| S_a | Spectral acceleration |
| $S_a(2.0)_{50/50}$ | Spectral acceleration at 2 s period with a probability of exceedance 50 % in 50 years |
| $S_a(2.0)_{2/50}$ | Spectral acceleration at 2 s period with a probability of exceedance 2 % in 50 years |
| M | Moment magnitude used in attenuation relationship presented in Section 3.12.1 |
| R | Distance used in attenuation relationship presented in Section 3.12.1 |

| | |
|----------|---|
| h | focal depth used in attenuation relationship presented in Section 3.12.1 |
| gg | factor used in used in attenuation relationship presented in Section 3.12.1 |
| Δ | near-saturation term used in attenuation relationship presented in Section 3.12.1 |
| D_f | near distance to the fault used in attenuation relationship presented in Section 3.12.1 |
| c_i | regression factors used in attenuation relationship presented in Section 3.12.1 |

Symbols used in Chapter 4:

| | |
|-----------------|---|
| n_c | number of columns |
| A_{col} | cross section area of a column |
| γ_{rc} | self weigh of reinforced concrete |
| A_{plan} | area of the building plan |
| th_w | thickness of the wall |
| CA_{trib} | cumulative tributary area |
| M_c | moment capacity |
| I_r | ratio of effective moment of inertia to the gross moment of inertia |
| V_{by} | yield base shear |
| $diff_{V_y}$ | difference between two successive estimates of yield base shear |
| Δ_{roof} | total roof displacement response |

| | |
|-----------------------|---|
| θ_{\max} | total maximum drift ratio response |
| V_b | total base shear response |
| V_{capacity} | shear capacity |
| d_v | effective shear depth |
| V_{bOP} | Base shear of the operational performance level |

Acronyms and Abbreviations

| | |
|---------------|--|
| ABSSUM | Absolute Sum |
| BC | British Columbia |
| CASR | Cascadia Mountain Region |
| CSA | Canadian Standard Association |
| COSMOS | Consortium of Organizations for Strong-Motion Observation System |
| DBSD | Displacement-based Seismic Design |
| DGG | Department of Geophysics and Geodesy (Chile) |
| DOF | Degree Of Freedom |
| DL | Dead Load |
| E | Earthquake Load |
| EBSD | Energy-Based Seismic Design |
| FBSD | Force-Based Seismic Design |
| FEMA | Federal Emergency Management Association |

| | |
|-------------|---------------------------------------|
| GM | Ground Motion |
| LL | Live Load |
| LLRF | Live Load Reduction Factor |
| MDOF | Multiple Degree of Freedom |
| MPA | Modal Pushover Analysis |
| NBCC | National Building Code of Canada |
| PBE | Performance-Based Engineering |
| PBSD | Performance-Based Seismic Design |
| PBSE | Performance-Based Seismic Engineering |
| PGA | Peak Ground Acceleration |
| PGV | Peak Ground Velocity |
| PNSN | Pacific Northwest Seismograph Network |
| PO | Performance Objective |
| RHA | Response History Analysis |

| | |
|--------------|---|
| SDOF | Single Degree of Freedom |
| SEAOC | Structural Engineers Association of California |
| SRSS | Square Root of the Sum of Squares |
| SSN | National Seismological Service (Servicio Sismológico Nacional, Mexico, in spanish) |
| UBC | Uniform Building Code |
| UCA | University of Central America (Universidad de Centro América, El Salvador, in spanish) |
| UHS | Uniform Hazard Spectrum |
| UMRHA | Uncoupled Modal Response History Analysis |
| UNAM | Independent National University of Mexico (Universidad Nacional Autónoma de México, in spanish) |
| UNR | University of Nevada at Reno (USA) |
| USGS | United States Geological Survey |

Chapter 1

Introduction

1.1. Introduction

The tremendous loss of life, suffering and injury, property damage and economic loss that both historical and recent earthquakes have caused has motivated designers and engineers to pay increasing attention to how they design and construct engineering structures. It is now recognized that while improvements in design and construction may have reduced the loss of life during an earthquake, the property loss and the loss suffered through suspension of economic activity is still very large and a serious set back for the society. These factors have motivated engineers to design and build structures that will not only survive an earthquake, but will also minimize nonstructural damage.

The concept of performance based design is that the structure should achieve a desired performance level during each of the hazard levels that it is likely to experience. Vision 2000 committee of SEAOC (SEAOC 1995) has described the various levels of hazard and desired performance that the structure may be required to achieve. The quantitative performance levels are defined in terms of displacements and drifts, because it is believed that drifts and displacements provide a better measure of performance than strength. This has in turn led to a renewed interest in displacement-based design.

Several shortcomings are inherent in a force-based seismic design. These problems become apparent when viewed in the context of the philosophy of performance-based seismic design. There is a clear recognition in the research community that the performance of the structure can be defined by the level of damage expected for a certain future demand. Researchers and engineers also agree that the level of damage is better defined by displacements or strains than forces or strengths. The displacement-based seismic design has emerged as an alternative method of design that captures the comprehensive concepts needed for the design based on multiple performance levels.

The displacement-based seismic design (DBSD) has been studied for the last 15 years and has seen several applications and improvements over the years. However, many areas still requires further research. One of these areas is the application of DBSD to the design of shear wall buildings. It is known that DBSD based on first mode deformation shape may lead to substantial underestimation of some response parameters in a shear wall building because of the large contribution that higher modes make in such a structure. It must be noted that most of DBSD procedures are based on modeling the structure according to its fundamental mode, regardless of the contribution from higher modes. Krawinkler and Seneviratna (1998) compared results from pushover analysis and nonlinear time history analysis in shear wall buildings. They reported that for taller wall buildings higher mode effects significantly amplify the storey shear forces that can be generated in the wall once a plastic hinge has formed at the base. Gupta and Kunnath (2000) studied recorded responses of instrumented buildings subjected to real earthquakes. They found that none of the studied buildings presented a response

dominated by the first mode, and that they were all affected by contributions from higher mode, especially the second mode. Priestley (2003) reported the substantial effect that higher modes make in cantilever shear walls. A conclusion of that study was that for buildings of 8 or more storeys the difference between modal response spectrum procedures and a displacement-based design were very marked for shear responses. These facts have motivated the present study of a displacement-based design method that complements the existing procedures by including a multi-modal analysis in order to account for higher mode effects. At the same time an attempt is made to keep the design procedure simple so that it can be used for the routine designs carried out in a structural design office.

The purpose of this thesis is to introduce a new simplified displacement-based seismic design (DBSD) method with emphasis on shear wall buildings having a symmetric configuration in plan. The new DBSD method for shear wall buildings takes into account the effect of higher modes in the total response by including a multi-modal analysis proposed by Chopra and Goel (2002), the so-called modal pushover analysis (MPA). The entire procedure, including the MPA, maintains the simplicity required for design office uses. At the same time it retains the comprehensive concepts needed for a seismic design based on structural performance. It must be mentioned that the design method presented here is an extension of the new displacement-based design presented by Humar and Ghorbanie (2004) and is part of a more general research involved in the application and evaluation of the new DBSD for several structures with different configurations. The intent is to develop a comprehensive methodology for seismic design based on

displacements to be evaluated by the research and professional community in order for it to be included in future codes and engineering practices.

1.2. Performance-based seismic design

There is a growing recognition among researchers, engineers, owner-users and the society that our infrastructure must be designed, evaluated and constructed so as to perform in a desirable manner under certain future demands (Krawinkler 1999). This new concept, or philosophy, is commonly referred to as performance-based engineering (PBE). When the source of demand is an earthquake, the PBE is called performance-based seismic engineering or PBSE (SEAOC 1995). One of the most important phases of the PBSE is the performance-based seismic design or PBSO. As described by Bertero and Bertero (2002), the PBSO includes identification of seismic hazards, selection of the performance levels and performance design objectives, conceptual design, numerical preliminary design, final design, design review, and other steps that must be taken during the construction and life-time of the building. The authors present a detailed discussion of these numerous steps and emphasize that the term 'design' should be applied to the whole building system, not just the structure.

One of the basic steps of the PBSE deals with the definition of the performance-based objectives (POs). According to the SEAOC Vision 2000 (SEAOC 1995), the POs are based on a combination of the performance levels and earthquake design levels (Figure 1.1). In other words, the PO for a given structure may require the structure to

achieve a different performance level for each of a series of different earthquake design levels. The current practice in seismic design is to achieve a single performance level, namely that of life safety. However, operational level considerations often require that the structure achieve other performance levels for lesser hazards. Thus, as an example, safety critical structures, such as a hospital, may need to remain operational during a very rare earthquake and fully operational during a rare earthquake.

Presently, many researchers are attempting to define seismic hazard levels and quantitative values for performance design objectives. Seismologists are focused on defining the different levels of seismic hazard by using probabilistic seismic hazard analysis. The design level seismic hazard that is obtained by this probabilistic analysis is commonly presented in the form of a uniform hazard spectrum (UHS). The UHS may be obtained for different probabilities of exceedance in a given period of time. For example, the UHS defined in the National Building Code of Canada (NBCC 2005) was obtained for a 2 % probability of being exceeded in 50 years, which is equivalent to a return period of 2500 years (Adams and Halchuck 2003). At the same time, researchers involved in earthquake engineering are working on defining performance levels for different earthquake demands. The performance level is usually described by a certain level of damage expected in the structure, which can be non-structural damage or local damage in the structural elements. The most common measure of performance level is specified in terms of a maximum inter-storey drift ratio, which would limit non-structural and structural damage. For example, NBCC 2005 defines a maximum drift ratio of 0.025 when the design earthquake level corresponds to a return period of 2500 years.

An important step in PBSD is the definition and application of a conceptual design methodology. This is the most critical step within the PBSD since most of the important design decisions are made in it (Krawinkler 1999). The conceptual design must be capable of considering multiple performance levels for the structure. Several simplified design methods are available in the literature, in the present codes, and in the current practice. According to the SEAOC Vision2000, these methods can be divided in three groups: (a) force-based design (FBSD), (b) displacement-based design (DBSD), and (c) energy-based design (EBSD). According to the research community DBSD is most adequate for performance-based design. Energy-based design is still in a preliminary stage. According to Bertero and Bertero (2002), most of the methods listed above sacrifice some important concepts for the sake of simplicity. An evaluation for force-based design (Priestley 2000) has shown that it has several weaknesses which make it unsuitable for performance-based design.

Priestley (2000) has described some conceptual and philosophical problems associated with a force-based design. One of the problems is associated with the use of force-reduction factors for seismic design. The use of such factors leads to structures with non-uniform risk, since these factors are poor indicators of damage potential. It has been shown (Kowalsky *et al.* 1995) that two structures designed to the same conditions and the same reduction factor may experience different levels of damage under a given earthquake. This situation arises because of the lack of a consistent relationship between strength and damage. It is generally accepted that damage is strain related (for structural components), or drift related (for non-structural damage) and therefore damage control

may not be achieved simply by providing a certain amount of strength. Another problem in using force-based design is related to the complexity of design process and the iterations needed to obtain an adequate characterization of the structure, which are necessitated for two reasons. First, most of the structures are governed by code drift limits, which implies that the original design must be modified during subsequent iterative process. Second, the force-based design is based on the invalid assumption that the stiffness is independent of the strength. It has been found (Priestley 1998) that the stiffness is, in fact, directly proportional to the strength, and the yield curvature is essentially independent of the strength.

The displacement-based design procedures have been developed in order to overcome the weaknesses in traditional design procedures. The goal of DBSD is to achieve uniform-risk structures by defining a performance objective for the structure and by ensuring that the structure meets that objective. This approach is compatible with the use of uniform-risk seismic design spectra included in most codes. A more extensive review of literature related to DBSD procedures is presented in the following sections.

1.3. Review of displacement-based seismic design methods

Most of the seismic design procedures based on displacements have been developed and studied during the last 15 years (Priestley 2000). Many variants of the procedure are available in the literature, and they differ in some of the concepts. In the opinion of the author the various methods can be classified in four groups: (a) assessment procedures,

(b) displacement-check procedures, (c) direct procedure based on equivalent linear systems, and (d) direct procedure based on inelastic spectrum.

1.3.1. Assessment procedures

An assessment procedure, also called capacity-demand method, is mainly intended to give a simpler alternative to the inelastic time-history analysis. This procedure was originally developed by Freeman *et al.* (1975) and some improvements have subsequently been made by Freeman (1998), Chopra and Goel (1999), and Fajfar (2000). The method was included in FEMA 273 (Federal Emergency Management Agency 1997) as a nonlinear static procedure and in ATC-40 (Applied Technology Council 1996) in the form of three procedures (A, B, and C), in order to estimate earthquake-induced deformation demands. The procedures A and B of ATC-40 are analytical and amendable to computer implementation, whereas procedure C is graphical and suitable for hand analysis. Procedures A and B were significantly improved by Chopra and Goel (1999). A description of the original methods and some of these modifications are presented in the following paragraphs.

The original methods (FEMA 273 and ATC-40) consist of obtaining the deformation demand from the intersection between the capacity curve of the structure and the demand diagram which are plotted together in an acceleration-displacement (A-D) format. The capacity curve is obtained by modifying the pushover curve for a multi-storey building (relationship between the base shear and roof displacement) to represent an equivalent

single-degree-of-freedom (SDOF) system. The SDOF system is characterized by the equivalent stiffness, K_e , and damping, ζ_e . The demand diagram is obtained by converting the design spectrum from the standard pseudo-acceleration versus natural period format to the A-D format, and then modifying it for the equivalent damping, ζ_e , of the SDOF system.

Chopra and Goel (1999) and Fajfar (2000) found some inconsistencies between deformations obtained from the method referred to in the previous paragraph and those obtained from inelastic design spectra. In order to solve this problem and to retain the original graphical features, they proposed some modifications to both the demand diagram and the capacity curve. In the modified method, the demand diagram is defined by an inelastic demand, which is a function of the forced-reduction factor, the ductility factor, and the natural period. The capacity curve is no longer represented by an equivalent linear system but by an elasto-plastic model of a SDOF system that is equivalent to the inelastic MDOF system.

1.3.2. Displacement-check procedures

Displacement-check procedures complement the force-based design procedures and are intended to reduce local damage or ductility demand in the structural model. A summary of these methods was presented by Kappos (1997), and later reviewed by Priestley (2000) within the context of performance-based design. Some of the procedures in this category use the force-based design code for preliminary strength determination and the inelastic

response history analysis (RHA) to check inelastic deformations. The preliminary design is often based on a simple SDOF model and successive design iteration are needed in order to reduce the inelastic deformations to acceptable limits. Kappos (1997) presented a modification to these procedures in which the SDOF model was not required. In his proposal the beam strengths were obtained by applying code force-reduction factors to the values obtained from a modal elastic analysis while the column strengths were determined from an inelastic RHA using code spectrum-compatible records. The inelastic RHA was also used to check that the storey drifts and local deformations were within the limits. Although, the procedure proposed by Kappos (1997) modifies the traditional design concept for columns, this type of methodologies are still based on the concepts of a force-based design. According to Priestley (2000), the savings obtained from these procedures are likely to be minimal and that the use of force-reduction factors for all modes in the modal elastic analysis can greatly underestimate the higher mode effects.

1.3.3. Direct procedure based on equivalent linear systems

The design methods in the third group are also called direct displacement-based seismic design methods. One of the first attempts in this direction was made by Calvi and Kingsley (1995) for seismic design of MDOF bridge structures and was based on the basic concepts presented by Priestley and Calvi (1997) and Priestley and Kowalsky (2000).

The direct DBSD procedure for a SDOF system is very simple and can be explained in just four steps (Priestley 2000). First, an equivalent damping ratio is obtained depending on a given ductility and the structural system (Figure 1.2 c). Second, for a given design displacement, the effective period is obtained from the design displacement response spectrum for the corresponding damping ratio (Figure 1.2 d). Third, the effective stiffness at maximum response displacement is computed from given effective mass and the previously obtained effective period (Figure 1.2 b). The design base shear is finally obtained from the product of the effective stiffness and the design displacement (Figure 1.2 a).

For a MDOF system, the aforesaid design procedure requires initial determination of the yield and design displacements, and the effective mass and damping of an equivalent SDOF “substitute structure”. The approach used to characterize the structure is based on the “substitute structure” analysis procedure developed by Shibata and Sozen (1976). The design displacement can be expressed in terms of the elastic yield drift and the plastic drift depending on the geometry of the structure. The effective mass is equivalent to the mass participation calculated from the inelastic displacement shape corresponding to the design displacement. The effective damping for the equivalent SDOF system considers the different effective damping values in individual elements, weighted in proportion to the shear in such each elements. The procedure described for an SDOF system is then applied and the resulting base shear is distributed in proportion to the vertical mass and the displacement profile.

1.3.4. Direct procedure based on inelastic spectrum

This group includes the design procedure presented by Chopra and Goel (2001) and uses the inelastic demand spectrum. The authors demonstrate the application of inelastic design spectra to direct DBSD of structures and show the differences between the proposed procedure and the procedures that use equivalent linear systems. The study carried out by the authors was intentionally restricted to SDOF systems having bilinear force-deformation relations to avoid any uncertainties introduced in modeling a MDOF system by an equivalent SDOF system.

The inelastic design spectrum is a constant-ductility spectrum representing the response of an elasto-plastic hysteretic system and is obtained by dividing the elastic design spectrum by appropriate reduction factors, R_y . The research community agrees that R_y depends on the elastic period, T_n , and the ductility factor, μ , of the system, and therefore R_y - μ - T_n relationships must be developed. Three such relationships were studied by Chopra and Goel (2001). These relationships were originally proposed by (a) Newmark and Hall (1982); (b) Krawinkler and Nassar (1992); and (c) Vidic, Fajfar, and Fischinger (1994). The inelastic spectrum obtained from the three relationships showed similar results for periods longer than 0.7, but they differed for shorter periods.

The procedure proposed by Chopra and Goel (2001) starts by reading the initial elastic period from the inelastic deformation design spectrum for given design displacement and ductility; these parameters require estimates of yield and plastic displacements. The

elastic period defines the initial elastic stiffness and the design shear is obtained from the product between this initial elastic stiffness and the yield displacement. The structure is now designed for this yield shear and new estimates of the elastic stiffness and yield displacement are obtained. The procedure is repeated until a satisfactory solution is obtained.

The study by Chopra and Goel showed that the procedure based on the use of inelastic design spectra provides displacement estimates that are consistent with those predicted by the concepts of inelastic design spectra, and produces a design that satisfies the design criteria of acceptable plastic rotation. On the other hand, the procedures based on equivalent elastic systems, such as the effective stiffness, provide displacement estimates that are significantly smaller than those obtained from inelastic analysis, and the ductility demand may be underestimated which leads to unconservatively less-ductile detailing.

1.4. Review of pushover and multi-modal analysis procedures

It is generally accepted that a non-linear time history analysis is best able to predict the forces and cumulative damage demands in the elements of the structure. However, such an analysis requires complicated modeling and sophisticated analytical tools, is cost- and time-consuming and impractical for widespread professional use. These limitations have led to the development of simpler, yet reasonably accurate methods for estimating the seismic demands. One such method is non-linear static analysis procedure, or pushover analysis, and it is becoming popular in the current engineering practice. In this method,

the seismic demands are computed by subjecting the structure to monotonically increasing lateral loads with an invariant height-wise distribution until a predetermined target displacement is reached (Chopra and Goel 2002). Both the force distribution and target displacement are based on a response controlled by the fundamental mode and an unchanged mode shape even after the structure yields.

The two assumptions mentioned in the preceding paragraph are, in fact, the shortcomings of a pushover analysis. Krawinkler and Seneviratna (1998) have carried out an extensive and complete study to evaluate the nonlinear static analysis procedure. They reported that the pushover analysis was likely to give reasonable results, provided the structure response was not severely affected by higher modes, or the structure had only a single load yielding mechanism that could be detected by an invariant load pattern. As an improvement, FEMA-356 (Federal Emergency Management Agency 2000) recommends the use of two lateral load patterns, namely first mode proportional and “uniform”. It is believed that these two patterns provide approximate bounds on the inertia force distribution.

None of the invariant force distributions can accurately account for the contributions of higher modes to response, or for a redistribution of inertia forces due to structural yielding and the corresponding changes in the structural vibration properties (Krawinkler and Seneviratna 1998). As a result, many researches have studied the use of adaptive load patterns (adaptive pushover methods) that follow more closely the time variant distribution of inertia forces. Adaptive pushover methods consist of updating the loading

pattern at each analysis step. Bracci *et al.* (1997) and later Gupta and Kunnath (2000) proposed the use of patterns in which the applied story loads were proportional to story shear resistances at the previous time step of analysis. This procedure uses the response spectral analysis to compute the story loads and create a new structure whenever one or more elements yield by changing the stiffness of the yielded element(s). Currently, a different approach to design is being investigated, which is based on displacement-based adaptive pushover analysis (Antoniou and Pinho 2004).

It is generally believed that the use of adaptive lateral load patterns may provide better estimates of seismic demands. However, within the context of performance-based seismic design, such methods are conceptually complicated and computationally demanding for application in structural engineering practice. Chopra and Goel (2002) have proposed an alternative to the traditional pushover analysis that retains the conceptual simplicity and computational attractiveness of the procedures which uses an invariant force distribution. This method, commonly referred to as modal pushover analysis (MPA), is based on a modification to the uncoupled modal response history analysis (UMRHA). The UMRHA uses the elastic mode shapes to transform the equations of motion but neglects the coupling effect inherently present in the traditional non-linear response history analysis. Thus, the structure is represented by a series of equivalent SDOF systems, one for each mode. The MPA determines these equivalent systems from a transformation of the pushover curve obtained from a nonlinear static analysis. A nonlinear static analysis is separately carried out for each mode by using lateral load patterns obtained from the product of the mass matrix and the corresponding elastic mode shape. The resulting

pushover curve is idealized by a bilinear relationship between the base shear and the roof displacement. The pushover curve is then transformed into a different coordinate system, giving the relationship for a SDOF system. The peak displacement of the equivalent SDOF system can be obtained from the inelastic response spectrum and then transformed back into the roof displacement of the original system. The seismic demands determined from individual modes are finally combined using an appropriate modal combination rule.

1.5. Review of design considerations on shear walls

Extensive literature and research studies exist on the seismic design of shear wall structures. Most of these studies are related to force-based design; studies related to displacement-based design are only recently being conducted. Some of the studies that can be included in literature related to displacement-based design are presented in this section.

Adebar *et al.* (2005) described fundamental principles for design of ductile shear walls that have now been included in the design codes, particularly in the 1984 and 1994 editions of the Canadian Standards Association (CSA) standard A23.3 for the design of concrete structures (CSA 1984 and CSA 1994). It has been stated that the objective of wall ductility provisions is to ensure that curvature capacity, ϕ_{cap} , of a concrete wall is greater than or equal to the curvature demand, ϕ_d , imposed on the wall by the design earthquake. The curvature capacity is given by the ratio between the maximum

compression strain and the flexural compression zone length. On the other hand, the demand curvature is given by the addition of the yield curvature, ϕ_y , and the inelastic curvature demand, ϕ_{id} . The authors show two different approaches to estimating the curvature demand: a displacement approach and a ductility approach, both of which lead to the same results. In the ductility approach, the inelastic displacement demand is estimated from displacement ductility demand and yield curvature, while in the displacement approach, the inelastic displacement demand is specified as an input.

The two approaches mentioned above need an estimate of the yield curvature. Priestley and Kowalsky (1998) evaluated rectangular walls with different axial load ratios, longitudinal reinforcement ratios, and reinforcement patterns in order to determine trends in their moment-curvature relationships. Results of the analysis were expressed in dimensionless terms, $\phi_y l_w = K_1 \varepsilon_y$, where l_w was the wall length, ε_y the yield strain, and K_1 a factor to be determined. They found that for shear walls with reinforcement ratio of 0.5% and end reinforcement the factor K_1 worked out to be 2.0 with a dispersion in the results of about 5%. The results of this study imply that the yield curvature is (a) independent of the strength, (b) proportional to the yield strength of the reinforcement used, (c) inversely proportional to the wall length, and (d) generally not affected by concrete compression loads commonly encountered in cantilever walls (Paulay 2001).

Another aspect to consider in the design of shear walls is the definition of the ductility demand. Kowalsky (2001) evaluated design requirements in the 1997 edition of the Uniform Building Code (UBC) (UBC 1997) relating to displacement-based design. He

compared the structural capacity limits of shear walls corresponding to a maximum concrete compression strain of 0.015 with the limit of damage given by drift ratios of 0.02 and 0.025 depending on the period of the structure. It was demonstrated that for a wide range of shear wall geometries and reinforcement the maximum drift employed by the UBC code, 0.02 and 0.025, governed the design as opposed to the concrete compression strain of 0.015. The same study was conducted by Humar and Ghorbanie (2004) regarding the provisions of the NBCC 2005, which showed similar results.

Adebar *et al.* (2005) addressed some observations with respect to the definition of the plastic hinge length. It was stated that the wall ductility provisions in the standards A23.3-84 and A23.3-94 assumed a plastic hinge length equal to a portion of the wall length plus a portion of the wall height. They also observed that it was a common practice to use a plastic hinge length equal to 50% of the wall length when making a conservative estimate of the inelastic displacement capacity.

1.6. Steps in the study

To fulfill the objective of this research, the following studies are performed:

1. Selection and generation of ground motions for the city of Vancouver.
2. Development of a simple procedure for seismic design of shear wall buildings based on displacement limits and including effects from higher modes.

3. Application of the proposed procedure to different structures.
4. Evaluation of higher mode effects on the response of shear wall buildings by means of modal pushover analysis.
5. Evaluation of structural responses obtained from DBSD through nonlinear response history analyses.
6. Evaluation of modal combination rules used in the modal pushover analysis through nonlinear response history analyses.

1.7. Objective and scope of the study

The main objective of this research is to introduce and evaluate a new displacement-based seismic design (DBSD) with emphasis on reinforced concrete shear wall buildings.

The following is a summary of the scope of the study:

1. The proposed method is intended to be applied to reinforced concrete shear wall buildings with a regular plan configuration. Gravity loads are considered according to the provisions of the National Building Code of Canada 2005 (NBCC 2005).
2. The proposed method is applied to the design of buildings to be constructed in the city of Vancouver, BC, Canada, on a site of NBCC class C. It is assumed that once the method is demonstrated to work for the western region of Canada, with its

- comparatively higher level of seismicity, it will also be applicable to other seismic regions.
- 3. Since the structures are located in the city of Vancouver, Canada, the requirements of reinforcement are adopted from the 1994 edition of the Canadian Standards Association (CSA) standard A23.3-94 (CSA 1994). Certain design assumptions particular to the proposed procedure are adopted from available literature.
- 4. The selection of ground motion is based on the seismic activity recorded until November 2005. As more records become available, the ground motion selection may need refinements.
- 5. The motions selected from the data base of previously required ground motions are scaled by a unique factor proposed by Somerville *et al.* (1997) to match as closely as possible the UHS for Vancouver.

1.8. Thesis layout

This thesis is organized into 6 Chapters and 3 Appendices. Motivation for the study, introductory materials, relevant published literature, and objectives of this research are presented in the current chapter. Chapter 2 presents a review of selection and scaling of ground motions to represent the seismicity of Vancouver and to match the UHS for the city. The proposed displacement-based seismic design procedure is described in Chapter 3. The method presented in Chapter 3 is applied to the design of a 6, 12, 15, and

20-storey shear wall building. Details of the design of 6-storey building are presented in Chapter 4. Also presented in that chapter are summaries of the design of the other 3 buildings. The results obtained from the non-linear response history analyses of the designed buildings to a suite of 20 spectrum compatible ground motions are presented in Chapter 5. The analytical results are compared with the estimates obtained from DBSD and a statistical evaluation of the comparative values is carried out. All of the resulting data are contained in Chapter 5. Conclusions, and recommendations for further work are presented in Chapter 6. Appendices A, B, and C contain details of the design of the 12, 15, and 20-storey buildings, respectively.

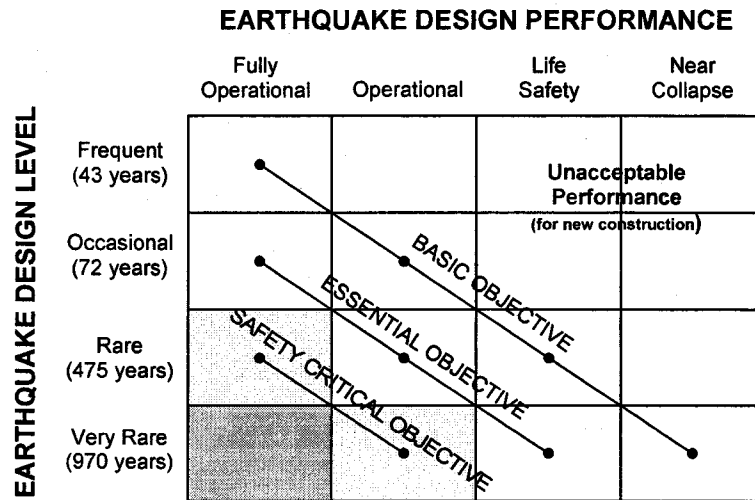


Figure 1.1: Recommended minimum seismic performance design objectives for buildings (adapted from SEAOC 1995)

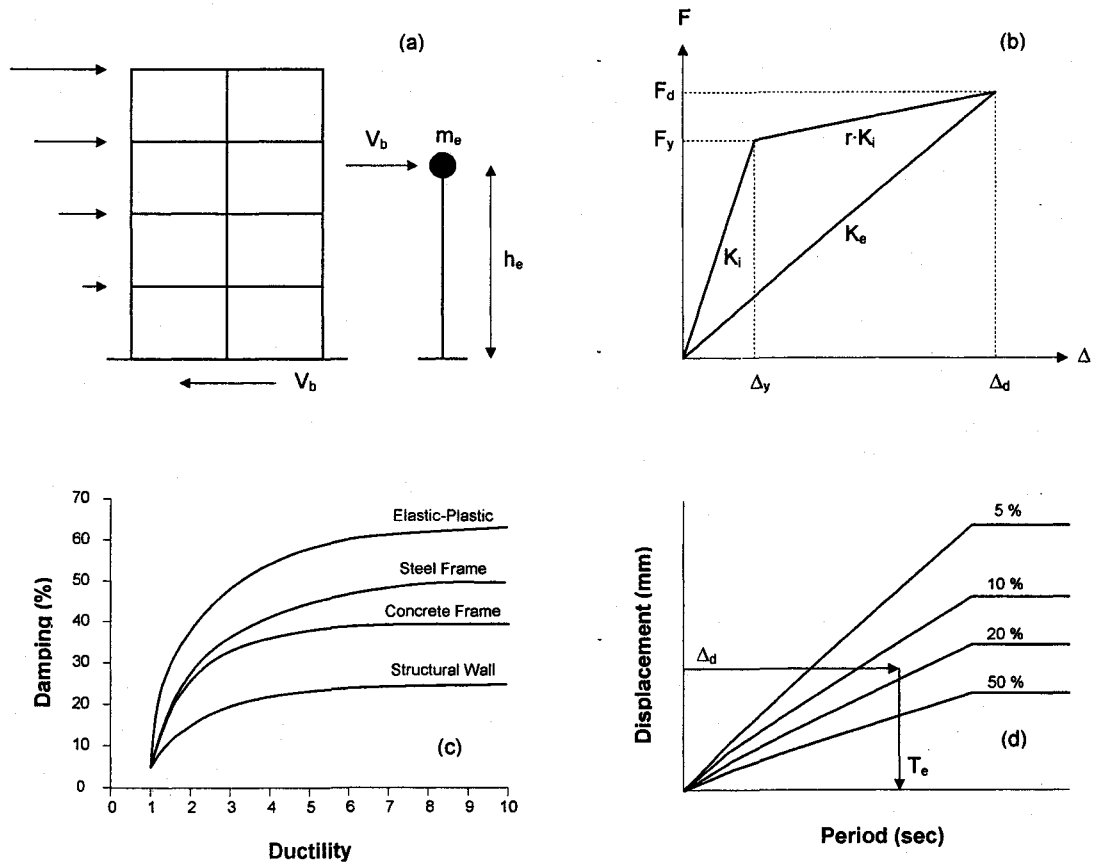


Figure 1.2: Fundamentals of direct displacement-based seismic design (adapted from Priestley 2000)

Chapter 2

Selection of Seismic Ground Motion Time Histories for Vancouver City

2.1. Introduction

The present work is primarily devoted to the evaluation of a new simplified displacement-based procedure for the seismic design of buildings (DBSD). When a new design methodology is proposed, such as the one studied here, the response of the designed structure to a representative design ground motion must be obtained to verify whether the structure performs as expected. In the present case, nonlinear time history analyses (RHA) are carried out on the structure to obtain its response. In the proposed DBSD the seismic demand is obtained from the uniform hazard spectra (UHS) presented in the National Building Code of Canada (NBCC 2005). Consequently, the ground motions used in the nonlinear time history analyses must be compatible with this UHS.

In the evaluation of the proposed DBSD, the structure is assumed as being located in the city of Vancouver. The selected input ground motions used in the RHA must therefore represent the seismicity of the city. For assistance in the selection it is important to know some of the site characteristics, such as the tectonic settings and the deaggregation of seismic hazard to ascertain the relative contributions of potential seismic events with

different magnitudes, distance, characteristics, etc. Once a record has been selected it must be scaled to match the corresponding UHS. Several different procedures exist for such matching. In the present work, a unique scaling factor is used, both to ensure simplicity and to prevent the distortion of frequency content in the motion.

2.2. Background

Several different methods exist for generating spectrum compatible ground motions (GMs). They can be classified in four groups (Kramer 1996): modification of previously recorded GMs, generation of artificial GMs in time domain, generation of artificial GMs in frequency domain, and generation of artificial GMs using Green's function technique. Many contributions have been made to each of these techniques. The modification of recorded GMs is the simplest approach and it is the preferred approach as long as enough real records exist. The use of artificial GMs is an alternative that is appropriate in some special cases, such as when few recorded GMs exist. In some cases where engineers need to evaluate existing structures, use of artificial GM time histories could represent a conservative approach to the determination of structural response (Lestuzzi *et al* 2004). Since spectrum compatible ground motions are obtained here by appropriate scaling of existing records, the following discussion focuses on methods of scaling existing records to match the target spectrum.

A commonly used scaling factor is obtained to match the peak ground acceleration at the site of the record to that at the site of the structure. This factor was originally proposed by

Krinitsky and Chang (1979) and was considered appropriate if it ranged between 0.25 and 4. It was also recommended that in the nonlinear analyses studies, several GMs with factors closest to one must be selected. Vanmarcke (1979) described the disadvantages of using scaling factors that did not consider the frequency content and duration of the excitation.

Dussom *et al.* (1991) and Ferrito (1992), recommended that parameters, other than PGA or PGV, such as magnitude, distance, local site characteristics and the acceleration level should be considered in selecting scaling factors. When these parameters match the earthquakes contributing most to the hazard, the selected motions will have frequency content and duration similar to those of the contributing earthquakes.

Some authors have tried scaling in the frequency domain. Naumosky (1998) modified the Fourier transform coefficients of a record until the response spectrum of the resulting modified motion matched the target spectrum. However, Naeim and Lew (1995) have cautioned against using this procedure because it may lead to unrealistic ground motions and the scaled GM could grossly overestimate the displacement and velocity responses.

It is also possible to modify the time history in the time domain. Abrahamson (1993) has presented a method that modifies a selected ground motion record, $a(t)$, by adding a small adjustment time history, $\delta a(t)$, so that the response spectrum of the modified record matches the target spectrum. The basic method of determining such an adjustment time history can be summarized in the following steps. First, the time history of the response

of a SDOF system characterized by the frequency, ω_i , and damping β_i , to the ground motion time history, $a(t)$, is obtained. The peak value (R_i) and its corresponding time, t_i , are determined from the time history response. From the target spectrum for the damping of β_i , the target value (Q_i) at frequency, ω_i , is obtained. Then, the difference between the target value, Q_i , and the peak value, R_i , is computed. This difference is referred to as the spectral misfit, ΔR_i . Finally, the adjustment time history, $\delta a(t)$, is determined such that the SDOF system response to $\delta a(t)$ at time t_i is equal to the spectral misfit, ΔR_i , for all values of i . It is assumed that the adjustment time history, $\delta a(t)$, will not perturb the time, t_i , of the peak response, R_i . The adjustment time history is, in fact, expressed as a sum of selected adjustment functions, each of which is weighted by a coefficient. These coefficients become the unknowns to be determined. The adjustment functions are chosen such as to preserve the non-stationary character of the reference ground motion $a(t)$ for a wide range of frequencies. The method includes an iterative process in order to obtain the adjustment function that satisfies the spectral misfits for all the SDOF systems. This procedure presents some numerical difficulties and is computationally cumbersome as compared to methods based on the frequency domain.

Frequency and time domain scaled time histories are also called spectrum compatible time histories (SCTH). Naeim and Lew (1995) pointed out that generating an acceleration-time history to be spectrum compatible to a UHS is neither reasonable nor realistic since UHS were intended to represent multiple events that correspond to a specified risk level. Abrahamson (1995) also described some objections to SCTH. First, SCTH are unrealistic by definition since they lead to a smooth spectrum and earthquakes

do not have smooth spectra. Second, SCTH will lead to a significant over-estimation of the response since they excite all periods in one earthquake. These observations lead to another consideration in selecting a methodology for generating modified time histories. As mentioned earlier, scaling of ground motion records by a single factor maintains simplicity and also preserves the variability of responses.

Somerville *et al.* (1997) have recently developed several suites of GMs for buildings located in three different zones of US. Their research was based on scaling actual motions to minimize the squared error between the spectral acceleration of the scaled motion and the target spectrum at several different periods. Four periods were considered: 0.3, 1, 2 and 4 seconds with weighting factors of 0.1, 0.3, 0.3 and 0.3, respectively. Ground motions for each zone were developed for two different probabilities of exceedance, 2 % and 10 % in 50 years.

A commonly accepted method of scaling ground motions for non-linear time history analysis is based on matching as closely as possible the response spectrum of the scaled motion and the target spectrum over a given range of periods. Shome *et al* (1998) proposed scaling to match the spectral acceleration at the fundamental period of the structure. Other researchers have used a range based on the likely range over which the fundamental period of the structure could vary as it under goes nonlinear response. Naumosky *et al.* (2004) studied a type of scaling for ground motions used to study the response of irregular concrete buildings based on the use of a period range between the second mode period and 1.2 times the fundamental period. This period range of the

excitation motions was assumed to have the largest effects on the structural response. The factor of 1.2 was intended to take into account the elongation of the fundamental structural period because of non-linear deformations during the response. The results from this method were quite similar to those obtained from the one proposed by Shome *et al.* (1998).

A more rigorous analytical approach was presented by Lestuzzi *et al.* (2004) who introduced a new definition of spectral intensity called modified spectral intensity, SI_b , in order to evaluate the "severeness" of the earthquake ground motion. This modification takes into account the fundamental period and the design ductility of the structure. The spectral intensity is calculated over a period range from the fundamental period to an elongated period that considers the nonlinear deformation of the structure. It was recommended that when modifying the acceleration time histories, the design spectral accelerations should be matched as closely as possible within this frequency range. After scaling, the "severeness" of several time history candidates can be ranked with the aid of the modified spectral intensity. A larger SI_b , leads to higher displacement and higher ductility demand. It is up to the user to decide whether to use the most "severe" time histories for worst case scenario studies or to use time histories that have neither particularly high nor particularly low values of SI_b .

2.3. Seismicity of Vancouver

According to the plate tectonic theory, there are three types of plate boundaries, namely: Spreading Ridge Boundaries, Subduction Zone Boundaries and Transform Fault Boundaries (Kramer 1996). Vancouver is located near a subduction zone called Cascadia. However, the city is 150 km east of this zone and its major hazard comes not from the subduction earthquakes themselves but from crustal and subcrustal earthquakes that originate in subduction zone (Halchuk and Adams 2004). Thus the presence of a subduction zone plays an important role in selection of ground motions for Vancouver, and one must search for the crustal and subcrustal activity in other similar subduction regions.

Based on a previous work by Onur, Cassidy and Rogers (2005) the seismic and tectonic setting for Vancouver can be classified by crustal, subcrustal and subduction earthquakes (Figure 2.1), The crustal earthquakes are produced by motions that originate at a depth of 20 km with little correlation to the surface faults, the subcrustal earthquakes are mainly concentrated at a depth of 50 km beneath the Georgia Strait (GOS) and the Puget Sound (PUG) areas (Figure 2.2), and the subduction earthquakes originate at a subduction interface between the Juan de Fuca Plate and the North American Continental Plate at approximately 150 km from Vancouver.

The earthquake hazard for Vancouver can be assessed from the deaggregation analysis carried out by Halchuk and Adams (2004). The pseudo-acceleration at 1 second period

presents a bimodal effect (Figure 2.3) due to crustal and subcrustal activity where the major contribution to hazard is from earthquakes with hypocenters less than 40 km from the site and having moment magnitudes greater than 7.0. The secondary hazard comes from earthquakes at hypocentral distances of between 40 and 80 km and magnitudes between 6.5 and 7.0. This bimodal effect is almost the same for several different periods, but the hazard at longer periods has greater contribution from subcrustal earthquakes, while the hazard at shorter periods is mainly from crustal earthquakes. In the case of subduction earthquakes, a deterministic approach is used to assess the hazard. Such earthquakes, in fact, make a smaller contribution to hazard than other two types. However, other similar regions such as South-western Japan (Geiyo Earthquake, 2001, from KiKnet), Southern Alaska (Alaska Earthquake, 1964, from USGS) West coast of Mexico (Mexico Earthquake, 1985, from SSN-UNAM) and Chile (Scholl and Thiel 1986) have shown significant damage to structures at hypocentral distances longer than 120 km. Therefore, these types of earthquakes must also be included in the selection of ground motions for Vancouver.

Another important aspect that must be considered in the selection of ground motions is the definition of the target response spectrum. The NBCC 2005 defines an uniform hazard spectrum (UHS) for different Canadian cities with a 2% probability of exceedance in 50 years. The corresponding pseudo-acceleration values for Vancouver are shown in Figure 2.4 for 9 different periods (0.1, 0.15, 0.2, 0.3, 0.4, 0.5, 1.0, 2.0, and 4.0 seconds). Values at other periods may be determined by linear interpolation. The figure also shows the spectral acceleration at zero second, which is equal to the peak

ground acceleration. In the present study pseudo-accelerations for periods longer than 4 seconds are assumed to be inversely proportional to the period. Ground motion having spectral responses that closely match this target spectrum will be selected according to the procedure presented in this chapter.

2.4. Selection of seismic regions and data

The first source of ground motion records should be the inventory of records produced during the local seismic events that made a major contribution to the hazard. In other words, events that occurred within a certain hypocentral distance and had a specified magnitude must be selected as the input ground motions. Details of some of the latest seismic activity, from 1996 until 2005, (Geological Survey of Canada) which was recorded at PGC station (Sidney, BC, 70 km South-west of Vancouver) are shown in Table 2.1. This summary shows both crustal and subcrustal seismic activity, but with very low contribution to hazard and only one event of magnitude higher than 5 (this event corresponds to the Nisqually earthquake 2001 which will be treated as one source for selecting ground motions). Records obtained during the local seismic activity may not therefore be adequate; and records from other seismic regions with similar tectonic settings must be included in the selection.

In seismic regions that have tectonic settings similar to these of Vancouver, the recorded ground motions would be expected to show characteristics (magnitude and distance) that are similar to earthquakes that contribute to the seismic hazard for the city. Selection of

regions having similar tectonic setting is based on an examination of the historic seismic activity of different subduction zones. Some regions with activity similar to Vancouver are presented in Table 2.2 with their respective references, type of earthquake and geographical location.

Only a few earthquakes with magnitude and distances that contribute to the hazard have been measured for many of regions presented on Table 2.2. However, three major earthquakes have occurred in zones with high density of instruments, such as the Geiyo (2001) and Tokachi Oki (2003) earthquakes in Japan and the Nisqually earthquake (2001) in Washington State, USA. Other important earthquakes within these regions that have been recorded include the Michoacan earthquakes (1994, 1997 and 2000) in Mexico, El Salvador earthquakes (2001) and some others in the North-west of USA. The characteristics of these earthquakes are presented on Table 2.3. A large number of records from the Geiyo, Nisqually and Tokachi Oki earthquakes have been processed in this research. However, these records have not all been listed in Table 2.3, instead only the range of distances to the recording station have been identified.

Another factor that must be taken into account in selecting the records, is the site condition at the site of the recording instrument. In this research, when possible, records measured by instruments located on sites of class C (NBCC 2005) are selected. Site class C is defined as having average shear wave velocities between 360 and 760 m/sec in the top 30 meter depth. This site class is the one used as the reference site for which the UHS in NBCC 2005 have been developed. For a number of instruments in the Japan networks

(Kik-net and K-net) additional estimations must be made in order to classify the site conditions for each instrument. Boore (2004) has estimated these values for 30 meter depth and their results are used in this research. For Washington stations, the geology defined by the Pacific Northwest Seismograph Network (PNSN) and the report presented by Williams *et al.* (1999a and 1999b) are used to classify the site conditions for this zone.

Most of the records obtained from the source are uncorrected, which means that some noise could be present in the signal. Hence, each of the uncorrected data is first mean-corrected and then bandpass filtered with a 6th order Butterworth filter having low and high frequencies of 0.05 Hz and 20 Hz, respectively. The low frequency allows correction of any baseline distortion, since the zero-frequency is included in the filtering process. Once data are corrected, pseudo-acceleration spectral response is obtained for each record by using the Newmark's method (average acceleration method). Scale factors required to match the calculated spectra are then determined.

2.5. Scaling method

The scaling method used in this work was adopted from Somerville *et al.* (1997). In this method the scaling factor is obtained by minimizing the weighted squared error between the target PSA (PSAt) and the average (between two horizontal records) ground motion PSA (PSAgm) assuming lognormal distribution of the amplitudes. The weight factors (w_i) used were 0.1, 0.3, 0.3 and 0.3 for periods of 0.3, 1, 2 and 4 seconds, respectively. The analytical expression for calculating the scale factor, α_{sm} , is given by

Equation (2.1). It will be noted that for similar response shapes the scale factor is equal to 1.

$$\alpha_{sm} = \prod_{i=1}^4 \left(\frac{PSA_{t_i}}{PSA_{gm_i}} \right)^{w_i} \quad (2.1)$$

An attempt is made here to further refine the selection process by following some of the recommendations from Lestuzzi *et al.* (2004). The procedure that is used consists of scaling the records so as to match the spectral response at the natural period of the structure (Shome *et al.* 1998) and then ranking the corrected ground motions according to their “severeness”. The “severeness” is measured in terms of a modified spectral intensity of the record, SI_b , which is directly related to the displacement and ductility demand.

The modified spectral intensity, SI_b , (Lestuzzi *et al.* 2004) is defined in Equation (2.2) and represents the area of the pseudo-velocity response spectrum (PSV) between two periods, divided by the period range (ΔT). The lower integration limit in Equation (2.2) is the fundamental period, T_0 , while the upper limit is an equivalent secant stiffness period, T_s .

$$SI_b = \frac{1}{\Delta T} \int_{T_0}^{T_s} PSV \cdot dT \quad (2.2)$$

The equivalent secant stiffness period, T_s , is obtained from an equivalent non-linear system defined by the reduction factor R_y and is given by Equation (2.3).

$$T_s = T_o \cdot \sqrt{R_y} \quad (2.3)$$

In this research, the records that rank higher in the SI_b or “severeness” are adopted as the preferred motions.

Although the ranking process based on “severeness” and the scaling factor based on the response at fundamental period can be useful, the definition of the parameters involved in the procedure are highly dependent on the type of structure being analyzed. In order to establish a general suite of GMs for Vancouver, a fundamental period of 1 second and a ductility factor of 4 are taken as being representative reasonable values for ductile mid-rise structures. Since this definition is arbitrary, the results coming from this process are only used as a reference to select the suite of GMs, and only the original scaling factor (α_{sm}) is used to modify a record.

Another important issue is the choice of the number of records needed for a non-linear analysis. Some design codes require at least five GMs to carry out a nonlinear time history analysis. For research purposes, however, this quantity must be larger in order to consider different GM characteristics, such as amplitude, frequency content and phase angles. According to Shome *et al.* (1998) the number of GMs, n , that should be selected can be obtained from:

$$n = 4.0 \cdot \left(\frac{\delta}{X} \right)^2 \quad (2.4)$$

where X is a factor that defines the confidence band of the median response; for instance the typical 95 % confidence is defined by a factor X equal to ± 0.1 . The factor, δ , is the dispersion in the nonlinear responses of a structure to several scaled ground motions. This dispersion was evaluated for earthquakes belonging to 4 different categories or Bins. Individual Bins are defined by given moment magnitudes, M , and epicenter distances, R . The median and dispersion obtained for two response parameters, ductility values related to maximum inter-storey drift ratios (Max. Inter-St.) and roof displacements (Global), are shown in Table 2.4. The Bins that are equivalent to the present study Bins II and III. Within these two Bins, the maximum dispersion, δ , is found to be 0.32. Therefore, if the number of GMs for nonlinear analysis, n , and the dispersion, δ , are set up as 20 and 0.32, respectively, the factor X obtained from Equation (2.4) will be around ± 0.14 representing 93 % confidence in the median response estimate. Assuming that this confidence level is adequate, 20 records will be used for the nonlinear time history analyses carried out in the present study.

2.6. Final selection criteria

There are several sources and institutions which collect, manage and store data obtained during seismic activity. Data is available either online or through file transfer protocol (ftp). For this work, more than 300 records were obtained for use in the selection process explained earlier. Most of these records come from three major earthquakes with a high density of instruments in the affected area: Nisqually (2001), Geiyo (2001) and Tokachi Oki (2003). Some criteria must be established in order to narrow down the

number of records to be processed. The following points are considered in choosing an initial set of records:

- Consider only those ground motions recorded by instrument with reliable information regarding site conditions;
- Include as many different earthquakes as possible, rather than selecting records from the same earthquake;
- Include records from both directions for each instrument;
- Define an upper limit on the scaling factor to avoid large modifications in the spectral response (e.g. increasing high-frequency responses);
- In cases where a large number of records are available, consider those records with smaller differences between the SI_b of the record and the SI_b of the target spectrum. Since, two records are selected from each instrument site, the average of the SI_b of the two may be used as the representative value.

Table 2.5 shows a summary of the 52 (26 pairs) records from which final selection will be made for Vancouver city, taking into account the considerations cited above. In choosing the 52 records the scaling factor was limited to 5 and the maximum difference between the spectral intensities (SI_b for the target spectrum is 0.594 m/s) was limited to 20 %. In Table 2.5 the number in parenthesis following the earthquake name indicates the

year of occurrence. The file name represents the original file name from the source, except for records from Geiyo, Tokachi Oki and Nisqually earthquakes where it represents the name of the station. The file names end with an indication of the direction of the instrument. The first factor, α_{sh} , is the scale factor required to match the spectral acceleration produced by the record at a period of 1 second to the corresponding value in the target spectrum. The spectral intensity, SI_b , was calculated between the periods of 1 and 2 seconds. The factor, α_{sm} , is the scale factor determined on the basis of the method proposed by Somerville *et al.* (1997). The last two columns show the time interval and number of points for each record.

It must be mentioned that most of the records shown in Table 2.5 come from Nisqually earthquake (2001). Each of these records is a strong candidate having characteristics that satisfy almost all of the criteria pointed out earlier, with the only exception that they all come from the same earthquake. This contradiction will be accepted in this work, so that sufficient number of records can be selected.

The pseudo-acceleration spectra of the scaled records are shown in Figure 2.5, Figure 2.6 and Figure 2.7. In most cases, the spectra are very similar in shape to the UHS with some differences for the lower periods. However, there are 5 cases where the spectral values at lower periods are three times (VAN06A-B) or even more (VAN20A-B and VAN24B) than the UHS. These differences in the spectral shapes can be explained by either of the following two reasons: the spectra of these 5 records may be closer to a different UHS

with a different probability of occurrence, and/or the use of a single scale factor may exaggerate a particular spectral value that was not considered on the matching process.

2.7. Comments

The selection of a suite of 26 pairs of records obtained from tectonic settings and seismic hazard similar to those of Vancouver was presented in this chapter. However, the engineer or researcher may limit the number to a more practical value. Based on research by others it is recommended that at least 20 of these records be used in a research study to obtain meaningful statistical results. A more detailed research study may be needed to establish the adequacy of the number in association with the scaling method proposed in the present study.

According to Shome *et al.* (1998) when a scaling factor based on the fundamental period of the structure is used, a suite of 20 ground motions may be adequate for nonlinear analyses of a MDOF system. The response spectra for some of the records presented here show large differences from the target spectrum at higher frequencies when a scaling factor based on the fundamental period is applied. It is known that the base shear response for shear walls is highly influenced by the higher modes (e.g. 2nd and 3rd mode). Therefore, the nonlinear RHA in this thesis will be based only on input ground motions that have been corrected by the scaling factor proposed by Somerville *et al.* (1997).

For future research, it is recommended that alternative scaling factors may be studied. The scale factors presented here are all based on matching the acceleration spectra.

However, the DBSD is based on the displacement demand rather than on the spectral acceleration. Therefore, it may be more appropriate to study scale factors that are based on matching of the displacement spectra.

Table 2.1: Seismic activity measures at PGC station within the period 1996-2005 (GSC)

| Epicenter Zone | Magnitude (ML) | Distance* (km) | Depth (km) | Date (YYYY/MM/DD) |
|---------------------------------|---------------------------|---------------------------|-----------------------|------------------------------|
| 21 km N from Nanaimo | 3.1 | 90 | 66.5 | 2004/08/03 |
| 28 km S from Richmond | 3.0 | 40 | 20.7 | 2004/01/30 |
| 9 km SE from Victoria | 2.4 | 30 | 44.8 | 2003/10/12 |
| 85 km S from Victoria | 4.6 | 115 | 51.3 | 2003/04/25 |
| 20 km E from Victoria | 4.3 | 30 | 26.2 | 2002/09/21 |
| 40 km SSE from Victoria | 3.0 | 65 | 16.0 | 2002/01/09 |
| 15 km E Victoria | 3.6 | 30 | 25.9 | 2000/06/29 |
| Victoria | 4.0 | 18 | 53.0 | 1999/12/11 |
| Strait of Georgia | 2.9 | 65 | 3.9 | 1999/01/21 |
| Near Saint Juan Island, WA, USA | 3.0 | 20 | 8.2 | 1997/09/24 |
| Strait of Georgia | 4.6 | 65 | 3.3 | 1997/06/24 |
| Strait of Georgia | 3.4 | 65 | 3.4 | 1997/06/13 |
| Near Duvall, WA, USA | 5.5 | 140 | 4.1 | 1996/05/03 |
| Coast Mountains | 4.0 | 140 | 2.0 | 1996/02/02 |

*Approximated Instrument Epicentral Distance (PGC station, Sidney, BC)

Table 2.2: Geographical and tectonic settings for different subduction regions with crustal and/or subcrustal seismicity

| Region | Reference | Type of Earthquake | Latitude | | Longitude | |
|---|--|-------------------------|----------|--------|-----------|-------|
| | | | Min | Max | Min | Max |
| Pacific North West (British Columbia, Washington, Oregon) | Seno & Yoshida (2004) | Crustal & Subcrustal | 47°N | 50.5°N | 122°W | 125°W |
| Southwestern Japan | Nakanishi, Kinoshita & Miura (2001) | Subcrustal | 34°N | 35°N | 131°E | 135°E |
| Central South Island (New Zealand) | Reyners (1987) | Subcrustal | 43.5°S | 44.5°S | 169°E | 171°E |
| Vrancea Region (Romania) | Radulian et al. (2001) | Subcrustal | 45°N | 46°N | 26°E | 27°E |
| Alpine Italy | Selvaggi & Amato (1992) | Subcrustal | 43°N | 44°N | 12°E | 13°E |
| Western Coast of Mexico | Seno & Yoshida (2004) | Crustal & Subcrustal | 15°N | 20°N | 105°W | 95°W |
| Central America (El Salvador) | Seno & Yoshida (2004); Japan Society of Civil Engineers (2001) | Crustal & Subcrustal | 8°N | 15°N | 92°W | 82°W |
| Pampean Ranges (Argentina) | Alvarado (2005); Araujo, Perez & Millan (2005) | Crustal | 26°S | 34°S | 64°W | 69°W |

Table 2.3: Selected earthquakes from zones with seismic hazard zones similar to that of Vancouver city.

| Epicenter Zone | Station (Number) | Source (Processed by) | Magnitude (type) | Distance* (km) | Depth (km) | Date (YYYY/MM/DD) | Type of EQ (Zone) |
|----------------------------|---|----------------------------|------------------|----------------|------------|-------------------|-------------------|
| Duval, WA, USA | Tolt River Dam (2199) | USGS (COSMOS) | 5.5 (ML) | 14.8 | 4.0 | 1996/05/03 | Crustal (SZ) |
| Duval (Nisqually), WA, USA | Several Stations (34 stations) | USGS (COSMOS) | 6.8 (Mw) | 111.0 | 52.0 | 2001/02/28 | Subcrustal (SZ) |
| Scot Mills, OR, USA | Detroit Dam (2133) | USGS (COSMOS) | 5.7 (ML) | 48.8 | 20.0 | 25/03/1993 | Crustal (SZ) |
| Satsop, WA, USA | Olympia, Halverson Residence (7008) | USGS (COSMOS) | 5.8 (Mw) | 58.0 | 41.0 | 1999/07/03 | Crustal (SZ) |
| Puget Sound, WA, USA | Seattle Federal Building (2102) | USGS (COSMOS) | 6.7 (Mw) | 63.1 | 59.0 | 1965/04/29 | Subcrustal (SZ) |
| Olympia, WA, USA | Washington Hwy Test Lab (2101) | USGS (COSMOS) | 6.9 (?) | 74.7 | 70.0 | 1949/04/13 | Subcrustal (SZ) |
| Helena, MN, USA | Carroll College (2202) | USGS (COSMOS) | 6.0 (Ms) | 3.5 | 6.0 | 1935/10/31 | Crustal (SZ) |
| Geiyo, Japan | Several Stations (64 stations) | KiKnet | 6.4 (Mw) | 60.0 – 150.0 | 60.0 | 2001/03/24 | Subcrustal (SZ) |
| Michoacan, Mexico | Caleta de Campos, Mexico | UNR (COSMOS) | 7.0 (Mw) | 17.6 | 9.0 | 2000/08/09 | Crustal (SZ) |
| Michoacan, Mexico | La Union | UNR (COSMOS) | 7.0 (Mw) | 62.6 | 9.0 | 2000/08/09 | Crustal (SZ) |
| Michoacan, Mexico | El Balcon | UNR (COSMOS) | 6.6 (ML) | 52.8 | 48.0 | 1994/12/10 | Subcrustal (SZ) |
| Michoacan, Mexico | La Union | UNR (COSMOS) | 6.6 (ML) | 68.4 | 48.0 | 1994/12/10 | Subcrustal (SZ) |
| Michoacan, Mexico | Zihuatanejo | UNR (COSMOS) | 6.6 (ML) | 76.6 | 48 | 1994/12/10 | Subcrustal (SZ) |
| Michoacan, Mexico | Caleta de Campos Mexico | UNR (COSMOS) | 7.1 (Mw) | 36.9 | 33 | 1997/01/11 | Subcrustal (SZ) |
| Michoacan, Mexico | Villita Mexico | UNR (COSMOS) | 7.1 (Mw) | 71.4 | 33 | 1997/01/11 | Subcrustal (SZ) |
| El Salvador | Unidad de Salud, Panchimalco, San Salvador (PA) | UCA | 6.6 (Mw) | 17.6 | 13.0 | 2001/02/13 | Crustal (SZ) |
| El Salvador | Unidad de Salud, Panchimalco, San Salvador (PA) | UCA | 7.6 (Mw) | 95.7 | 60.0 | 2001/01/13 | Subcrustal (SZ) |
| Tokachi-oki, Japan | Several Stations (16 stations) | KiK-net | 8.0 (Mw) | 120.0 – 200.0 | 33.0 | 2003/09/25 | Subduction (SZ) |
| Valparaiso, Chile | Endesa Building, Santiago (4400) | DGG Celebi (1988) (COSMOS) | 7.2 | 120.0 | 37.8 | 1985/04/09 | Subduction (SZ) |

*Hypocentral Distance

Table 2.4: Median and dispersion results of ductility responses obtained from scaled records of Bin-I, Bin -II, Bin-III, and Bin-IV (adapted from Shome *et al.* 1998).

| Case | Case definition | Ductility response | Median | Dispersion |
|-------------|------------------------|---------------------------|---------------|-------------------|
| Bin-I | M = 5.25-5.75 | Global | 1.6 | 0.19 |
| | D = 5-25 km | Max. Inter-St. | 2.6 | 0.28 |
| Bin-II | M = 6.5-7.0 | Global | 1.4 | 0.19 |
| | D = 50-70 km | Max. Inter-St. | 2.0 | 0.25 |
| Bin-III | M = 6.7-7.3 | Global | 1.3 | 0.20 |
| | D = 10-30 km | Max. Inter-St. | 1.9 | 0.32 |
| Bin-IV | M = 6.5-7.0 | Global | 3.5 | 0.39 |
| | D = 15-35 km | Max. Inter-St. | 6.9 | 0.42 |

Table 2.5: Selected Records for Vancouver city.

| GM | Earthquake | File Name | New Name | Factor | SI_b | Diff. SI_b | Factor | Δt | Number |
|-----------|--------------------|------------------|-----------------|---------------|-----------------------|-----------------------------|---------------|------------|------------------|
| # | name | | | ash | m/sec | % | asm | (s) | of points |
| 1 | Tokachi Oki (2003) | HKD0109_NS | VAN01A | 1.04 | 0.41 | 18.85 | 0.99 | 0.010 | 15709 |
| 2 | Tokachi Oki (2003) | HKD0109_EW | VAN01B | 1.34 | 0.41 | 18.85 | 0.99 | 0.010 | 15709 |
| 3 | Tokachi Oki (2003) | HKD096_EW | VAN02A | 1.53 | 0.60 | 0.62 | 1.25 | 0.010 | 23449 |
| 4 | Tokachi Oki (2003) | HKD096_NS | VAN02B | 1.83 | 0.60 | 0.62 | 1.25 | 0.010 | 23449 |
| 5 | Olympia (1949) | 103156o1_N04W | VAN03A | 1.49 | 0.55 | 4.15 | 1.65 | 0.020 | 4454 |
| 6 | Olympia (1949) | 103156o1_N86E | VAN03B | 1.84 | 0.55 | 4.15 | 1.65 | 0.020 | 4454 |
| 7 | Tokachi Oki (2003) | HKD0107_NS | VAN04A | 2.04 | 0.44 | 14.92 | 1.67 | 0.010 | 18509 |
| 8 | Tokachi Oki (2003) | HKD0107_EW | VAN04B | 1.92 | 0.44 | 14.92 | 1.67 | 0.010 | 18509 |
| 9 | Nisqually (2001) | BHD_01_NS | VAN05A | 3.03 | 0.67 | 7.30 | 2.62 | 0.010 | 17300 |
| 10 | Nisqually (2001) | BHD_01_EW | VAN05B | 1.32 | 0.67 | 7.30 | 2.62 | 0.010 | 17300 |
| 11 | Michoacan (1997) | CALE9701_EW | VAN06A | 2.32 | 0.54 | 5.05 | 2.63 | 0.005 | 13101 |
| 12 | Michoacan (1997) | CALE9701_NS | VAN06B | 1.29 | 0.54 | 5.05 | 2.63 | 0.005 | 13101 |
| 13 | Nisqually (2001) | LAP_01_NS | VAN07A | 1.69 | 0.57 | 2.50 | 2.83 | 0.010 | 17000 |
| 14 | Nisqually (2001) | LAP_01_EW | VAN07B | 2.57 | 0.57 | 2.50 | 2.83 | 0.010 | 17000 |
| 15 | Nisqually (2001) | KIMB_01_EW | VAN08A | 1.77 | 0.59 | 0.02 | 3.16 | 0.010 | 48001 |
| 16 | Nisqually (2001) | KIMB_01_NS | VAN08B | 2.54 | 0.59 | 0.02 | 3.16 | 0.010 | 48001 |
| 17 | Nisqually (2001) | CRO_01_NS | VAN09A | 1.85 | 0.60 | 0.57 | 3.32 | 0.010 | 17900 |
| 18 | Nisqually (2001) | CRO_01_EW | VAN09B | 3.90 | 0.60 | 0.57 | 3.32 | 0.010 | 17900 |
| 19 | Nisqually (2001) | GAR_01_NS | VAN10A | 3.62 | 0.75 | 15.86 | 3.38 | 0.010 | 16300 |
| 20 | Nisqually (2001) | GAR_01_EW | VAN10B | 2.32 | 0.75 | 15.86 | 3.38 | 0.010 | 16300 |
| 21 | Nisqually (2001) | THO_01_NS | VAN11A | 2.31 | 0.55 | 4.44 | 3.85 | 0.010 | 104900 |
| 22 | Nisqually (2001) | THO_01_EW | VAN11B | 3.57 | 0.55 | 4.44 | 3.85 | 0.010 | 104900 |
| 23 | Nisqually (2001) | SEU_01_NS | VAN12A | 3.37 | 0.68 | 9.13 | 3.88 | 0.010 | 20600 |
| 24 | Nisqually (2001) | SEU_01_EW | VAN12B | 4.05 | 0.68 | 9.13 | 3.88 | 0.010 | 20600 |
| 25 | Nisqually (2001) | HAL_01_NS | VAN13A | 1.57 | 0.65 | 5.36 | 4.02 | 0.010 | 17500 |
| 26 | Nisqually (2001) | HAL_01_EW | VAN13B | 3.70 | 0.65 | 5.36 | 4.02 | 0.010 | 17500 |
| 27 | Nisqually (2001) | ALO_01_NS | VAN14A | 2.77 | 0.68 | 8.48 | 4.08 | 0.010 | 13400 |
| 28 | Nisqually (2001) | ALO_01_EW | VAN14B | 4.72 | 0.68 | 8.48 | 4.08 | 0.010 | 13400 |

| GM # | Earthquake name | File Name | New Name | Factor ash | Slb m/sec | Diff. Slb % | Factor asm | Δt (s) | Number of points |
|------|----------------------|--------------|----------|------------|-----------|-------------|------------|--------|------------------|
| 29 | Nisqually (2001) | EVA_01_NS | VAN15A | 2.37 | 0.56 | 3.83 | 4.19 | 0.010 | 20500 |
| 30 | Nisqually (2001) | EVA_01_EW | VAN15B | 3.13 | 0.56 | 3.83 | 4.19 | 0.010 | 20500 |
| 31 | Nisqually (2001) | SEA_01_EW | VAN16A | 3.31 | 0.65 | 5.55 | 4.47 | 0.010 | 48001 |
| 32 | Nisqually (2001) | SEA_01_NS | VAN16B | 3.11 | 0.65 | 5.55 | 4.47 | 0.010 | 48001 |
| 33 | Nisqually (2001) | WISC_01_EW | VAN17A | 4.79 | 0.54 | 4.94 | 4.63 | 0.010 | 48001 |
| 35 | Nisqually (2001) | WISC_01_NS | VAN17B | 2.67 | 0.54 | 4.94 | 4.63 | 0.010 | 48001 |
| 36 | Nisqually (2001) | MPL_01_EW | VAN18A | 3.60 | 0.44 | 15.83 | 4.64 | 0.010 | 48001 |
| 37 | Nisqually (2001) | MPL_01_NS | VAN18B | 2.38 | 0.44 | 15.83 | 4.63 | 0.010 | 48001 |
| 34 | Nisqually (2001) | CTR_01_NS | VAN19A | 2.75 | 0.63 | 3.49 | 4.68 | 0.010 | 94800 |
| 38 | Nisqually (2001) | CTR_01_EW | VAN19B | 5.18 | 0.63 | 3.49 | 4.68 | 0.010 | 94800 |
| 39 | Geiyo (2001) | EHHM08_EW | VAN20A | 3.70 | 0.41 | 18.62 | 4.71 | 0.005 | 37400 |
| 40 | Geiyo (2001) | EHHM08_NS | VAN20B | 2.36 | 0.41 | 18.62 | 4.71 | 0.005 | 37400 |
| 41 | Nisqually (2001) | RBEN_01_EW | VAN21A | 3.33 | 0.52 | 7.41 | 4.74 | 0.010 | 48001 |
| 42 | Nisqually (2001) | RBEN_01_NS | VAN21B | 2.52 | 0.52 | 7.41 | 4.74 | 0.010 | 48001 |
| 43 | Nisqually (2001) | MAR_01_NS | VAN22A | 3.33 | 0.55 | 4.10 | 4.74 | 0.010 | 157100 |
| 44 | Nisqually (2001) | MAR_01_EW | VAN22B | 2.61 | 0.55 | 4.10 | 4.74 | 0.010 | 157100 |
| 45 | Puget Sound (1965) | UCACA02_S32E | VAN23A | 5.22 | 0.35 | 24.22 | 4.75 | 0.020 | 3706 |
| 46 | Puget Sound (1965) | UCACA02_S58W | VAN23B | 2.63 | 0.35 | 24.22 | 4.75 | 0.020 | 3706 |
| 47 | El Salvador (1/2001) | pa01001_EW | VAN24A | 4.32 | 0.42 | 16.98 | 4.80 | 0.005 | 10879 |
| 48 | El Salvador (1/2001) | pa01001_NS | VAN24B | 2.03 | 0.42 | 16.98 | 4.80 | 0.005 | 10879 |
| 49 | Nisqually (2001) | KITP_01_EW | VAN25A | 3.59 | 0.70 | 10.48 | 4.83 | 0.010 | 48001 |
| 50 | Nisqually (2001) | KITP_01_NS | VAN25B | 3.39 | 0.70 | 10.48 | 4.83 | 0.010 | 48000 |
| 51 | Helena (1935) | 304138hc_EW | VAN26A | 1.89 | 0.52 | 7.49 | 4.95 | 0.020 | 2551 |
| 52 | Helena (1935) | 304138hc_NS | VAN26B | 11.19 | 0.52 | 7.49 | 4.95 | 0.020 | 2551 |

Note: All of the records were measured on sites similar to class C site of NBCC 2005.

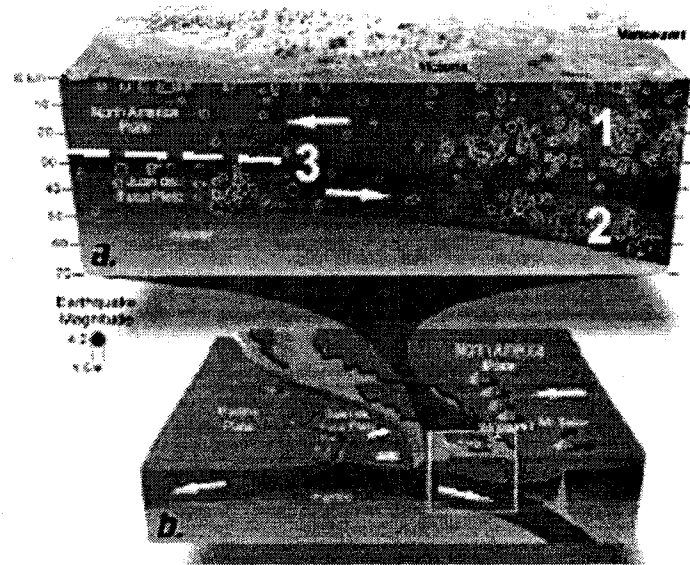


Figure 2.1: Cascadia Subduction Zone. (a) 1: Crustal Earthquakes on North America plate; 2: Subcrustal Earthquakes on Juan de Fuca plate; 3: Subduction earthquakes.
 (b) General view (reproduced from Onur, Cassidy and Rogers 2005)

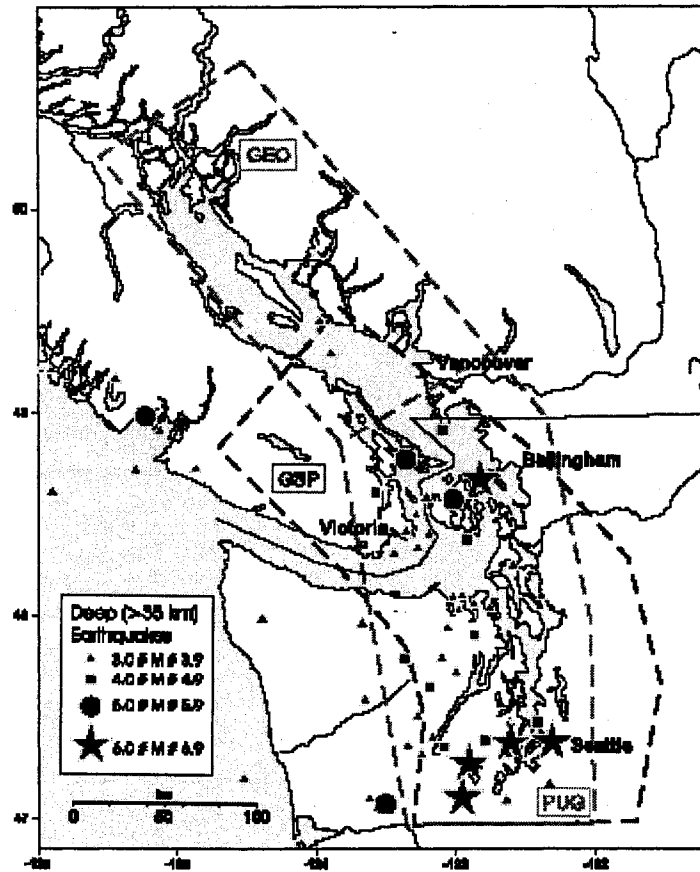


Figure 2.2: Deep earthquake (subcrustal) sources for Western British Columbia and Western Washington State. GEO: Georgia Strait, GSP: Georgia Strait/Puget Sound, PUG: Puget Sound (reproduced from Adams and Halchuk 2000)

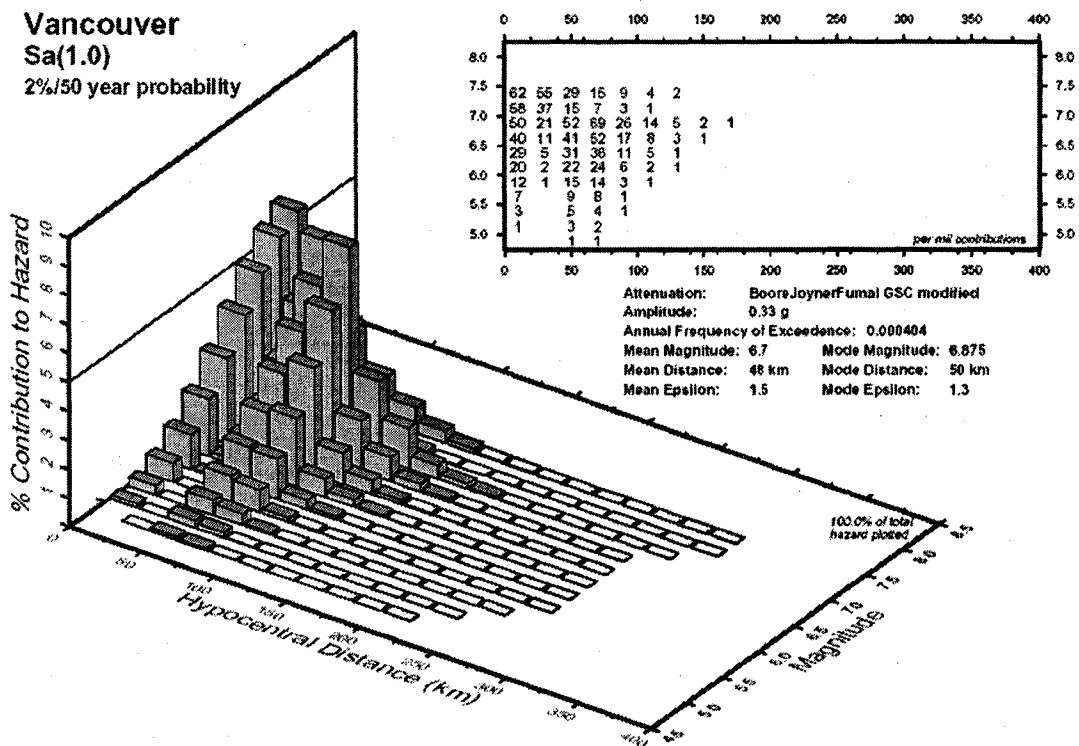


Figure 2.3: Deaggregation results for the seismicity of Vancouver city for 2% probability of exceedance in 50 years at Sa(1.0s) (reproduced from Halchuk and Adams 2004)

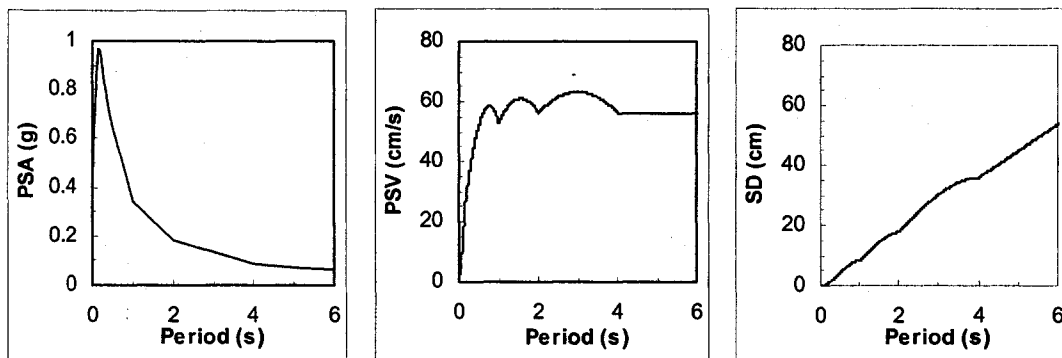


Figure 2.4: UHS for Vancouver city on site class C and 5% damping ratio(NBCC 2005)

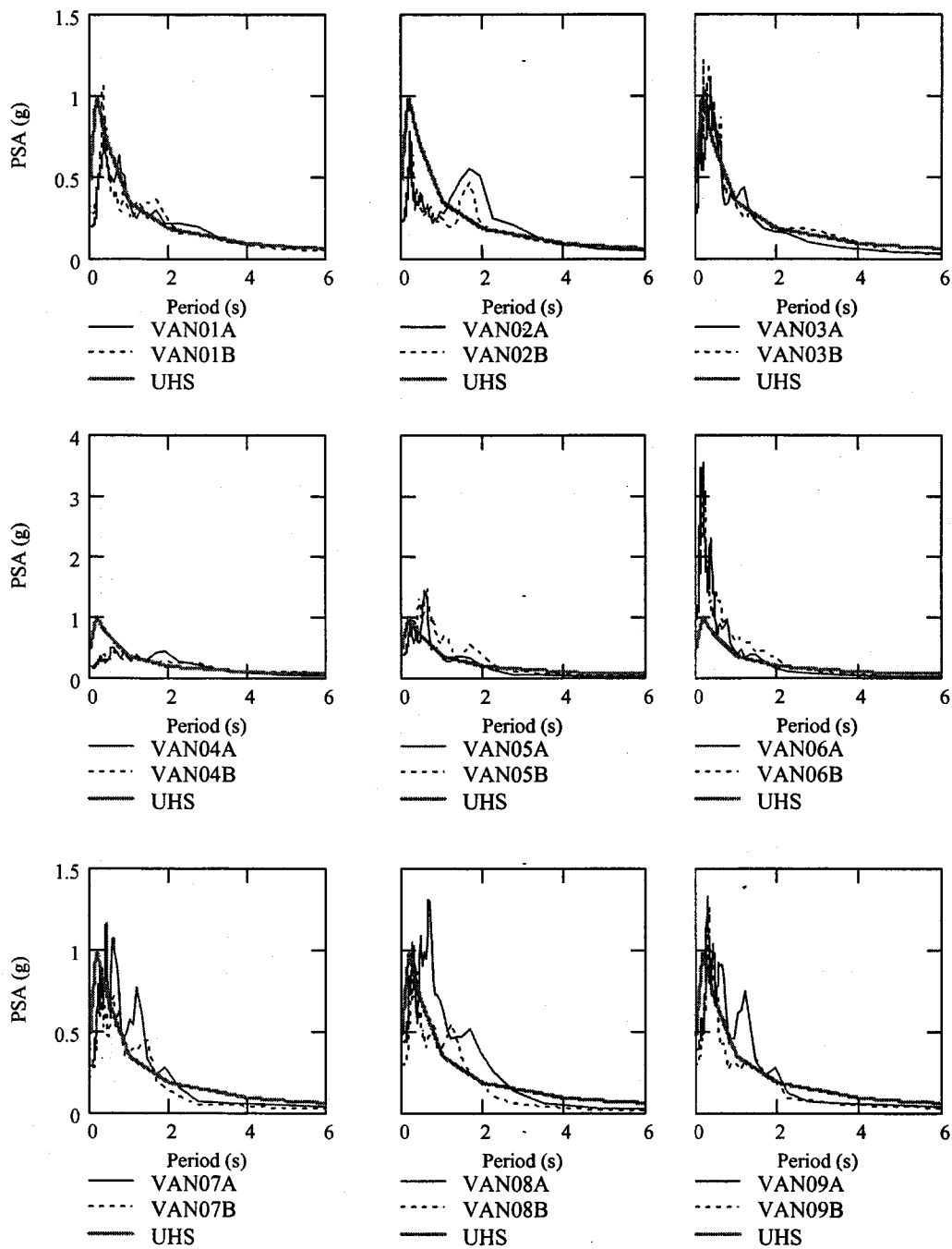


Figure 2.5: Pseudo-acceleration response spectra of selected ground motions for Vancouver (Part 1)

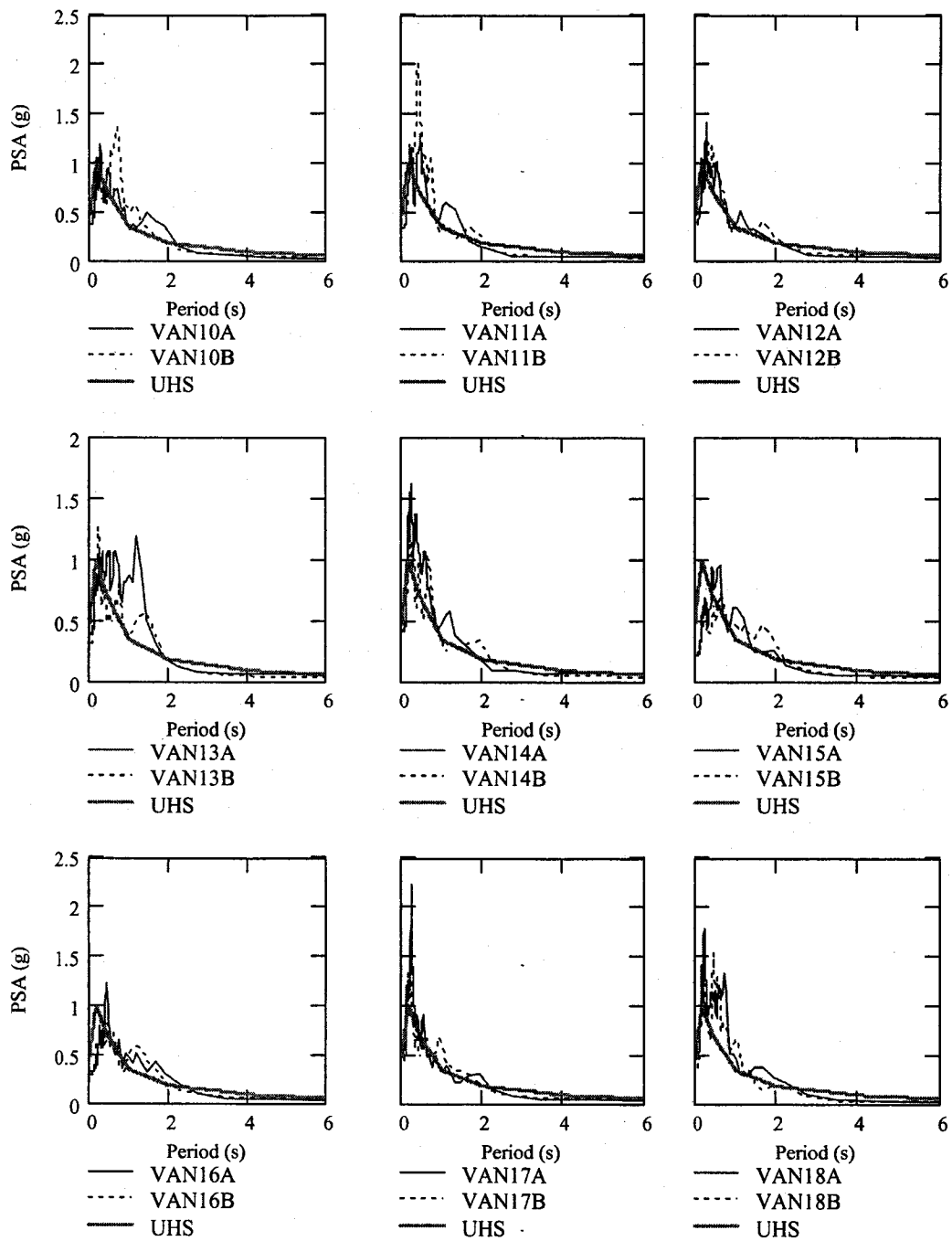


Figure 2.6: Pseudo-acceleration response spectra of selected ground motions for Vancouver (Part 2)

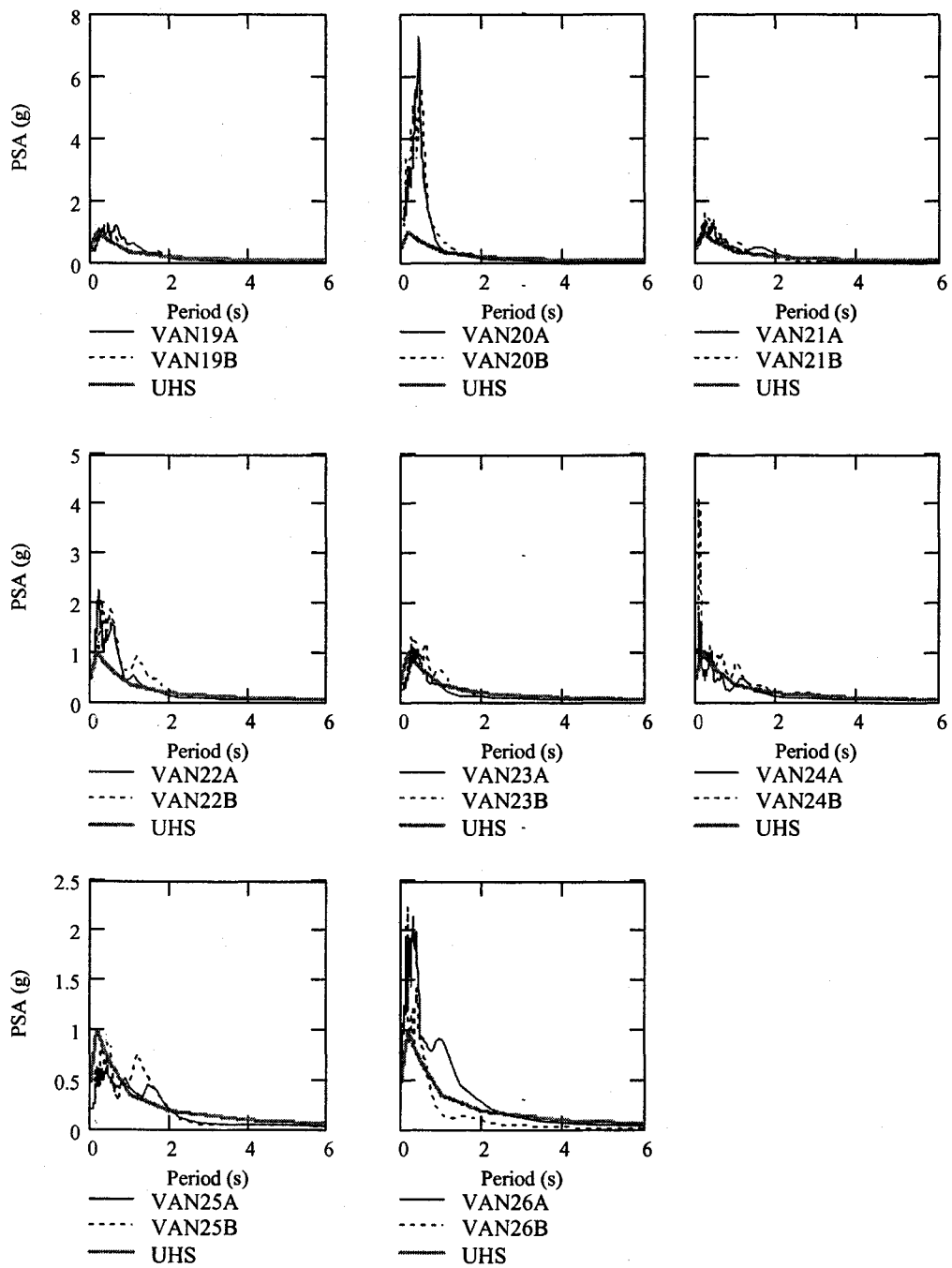


Figure 2.7: Pseudo-acceleration response spectra of selected ground motions for Vancouver (Part 3)

Chapter 3

Displacement-based Seismic Design

3.1. Introduction

Three different methods have been used for seismic design of structures: (a) force-based design, (b) displacement-based design, (c) energy-based design. Among these, the force-based seismic design is the most commonly used and the most developed method. However, there is a growing recognition that the performance of a structure under seismic loads needs to be measured by the level of damage, which is better defined by displacements rather than by forces. The displacement-based design therefore presents a better approach for performance-based seismic design. However, this method of design is still not widely accepted and is presented in only a few design codes. Current research effort has been focused on improving or testing the displacement-based design methods for different type of structures and different level of seismic demand.

In this chapter, a displacement-based method of seismic design (DBSD) is presented with specific reference to cantilever shear wall buildings with a symmetric plan. This method can be applied to achieve any desired level of performance. Two performance levels will be considered in this study. However, the design procedure will only be focused on the near collapse level and the operational level will just be included as an evaluation of the

final design. For near collapse level, the corresponding design earthquake is defined by the NBCC (2005) as having a 2 % probability of exceedance in 50 years (herein referred to 2%/50 year probability). In evaluation of operational level, a different earthquake design level (frequent earthquake) must be used with a shorter return period than the spectrum defined by the NBCC 2005. In order to show the applicability of the operational level, a design spectrum corresponding to a 50 % probability of exceedance in 50 years, which is equivalent to a return period of 72 years, is assumed.

The material presented in this chapter follows the same sequence as the steps involved in a real design. The last section provides a summary of the entire procedure. Also included is some additional information that would be useful in a preliminary selection of the amount of reinforcement and a brief description of the P- Δ effect in inelastic systems.

3.2. Conceptual basis and implementation of DBSD

The DBSD is based on a capacity spectrum method (Freeman *et al.* 1975) which consists of obtaining a performance point at the intersection of the capacity curve and the inelastic demand spectrum, plotted in the acceleration-displacement format (Figure 3.1). The capacity curve represents the relationship between applied force and displacement. As will be shown later, for a multi-degree-of-freedom (MDOF) structure a pushover analyses of the structure is carried out first. The relationship obtained between the base shear and roof displacement is then converted to the capacity diagram for a SDOF system.

In the practical application to the design of a structure a step-by-step procedure such as the one described by Humar and Ghorbanie (2004) may be used, and is adopted in this work.

In the proposed method approximate values of the target roof displacement Δ_u and roof yield displacement Δ_y are determined first according to the procedures outlined in the following sections. The required ductility capacity of the structure is then given by

$$\mu = \frac{\Delta_u}{\Delta_y} \quad (3.1)$$

However, if a lower value is recommended in the code it should be the one to be used in the design.

3.3. Yield displacement

As will be shown later, DBSD requires estimates of the yield and ultimate displacements. The yield displacement is defined as the roof displacement when the first yield occurs in the shear wall (Figure 3.2). For a cantilever shear wall, and assuming that the curvature varies linearly across the height the yield displacement, Δ_y and yield rotation, θ_y , at the roof level are given by

$$\Delta_y = \frac{\phi_y H^2}{3} \quad (3.2)$$

$$\theta_y = \frac{\phi_y H}{2} \quad (3.3)$$

where ϕ_y is the effective yield curvature and H the height of the wall. An approximate value of ϕ_y can be obtained from empirical relationship, for example, that given by Priestley (1998)

$$\phi_y \approx \frac{2.0\epsilon_y}{l_w} \quad (3.4)$$

where ϵ_y is the yield strain of reinforcing steel and l_w is the length of the wall in cross section.

3.4. Ultimate inter-storey drift and roof displacement

In a shear wall the maximum inter-storey drift is at the roof level and is approximately equal to the rotation at the roof level, θ_u , which is given by

$$\theta_u = \theta_y + \theta_p \quad (3.5)$$

where θ_y is given by Equation (3.3) and θ_p is the plastic rotation obtained from

$$\theta_p = (\phi_u - \phi_y)L_p \quad (3.6)$$

In Equation (3.6) ϕ_u is the ultimate curvature and L_p is the length of the plastic hinge.

The ultimate displacement corresponds to the roof displacement when the structure experiences a defined performance level (Figure 3.2). When this level goes beyond the yield displacement, a plastic deformation is developed in the structure. The addition of the two displacements gives the ultimate displacement, which takes its maximum value at the top of the structure (Kowalsky 2001). Thus, the maximum roof displacement Δ_u can be expressed as

$$\Delta_u = \Delta_y + \Delta_p \quad (3.7)$$

where Δ_p is the plastic displacement at the roof and is given by

$$\Delta_p = \theta_p (H - 0.5L_p) \quad (3.8)$$

In a near collapse level, the acceptable ultimate displacement would be governed by one of the following limits:

- Drift limits to achieve near-collapse performance goal;
- Local ductility capacity limit;
- Limit to preclude instability caused by P- Δ effect

It should be noted that the first limit is a consensus judgment that attempts to ensure that inelastic deformation will not be excessive, P- Δ instability would not be likely, and that non-structural damage that jeopardize life safety would be prevented (Federal Emergency

Management Agency 1998). However, in this study specific limits will be defined to ensure that member ductility capacities will not be exceeded and P-Δ instability will be prevented.

3.4.1. Drift limits to achieve near-collapse performance goal

Most codes and guidelines base this limit on the inter-storey drift ratio. The NBCC 2005 sets this ratio to 0.025 for a design earthquake with a probability of exceedance of 2 % in 50 years (2500 years return period). It is assumed that beyond this drift large non-structural damage will occur jeopardizing life safety, and major structural damage may also be caused. In this study we assume that the limit of 2.5% for a 2500 year earthquake as recommended by NBCC is an appropriate limit for near collapse performance objective (DeVall 2003). When this limit governs, Δ_u may be obtained by setting $\Theta_u = 0.025$ in the Equation (3.5) and substituting the result in Equations (3.6), (3.7) and (3.8), which gives

$$\Delta_u = \frac{\phi_y H^2}{3} + (H - 0.5 \cdot L_p) \cdot \left(0.025 - \frac{\phi_y \cdot H}{2} \right) \quad (3.9)$$

3.4.2. Local ductility capacity limit

The definition of the local ductility capacity limit depends on the inelastic behavior of the shear wall in the most critical cross section. This section is usually located at the base of the wall. The inelastic behavior is governed by the geometry of the section and characteristics of the materials. Two limits can be defined for the concrete compression

strain: 0.015 for confined concrete and 0.004 for unconfined concrete. Humar and Ghorbanie (2005) have shown that drift ratios obtained from the confined concrete cases do not control the design since these values are always larger than the code-specified drift limit (0.025). On the other hand, it is often difficult and expensive to provide confinement to the longitudinal steel in a shear wall. The local ductility capacity may therefore be related to the maximum acceptable concrete compression strain of 0.004.

Moment curvature analyses using strain compatibility indicate that the depth of neutral axis varies between $0.2l_w$ and $0.3l_w$ for several cross sections and steel distributions. Substituting these two lengths, a plastic hinge length of $0.5l_w$, and different material properties in Equations (3.3) through (3.6) limits on the drift ratios are obtained. The results are plotted in Figure 3.3. It will be observed from the figure that for aspect ratios less than 8 and 10 (for $f_y = 500$ MPa and 400 MPa, respectively) the drift ratio limit of 0.025 does not control the design and the local ductility capacity governs.

3.4.3. Limit to preclude instability caused by P- Δ effect

The P- Δ effect is a function of the axial load and the height of the wall. It decreases the stiffness of the structure and modifies its elastic and inelastic response. If the structure is idealized by an elasto-plastic force displacement relationship this effect will cause the stiffness to become negative as soon as yield takes place. This negative stiffness may cause instability in the structure and, theoretically, the structure should not be stressed beyond yield to prevent any chance of P- Δ instability. In other words, the structure should

be designed to remain elastic. Nevertheless, it is observed that the structure usually remains stable as long as the excursion into the zone of instability is not excessive. At the beginning of design the structure would normally be designed by using one of the first two limits. At the end of the design process, the excursion into the zone of instability can be evaluated, by taking the ratio of the base shear at maximum displacement to that at yield.

3.5. Equivalent SDOF system

In order to apply the DBSD method to a MDOF system the latter should first be represented by an equivalent SDOF system (Chopra and Goel 2002). This requires the selection of a displaced shape for the structure. Any logical shape including an inverted triangular shape, or a shape similar to the first mode shape could be selected. Assuming that the selected shape is represented by the vector ϕ , the following parameters are calculated:

$$\Gamma = \frac{(\phi^T \mathbf{M} \mathbf{1})}{(\phi^T \mathbf{M} \phi)} \quad (3.10)$$

$$M^* = \frac{(\phi^T \mathbf{M} \mathbf{1})^2}{(\phi^T \mathbf{M} \phi)} \quad (3.11)$$

where \mathbf{M} is the mass matrix, $\mathbf{1}$ is the unit vector, Γ is the modal participation factor, and M^* is the effective modal mass. The yield and target displacement for the equivalent SDOF system are given by

$$\delta_y = \frac{\Delta_y}{\Gamma\phi^r} \quad (3.12)$$

$$\delta_u = \frac{\Delta_u}{\Gamma\phi^r} \quad (3.13)$$

where ϕ^r is the value of ϕ at the roof.

3.6. Inelastic demand spectrum

The demand is defined by the UHS of Vancouver city (NBCC 2005) which corresponds to 2 % probability of exceedance in 50 years and 5 % of damping ratio. The values are given in acceleration-period format at specified vibration periods, linear interpolation being used for intermediate values of the period. The UHS must first be converted to the acceleration-displacement (A-D) format in order to plot it on the same graph as the capacity diagram referred to earlier (Figure 3.1 c, d).

The UHS represents elastic response of a SDOF system. When the structure develops inelastic deformations the demand curve may be modified according to the R_y - μ - T_n relationship (Figure 3.1e). Chopra and Goel (1999) have studied three different such relationships with very similar results. Among the three, the equation proposed by Krawinkler and Nassar (1992) represents an average. This equation is based on the response of bilinear systems and is given by

$$R_y = [c(\mu - 1) + 1]^{1/c} \quad (3.14)$$

where

$$c = \frac{T_n^a}{1 + T_n^a} + \frac{b}{T_n} \quad (3.15)$$

and parameters a and b depend on post-yield stiffness. For an elasto-plastic system $a = 1$ and $b = 0.42$.

Finally, the displacement of the inelastic system is defined as follows:

$$D = \frac{\mu}{R_y} \left(\frac{T_n}{2\pi} \right)^2 A \quad (3.16)$$

where A is the elastic spectral acceleration at the period T_n . The inelastic spectrum (Figure 3.1 e) can thus be defined for a constant ductility factor (Equation (3.1)) with displacements obtained from Equation (3.16) and accelerations given by A/R_y .

For preliminary design, the period and elastic spectral acceleration may be obtained from the elastic UHS by entering it with the previously described ultimate displacement. Using this period and ductility capacity, the reduction factor R_y can be determined from Equation (3.14). Finally, the inelastic acceleration can be obtained by dividing the elastic acceleration by the reduction factor.

3.7. P-delta effect in inelastic systems

As stated earlier, the stiffness becomes negative after yielding due to the P- Δ effect. On the other hand, we are using a $R_y-\mu-T_n$ equation based on an elasto-plastic model. These two statements clearly contradict each other. Therefore, a brief evaluation of the response of an inelastic system is carried out including the P- Δ effect.

The inelastic response of an SDOF system idealized as an elasto-plastic model (Model 1) is compared with the inelastic response of an SDOF system idealized as a model that includes the P- Δ effect in the inelastic part (Model 2). Both models are assumed to have the same elastic behaviour. Model 2, however, includes a negative slope in the inelastic zone. In the post yield region of the force displacement relationship a constant negative slope of 0.1 times the initial elastic slope is assumed, representing the P- Δ effect caused by the dead load and the contributing live load.

The elasto-plastic model used in the analysis is based on the Wen's hysteretic model included as one of the non-linear models within the software SAP2000 nonlinear. This model is explained by Wilson (1998) and consist of a bilinear model with independent internal deformation for each DOF. This model allows the specification of a negative slope in the inelastic zone and assumes that the unloading curve has the same slope as the elastic loading curve. For a partial verification of the method of analysis, Wen's model with zero post yield stiffness was used to analyze the response of an elasto-plastic system

to El Centro 1940 ground motion; the results obtained were identical to these obtained by Chopra (2004b) for a similar problem.

Constant ductility spectra are obtained by following the procedure described by Chopra (2004). A ductility of 2 is selected for this study for a system with 5 % of damping ratio and the ground motion is selected as the El Centro 1940 ground motion. Figures 3.4, 3.5, and 3.6 show the displacement, pseudo-velocity and pseudo-acceleration responses, respectively.

Differences between two models are small for periods shorter than 5 seconds. After a period of 6 seconds, the structure fails by instability problems due to the P- Δ effect. Considering that most of the structures (regular buildings) studied have periods between 0.5 and 5 seconds with inelastic performance restricted to the first mode, an elasto-plastic model can be used to obtain the demand spectrum even when P- Δ effect is present. A detailed study for frame structures presented by Mahgoub (2004) shows that the P- Δ effect on structure is very sensitive to the nature of earthquakes and the strength of the structure. It was recommended that the ductility demand on the structure be limited in order to avoid instability problems. However, the study only focused on structures that experienced ductilities that were significantly larger than those expected for the shear wall structures studied here. Nevertheless, it may be noted that the conclusion on this section is valid provided P- Δ effect does not lead to instability. Therefore, a more refined study may be needed in order to evaluate the P- Δ effect of shear wall buildings with different ductility factors and subjected to different earthquakes.

3.8. Preliminary design

For a preliminary design of the structure the spectral acceleration A_y on the inelastic spectrum corresponding to the ultimate displacement δ_u is determined. The initial capacity curve, in fact, is obtained by drawing a horizontal line from point (δ_u, A_y) on the inelastic spectrum to displacement δ_y and then connecting the end of the line to the origin. The process is presented in Figure 3.7. The design base shear for the structure is then given by

$$V = A_y M^* \quad (3.17)$$

The base shear is distributed across the height of the structure in proportion to the element of the vector $M\phi$, where ϕ is the assumed displacement shape vector.

An elastic analysis of the structure is now carried out for the storey level forces, determined as above, to obtain the design moments and shears. Such an analysis may require estimated values of the member cross-section properties. The member size and reinforcement are next determined. The procedure used in this work is based on the edition 1994 of the Canadian Standards Association (CSA) standard A23.3-94 (CSA 1994), herein referred to as CSA A23.3-94, and is described briefly in the following sections along with some recommendations from Paulay and Priestley (1992) that are used in the design.

3.8.1. Stability of wall section

One basic design requirement is to define the cross section properties of the shear wall. The section must be chosen such that the full capacity of the wall can be utilized. In other words, the selected section should need an amount of vertical reinforcement larger than the minimum requirements. Another condition in the selection of cross section is to ensure its stability under vertical loads. According to Paulay and Priestley (1992), the cross section thickness in the plastic region must be larger than the critical wall thickness, b_c , which can be estimated by the empirical formula:

$$b_c = 0.017l_w \sqrt{\mu_\phi} \quad (3.18)$$

where μ_ϕ is the curvature ductility. This formula is valid only when two layers of reinforcement are placed on both sides of the wall, which is the most common case for shear walls. Equation (3.18) implies that the potential buckling of the section depends also on the magnitude of the inelastic deformation, which is mainly defined by the inelastic tensile strains experienced by the vertical reinforcement. Instability may occur during a subsequent moment reversal when the strain change from tensile to compressive.

The CSA A23.3-94 recommends a minimum thickness of a tenth of the free height to prevent buckling failure in the wall. This limit gives a conservative approach in most cases when compared to the limit proposed by Paulay and Priestley (1992). The authors have suggested that the limit of one tenth of the free height is based on the traditional concept of Eulerian buckling of struts and on engineering judgment rather than on

experimental results. It must be noticed that by on substituting the limit proposed by the code in Equation (3.18) the curvature ductility works out to 34.6, which is impractical to achieve in shear walls.

3.8.2. Base design forces and moment

There are two base forces and a moment to consider in the design. The axial load is directly obtained from the gravity loads acting on the structure and will later be included in the moment-curvature analysis. For preliminary design, the base shear is obtained from Equation (3.17). However in subsequent iterations the first mode pushover analysis is used to provide the base shear. The base shear is expected to have important contributions from higher modes and the first mode base shear will be used only to define the base design moment.

3.8.3. Vertical concentrated reinforcement

The concentrated reinforcement is obtained by assuming a rectangular stress distribution as given by the CSA A23.3-94 and also that both compressive and tensile concentrated reinforcements yield. Based on these assumptions, equilibrium of internal forces, and strain compatibility, the reinforcement can be determined from the following procedure:

- Define the compression zone length, c

$$c = \frac{P + A_d \phi_s f_y l_w}{\alpha_1 \phi_c f_c \beta_1 b_w + 2A_d \phi_s f_y} \quad (3.19)$$

where P is the axial load, A_d the area of the distributed reinforcement per unit length, f_y the steel yield strength, f_c the concrete strength, ϕ_s and ϕ_c are the performance factors for steel and concrete, respectively, $\alpha_1 = 0.85 - 0.0015f_c$, $\beta_1 = 0.97 - 0.0025f_c$, and b_w is the wall thickness.

- Determine the concrete resistant moment, M_c

$$M_c = \alpha_1 \phi_c f_c c^2 \beta_1 b_w (1 - 0.5\beta_1) \quad (3.20)$$

- Determine the resisting moment contributing by the distributed reinforcement, M_{Ad}

$$M_{Ad} = A_d \phi_s f_y c^2 \left[1 + \left(\frac{l_w}{c} - 1 \right)^2 - \frac{2}{3} \left(\frac{\epsilon_y}{\epsilon_{cu}} \right)^2 \right] \quad (3.21)$$

where ϵ_{cu} is the ultimate concrete strain.

- Determine the restoring moment derived from the axial load, M_p

$$M_p = P \cdot \left(\frac{l_w}{2} - c \right) \quad (3.22)$$

- Obtain the resisting moment offered by the concentrated reinforcement, M_{cr}

$$M_{cr} = M_e - M_c - M_{Ad} - M_p \quad (3.23)$$

where M_e is the external moment to be resisted.

- Determine the required concentrated reinforcement, A_{cr}

$$A_{cr} = \frac{M_{cr}}{\phi_s f_y (l_w - 2h_m)} \quad (3.24)$$

where h_m represents the distance between the edge of the wall and the middle point of the concentrated steel arrangement.

3.8.4. Moment curvature relationship

For a more refined analysis of the moment resisting capacity of the wall cross section and the effective moment of inertia, a moment curvature analysis needs to be carried out. Such an analysis requires that the geometric and material properties of the shear wall be defined. The material properties are defined by an idealized stress-strain curve for steel (Figure 3.8 a) and by Hognestad's model for concrete (Figure 3.8 b). The resulting moment-curvature relationship can be idealized as a bi-linear curve (Figure 3.8 c). The procedure has been explained in detail by Yavari (2001) and has been programmed by Humar (personal communication) using MATLAB software.

The principal results obtained from this analysis are the effective moment of inertia, and the yield and ultimate points (curvatures and moments). These results define the

parameters of the plastic hinge for carrying out the pushover analysis and also for refining the assumptions made in the preliminary design.

3.9. Pushover Analysis

After a preliminary design has been completed, subsequent iterations in design require a pushover analysis of the structure. The pushover analysis consists of a nonlinear static analysis of the structure. The structure must be modeled in order to define its distributed nonlinear properties. The most common models use frame elements with plastic hinges placed at both ends. The elastic component of the frame element represents the elastic properties of the wall while the plastic hinge represents the nonlinear properties as obtained from the moment curvature relationship.

The nonlinear static analysis requires that a predefined pattern of lateral forces be applied on the wall. It is usual to assume that the lateral forces are given by product of mass matrix, \mathbf{M} , and the first mode shape, ϕ_1 . This assumption implies that a modal analysis must first be carried out in order to obtain the modal response. The lateral forces needed in the pushover analysis are thus obtained from Equation (3.25).

$$\mathbf{s}_1^* = \mathbf{M}\phi_1 \quad (3.25)$$

The pushover curve shows the relationship between the roof displacement response and the base shear response (Figures 3.9 a, b). For cantilever shear walls, the resulting pushover curve is characterized by a bi-linear curve with a break at the yield point. The

yield point corresponds to the yield roof displacement and the yield base shear at the moment when the wall reaches its moment capacity.

3.10. Subsequent iterations in design

The preliminary design must be refined further based on more up-to-date information that is available. As stated earlier, a modal analysis of the preliminary design gives the characteristics of the first and several higher modes. A pushover curve obtained from the forces distributed according to first mode now provides the yield displacement. At the same time the moment curvature analysis on the wall section gives the yield curvature, ϕ_y and the ultimate curvature ϕ_u . Using these values and Equations (3.6), (3.7), and (3.8) we obtain the ultimate displacement. Another value of Δ_u is obtained from Equation (3.9), which corresponds to the drift limit of 0.025. The smaller of the two values governs the design.

The ductility requirement is now determined from Equation (3.1), and the inelastic demand spectrum corresponding to this value of ductility is determined. The MDOF system is converted to an equivalent SDOF system using the first mode and Equations (3.10) and (3.11). The yield and ultimate displacements of the SDOF are calculated from Equations (3.12) and (3.13). The interaction of the vertical from Δ_u and the inelastic demand spectrum gives the performance point (Figure 3.7).

The inelastic spectral acceleration corresponding to the performance point times the effective modal mass, M_i^* , gives a new base shear. The DBSD converges when this new base shear is similar or equal to the yield base shear obtained from the pushover curve. If the difference between these two base shears is substantial a new reinforcement arrangement must be defined and new moment-curvature, modal, and pushover analyses must be performed. In those cases where the required reinforcement is less than the minimum a smaller cross section may be selected.

3.11. Modal pushover analysis

Once the DBSD procedure shows convergence based on the first mode pushover analysis, the contribution from higher modes must be considered. The modal pushover analysis (MPA) for buildings with symmetric plans has been presented by Chopra and Goel (2002, 2004) and consists of combining the responses from pushover analyses based on the first few, say three, modal displacement shapes and assuming that they are uncoupled. Such an analysis to the i^{th} mode can be summarized as follows:

1. From the modal analysis performed earlier obtain the period, T_i , the vector of the i^{th} mode shape, ϕ_i , the modal participation factor, Γ_i , and the effective modal mass, M_i^* , where i varies from 2 to n .
2. Perform a nonlinear static analysis with a force distribution, s_i^* given by

$$\mathbf{s}_i^* = \mathbf{M}\boldsymbol{\phi}_i \quad (3.26)$$

where \mathbf{M} is the mass matrix.

From this analysis obtain the relationship between the base shear, V_b , and roof displacement, Δ (pushover curve), shown in Figure 3.10 for the first three modes.

3. Convert the pushover curve into the capacity diagram by using Equations (3.10), (3.11), and (3.12), and the following expression to determine both the yield displacement and the acceleration at yield.

$$A_y = \frac{V_b}{M^*} \quad (3.27)$$

4. Obtain the performance point which corresponds to the intersection between the capacity curve and the inelastic spectrum in A-D format. As different from the procedure presented for the first mode in previous sections, the convergence for higher modes must be found with inelastic displacements rather than accelerations and the iterative process must be started with tentative ductility factors rather than periods.
5. Compute the ultimate roof displacement by multiplying the yield displacement by the ductility factor obtained in Step 4.

6. From the pushover database, extract the responses corresponding to the pushover step for the ultimate displacement calculated in Step 5.
7. Repeat previous steps for as many modes as needed for sufficient accuracy in the total response. The number of modes required for shear wall type of buildings will be part of the objectives of this research.
8. Combine the responses from each MPA by using some combination rule. It is recommended that the square root of the sum of the squared (SRSS) responses be used as the combination rule.

As stated earlier, for shear walls the modal pushover analysis is required to account for the contribution of higher modes to the design shears. The wall section already selected should be reinforced with adequate reinforcement to provide a shear resistant that is greater than the shear demand. If this can not be achieved a larger wall section must be selected and the design repeated.

3.12. Multiple performance objectives

As outlined in Chapter 1, it is often required that the structure be designed to satisfy multiple performance objectives, each of which is associated with a given level of hazard. For example the structure designed to meet basic standard should satisfy near collapse condition for an earthquake with 2 % probability of exceedance in 50 years. At the same

time it should be operational under an earthquake that has 50 % probability of exceedance in 50 years.

The design procedure presented in this work focuses on design for earthquakes with probability of exceedance of 2 % in 50 years, because the UHS available in NBCC (2005) are for this probability. However, the design can be verified, and if necessary modified, to satisfy the performance at the other levels of hazard. This will be illustrated in this work by designing the structure to meet the performance required under an earthquake with 50 % probability of exceedance in 50 years. For this to be accomplished we need a quantitative measure of performance as well as the UHS for 50 % probability of exceedance in 50 years. Vision 2000 (SEAOC 1999) specifies that for the structure to remain operational the inter-storey drift should not exceed 0.5 %; we will use this performance criterion. A procedure for obtaining the 50 % in 50 year probability UHS is described in the following section.

3.12.1. Estimated UHS corresponding to 50%/50 year probability

A simple procedure for estimating the UHS for an earthquake with 50 % probability of exceedance in 50 years (72 years of return period) for the city of Vancouver, referred to $UHS_{50/50}$, is outlined in this section. The estimated $UHS_{50/50}$ is obtained by scaling down the UHS corresponding to 2 % probability of exceedance in 50 years (NBCC 2005), herein referred to $UHS_{2/50}$. It is proposed that the scaling factor be defined as the ratio of the spectral accelerations obtained from the $UHS_{2/50}$, $S_{a2/50}$, to the spectral acceleration

obtained from the $UHS_{50/50}$, $Sa_{50/50}$, at a certain period. A period of 2 s is chosen here as the representative vibration period of the structures studied in this thesis. For increased accuracy, the spectral values need to be modified by using a series of period dependent scale factor.

Two assumptions are involved in the calculation of the spectral acceleration at 2.0 s period, $Sa(2.0s)$. First, it is assumed that the maximum contribution to hazard for the $UHS_{50/50}$ is due to subcrustal earthquakes. This assumption is based on the high contribution to hazard observed from more frequent subcrustal earthquakes in deaggregation analysis (Adams and Halchuk 2003). For example, the highest contribution to hazard for the $Sa(2.0s)$ with 475 years of return period comes from earthquakes with magnitudes between 6.5 and 7.0 and for distances between 50 and 80 km (Figure 3.13). The second assumption consists of obtaining the spectral value from a single combination of magnitude and hypocentral distance. This is a very approximate procedure, but it retains the simplicity of calculations. However, there certainly is a need to carry out more elaborate, accurate and comprehensive studies for obtaining different UHS corresponding to different levels of earthquake hazard.

The following computations are based on the attenuation relationship presented by Atkinson and Boore (2003) for in-slab earthquakes in the Cascadia region. The magnitude-recurrence relation used here corresponds to the CASR case (Casadia mountain region) presented by Adams and Halchuk (2003).

The calculations for estimating the UHS_{50/50} can be summarized in the following steps:

1. From the deaggregation of hazard for 2%/50 year probability (Adams and Halchuk 2003) observe that the spectral acceleration at a period of 2.0 s, $Sa(2.0s)_{2/50}$, is 0.17 g (Figure 3.14).
2. The attenuation relationship for a site class C (NBCC 2005) and periods longer than 1 s is given by (Atkinson and Boore 2003):

$$\log(Sa) = c_1 + c_2M + c_3h + c_4R - gg \log R + c_5 \quad (3.28)$$

where M is the magnitude, h is the focal depth in kilometers, $gg = 10^{0.301-0.01M}$, and $R = \sqrt{D_f^2 + \Delta^2}$ in which D_f is the near distance to the fault, in kilometers, and Δ a near-saturation term, given by $\Delta = 0.0724 \times 10^{0.507M}$. The c_i factors are the regression factors, whose values for in-slabs events in the Cascadia region are defined as: $c_1 = -2.25$, $c_2 = 0.9964$, $c_3 = 0.00364$, $c_4 = -0.00118$, and $c_5 = 0.10$.

3. The magnitude for the UHS_{50/50}, $M_{50/50}$, is estimated from the magnitude-recurrence curves for CASR shown in Figure 3.15 (Adams and Halchuk 2003). For a recurrence of 0.014 (72 year return period) $M_{50/50} = 6.84$, approximately. Substitution of $M_{50/50}$ in Equation (3.28) gives:

$$\log(Sa) = -2.25 + 0.9964 \times 6.84 + 0.00364 \times h - 0.00118 \times R - gg \log R + 0.10$$

where h is set to 40 km and D_f to 65 km, which corresponds to a hypocentral

distance of 76.3 km. Other factors are obtained as follows:

$$\Delta = 0.00724 \times 10^{0.507 \times 6.84} = 21.263$$

$$R = \sqrt{65^2 + 21.263^2} = 68.39 \text{ km}$$

$$gg = 10^{0.301 - 0.01 \times 6.84} = 1.708$$

4. Substituting the foregoing values in Equation (3.28), the $Sa(2.0s)_{50/50}$ is obtained as 0.04 g. Thus, the scale factor to be applied to the $UHS_{2/50}$ is:

$$\frac{Sa(2.0s)_{50/50}}{Sa(2.0s)_{2/50}} = \frac{0.04g}{0.17g} = 0.325$$

3.13. Summary

The procedure presented here is intended to be used for two performance-level. The near collapse performance level corresponds to Steps 1 through 13. The last two steps, 14 and 15, are included in order to evaluate the operational performance level.

The new DBSD for the near collapse performance level can be separated in two groups: the preliminary design (Figure 3.11) and the iterative process (Figure 3.12). The preliminary design is performed in Steps 1 through 7, while the iterative process is carried out in Steps 8 through 11. It is assumed that at the beginning of design a reasonable geometric shape for the wall has been selected. The complete step-by-step DBSD is summarized as follows:

1. Obtain a preliminary estimate of the yield displacement, as described in Section 3.3.
2. Obtain a preliminary estimate of the ultimate displacement as described in Section 3.4, and calculate the ductility capacity.
3. Obtain the modal participation factor (Equation (3.10)) and the effective modal mass (Equations (3.11)) assuming an inverted triangle displacement shape.
4. Obtain yield and ultimate displacements of the equivalent SDOF system (Equations (3.12) and (3.13), respectively)
5. Using the ductility factor and displacements from Step 4, obtain inelastic demand spectrum and the performance point for the equivalent SDOF system (Figure 3.7).
6. Compute the design base shear as the product of the inelastic spectral acceleration obtained from Step 5 and the effective modal mass obtained from Step 3.
7. Obtain the base moment by distributing the base shear along the height according to the weight distribution and the assumed displacement shape.
8. Calculate the concentrated reinforcement and carry out a moment curvature analysis. From the moment-curvature relationship find the yield and ultimate curvature corresponding to the limiting concrete strain. Using these new

- curvatures, refine the values of plastic rotation (Equation (3.6)) and plastic roof displacement (Equation (3.8)).
9. Perform a modal analysis and obtain the first mode shape. Compute the modal participation factor (Equation (3.10)) and the effective modal mass (Equation (3.11)).
 10. Perform a pushover analysis using the first mode distribution of the lateral forces. From the pushover curve find the yield roof displacement, add the plastic roof displacement (Step 8), and obtain the ultimate roof displacement (Equation (3.7)). Compute the new ductility factor.
 11. Convert the yield and ultimate displacement of the MDOF system to those of the equivalent SDOF system using the first mode shape (Step 8) and Equations (3.12) and (3.13). Find the inelastic spectral acceleration corresponding to the calculated ultimate displacement (Figure 3.7) and determine the base shear using Equation (3.17).
 12. Compare the base shear obtained in Step 11 with that obtained from the pushover analysis. If the two are not close, modify the base moment according to this difference and repeat steps 8 through 12.
 13. Perform a MPA for the several higher modes and combine the modal base shear to obtain a more accurate estimate of the base shear.

14. Using the fundamental period of structure find the demand acceleration from the UHS corresponding to 50%/50 year probability and determine the base shear.
15. Distribute the base shear determined in Step 14 across the height and carry out an elastic analysis for the resulting story level forces. Verify that the inter-storey drift ratios is less than 0.5%. As an alternative, obtain the inter-storey drift ratio from the pushover data base at the corresponding value of the base shear. If the limits on drift ratio is not satisfied, revise the design appropriately by increasing the strength so that the stiffness also increases proportionally.

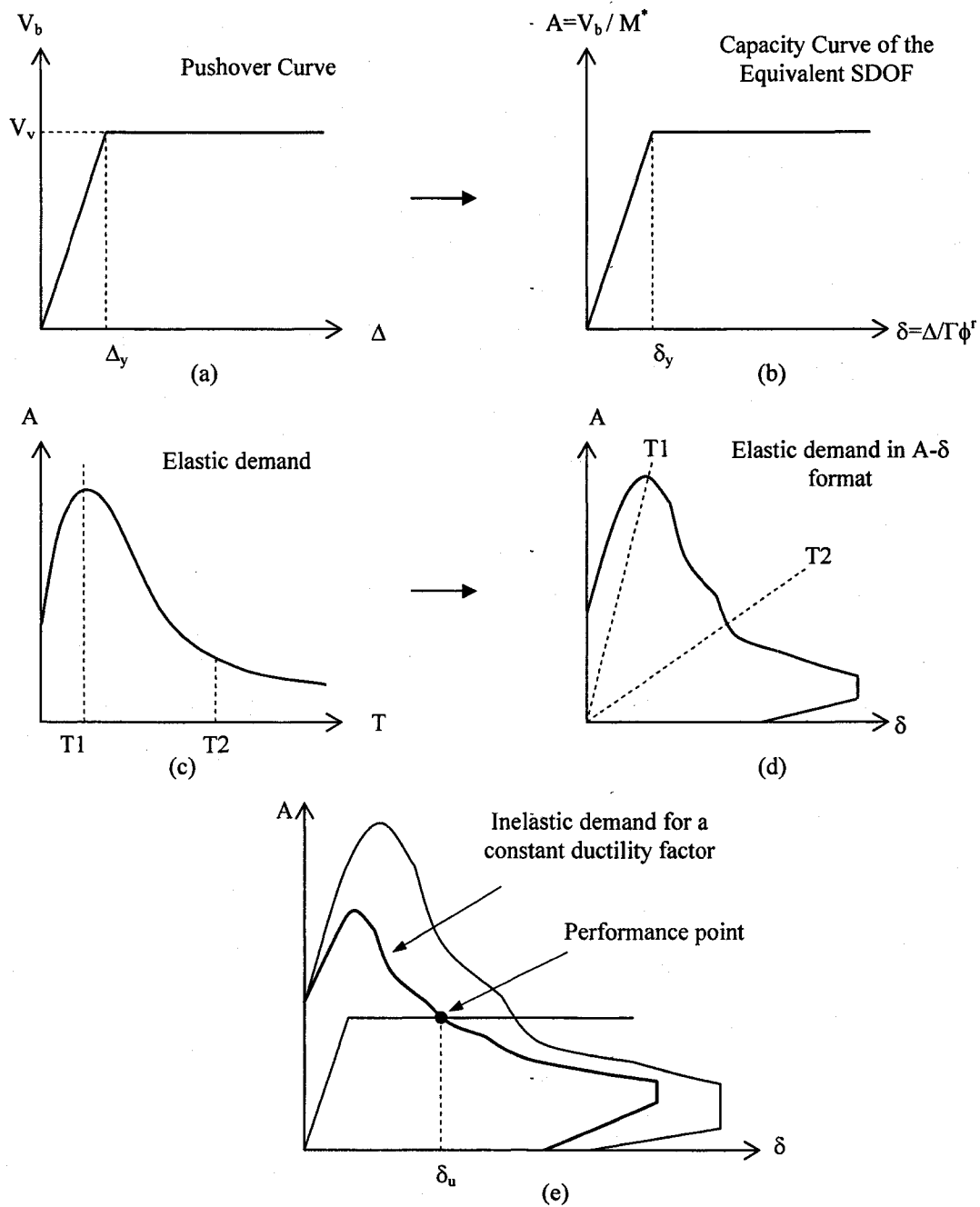


Figure 3.1: Summary of capacity-diagram method: (a) Pushover curve, (b) Capacity diagram of the equivalent SDOF system, (c) Elastic demand, (d) Elastic demand diagram, (e) Determination of performance point (adapted from Chopra and Goel 1999).

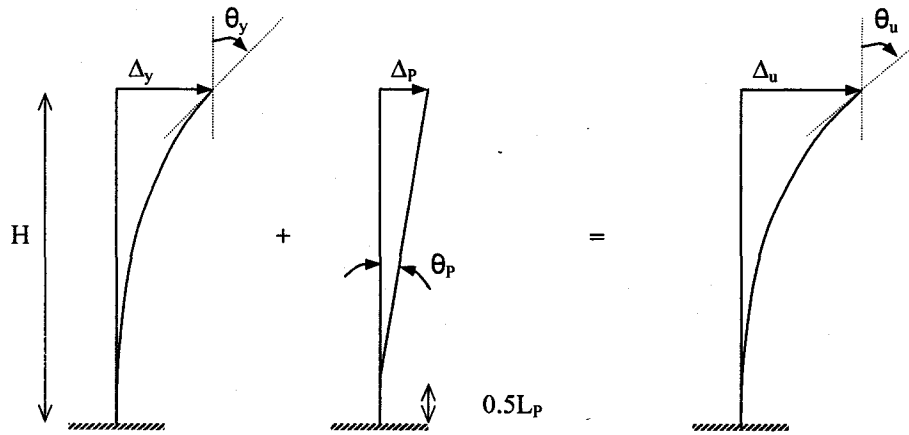


Figure 3.2: Models of cantilever shear wall showing yield, plastic and ultimate displacements and drifts

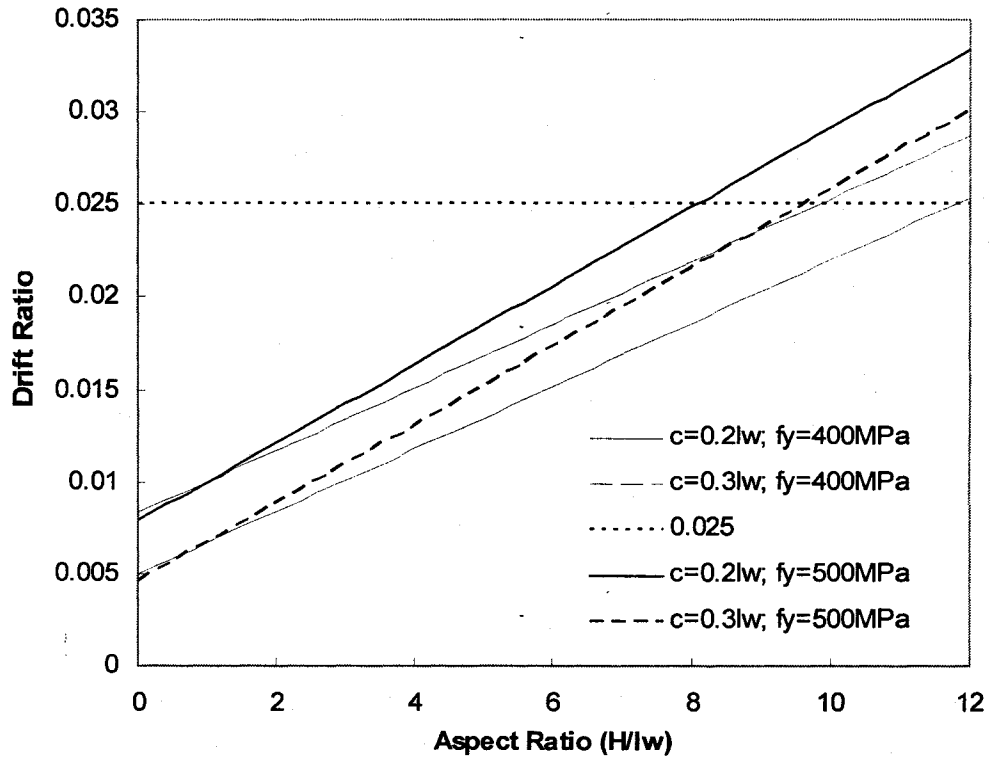


Figure 3.3:Ultimate drift ratios for shear walls

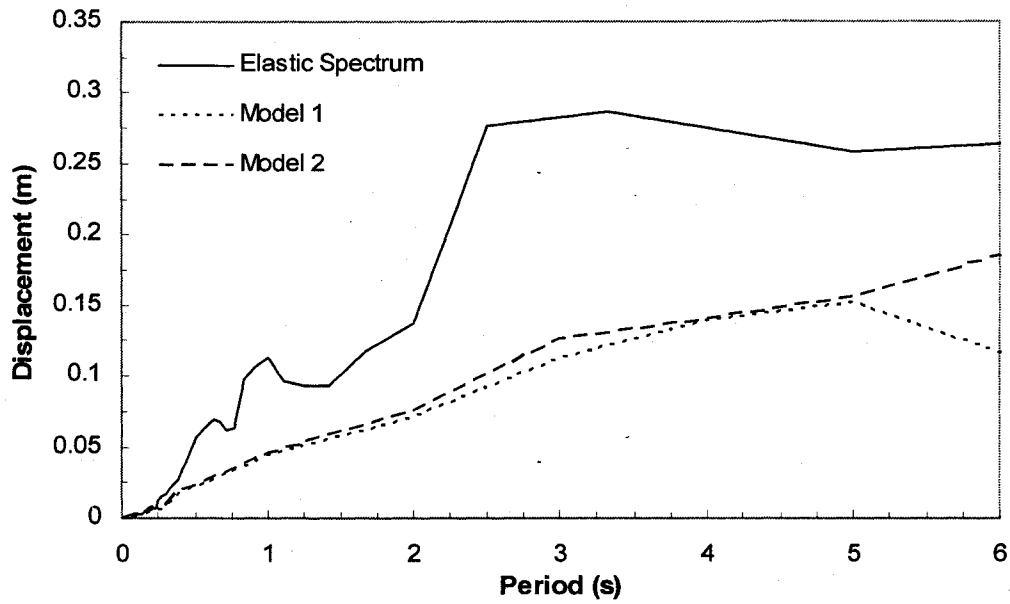


Figure 3.4: Constant-ductility ($\mu = 2$) displacement response spectrum for El Centro ground motion (1940) and 5 % damping, for Model 1 (Elasto-plastic) and Model 2 (Elasto-plastic plus P- Δ effect)

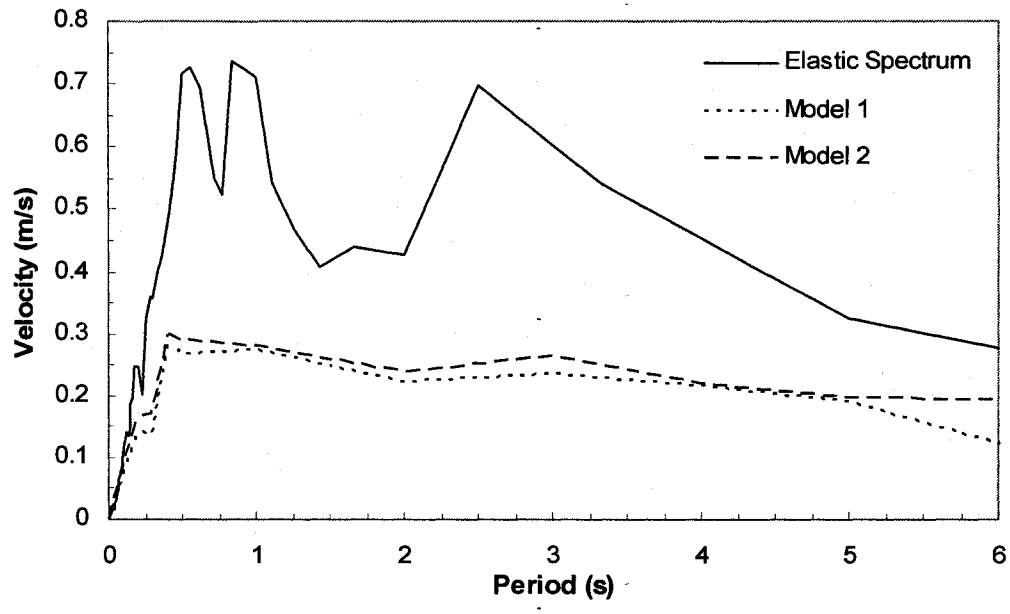


Figure 3.5: Constant-ductility ($\mu = 2$) velocity response spectrum for El Centro ground motion (1940) and 5 % damping, for Model 1 (Elasto-plastic) and Model 2 (Elasto-plastic plus P- Δ effect)

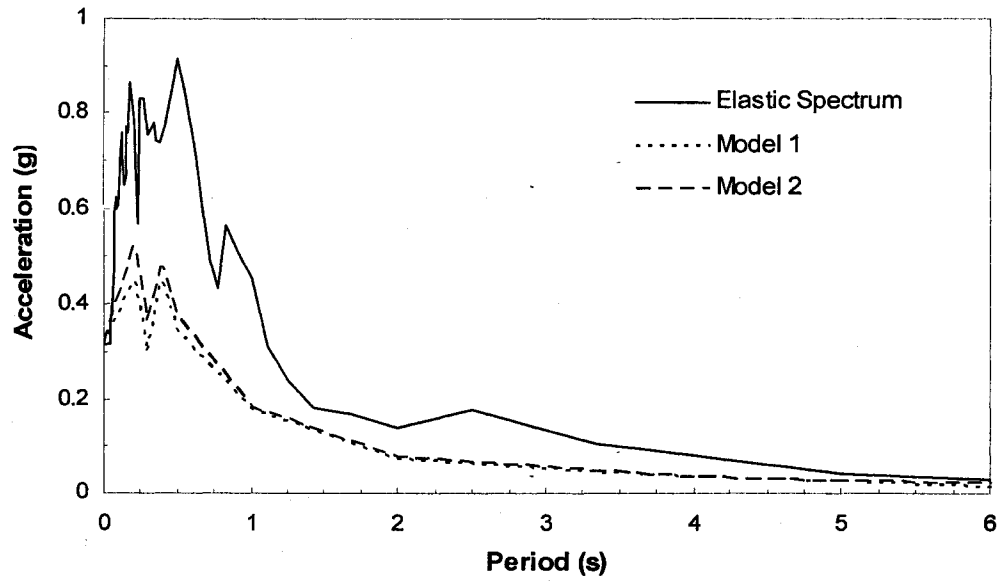


Figure 3.6: Constant-ductility ($\mu = 2$) acceleration response spectrum for El Centro ground motion (1940) and 5 % damping, for Model 1 (Elasto-plastic) and Model 2 (Elasto-plastic plus P- Δ effect)

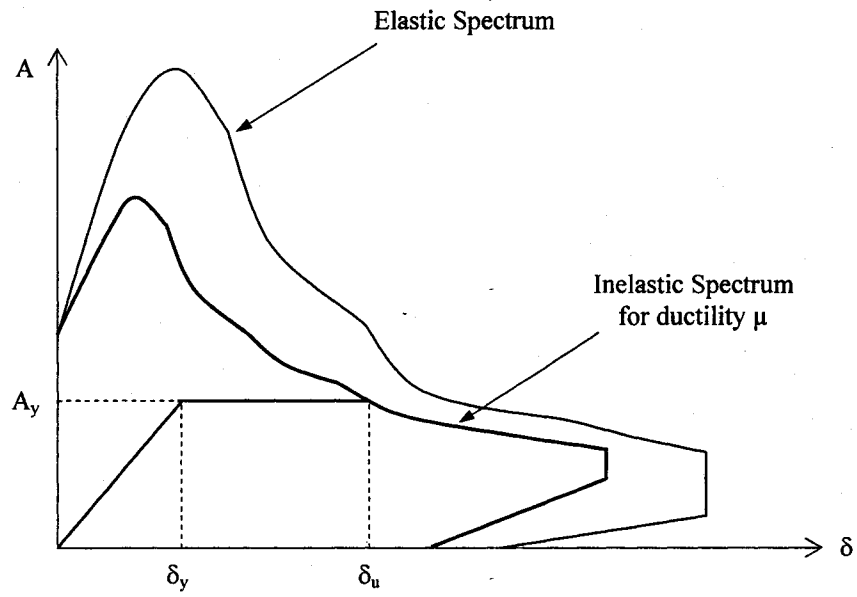


Figure 3.7: Demand and capacity diagram for the equivalent SDOF system.

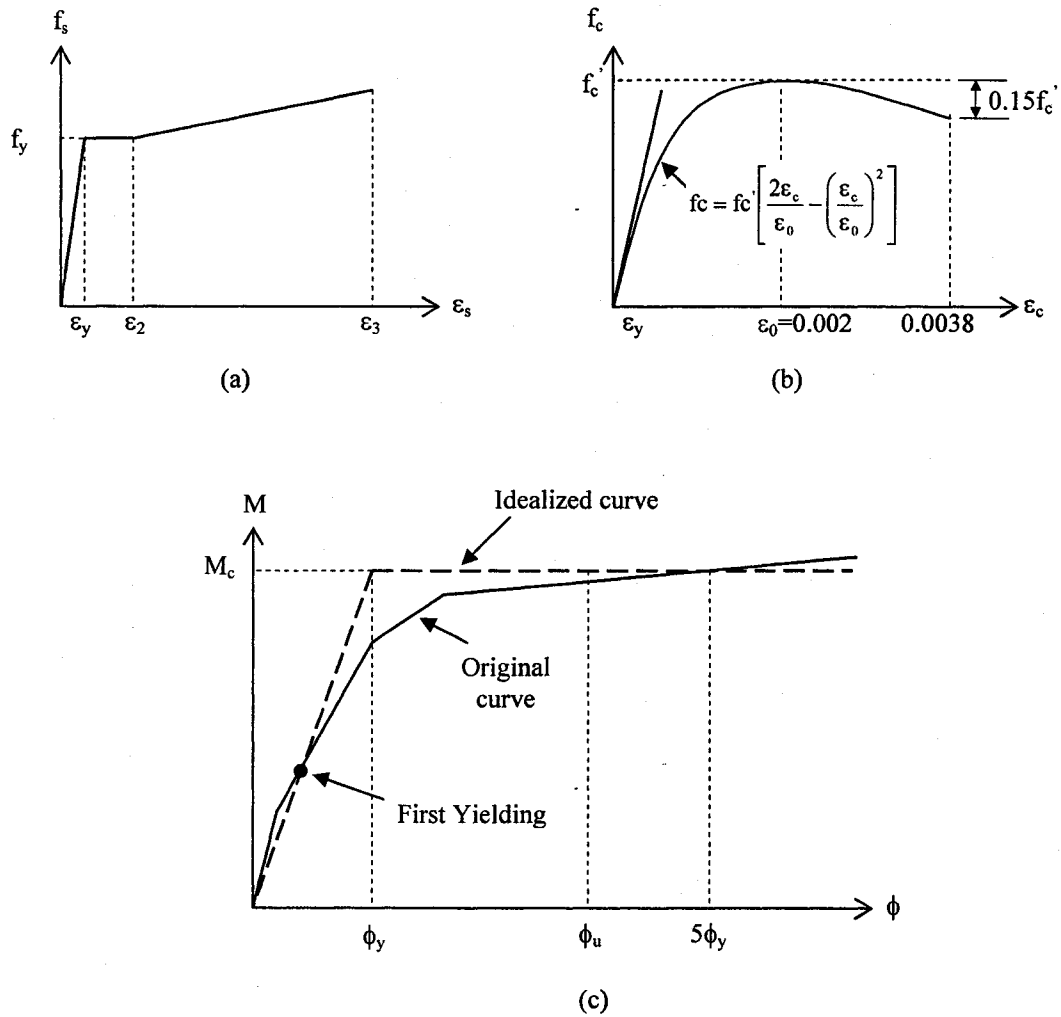


Figure 3.8: Moment-curvature analysis: (a) tri-linear stress-strain relationship for reinforcing steel, (b) Idealized stress-strain curve for concrete uniaxial compression, (c) moment-curvature relationship for a rectangular concrete wall (adapted from Yavari 2001)

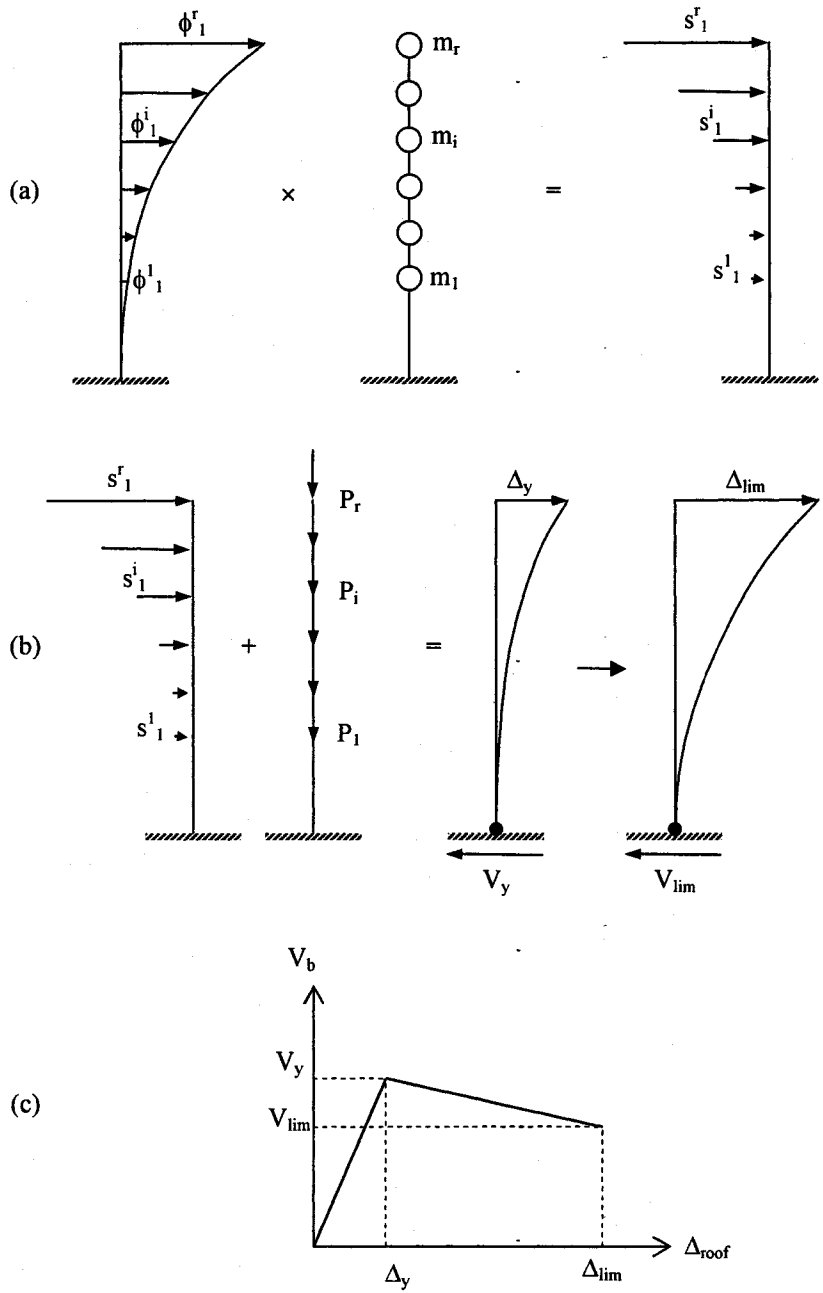


Figure 3.9: Pushover analysis using first mode: (a) determination of lateral loads, (b) static analysis displacement response, (c) pushover curve.

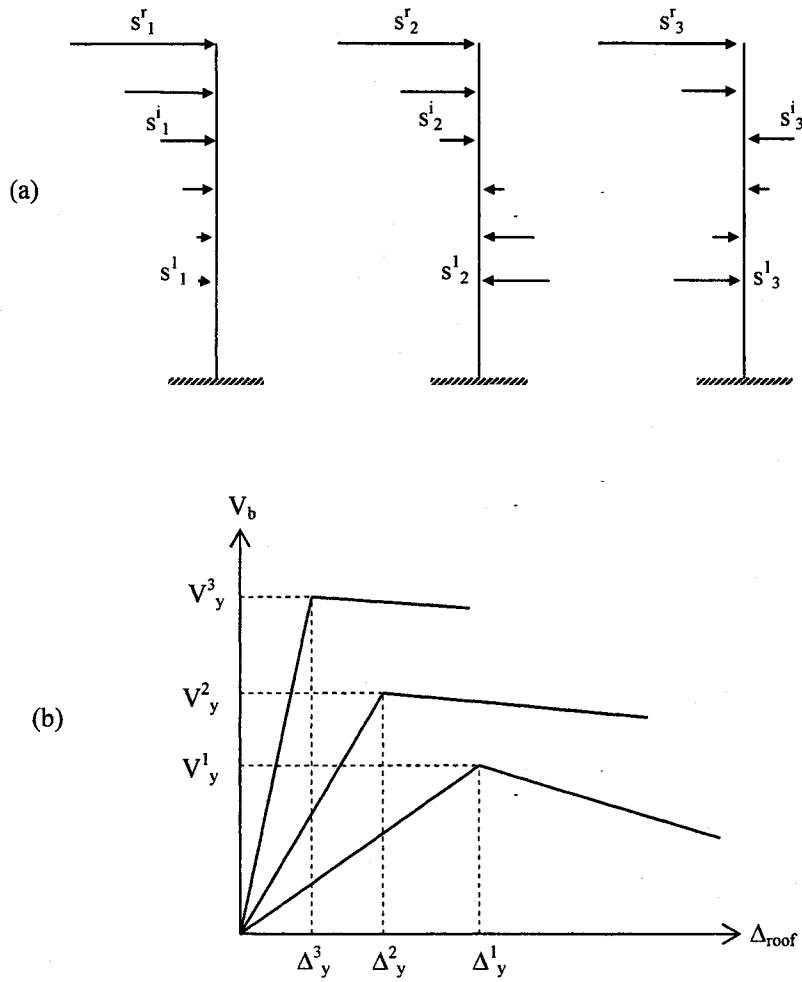


Figure 3.10: Modal pushover analysis for three first modes: (a) lateral forces, (b) pushover curves.

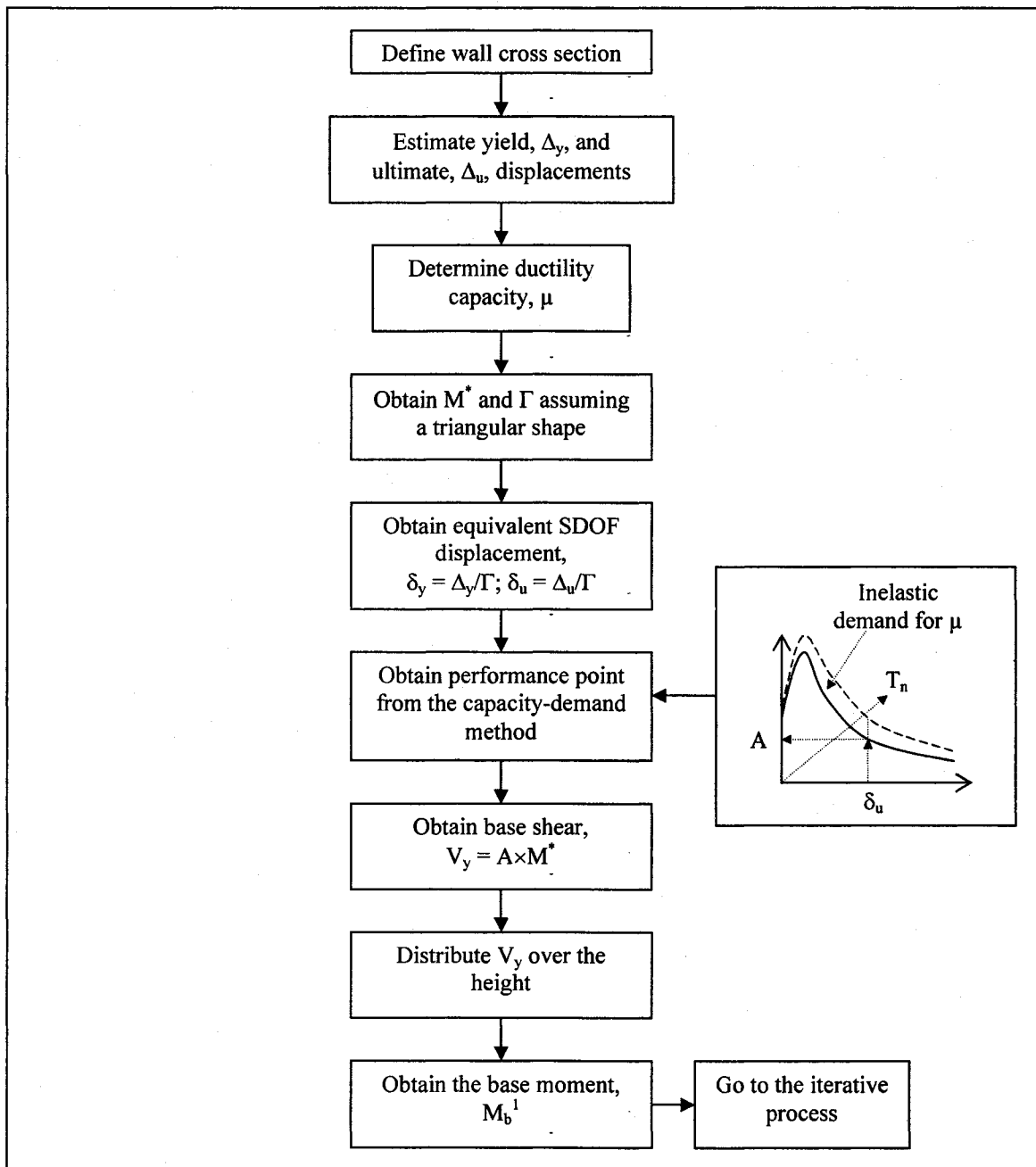


Figure 3.11: Flow chart for the preliminary part of the DBSD for shear wall buildings.

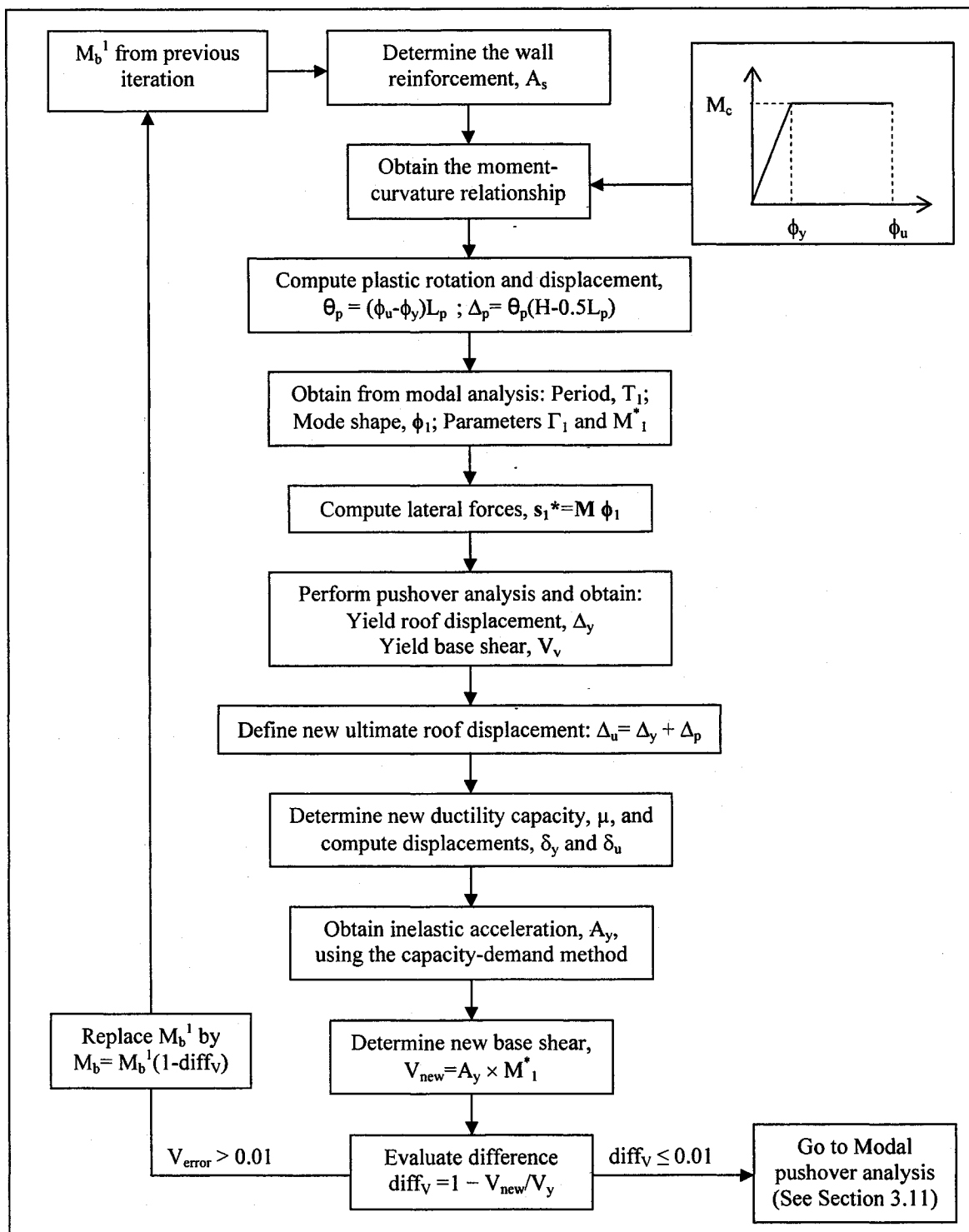


Figure 3.12: Iterative process of the DBSD for shear wall buildings.

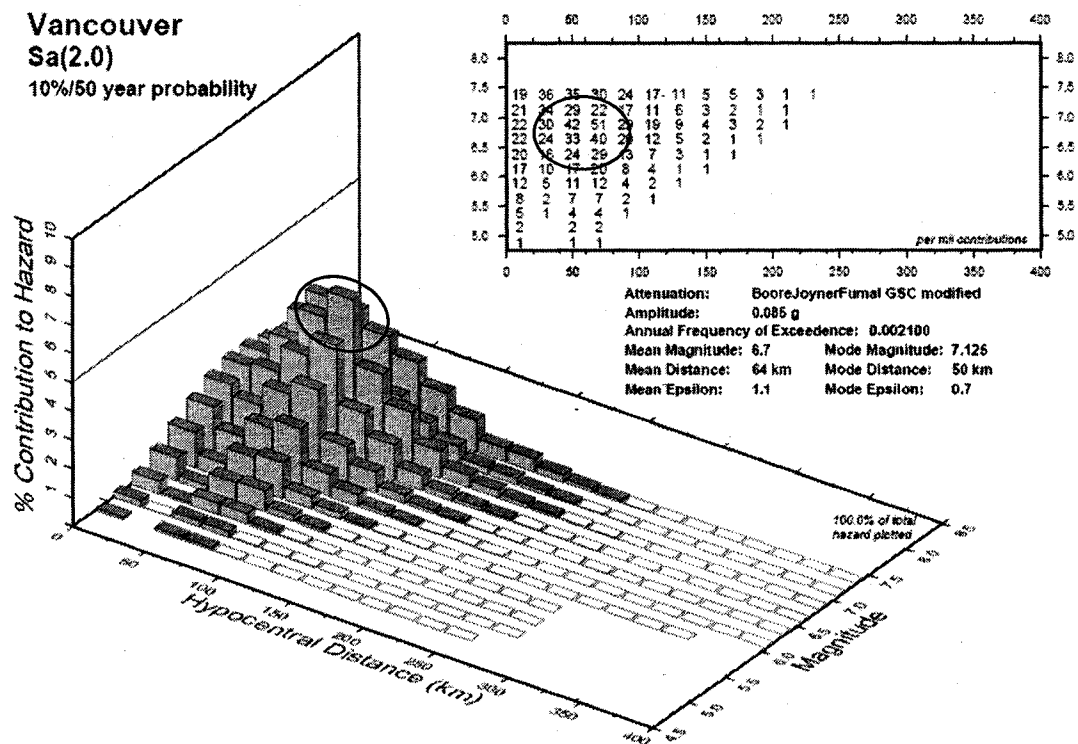


Figure 3.13: Deaggregation of hazard for the city of Vancouver with 10% probability of exceedance in 50 years (475 years of return period). The circles shows the maximum contribution to hazard (reproduced from Adams and Halchuk 2003)

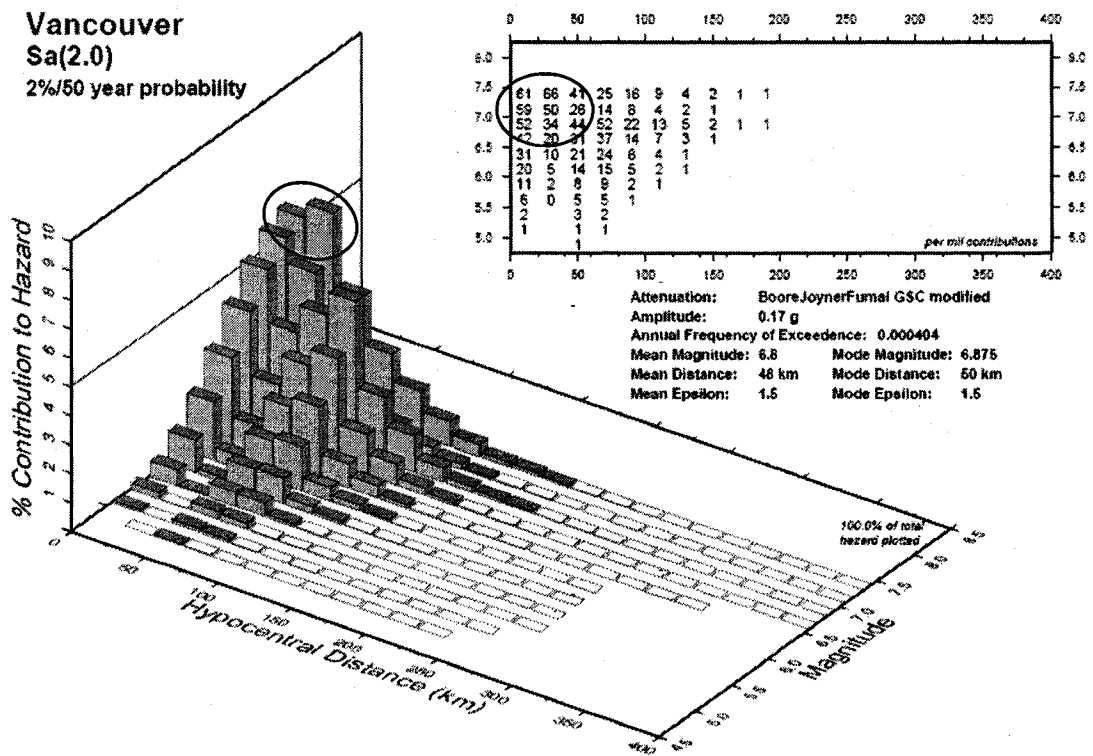


Figure 3.14: Deaggregation of hazard for the city of Vancouver with 2% probability of exceedance in 50 years (2500 years of return period). The circles shows the maximum contribution to hazard (reproduced from Adams and Halchuk 2003)

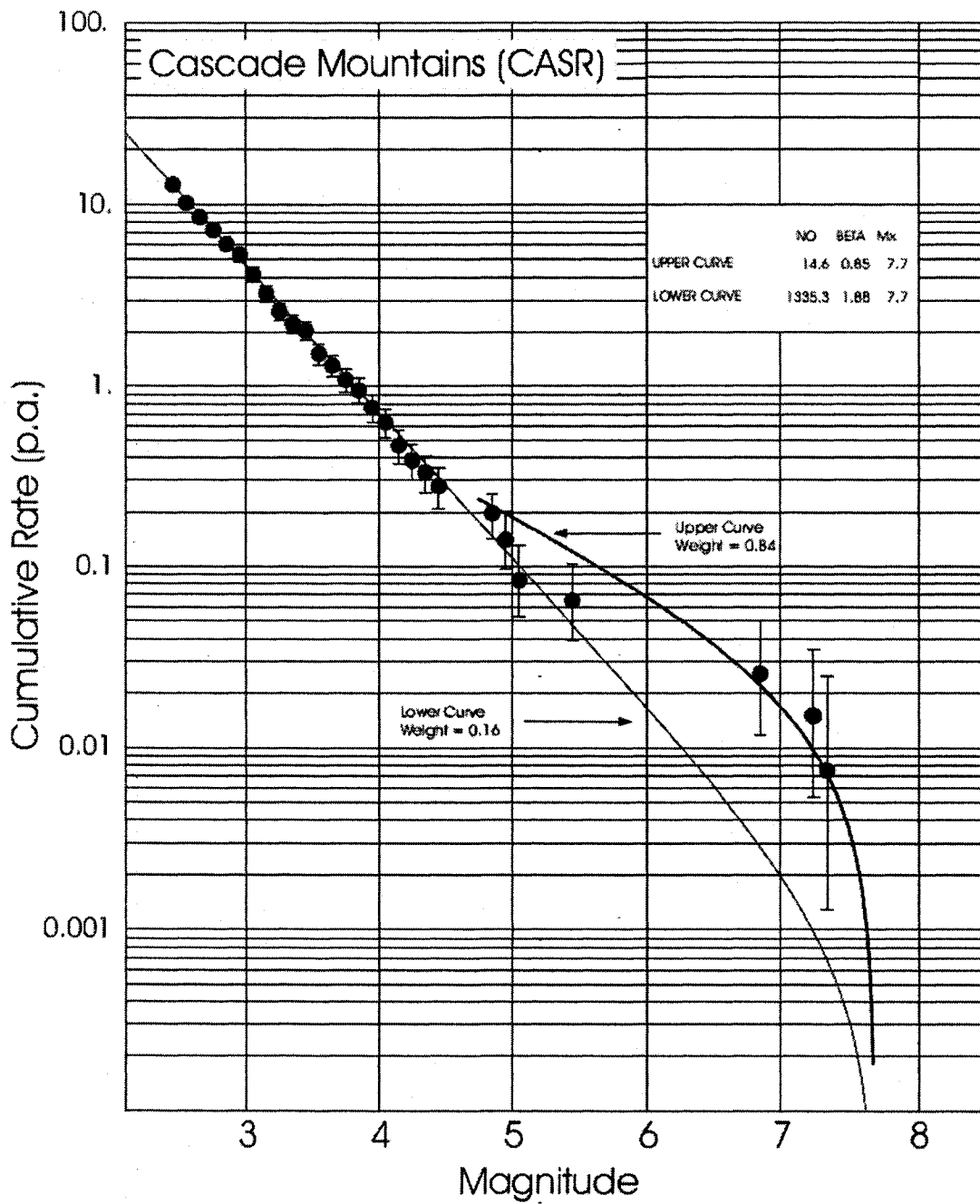


Figure 3.15: Magnitude-recurrence curve for CSAR, Cascadia mountain region.

(reproduced from Adams and Halchuk 2003)

Chapter 4

Application of Displacement-based Seismic Design

4.1. Introduction

In this chapter a detailed description of DBSD for a 6-storey shear wall building is presented. Another 3 buildings (12, 15 and 20-storey) have also been designed by this method; a summary of those designs is presented. The application of the DBSD is based on the procedure described in Chapter 3. The important parameters that govern the design are the inter-storey drift ratio, the roof displacement and the base shear. As mentioned in the scope of this research, the buildings are assumed to be located in Vancouver city on a site of class C as defined in NBCC 2005. The buildings are assumed to have a symmetric plan; the torsional vibration is therefore ignored and only two-dimensional analyses are carried out. Finally, every model (structure) is assumed to develop a plastic hinge only at the base and the pushover analyses are carried out by using the software SAP2000 nonlinear.

4.2. Building definition

4.2.1. Geometry

The buildings are built in reinforced concrete and each of them has the plan shown in Figure 4.1. This plan has 3 bays, each 8 m wide, in the E-W (East-West) direction and 6 bays, each 6m wide, in the N-S (North-South) direction. Each building has a first-storey height of 4.85 m; the height of each of the remaining storeys is 3.85 m. The lateral resistance is provided by two shear walls in each direction. Shear walls in the N-S direction are located in the 1st and 4th framing lines; the shear walls in the E-W direction are located in the 2nd and 6th framing lines. Only the shear walls running in the E-W direction are designed.

The RC flat slab thickness is assumed as being 200 mm. Other parameters, such as the number of columns, n_{col} , column section, A_{col} , wall thickness, t_{w} , shear wall length, l_w , total building height, H , and shear wall aspect ratio, A_r , are shown in Table 4.1

4.2.2. Load definition

Three type of loads are considered to be acting on the building: Dead Loads (DL), Live Loads (LL) and Lateral Loads due to earthquakes (E). Earthquake loads are inherently considered in the DBSD and only the first two loads are defined in this section.

Dead loads

| | |
|--|-----------------------|
| Partitions, q_P | 0.5 kN/m ² |
| Electrical, mechanical, ceiling, q_{EMC} | 0.5 kN/m ² |
| Roof insulation and water proofing, q_R | 0.5 kN/m ² |

Live loads

| | |
|--------------------------|-----------------------|
| Snow load on roof, q_S | 2.2 kN/m ² |
| Floor load, q_F | 2.4 kN/m ² |

4.2.3. Material properties

Concrete

| | |
|--|----------------------|
| Specified compressive strength, f_c' | 30 MPa |
| Elastic modulus, E_c | 24,500 MPa |
| Strain at f_c' | 0.002 |
| Modulus of rupture, f_r | 3.286 MPa |
| Resistance factor, ϕ_c | 0.6 |
| Cover, h_c | 40 mm |
| Self weight, γ_{rc} | 24 kN/m ³ |

Steel

| | |
|--|---------|
| Yield strength, f_y | 400 MPa |
| Elastic modulus, E_s | 200 GPa |
| Factored ultimate strength, f_{cu} | 600 MPa |
| Strain at onset of strain hardening, ϵ_{st} | 0.02 |
| Resistance factor, ϕ_s | 0.85 |

4.3. DBSD of a 6-storey building

4.3.1. General Calculation

Floor dead load, q_f

| | |
|---------------------------------|--|
| Slab | $q_{slab} = t h_s \times \gamma_{rc} = 0.2 \times 24 = 4.8 \text{ kN/m}^2$ |
| Partition | $q_p = 0.5 \text{ kN/m}^2$ |
| Electrical, mechanical, ceiling | $q_{EMC} = 0.5 \text{ kN/m}^2$ |
| Total | $q_f = q_{slab} + q_p + q_{EMC} = 5.8 \text{ kN/m}^2$ |

The roof dead load is also 5.8 kN/m^2 since partition load is replaced by the same amount of load due to insulation and roofing.

Load due to self weight

Upper floor columns

$$q_{fc} = \frac{n_c \times A_{col} \times \gamma_{rc} \times 3.65m}{A_{plan}} = \frac{22 \times 0.4 \times 0.4 \times 24 \times 3.65}{24 \times 36} = 0.357 \text{ kN/m}^2$$

1st level columns

$$q_{lc} = \frac{n_c \times A_{col} \times \gamma_{rc} \left(\frac{3.65 + 4.85}{2} \right)}{A_{plan}} = \frac{22 \times 0.4 \times 0.4 \times 24 \times 4.25}{24 \times 36} = 0.416 \text{ kN/m}^2$$

Roof level columns

$$q_{roofc} = \frac{n_c \times A_{col} \times \gamma_{rc} \left(\frac{3.65}{2} \right)}{A_{plan}} = \frac{22 \times 0.4 \times 0.4 \times 24 \times 1.825}{24 \times 36} = 0.178 \text{ kN/m}^2$$

Upper floor walls

$$q_{fsw} = \frac{4 \times l_w \times th_w \times \gamma_{rc} \times 3.65m}{A_{plan}} = \frac{4 \times 4 \times 0.4 \times 24 \times 3.65}{24 \times 36} = 0.649 \text{ kN/m}^2$$

1st level walls

$$q_{lsw} = \frac{4 \times l_w \times th_w \times \gamma_{rc} \left(\frac{3.65 + 4.85}{2} \right)}{A_{plan}} = \frac{4 \times 4 \times 0.4 \times 24 \times 4.25}{24 \times 36} = 0.756 \text{ kN/m}^2$$

Roof level walls

$$q_{\text{roofsw}} = \frac{4 \times l_w \times t_{h_w} \times \gamma_{rc} \left(\frac{3.65}{2} \right)}{A_{\text{plan}}} = \frac{4 \times 4 \times 0.4 \times 24 \times 1.825}{24 \times 36} = 0.324 \text{ kN/m}^2$$

Total dead load and mass

Floor

$$q_{\text{IDL}} = q_f + q_{fc} + q_{fsw} = 5.8 + 0.357 + 0.649 = 6.806 \text{ kN/m}^2$$

1st level

$$q_{\text{IDL}} = q_f + q_{lc} + q_{lsw} = 5.8 + 0.416 + 0.756 = 6.971 \text{ kN/m}^2$$

Roof (including 25% of snow load)

$$q_{\text{IDL}} = 0.25q_s + q_f + q_{\text{roofc}} + q_{\text{roofsw}} = \\ 0.25 \cdot 2.2 + 5.8 + 0.178 + 0.324 = 6.853 \text{ kN/m}^2$$

Considering a tributary area of 432 m² (half of the plan area), the distribution of dead loads and masses for each wall and floor presented on Table 4.2.

4.3.2. Gravity loads

The gravity loads are divided in two types: design axial load, and axial load for P-Δ effect. The design load or maximum axial load is computed at the shear wall base and will be used in the moment-curvature analysis. Another load is calculated assuming that the two shear walls together resist the P-Δ effect produced by the entire gravity load

4.3.2.1. Design axial load, P_b

The gravity loads on the shear wall will be obtained from the floor loads acting on a tributary area of 84 m^2 ($14 \text{ m} \times 6 \text{ m}$) plus the self weight. These loads are calculated as follows:

Upper floor level self weight, P_{wf}

$$P_{wf} = 3.65 \times l_w \times th_w \times \gamma_{rc} = 3.65 \times 4 \times 0.4 \times 24 = 140.16 \text{ kN}$$

1st level self weight, P_{w1}

$$P_{w1} = 4.85 \times l_w \times th_w \times \gamma_{rc} = 4.85 \times 4 \times 0.4 \times 24 = 186.24 \text{ kN}$$

Bottom of top storey, P_{top}

| | |
|------------|---|
| Snow load, | $P_s = 0.25 \times q_s \times A_{trib} = 0.25 \times 2.2 \times 84 = 46.2 \text{ kN}$ |
|------------|---|

| | |
|------------|--|
| Roof load, | $P_r = q_r \times A_{trib} = 5.8 \times 84 = 487.2 \text{ kN}$ |
|------------|--|

| | |
|-------|--|
| Total | $P_{top} = P_{wf} + P_s + P_r = 673.56 \text{ kN}$ |
|-------|--|

Bottom of typical storey, P_{ts}

| | |
|-------------|--|
| Floor load, | $P_f = q_f \times A_{trib} = 5.8 \times 84 = 487.2 \text{ kN}$ |
|-------------|--|

| | |
|-------|---|
| Total | $P_{ts} = P_{wf} + P_f = 627.36 \text{ kN}$ |
|-------|---|

Bottom of first storey, P_1

$$P_1 = P_{w1} + P_f = 673.44 \text{ kN}$$

The live load is included according to the NBCC 2005 requirements. This load is reduced by the live load reduction factor, LLRF, which is given by:

$$\text{LLRF} = 0.3 + \sqrt{\frac{9.8}{CA_{\text{trib}}}} \quad (4.1)$$

where CA_{trib} is the cumulative tributary area in m^2 . The calculations are presented in Table 4.3.

Finally, the factored dead and live loads are combined by using two load combination rules: $1.25 D + 1.50 L$ and $1.0D + 0.5 L$, where L is the reduced live load. The results are presented in Table 4.4. The design gravity load in the presence of earthquake loads is obtained from the combination $D + 0.5 L$ and is seen to be 4,084.63 kN.

4.3.2.2. Axial load for P-delta effect

In this case, the tributary area will be assumed to be half of the total plan area, 432 m^2 . The live loads are computed using the same procedure as the previous section and the results are shown on Table 4.5. The factored dead load and reduced live loads are finally combined using the rule: $1.0 D + 0.5 L$ and the results for each wall and floor are shown in Table 4.6.

4.3.3. DBSD

The calculations presented bellow follow the steps presented in the summary Chapter 3.

1. The yield displacement and rotation are given by Equations (3.2) and (3.3) where

$$\varepsilon_y = \frac{f_y \times \phi_s}{E_s} = \frac{400 \times 0.85}{200000} = 0.0017$$

is the factored yield steel strain. The yield curvature is given by Equation (3.4)

$$\phi_y = \frac{2.0\varepsilon_y}{l_w} = \frac{2 \times 0.0017}{4000} = 8.5 \times 10^{-7} \text{ 1/mm}$$

Hence the yield rotation is

$$\theta_y = \frac{\phi_y H}{2} = \frac{8.5 \times 10^{-7} \times 23100}{2} = 0.00982 \text{ rad}$$

and the yield displacement is

$$\Delta_y = \frac{\phi_y H^2}{3} = \frac{8.5 \times 10^{-7} \times 23100^2}{3} = 151.19 \text{ mm}$$

2. The ultimate rotation and displacement are defined by Equations (3.5) and (3.7), and together provide the required local ductility. The ultimate curvature is given by

$$\phi_u = \frac{\varepsilon_{cu}}{0.3l_w} = \frac{0.004}{0.3 \times 4000} = 3.33 \times 10^{-6} \text{ 1/mm.}$$

Assuming a plastic hinge length of $0.5l_w$ the plastic rotation and displacement are obtained from Equations (3.6) and (3.8) as follows:

$$\theta_p = (\phi_u - \phi_y)L_p = (33.3 - 8.5) \times 10^{-7} \times 0.5 \times 4000 = 0.00497 \text{ rad}$$

$$\Delta_p = \theta_p (H - 0.5L_p) = 0.00497 \times (23100 - 0.5 \times 2000) = 109.76 \text{ mm.}$$

Finally, the ultimate rotation is given by

$$\theta_u = \theta_y + \theta_p = 0.00982 + 0.00497 = 0.01479 \text{ rad}$$

and the ultimate displacement is

$$\Delta_u = \Delta_y + \Delta_p = 151.2 + 109.8 = 261 \text{ mm.}$$

Note that by using the drift limit establish by the NBCC 2005, the ultimate displacement is given by (Equation (3.9))

$$\Delta_u = 151.2 + (23100 - 0.5 \times 2000) \cdot \left(0.025 - \frac{8.5 \times 10^{-7} \times 23100}{2} \right) = 486.7 \text{ mm}$$

which is larger than that obtained from limiting the concrete strain to 0.004.

Therefore, the ultimate displacement is set at 261 mm and the ductility capacity is given by

$$\mu = \frac{\Delta_u}{\Delta_y} = \frac{261}{151.19} = 1.726$$

3. The mass distribution is shown in Table 4.2 and the displacement shape assumed to be in the form of an inverted triangle is obtained from the following

$$\begin{aligned} \phi_T &= \frac{h}{H} = \frac{\{4.85 \quad 8.5 \quad 12.15 \quad 15.8 \quad 19.45 \quad 23.1\}}{23.1} \\ &= \{0.21 \quad 0.37 \quad 0.53 \quad 0.68 \quad 0.84 \quad 1\} \end{aligned}$$

The modal participation factor and effective modal mass are now calculated from Equations (3.10) and (3.11), respectively

$$\Gamma = \frac{(\phi^T \mathbf{M} \mathbf{1})}{(\phi^T \mathbf{M} \phi)} = 1.379$$

$$M^* = \frac{(\phi^T \mathbf{M} \mathbf{1})^2}{(\phi^T \mathbf{M} \phi)} = 1505.2 \text{ tonne}$$

4. The yield and ultimate displacements for the equivalent SDOF system are thus given by

$$\delta y = \frac{\Delta_y}{\Gamma \phi^r} = \frac{151.19}{1.379 \times 1} = 109.63 \text{ mm}$$

$$\delta u = \frac{\Delta_u}{\Gamma \phi^r} = \frac{261}{1.379 \times 1} = 189.23 \text{ mm}$$

5. From the capacity-demand method (Figure 4.2) and using δy , δu and μ , the inelastic pseudo-acceleration is obtained as

$$A = 0.1 \text{ g}$$

6. The corresponding base design shear is

$$V_b = A \cdot M^* = 0.1 \times 9.81 \times 1505.2 = 1477.9 \text{ kN}$$

7. The base shear is distributed according to the product of the floor weights and the floor height shown in Table 4.2:

$$F^T = V_b \times \frac{W \cdot h}{\sum W \cdot h} = \{87.27 \quad 149.32 \quad 213.44 \quad 277.55 \quad 341.67 \quad 408.60\} \text{ kN}$$

The base moment is then given by

$$M_b = \sum [F(h_{i+1} - h_i)] = 24755.29 \text{ kN} \cdot \text{m}$$

8. The structure is now designed to resist P_b , V_b and M_b . The minimum requirements are taken from the CSA A23.3-94.

The minimum area of concentrated reinforcement is given by

$$A_{s_{\min}} = 0.002 \cdot t h_w \cdot l_w = 0.002 \times 400 \times 4000 = 3200 \text{ mm}^2$$

The minimum distributed reinforcement is obtained from

$$A_{s_{d\min}} = 0.0025 \cdot t h_w = 0.0025 \times 400 = 1000 \text{ mm}^2 / \text{m}$$

and is provided by 2 layers of #10 at 200 mm spacing.

The required vertical concentrated reinforcement is calculated by following the simplified method presented on Chapter 3. The depth of the compression zone is given by

$$c = \frac{P_b + A_d \phi_s f_y l_w}{\alpha_1 \phi_c f_c \beta_1 b_w + 2 A_d \phi_s f_y}$$

$$= \frac{4084.63 + 1000 \times 0.85 \times 400 \times 4000}{0.805 \times 0.6 \times 30 \times 0.895 \times 400 + 2 \times 1000 \times 0.85 \times 400} = 927.94 \text{ mm}$$

The concrete resistant moment is obtained from

$$M_c = \alpha_1 \phi_c f_c c^2 \beta_1 b_w (1 - 0.5 \beta_1)$$

$$= 0.805 \times 0.6 \times 30 \times 927.94^2 \times 0.895 \times 400 \times (1 - 0.5 \times 0.895) = 2467.9 \text{ kN} \cdot \text{m}$$

The resistant moment from the distributed reinforcement is give by

$$M_{Ad} = A_d \phi_s f_y c^2 \left[1 + \left(\frac{l_w}{c} - 1 \right)^2 - \frac{2}{3} \left(\frac{\epsilon_y}{\epsilon_{cu}} \right)^2 \right]$$

$$= 1000 \times 0.85 \times 400 \times 927.94^2 \left[1 + \left(\frac{4000}{927.94} - 1 \right)^2 - \frac{2}{3} \left(\frac{0.002}{0.0035} \right)^2 \right] = 1718.9 \text{ kN} \cdot \text{m}$$

The restoring moment provided by the axial load is obtained from

$$M_p = P_b \cdot \left(\frac{l_w}{2} - c \right) = 4086.63 \left(\frac{4000}{2} - 927.94 \right) = 4379 \text{ kN} \cdot \text{m}$$

Thus, the resistant moment to be contributed by the concentrated reinforcement is obtained from

$$M_{cr} = M_b - M_c - M_{Ad} - M_p$$

$$= 24755.3 - (2467.9 + 1718.9 + 4379) = 16189.5 \text{ kN} \cdot \text{m}$$

and the corresponding steel area is given by

$$A_{cr} = \frac{M_{cr}}{\phi_s f_y (l_w - 2h_m)} = \frac{16189.5}{0.85 \times 400 \times (4000 - 2 \times 437.5)} = 15237.2 \text{ mm}^2$$

This area is larger than the minimum area required by the code, $A_{s_{min}} = 3200 \text{ mm}^2$.

Therefore, an arrangement of 15 bars #35 is adopted which gives an area of 15000 mm^2 . The value of h_m was obtained by assuming a spacing of 190 mm plus a cover of 40mm, and half of the steel section diameter, 17.5 mm (see reinforcement detail in Figure 4.3). Using this reinforcement, the moment-curvature analysis gives the curve shown on Figure 4.4. From the idealized curve shown with a dotted line, the following results are obtained

| | |
|---------------------------|------------------------------------|
| Moment capacity, M_c | 23686 kN m |
| Yield curvature, ϕ_y | $9.05 \times 10^{-7} \text{ 1/mm}$ |

Ultimate curvature, ϕ_u 4.14×10^{-6} 1/mm

Ratio of effective moment of
inertia to the gross moment of inertia, I_r 0.5006

From these results the refined plastic rotation and roof displacement can be computed as follows

$$\theta_p = (\phi_u - \phi_y)L_p = (41.4 - 9.05) \times 10^{-6} \times 2000 = 0.00647 \text{ rad}$$

$$\Delta_p = 0.00647(23100 - 0.5 \times 2000) = 142.88 \text{ mm}$$

Also from these results, the stability of this shear wall can be checked by obtaining the critical thickness according to Equation (3.18) as follows

$$b_c = 0.017 \cdot l_w \cdot \sqrt{\mu_\phi} = 0.017 \times 4000 \times \sqrt{\frac{41.4}{9.05}} = 145.4 \text{ mm}$$

Thus 400 mm thickness will avoid any instability problem.

9. The modal analysis including the P- Δ effect gives the following properties related to the first mode

| | |
|--------------------------------|--------------|
| Period of vibration, T_1 | 2.039 s |
| Mode shape at roof, ϕ^r | 0.0398 |
| Participation factor, Γ | 1.414 |
| Effective modal mass, M^* | 1263.7 tonne |

10. Distributing the forces according to Equation (3.26) a first mode pushover analysis is carried out. The roof displacement versus base shear relationship obtained is shown in Figure 4.5. The important result from this curve is the yield point which is

12. The difference between the two successive estimates is

$$\text{diff}_{V_y} = \frac{V_y - V_{y\text{new}}}{V_y} = 15.74 \%$$

Therefore, a new design will be carried out. The new base design moment is obtained from

$$M_b = M_c(1 - \text{diff}_{V_y}) = 23686 \times (1 - 0.1574) = 19958.71 \text{ kN} \cdot \text{m}$$

The computations presented in Steps 8 through 12 are repeated; results of the moment-curvature analysis, modal analysis, and pushover analysis are shown in Table 4.7, Table 4.8, and Table 4.9 for 4 different tries, including the results from the first try. Four tries were needed to find an error less than 1%. From the last column of Table 4.9, it is noticed how the procedure converges over the 4 attempts. The results obtained from the last attempt are shown in Figure 4.7 through Figure 4.10. This design gives an ultimate base shear of $V_u = 765 \text{ kN}$, and the corresponding ratio of the ultimate base shear to yield shear $V_u/V_y = 0.878$, which is a measure of the excursion into the unstable part of the pushover curve.

13. The method was seen to converge on the fourth attempt. It may be noted that all of the preceding computations were based on the first mode. The moment estimate obtained from the first mode is expected to be reasonable. However, in a shear wall structure the higher modes make significant contribution to the base shear. Hence two higher modes, 2nd and 3rd are included and analysis is repeated with these modes following the procedure presented in Section 3.11 of modal pushover analysis. The modal analysis results are shown in Table 4.10 for three modes. The

pushover curves obtained by using distribution of forces according to the second and third mode shapes are shown in Figure 4.11. These curves are transformed into equivalent SDOF systems and then plotted on the capacity-demand diagrams presented in Figure 4.12. That figure, as well as the data summarized in Table 4.11, show that the performance points do not lie in the inelastic zone of the capacity diagram, which means that both responses remain elastic. The responses in the first, second and third modes are combined according to the SRSS and ABSSUM rules and the results are shown in Figure 4.13 for the inter-storey drifts and displacements and in Figure 4.14 for shear forces. As examples, three particular results are obtained as follows:

Roof displacement

$$\Delta_{\text{roof}} = \sqrt{\Delta_{u1}^2 + \Delta_{u2}^2 + \Delta_{u3}^2} = \sqrt{304.8^2 + 15.0^2 + 1.0^2} = 305.2 \text{ mm}$$

Maximum drift ratio

$$\theta_{\text{max}} = \sqrt{\theta_{\text{max}1}^2 + \theta_{\text{max}2}^2 + \theta_{\text{max}3}^2} = \sqrt{0.015^2 + 0.004^2 + 0.001^2} = 0.016$$

Base shear

$$V_b = \sqrt{V_{b1}^2 + V_{b2}^2 + V_{b3}^2} = \sqrt{871^2 + 2892^2 + 1029^2} = 3191 \text{ kN}$$

where the numeric subscript indicates the mode number.

For the purpose of comparison the base shear is obtained with 4 modes; the shear in the fourth mode is 280 kN, so that the total response is 3203 kN. This is not significantly different from the value obtained with 3 modes, hence for this building inclusion of 3 modes in MPA should be adequate.

Assuming a horizontal reinforcement of #15 at 150 mm and an effective depth of $d = 0.81w$, the simplified method gives a shear capacity of (Clause 11.3 of the CSA 1994):

$$V_{\text{capacity}} = 0.2\phi_c \sqrt{f_c} \cdot t h_w d_v + \phi_s \frac{A_v f_y}{s} d =$$

$$0.2 \times 0.6 \times \sqrt{30} \times 400 \times 0.8 \times 4000 + 0.85 \frac{400 \times 400}{150 \times 1000} 0.8 \times 4000 = 3742.6 \text{ kN}$$

Thus, the provided horizontal reinforcement will ensure sufficient capacity to resist the shear demand of 3,191 kN.

14. The design spectrum corresponding to 50%/50 year probability is obtained by scaling down the UHS corresponding to 2%/50 year probability by the ratio obtained in Section 3.12.1, that is, 0.325. The spectral acceleration from the UHS corresponding to 2%/50 year probability at $T_1 = 2.337 \text{ s}$ is 0.165 g. Thus, the demand acceleration for the operational level is $0.165 \times 0.325 = 0.039 \text{ g}$. Considering the equivalent modal mass for the final design $M1^* = 1262.05 \text{ tonne}$, the demand base shear, V_{bOP} , is given by

$$V_{\text{bOP}} = 1262.05 \times 9.81 \times 0.039 = 481.8 \text{ kN}$$

15. From the pushover curve shown in Figure 4.9, the roof displacement is 74.7 mm for the calculated base shear, V_{bOP} . From pushover analysis data base, the maximum drift ratio at this roof displacement is 0.54 %, which is close to the 0.5% limit. The design is assumed to be satisfactory for the operational performance level.

4.4. Summary of DBSD for 6, 12, 15, and 20-storey buildings

Another 3 buildings are designed by the same procedure as adopted for the 6-storey building. Since the calculations are similar to these for the 6-storey building, the detailed designs are presented in Appendices A, B, and C, and only a summary of the results is presented in this section.

Table 4.12 sums up some of the results obtained from the DBSD of each building. In each case convergence is assumed to have been achieved when the variation in the base shear in the last try is less than 1 %. The total responses are obtained by combining the results from several modes as illustrated for the 6-storey building. In each case the first mode period is quite long since the reduced moment of inertia is applied over the entire height of the cantilever wall resulting in a more flexible structure. For the 15 and 20-storey buildings 4 and 5 modes, respectively, are included in calculating the building response, since for such tall buildings more modes are expected to contribute to the response. These results will later be compared with those obtained from nonlinear RHA. The last two columns show the moment capacities and the ductility factors that are equal or close to the moment and ductility demands for each building. The shear walls in each building are designed to have a capacity that can be achieved only when the amount of reinforcing steel is larger than the minimum requirement defined by the code.

The total responses, such as inter-storey drift ratios, roof displacements, and shear forces are presented in the next section.

4.4.1. Total responses

The total responses obtained by combining the modal responses are shown in Table 4.13. The results indicate that the ABSSUM rule may be conservative, particularly in estimating the base shear. This observation will be validated on the basis of nonlinear RHA. Table 4.13 also shows the plastic rotation at the base of each building obtained from the pushover analysis database.

Results of the response are also presented in Figure 4.13 through Figure 4.20. In those figures the number following the combination rule name corresponds to the number of modes used to get the total response. The first mode response is identified as Mode-1. The results for individual buildings are separately presented in the following sections.

4.4.1.1. Response of 6-storey building

When the SRSS rule is used the higher modes are seen to contribute very little to the inter-storey drift ratio and roof displacement. When the ABSSUM rule is used, inclusion of the second mode significantly changes the values of these two parameters although a major portion of the response is still from the first mode. Again, the 3rd mode makes only a small contribution in any rule. The maximum response is obtained at the top level for both displacement and drift ratio. In some cases the higher modes appear to contribute very little to the drift ratio and displacement. This is so as the 3rd level for drift and the 5th storey for displacement. One plausible reason for that is the fact that 2nd mode has a node near these levels and hence makes a little contribution to the drifts and displacement responses.

Results are very different for shear force response. SRSS-3 is almost 3 times the shear in Mode-1 and ABSSUM-3 is almost 5 times the value in Mode-1, which indicates the large contribution of the 2nd and 3rd modes to this response. The results of SRSS rule show a small impact of the 3rd mode. The ABSSUM, on the other hand, shows an important contribution from the 3rd mode. However, the 2nd mode plays the major role in either case.

4.4.1.2. Response of 12-storey building

The results for the 12-storey building are similar to those for six storey building. When the SRSS rule is used, the higher modes are seen to make minimum contribution to the drifts and displacements. When the ABSSUM rule is used, the 2nd mode is seen to make a significant contribution to the inter-storey drift although the major contribution still comes from the first mode.

The total shear response using SRSS-3 rule is almost 3 times the Mode-1 response. The ABSSUM-3 is now almost 6 times the first mode response. The difference between response obtained using 2 and 3 modes also increases; ABSSUM-2 represents about 70 % of the total response, implying that the third mode contributes about 30 % to the response.

4.4.1.3. Response of 15-storey building

The pattern of inter-storey drift and storey displacement are similar to those for 6 and 12-storey buildings. In this case, the 4th mode was added in the modal analysis but the contribution of this mode is seen to be quite small.

Regarding the shear response, the 2nd mode shows the largest contribution when the SRSS rule is used with only 22 % of the response coming from the first mode. When the ABSSUM rule is used even the third mode is seen to have a high effect on the total response. In this case, the first mode represents only one eighth of the 4-mode response.

4.4.1.4. 20-storey building responses

Again, the contribution of the higher modes to the inter-storey drifts and storey displacements is small. An additional 5th mode was included in the analysis but the combined response from 5 modes is almost the same as that from 3 modes, implying that the 4th and 5th modes make very small contribution.

The base shear response from the first mode is about 1/4 of the total response obtained by using the SRSS rule, and about 1/8 the total response obtained using the ABSSUM rule. The main contribution is again from the 2nd mode for the SRSS rule and the 2nd and 3rd modes for the ABSSUM rule.

4.4.2. Discussion on the results

The target displacement in each case was set by a local ductility limit rather than the inter-storey drift limit of 0.025. The results presented on Table 4.12 show decreasing ductility requirements for taller buildings. Since the taller structures are more flexible, most of their displacements comes from the yield displacement and the plastic deformation is comparatively small. As a result, the ductility requirement is low and is

mainly defined by local damage limit on structural elements such as the limit on concrete strain of 0.004 for unconfined sections.

Although the error in only the last iteration is shown in Table 4.12, the DBSD converged in every case and by defining reasonable shear wall aspect ratios no more than 4 iterations were needed in order to reach the final design. The method showed convergence whether the moment capacity obtained from the preliminary design was smaller or larger than the next attempt and the assumption of 1 % difference between base shears of two tries gave a practical limit for design.

The inter-storey drift ratio and displacement responses are not affected much by contributions from the higher modes. The first-mode response is very close to the total response implying that the DBSD based on first mode alone is adequate for controlling these responses.

One of the most important results obtained from the DBSD and the MPA, is that the higher modes make substantial contribution to the shear. The 2nd mode makes a major contribution to the base shear and the contribution from even the 3rd, 4th, and 5th modes may be significant depending on the number of storeys in the building. The ABSSUM rule provides even larger values for the base shear and is expected to be conservative. These observations can be validated by carrying out a series of nonlinear analyses.

Table 4.1: Geometric parameters for the 4 shear wall buildings

| Number of storeys | Number of columns | Column section | Shear wall thickness | Shear wall length | Building height | Shear wall aspect ratio |
|-------------------|-------------------|-------------------------------|-------------------------|-------------------|-----------------|-------------------------|
| n | n _{col} | A _{col} (mm x mm) | th _w (mm) | lw (m) | H (m) | A _r |
| 6 | 22 | 400 × 400 | 400 | 4.0 | 23.10 | 5.78 |
| 12 | 18 | 500 × 500 | 400 | 7.5 | 45.00 | 6.00 |
| 15 | 18 | 600 × 600 | 400 | 8.5 | 55.95 | 6.58 |
| 20 | 18 | 700 × 700 | 400 | 10.0 | 74.20 | 7.42 |

Table 4.2: Floor dead loads and masses tributary to each wall in the 6-storey building

| Storey | Height above base | Dead Load | Mass |
|--------|-------------------|-----------|---------|
| Number | (m) | (kN) | (tonne) |
| 1 | 4.85 | 3011.5 | 306.99 |
| 2 | 8.50 | 2940.1 | 299.70 |
| 3 | 12.15 | 2940.1 | 299.70 |
| 4 | 15.80 | 2940.1 | 299.70 |
| 5 | 19.45 | 2940.1 | 299.70 |
| 6 | 23.10 | 2960.5 | 301.78 |

Table 4.3: Reduced live load calculations for each wall of the 6-storey building

| Storey | Live Load | Cumulative Live Load | Cumulative Tributary Area | Live Load Reduction Factor | Reduced Cumulative Live Load |
|--------|------------|----------------------|---|----------------------------|------------------------------|
| n | LL (kN) | CLL (kN) | CA _{trib} (m ²) | LLRF | RCLL (kN) |
| 1 | 201.6 | 1008.0 | 420 | 0.453 | 456.38 |
| 2 | 201.6 | 806.4 | 336 | 0.471 | 379.64 |
| 3 | 201.6 | 604.8 | 252 | 0.497 | 300.71 |
| 4 | 201.6 | 403.2 | 168 | 0.542 | 218.34 |
| 5 | 201.6 | 201.6 | 84 | 0.642 | 129.34 |
| 6 | 0 | 0 | 0 | 0 | 0 |

Table 4.4: Gravity load combinations for each wall of the 6-storey building

| Storey | Dead Load | Cumulative Dead Load | Reduced Cumulative Live Load | Cumulative 1.25D+1.5L | Cumulative 1.0D+0.5L |
|--------|-----------|----------------------|------------------------------|-----------------------|----------------------|
| n | DL (kN) | CDL (kN) | RCLL (kN) | (kN) | (kN) |
| 1 | 673.44 | 3856.44 | 456.38 | 5505.11 | 4084.63 |
| 2 | 627.36 | 3183.00 | 379.64 | 4548.21 | 3372.82 |
| 3 | 627.36 | 2555.64 | 300.71 | 3645.61 | 2705.99 |
| 4 | 627.36 | 1928.28 | 218.34 | 2737.86 | 2037.45 |
| 5 | 627.36 | 1300.92 | 129.34 | 1820.16 | 1365.59 |
| 6 | 673.56 | 673.56 | 0 | 841.95 | 673.56 |

Table 4.5: Reduced tributary live loads for calculating the P- Δ effect for each wall of the 6-storey building

| Storey | Live Load | Cumulative Live Load | Cumulative Tributary Area | Live Load Reduction Factor | Reduced Cumulative Live Load | Reduced Live Load |
|--------|-----------|----------------------|--------------------------------------|----------------------------|------------------------------|-------------------|
| n | LL (kN) | CLL (kN) | CA _{trib} (m ²) | LLRF | RCLL (kN) | RLL (kN) |
| 1 | 1036.8 | 5184.0 | 4320 | 0.348 | 1802.11 | 337.11 |
| 2 | 1036.8 | 4147.2 | 3456 | 0.353 | 1465.00 | 340.63 |
| 3 | 1036.8 | 3110.4 | 2592 | 0.361 | 1124.38 | 346.14 |
| 4 | 1036.8 | 2073.6 | 1728 | 0.375 | 778.24 | 356.78 |
| 5 | 1036.8 | 1036.8 | 864 | 0.407 | 421.46 | 421.46 |
| 6 | 0 | 0 | 0 | 0 | 0 | 0 |

Table 4.6: Floor gravity loads tributary to each wall for calculating the P- Δ effect in the 6-storey building

| Storey | Dead Load | Reduced Live Load | Combined Load 1.0D+0.5L |
|--------|-----------|-------------------|-------------------------|
| n | CDL (kN) | RCLL (kN) | (kN) |
| 1 | 3011.5 | 337.11 | 3180.07 |
| 2 | 2940.1 | 340.63 | 3110.41 |
| 3 | 2940.1 | 346.14 | 3113.16 |
| 4 | 2940.1 | 356.78 | 3118.49 |
| 5 | 2940.1 | 421.46 | 3150.83 |
| 6 | 2960.5 | 0 | 2960.45 |

Table 4.7: Results of moment-curvature analysis in the four iterations in the design of the 6-storey building

| Iteration | Moment Capacity | Yield curvature | Ultimate curvature | Moment of Inertia ratio | Plastic rotation |
|-----------|-----------------|-----------------|--------------------|-------------------------|-----------------------------|
| Number | M_c (kN m) | ϕ_y (1/mm) | ϕ_u (1/mm) | I_r | θ_p (10^{-2} rad) |
| 1 | 23686 | 9.05E-07 | 4.14E-06 | 0.501 | 0.497 |
| 2 | 19006 | 8.57E-07 | 4.70E-06 | 0.424 | 0.647 |
| 3 | 16991 | 8.45E-07 | 4.68E-06 | 0.385 | 0.769 |
| 4 | 17108 | 8.45E-07 | 4.69E-06 | 0.387 | 0.767 |

Table 4.8: First mode analysis results for the 4 design iterations of the 6-storey building

| Iteration | First mode period | Participation factor | Modal mass participation | Effective modal mass |
|-----------|-------------------|----------------------|--------------------------|----------------------|
| Number | T_1 (s) | Γ | (%) | M^* (tonne) |
| 1 | 2.039 | 1.414 | 69.91 | 1263.68 |
| 2 | 2.226 | 1.414 | 69.85 | 1262.59 |
| 3 | 2.346 | 1.414 | 69.82 | 1262.05 |
| 4 | 2.337 | 1.414 | 69.82 | 1262.05 |

Table 4.9: Results from pushover analyses for the 4 design iterations of the 6-storey building

| Iteration | Yield base shear | Yield Roof Displ. | Ultimate Roof Displ. | Ductility Factor | Reduction Factor | Inelastic PSA | New Yield Shear | Base Shear Error |
|-----------|------------------|-------------------|----------------------|------------------|------------------|---------------|-----------------|------------------|
| Number | V_{by} (kN) | Δ_y (mm) | Δ_u (mm) | μ | R_y | A(g) | V_y (kN) | (%) |
| 1 | 1230.0 | 145.0 | 287.88 | 1.99 | 2.03 | 0.084 | 1036.4 | 15.74 |
| 2 | 974.4 | 137.0 | 306.90 | 2.24 | 2.31 | 0.071 | 882.2 | 9.46 |
| 3 | 867.2 | 135.5 | 305.05 | 2.25 | 2.33 | 0.071 | 879.4 | -1.40 |
| 4 | 870.9 | 135.0 | 304.82 | 2.26 | 2.33 | 0.071 | 876.8 | -0.68 |

Table 4.10: Modal analysis results for the 4th design iteration of the 6-storey building

| Mode | Period | Participation factor | Modal mass participation | Effective modal mass |
|----------------|-----------|----------------------|--------------------------|----------------------|
| N ^o | T_n (s) | Γ | (%) | M^* (tonne) |
| 1 | 2.337 | 1.414 | 69.82 | 1262.05 |
| 2 | 0.367 | 0.578 | 21.11 | 381.58 |
| 3 | 0.137 | 0.234 | 6.22 | 112.41 |

Table 4.11: Results from modal pushover analysis in the 4th design iteration of the 6-storey building

| Mode | Yield base shear | Yield Roof Displ. | Yield PSA | Elastic PSA | Reduction Factor | Ultimate Roof Displ. | Ultimate Base Shear |
|----------------|------------------|-------------------|-----------|-------------|------------------|----------------------|---------------------|
| N ^o | V_{by} (kN) | Δ_y (mm) | A (g) | PSA (g) | R_y | Δ_u (mm) | V_y (kN) |
| 2 | 3284.7 | 17.0 | 0.88 | 0.77 | 0.88 | 14.97 | 2892.1 |
| 3 | 5358.0 | 5.3 | 4.86 | 0.93 | 0.19 | 1.02 | 1029.2 |

Table 4.12: Summary of DBSD for the 6, 12, 15 and 20-storey buildings

| Storey | No. of iterations | Relative error in last iteration | Modes considered | 1st Period | 2nd Period | 3rd Period | 4th Period | 5th Period | Moment Capacity | Ductility Factor |
|--------|-------------------|----------------------------------|------------------|------------|------------|------------|------------|------------|-------------------------------|------------------|
| # | # | (%) | # | (s) | (s) | (s) | (s) | (s) | $M_c(\text{kN}\cdot\text{m})$ | μ |
| 6 | 4 | -0.68 | 3 | 2.34 | 0.37 | 0.14 | - | - | 17108 | 2.26 |
| 12 | 1 | 0.70 | 3 | 3.73 | 0.58 | 0.22 | - | - | 50528 | 1.91 |
| 15 | 2 | -0.08 | 4 | 4.74 | 0.73 | 0.27 | 0.14 | - | 70094 | 1.69 |
| 20 | 3 | 0.23 | 5 | 6.14 | 0.93 | 0.34 | 0.18 | 0.12 | 118530 | 1.47 |

Table 4.13: Maximum total responses for the 6, 12, 15 and 20-storey buildings

| Storey | Plastic Rotation from Pushover Analysis | Inter-storey Drift Ratio | | Roof Displacement | | Base Shear | |
|--------|---|--------------------------|--------|-----------------------------|--------|------------|---------|
| # | θ_p (rad) | θ_{i-s} | | Δ_{roof} (mm) | | V_b (kN) | |
| | Mode-1 | SRSS | ABSSUM | SRSS | ABSSUM | SRSS | ABSSUM |
| 6 | 0.0074 | 0.0160 | 0.0200 | 305.2 | 320.8 | 3190.9 | 4792.2 |
| 12 | 0.0056 | 0.0145 | 0.0191 | 518.6 | 558.0 | 5617.9 | 8710.1 |
| 15 | 0.0047 | 0.0147 | 0.0201 | 634.3 | 690.5 | 6531.4 | 12360.1 |
| 20 | 0.0037 | 0.0148 | 0.0203 | 836.2 | 911.0 | 7624.1 | 15181.9 |

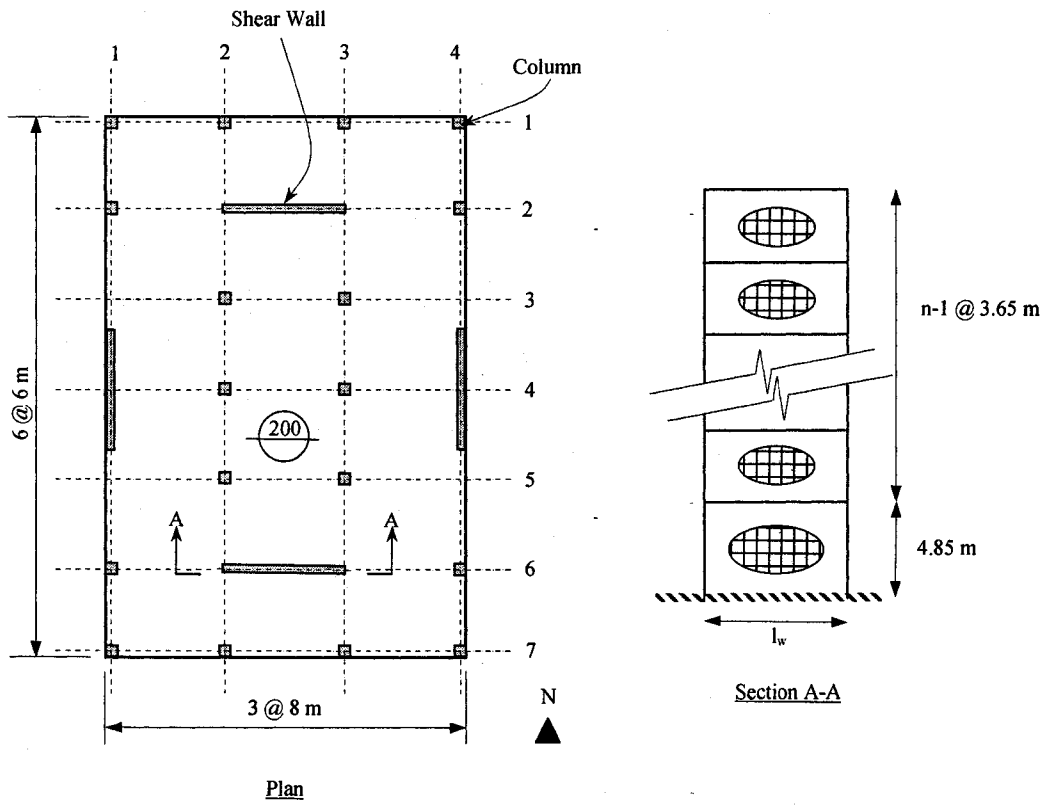


Figure 4.1: Building plan and elevation of one cantilever shear wall.

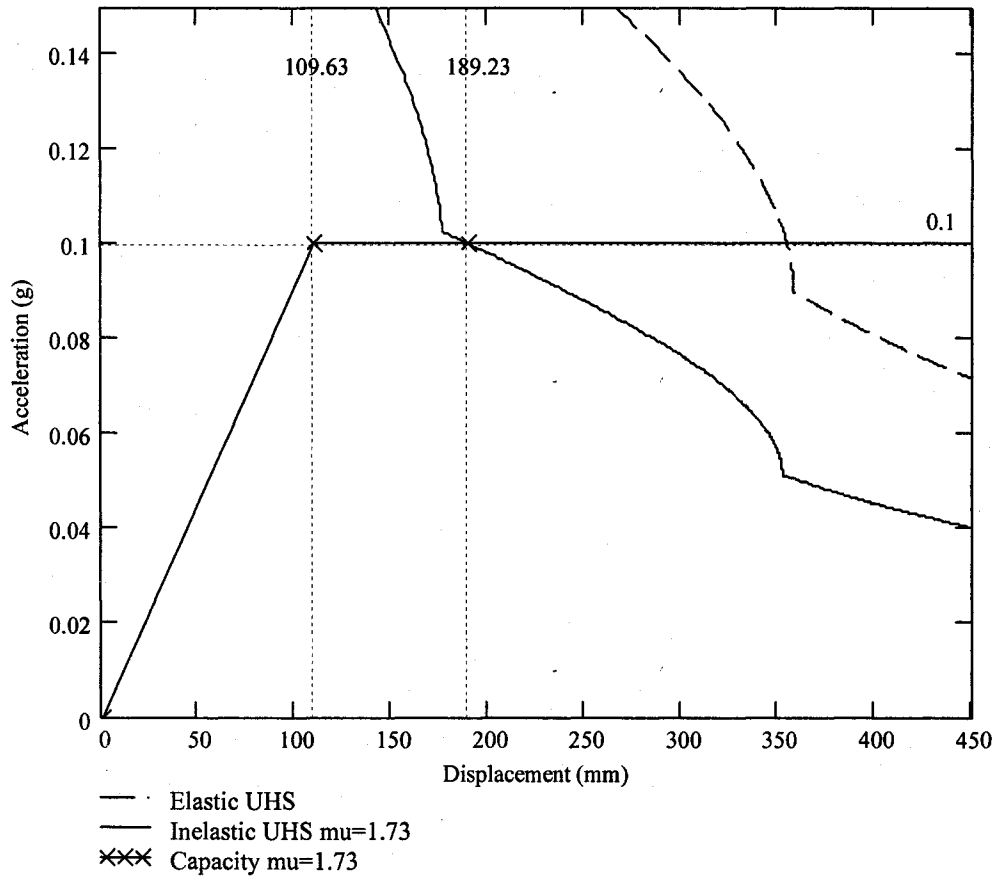


Figure 4.2: Capacity-demand diagram for the preliminary design of shear wall for the 6-storey building

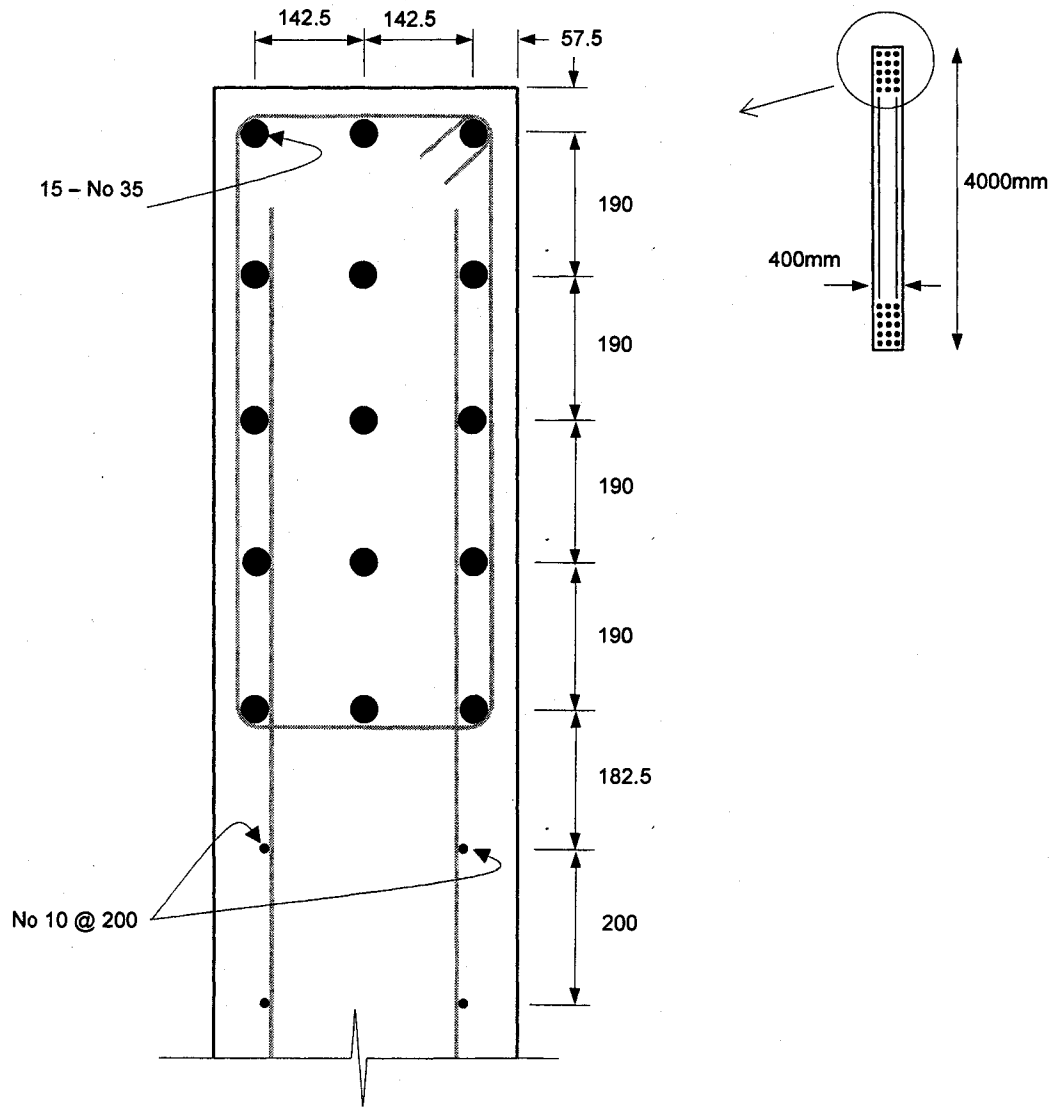


Figure 4.3: Detail of reinforcement for the preliminary design of shear wall for the 6-storey building

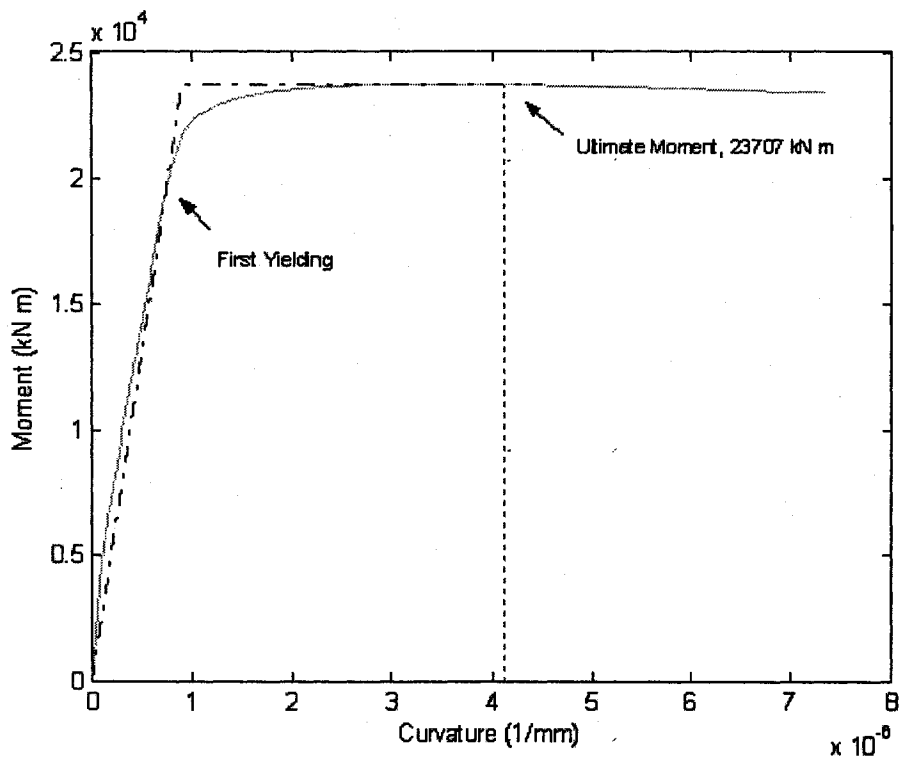


Figure 4.4: Moment-curvature relationship for the preliminary design of shear wall for the 6-storey building

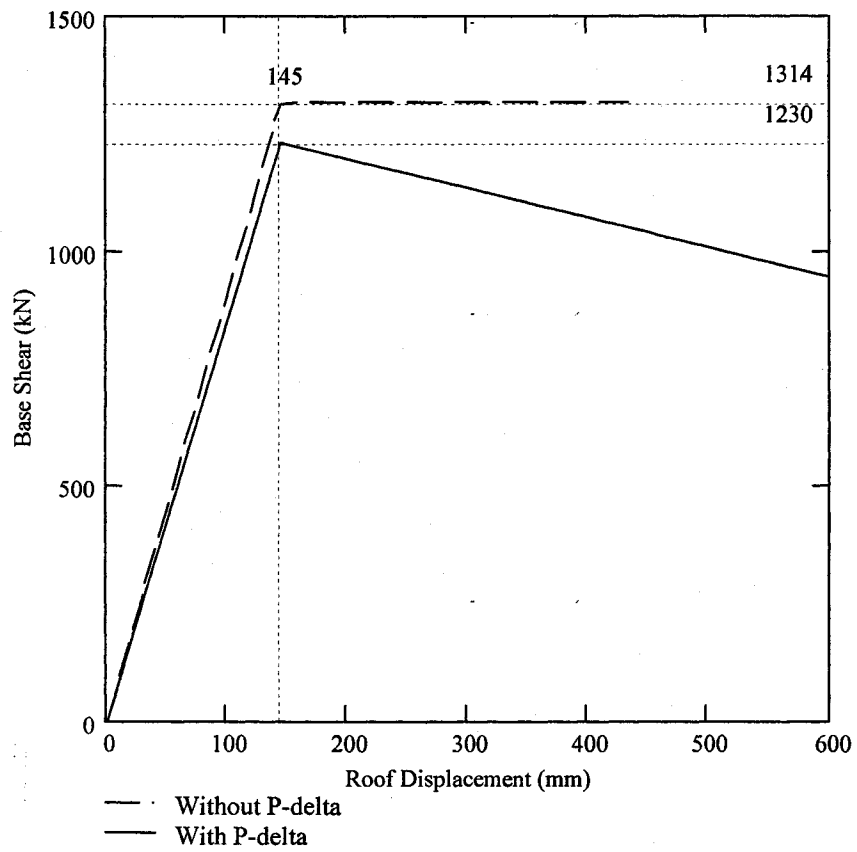


Figure 4.5: Pushover curves with and without P- Δ effect for the preliminary design of shear wall for the 6-storey building

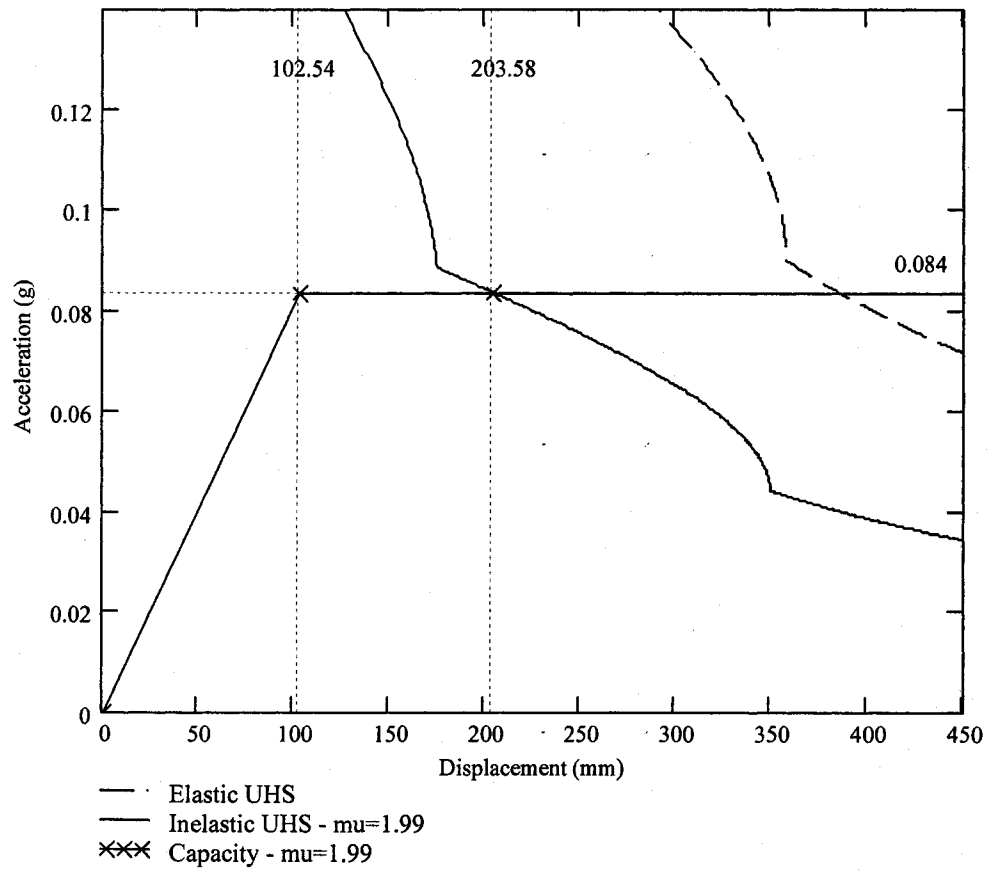


Figure 4.6: Capacity-demand diagram for the first design iteration of the 6-storey building

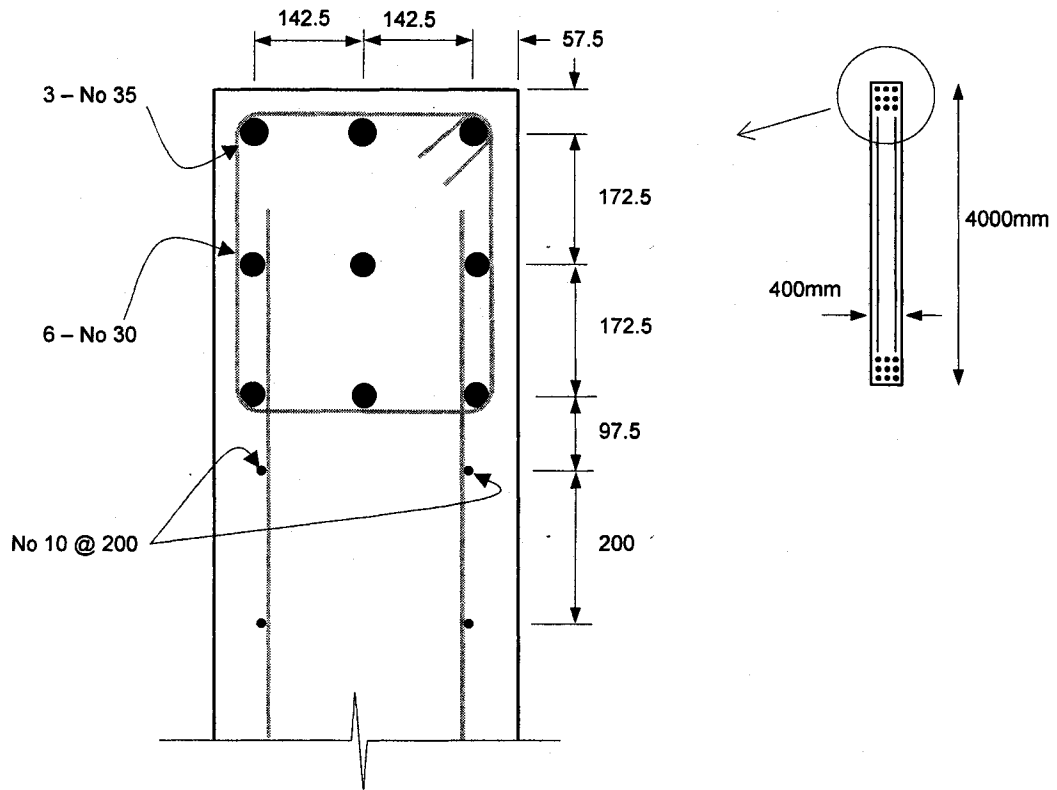


Figure 4.7: Detail of reinforcement for the final design of shear wall for the 6-storey building

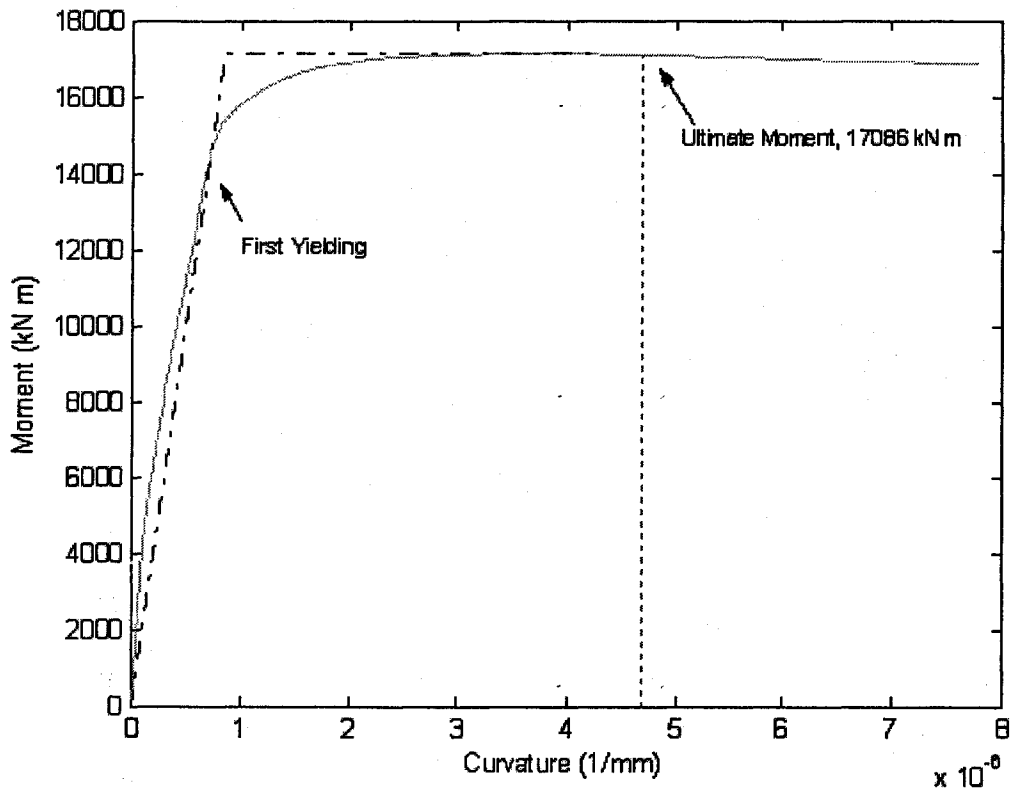


Figure 4.8: Moment-curvature relationship for the final design of shear wall for the 6-storey building

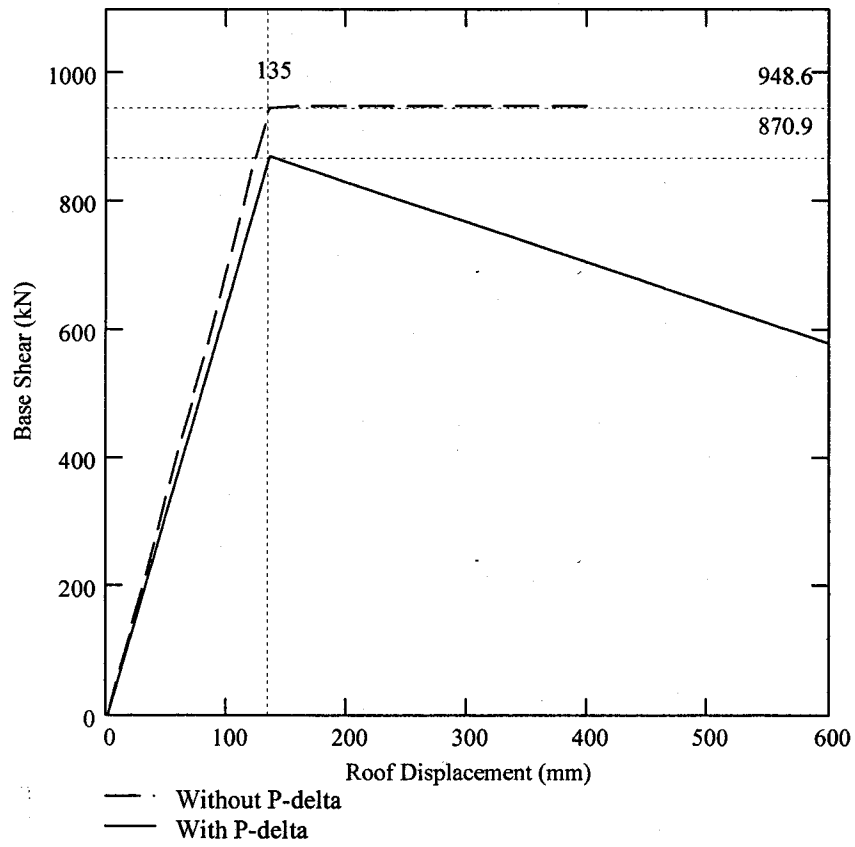


Figure 4.9: Pushover curves with and without P- Δ effect for the final design of shear wall for the 6-storey building

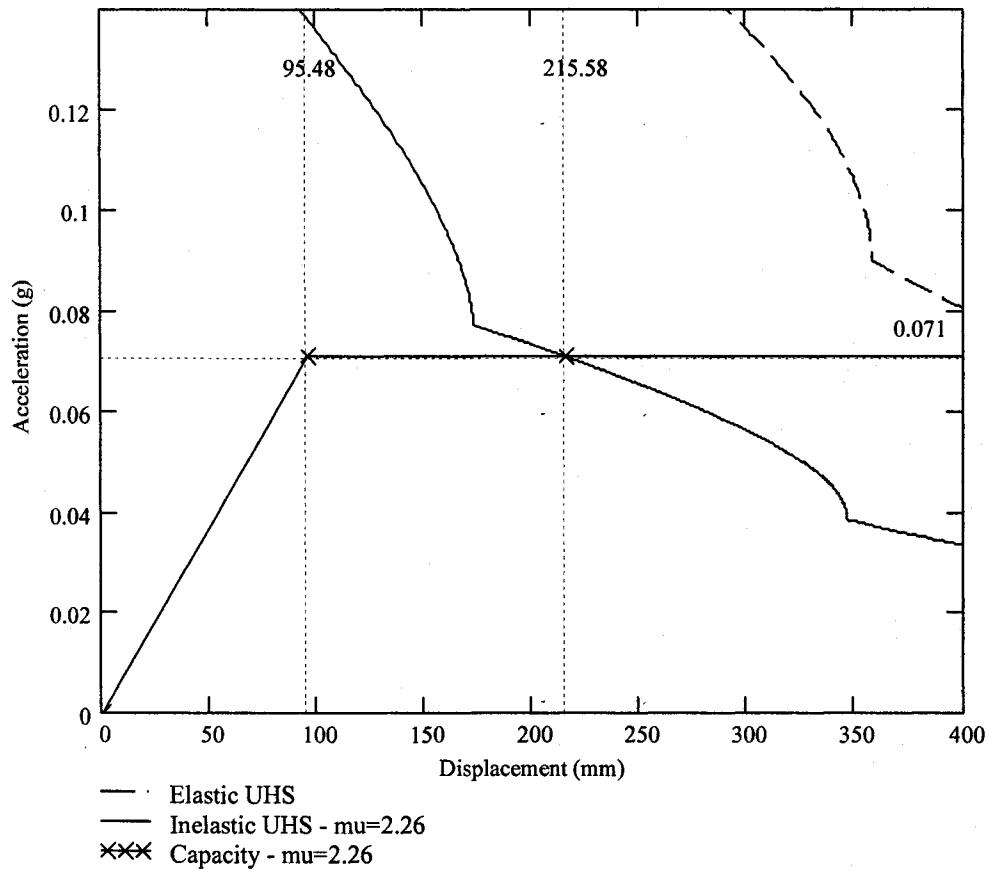


Figure 4.10: Capacity-demand diagram for the final design of shear wall for the 6-storey building

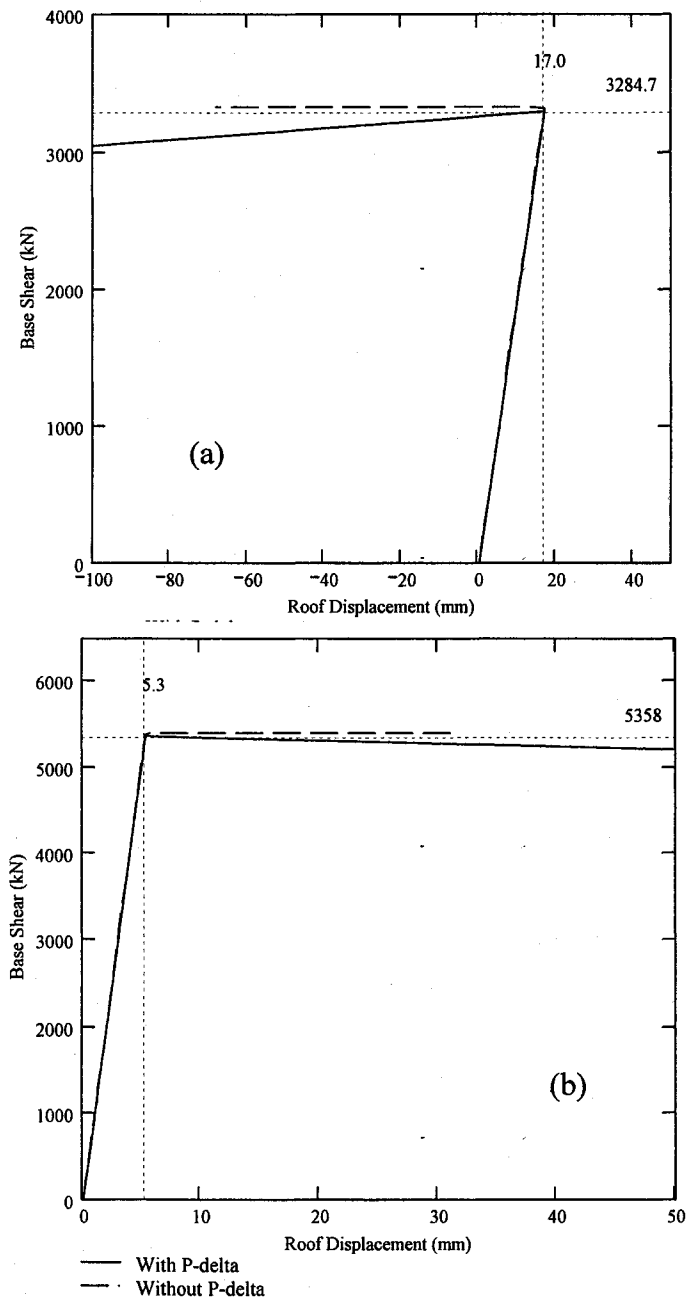


Figure 4.11: Pushover curves with and without P- Δ effect for the final design of shear wall for the 6-storey building obtained by distributing the lateral forces according to (a) the second mode shape, and (b) the third mode shape

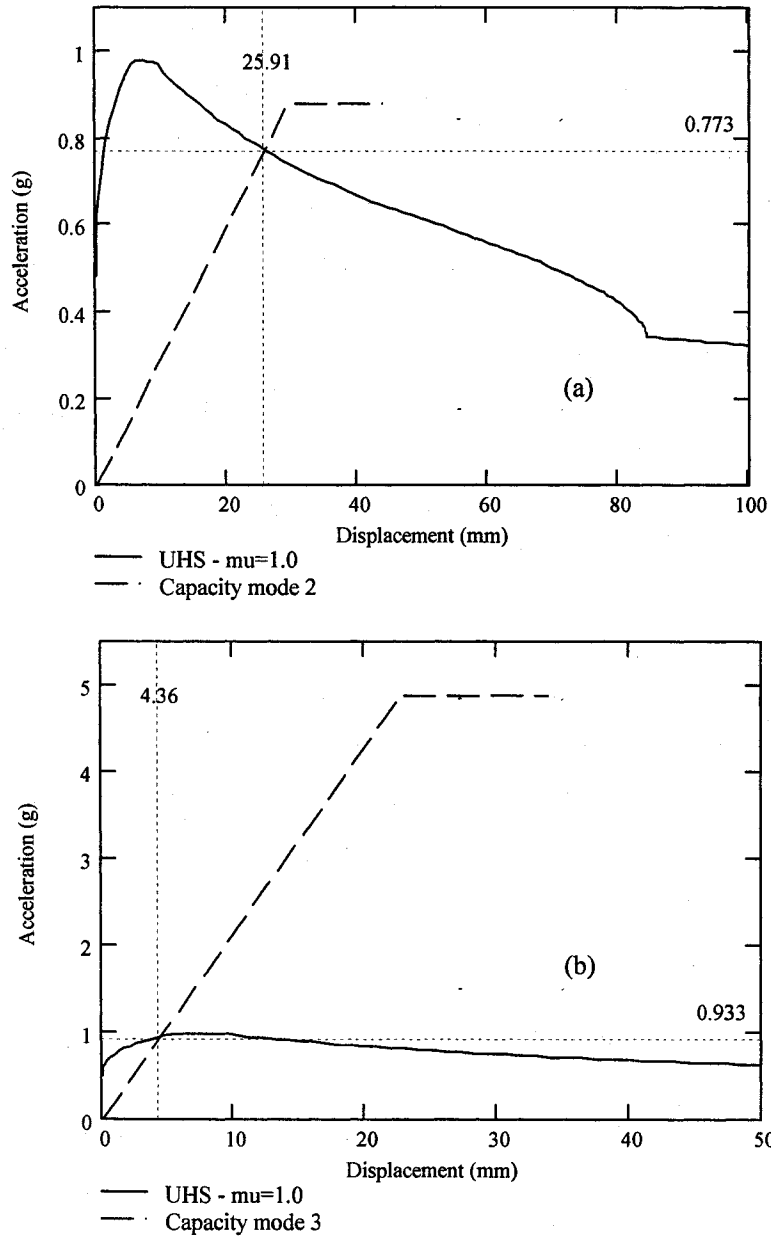


Figure 4.12: Capacity-demand diagrams for the final design of shear wall for the 6-storey building obtained by distributing the lateral forces according to (a) the second mode shape, and (b) the third mode shape

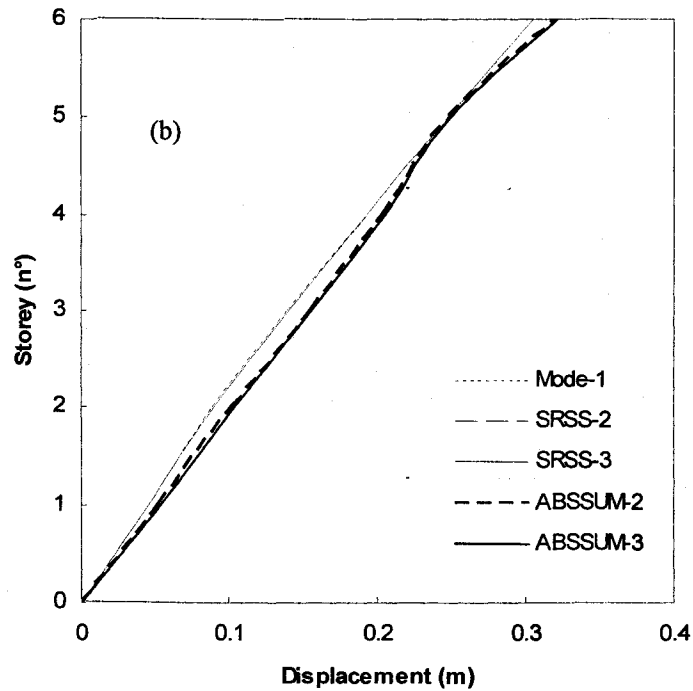
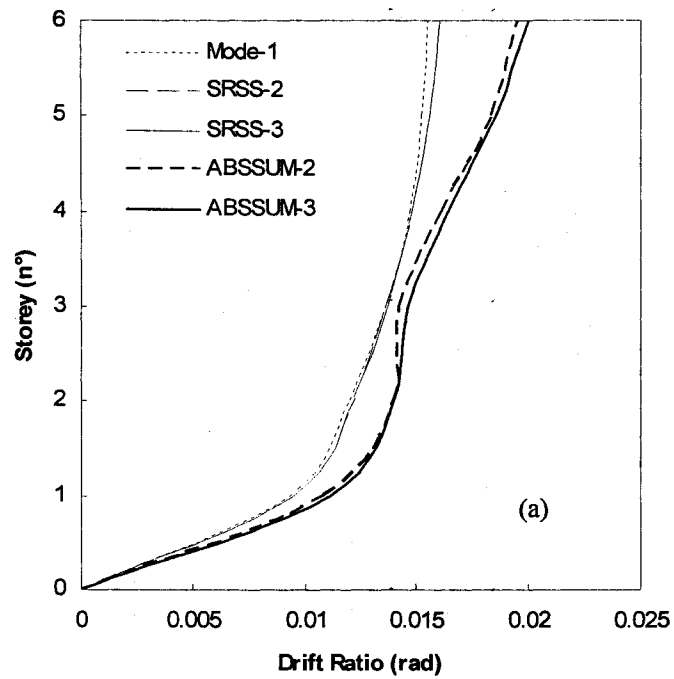


Figure 4.13: (a) Inter-storey drifts ratios and (b) displacements for the 6-storey building

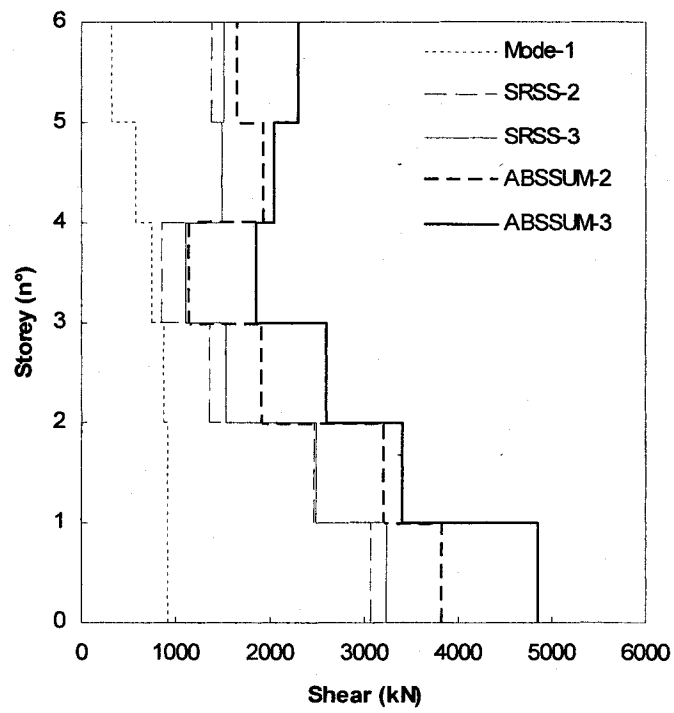


Figure 4.14: Shear forces for the 6-storey building

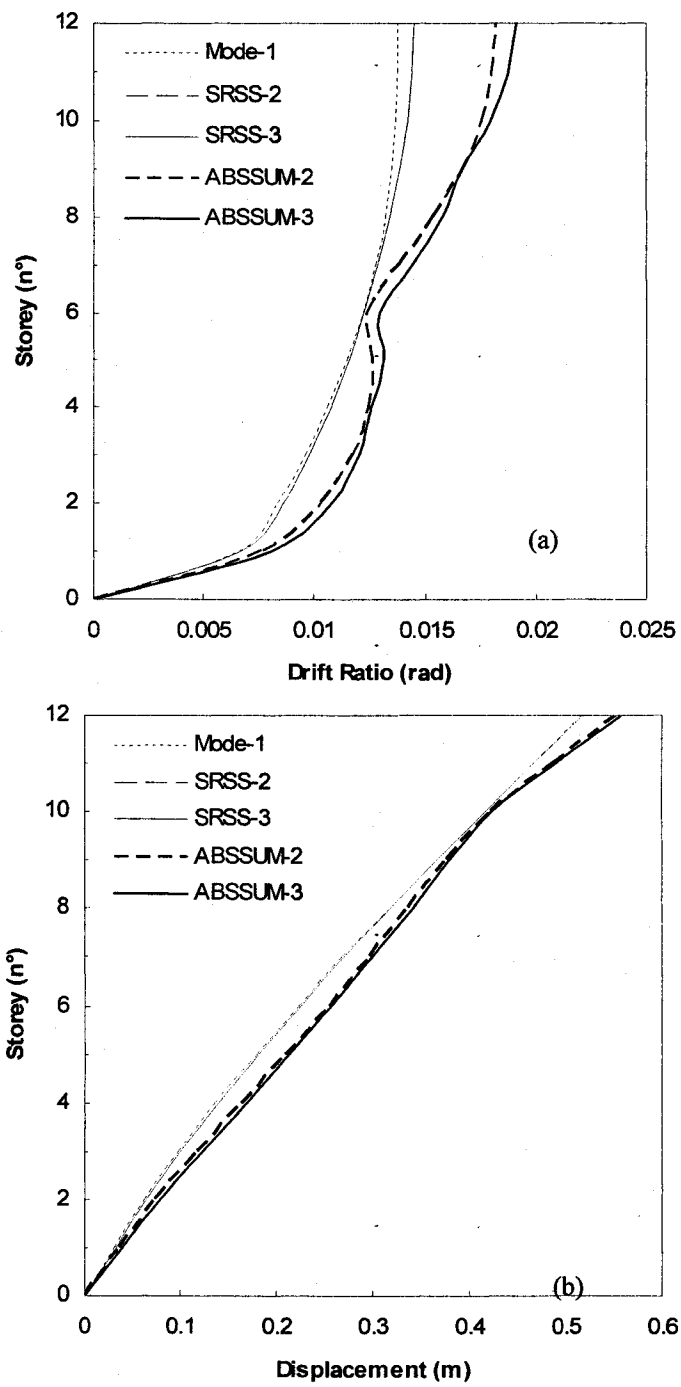


Figure 4.15: (a) Inter-storey drifts ratios and (b) displacements for the 12-storey building

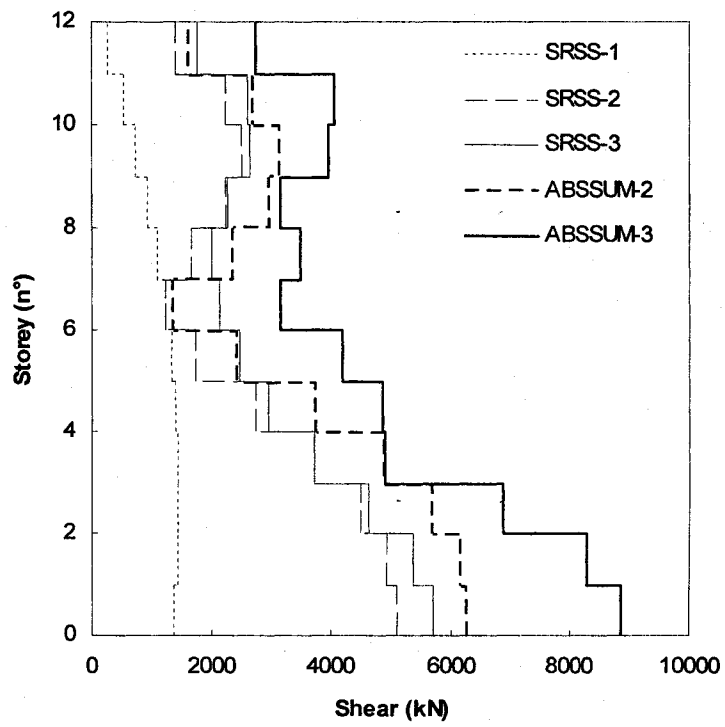


Figure 4.16: Shear forces for the 12-storey building

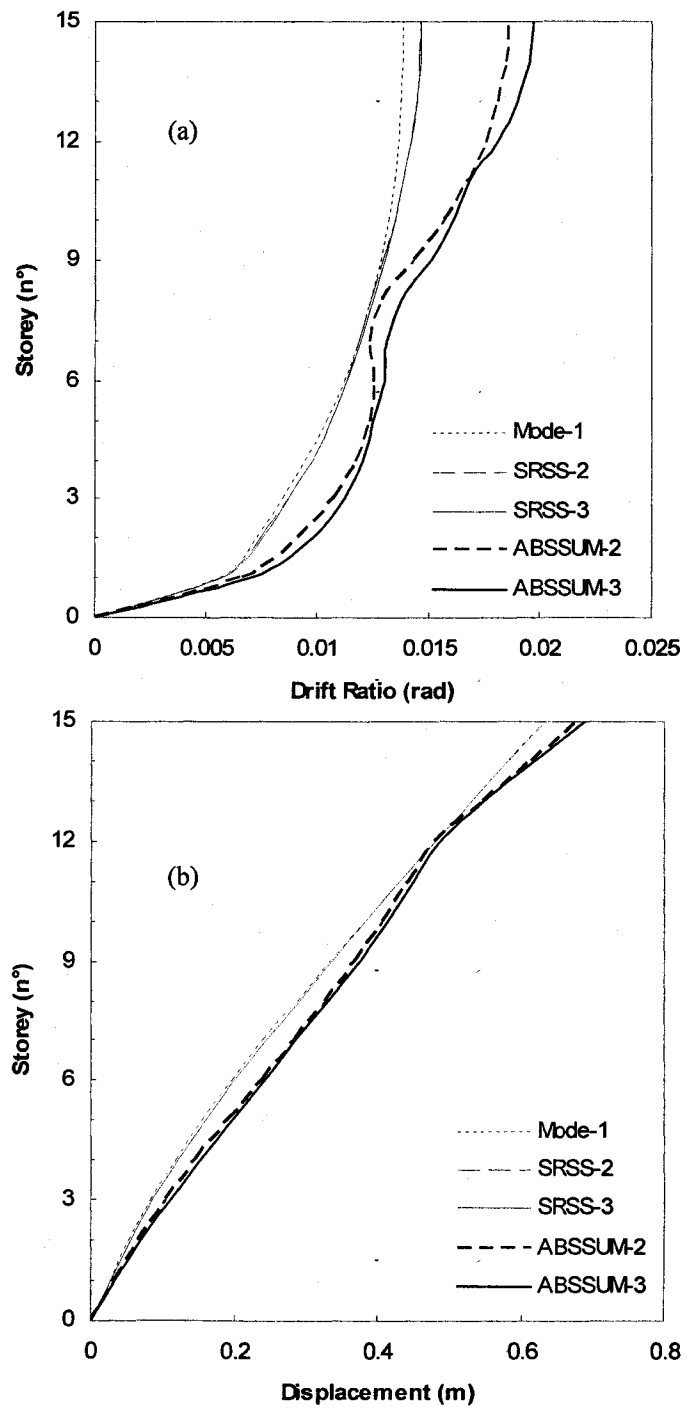


Figure 4.17: (a) Inter-storey drifts ratios and (b) displacements for the 15-storey building

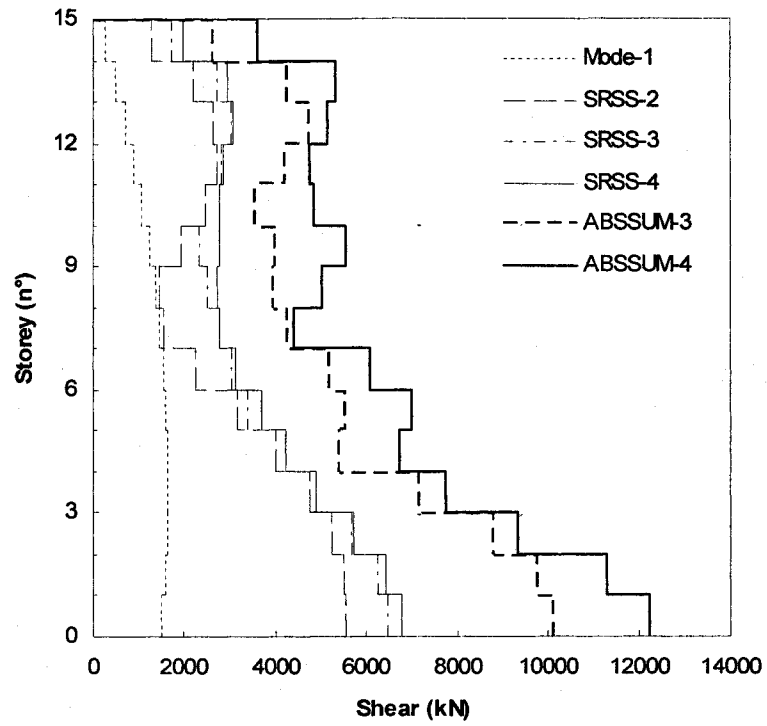


Figure 4.18: Shear forces for the 15-storey building

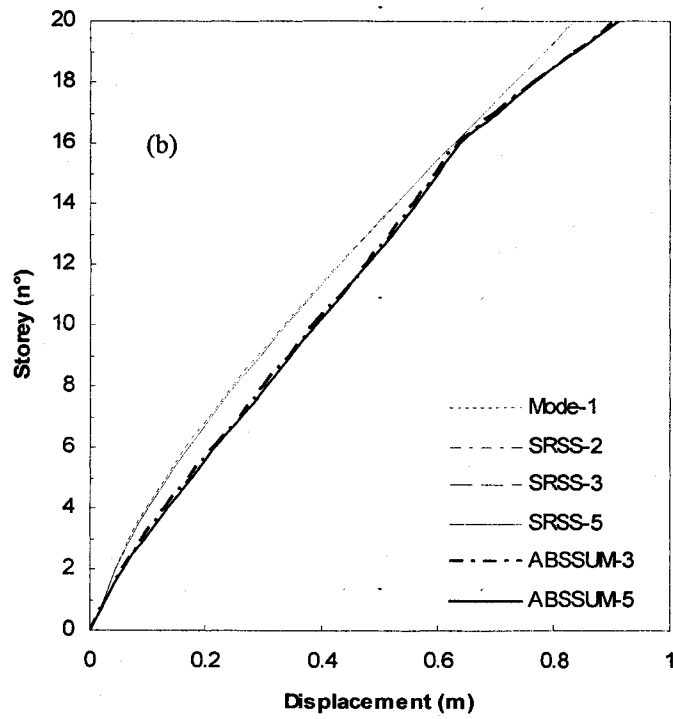
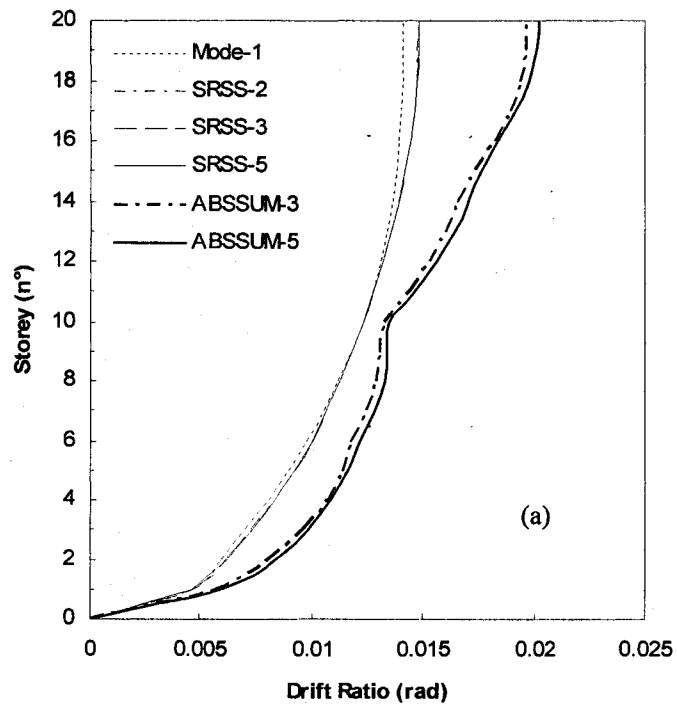


Figure 4.19: (a) Inter-storey drift ratios and (b) displacements for the 20-storey building

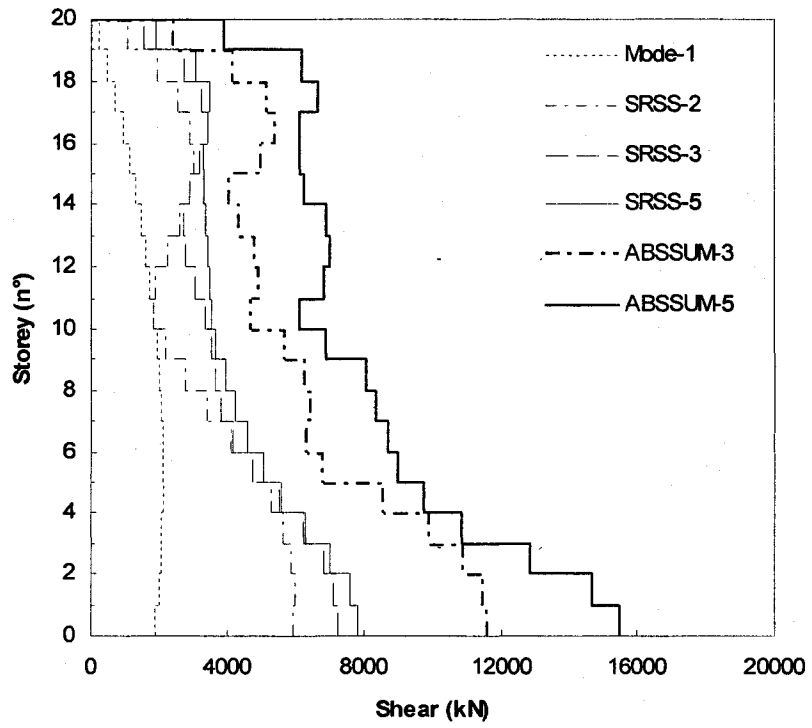


Figure 4.20: Shear forces for the 20-storey building

Chapter 5

Evaluation of the Displacement-based Seismic Design

5.1. Introduction

This chapter deals with an evaluation of the accuracy of displacement-based seismic design (DBSD) procedure presented in this thesis. The final responses obtained from the DBSD are compared with more “exact” solutions, such as those obtained from nonlinear response history analyses (RHA). The responses evaluated are maximum inter-storey drift ratios, maximum displacements and maximum shear forces for each of the buildings whose design has been presented in the previous chapter.

Two combination rules, square root of the sum of squares (SRSS) and absolute sum (ABSSUM), were used in the DBSD for several modal responses. This chapter will evaluate the accuracy of the solutions obtained with the two combination rules and the number of modes needed to obtain a more accurate solution when a multi-modal analysis is applied to the design.

The nonlinear RHA is based on input ground motions selected from the results and recommendations given in Chapter 2. In general, 10 pairs of ground motions, which are matched with UHS of Vancouver city assuming a site type C, are selected. Several results

are obtained from the analysis and processed statistically. The geometric mean and the 84th percentile are obtained with reference to the “exact” solutions.

The bias in the results obtained from the DBSD and RHA are presented along with a discussion on the results in the last two sections. The dispersions in the responses for the 20 ground motions are also shown. Opportunities for further research are pointed out.

5.2. Inelastic Systems

The shear wall buildings are modeled by frame elements, the base element being fixed at the bottom. The plastic hinge is expected to form at the base, although the analytical formulation allows the formation of a plastic hinge at either one or both ends of any element. The properties of the plastic hinge are obtained from the moment-curvature relationship of the final design. In the analysis every element is assumed to have cracked and to possess a reduced moment of inertia, as also assumed in the DBSD.

The nonlinear RHA is performed with the computer program DRAIN-2DX using a plastic hinge beam-column element (Type 02). This is a simple inelastic element which computes the properties from a pre-defined yield surface. In this case, a constant moment capacity is set at the base avoiding any interaction with the axial load that contributes to the P- Δ effect. The moment capacity is obtained from a moment-curvature analysis and takes into account the gravity induced axial load. This definition allows having an elasto-plastic model with a negative slope on the inelastic branch of the model.

One of the factors affecting the dynamic response is the definition of the damping properties of the structure. According to published literature (Chapter 11, Chopra 2004) higher modes are expected to have smaller damping ratios, ξ . On the other hand, in the DBSD the responses from higher modes are obtained from a UHS for a 5% damping. Therefore, to be consistent a Rayleigh damping is assumed with 5 % damping in the first and the fourth mode. Table 5.1 shows the mass and stiffness proportional coefficients used to define the Rayleigh damping.

5.3. Ground motions for Vancouver

In Chapter 2, 26 pairs of ground motions were collected, filtered and modified for matching with the UHS of Vancouver city. It was also recommended that at least 10 pairs of motions be used for nonlinear RHA in order to increase the confidence in the results. Therefore, 20 ground motions are finally selected considering the following criteria:

- Select ground motions from different sources and different events;
- Within the same event, select those with smaller scaling factors;
- Select the motions whose spectral shape is close to the target spectrum over the entire range of periods.

Table 5.2 summarizes this final selection showing the name of each earthquake and its year, the file or record name, the scaling factor, the time step, and number of points in the

record. This summary is shown in ascending order of the scaling factor. It must be recalled that this factor minimizes the square error between the spectral response of the average of two pairs (A and B) and the UHS for 4 different periods, namely 0.3, 1, 2 and 4 seconds (Somerville *et al.*, 1997). Thus, this factor ensures that higher modes are considered in the matching process.

5.4. Response statistics

In the elastic range if the response spectrum of each of the ground motions in a series matches a target spectrum, the responses of a given structure to the ground motions in the series would all be identical. However, this is not true of nonlinear responses, which may vary significantly from record to record. In addition, several simplifying assumptions are implied in DBSD. These factors may lead to significant variation between the responses obtained from nonlinear RHA and that provided by DBSD. The confidence with which the results of DBSD can be used depends on the quality of statistical variation between the two sets of results. The statistical parameters or estimators used here will follow the recommendations and theory put forward by Benjamin and Cornell (1970) which have also served as the reference for the research carried out by Chopra and Goel (2004a) and Shome *et al.* (1998).

The definition of estimators depends on the type of distribution expected for the solution or final response. It is common to use the lognormal probability law in civil engineering. Some of the applications of such distribution are: hydrological data, fatigue failures,

earthquake magnitudes, strength of plastic materials, yield stress in reinforcing bars, etc. This distribution was also assumed by Chopra and Goel (2004) and Shome *et al.* (1998) in analyzing the results of nonlinear RHA.

According to Benjamin and Cornell (1970) the best or the most logical estimators for a lognormal distribution are the geometric mean (position) and the standard deviation of the lognormal values (dispersion). The median or geometric mean, \tilde{X} is given by

$$\tilde{X} = \exp \left[\frac{\sum_{i=1}^n \ln(X_i)}{n} \right] \quad (5.1)$$

And the standard deviation, δ_x , is given by

$$\delta_x = \left[\frac{\sum_{i=1}^n [\ln(X_i) - \ln(\tilde{X})]^2}{n-1} \right]^{1/2} \quad (5.2)$$

An additional benchmark used to assess the data is the response represented by the 84th percentile, p_{84} . This benchmark is defined by

$$p_{84} = \tilde{X} \cdot \exp(\delta_x) \quad (5.3)$$

When one or more ground motions cause collapse of the structure, the position and dispersion of data are determined by a counting method proposed by Chopra and Goel (2004). This method consists of sorting the results in ascending order, considering the failing datum at the end, and when the number of data points is 20 obtaining the median as the average between the 10th and 11th data. The 84th percentile corresponds to the 17th value and the dispersion is thus obtained by subtracting the lognormal median from the lognormal 84th percentile. On the other hand, when one or more ground motions do not cause yield of the structure, and if is not possible to obtain plastic rotations the data corresponding to no yield condition are not considered in the statistical evaluation, but the event is reported.

The bias of the DBSD is finally deduced from the ratio between the responses obtained from the MPA and the position measures of the nonlinear RHA defined earlier. For each case being analyzed there will be two ratios since two positions are defined, geometric mean and 84th percentile. In either case, the DBSD will be biased toward underestimating the response when this ratio is less than one and overestimating the response when the ratio exceeds one.

5.5. Results

The final results from the response statistic of the nonlinear RHA are presented on this section. First, in order to evaluate the assumed lognormal distribution, four responses: roof displacement, maximum drift ratio, base shear, and base plastic rotation, are showed

in Figure 5.1 through Figure 5.4 for the 6, 12, 15 and 20-storey buildings. The position of the distribution is defined by the median obtained from Equation (5.1). These figures clearly show that the lognormal distribution as well as the geometric mean are good assumptions to describe the results obtained from the nonlinear RHA. The results also show the comparatively large variation in the results.

Results for each of the buildings or structures are separately presented here (from Figure 5.5 through Figure 5.8). Included also are the results obtained from the DBSD for two combination rules and several modes. For each structure, the variation of three responses over the height are presented: inter-storey drift ratio, displacement, and shear forces. Each response is plotted in two graphs: maximum responses (left hand side) and bias results (right hand side). The dispersion of the nonlinear RHA of the three responses is shown in Figure 5.9 for each building.

As stated earlier, four different response parameters are obtained: roof displacement, maximum drift ratio, base shear, and base plastic rotation. The response obtained from DBSD using the SRSS rule is divided by the corresponding response obtained from the nonlinear RHA to obtain the bias in the response. Bias results are presented in the form of histograms in Figure 5.10 through Figure 5.13. Each of these figures also show two vertical lines; the solid line indicates the position of unbiased result and the dashed line shows the median (geometric mean) of the bias values. The range over which the 20 data values vary is also shown. A detailed discussion of the results is presented in the following subsections.

5.5.1. Results for the 6-storey building results

The results for this building are presented in Figure 5.5 and Figure 5.9

5.5.1.1. Inter-storey drift ratios

The 1st level drift ratio has median and 84th percentile values of 0.008 and 0.015, respectively. The top level drift shows a median of 0.016 and a 84th percentile of 0.022. The drift ratios from the DBSD obtained by the SRSS rule closely follow the median response. The ABSSUM rule instead gives values that lie between the median and the 84th percentile. The bias results give a clear indication that the DBSD using both the SRSS and ABSSUM rules underestimates the response when compared with the 84th percentile, the bias values at the top level being 0.74 and 0.92, respectively. On the other hand, when compared with the median response, DBSD results using the SRSS rule are fairly unbiased with the bias value being 1.02 at the top level. The ABSSUM rule clearly overestimates the median response with a bias value at the top level being 1.27.

Minimum dispersion in the drift ratio is found at the top level, being 0.32, and the maximum is found at the base, being 0.57.

5.5.1.2. Displacements

Results of the two combination rules do not differ much from the median response, which has a value of 289 mm at the roof level. However, the 84th percentile value is 433 mm at

the roof. It is also clear from the bias results that the response is underestimated when compared to the 84th percentile, the bias at roof being 0.70 (SRSS) and 0.74 (ABSSUM). On the other hand, the results are almost unbiased with respect to the median, the bias values at the roof being 1.06 (SRSS) and 1.11 (ABSSUM).

The displacement has a dispersion of 0.41 at the roof level and 0.57 at the first level, which is obviously similar to the dispersion in the drift ratio response.

5.5.1.3. Shear Forces

The median and the 84th percentile responses for shear forces are fairly close. The first gives a base shear of 3,053 kN and the later gives 3,929 kN. The SRSS rule is close to the median response over the full height. On the other hand, the ABSSUM rule gives values that are even larger than the 84th percentile. The bias results clearly show that the responses obtained from the ABSSUM rule are larger than both the median and 84th percentile values, the bias value at the base being 1.23 and 1.59, respectively. On the contrary, the SRSS rule presents an almost unbiased response with a bias value of 1.06 at the base compared to the median response. This combination slightly underestimates the response when compared to the 84th percentile, the bias being 0.82 at the base.

Shear force dispersion varies between 0.12 and 0.33. In particular, the base shear dispersion is 0.25.

5.5.2. Results for the 12-storey building

The results for this building are presented in Figure 5.6 and Figure 5.9

5.5.2.1. Inter-storey drift ratios

The median response is characterized by a drift ratio of 0.005 and 0.012 at the 1st and top level, respectively. The 84th percentile values are 0.010 and 0.017 for the same two levels. The SRSS response lies between the median and 84th percentile while the ABSSUM follows the 84th percentile response. This can also be seen on the bias results, where the ratio between the ABSSUM and the 84th percentile is almost 1 over the entire height. Obviously, the ABSSUM rule is conservative in its predictions having a bias of 1.56 at the top level with respect to the median. The SRSS rule gives biased results with respect to both measures; overestimating the response (bias at the top level of 1.18) with respect to the median and underestimating the response (bias at the top level of 0.84) compared with the 84th percentile.

Drifts from 1st through 8th level show comparatively large dispersion, the maximum being at the first level with a value of 0.73. The minimum dispersion is at the top level, being 0.34.

5.5.2.2. Displacements

This roof displacement has a median value of 377 mm and an 84th percentile value of 622 mm. The SRSS and ABSSUM combination rules give responses that lie between the median and the 84th percentile, the ABSSUM rule being closer to the 84th percentile. The bias values clearly show that both the SRSS and the ABSSUM rules overestimate the response when compared with the median value, the bias at the top level being 1.38 and 1.48, respectively. On the contrary, both rules underestimate the response when compared to the 84th percentile with bias values at the roof being 0.83 (SRSS) and 0.90 (ABSSUM).

Dispersion is roughly constant above the 4th level, with a minimum value of 0.50 at the roof. The maximum dispersion is seen at the first level, being 0.73.

5.5.2.3. Shear Forces

The maximum value of the shear is at the base, being 5,843 kN and 7,330 kN for the median and 84th percentile response, respectively. The ABSSUM rule response is larger than the 84th percentile response, while the SRSS rule response is very close to the median response. The bias values confirm this last statement; The ABSSUM rule overestimates the median as well as the 84th percentile responses, with bias ratios of 1.52 and 1.21, respectively. However, the SRSS rule response underestimates the 84th percentile response with a bias value of 0.78 and is practically unbiased with respect to the median response, the bias being 0.98 at the base.

Dispersion is found to vary between 0.14, at the 8th level, and 0.31, at the top level. Base shear has a dispersion of 0.23.

5.5.3. Results for the 15-storey building

The results for this building are presented in Figure 5.7 and Figure 5.9

5.5.3.1. Inter-storey drift ratios

The median responses at the 1st and top levels are 0.004 and 0.012, respectively. The 84th percentile drift at the 1st level is 0.008 and at the top level it is 0.016. The SRSS rule gives results that lie between the median and 84th percentile responses, being slightly closer to the 84th percentile. The ABSSUM rule follows the same pattern over the first nine levels as the 84th percentile. Above the ninth level the ABSSUM values are somewhat larger than the 84th percentile. These observations are confirmed by the bias results which show that the SRSS rule is biased toward underestimating the response with respect to the 84th percentile, the bias being 0.90 at the top level, and overestimating the response with respect to the median, the bias being 1.19 at the same level. The ABSSUM is practically unbiased for the first nine levels with respect to the 84th percentile but overestimates the response at upper levels with a value at the top of 1.21. The ABSSUM also overestimates the drift with respect to the median response, the bias being 1.59 at the top level.

Dispersions at levels 7 and lower are somewhat high, the value at the base being 0.74. The minimum dispersion is found to be at the top level and is 0.27.

5.5.3.2. Displacements

The ABSSUM rule follows almost the same pattern as the 84th percentile response, while the SRSS rule gives results that lie between the median and the 84th percentile with a clear tendency to be closer to the 84th percentile response. The 84th percentile response presents a value of 720 mm at the roof while the median is 473 mm. The bias results show little bias results between the ABSSUM rule response and the 84th percentile, the bias being 0.96 at the roof. The SRSS rule underestimates the 84th percentile, with a bias value of 0.88 at the roof. Both combination rules clearly overestimate the response with respect to the median, with bias values of 1.34 (SRSS) and 1.46 (ABSSUM) at the roof.

The dispersion for the lower floors (from 1st through 6th) is quite large with a value of 0.74 at the first storey. Above level 6, an almost constant dispersion exists with a minimum value of 0.42 at the roof.

5.5.3.3. Shear Forces

The median base shear is 6,377 kN and the 84th percentile is 7,812 kN. In this case the first four modes are included in the MPA and the SRSS rule response is close to the median response, while the ABSSUM is larger than the 84th percentile response. Bias results show that the SRSS results are almost unbiased with respect to the median

response, with a bias value of 1.06 at the base. However, the SRSS rule underestimates the response when compared to the 84th percentile, with a bias value of 0.87 at the base. The ABSSUM rule clearly overestimates both the median and 84th percentile responses, with bias values of 1.92 and 1.56 at the base, respectively.

The minimum dispersion is found to be at the 10th level, its value being 0.16 while the maximum is 0.27 at the top level. Base shear has a dispersion of 0.34.

5.5.4. Results for the 20-storey building

The results for this building are presented in Figure 5.8 and Figure 5.9

This building was the only one that experienced no yielding under the excitation from one input ground motion. The structure was designed to resist a base moment of 118,500 kNm before developing plastic deformation. However, this building experienced a base moment of only 115,800 kNm when subjected to the VAN12B input ground motion. Clearly, the structure remained elastic and no plastic rotation took place. Also, this building developed only limited amount of plastic deformation under several other input ground motions. This fact will be reflected in the following results.

5.5.4.1. Inter-storey drift ratios

The median inter-storey drifts at the 1st and top levels are 0.003 and 0.011, respectively, while the 84th percentile values are 0.004 and 0.013, respectively. Both combination rules

give responses that are larger than the 84th percentile response. The bias ratios with respect to the median are 1.40 (SRSS) and 1.86 (ABSSUM) at the top level. The bias results are conservative even when compared to the 84th percentile, with bias values of 1.15 (SRSS) and 1.53 (ABSSUM).

Maximum dispersion exists at the 1st and 2nd levels with values of 0.51 and 0.37, respectively. Above the 2nd level and upto the 9th level, dispersion is almost constant with a value of 0.33 at the 9th level. Dispersion above the 9th level decreases over the height, reaching its minimum at the top level, being 0.20.

5.5.4.2. Displacements

Maximum displacement is experienced at the roof with a median value of 448 mm and an 84th percentile value of 621 mm. Results of DBSD using either combination rule are larger than the 84th percentile response. In other words, the SRSS and ABSSUM rules overestimate both the median and 84th percentile responses. When compared to the median response, the bias values at the roof are 1.86 (SRSS) and 2.03 (ABSSUM). The results obtained from both combination rules are conservative even with respect to the 84th percentile, with roof level bias values of 1.35 (SRSS) and 1.46 (ABSSUM).

The first storey has the maximum dispersion with a value of 0.51. Above the 3rd level, dispersion is fairly constant, with a minimum value of 0.33 at the roof.

5.5.4.3. Shear Forces

The base shear has a median value of 8,537 kN and an 84th percentile value of 10,017 kN. In this case the first five modes are included in the MPA and the SRSS is close to the median response. The ABSSUM rule response gives very large values over the entire height, even larger than the 84th percentile. The bias shows a clearly overestimated response when the ABSSUM rule is used, with bias values at the base of 1.55 and 1.82 when compared to the median and 84th percentile, respectively. On the other hand, the SRSS rule shows an underestimated response when compared to both the median and the 84th percentile, with bias values at the base of 0.92 and 0.78, respectively.

Maximum dispersion is found at 11th level, being 0.28, while the minimum is at the 1st, being 0.16.

5.5.5. Summary of results for different response parameters

The following discussion refers to the results presented in Figure 5.10 through Figure 5.13. Those results are based on a DBSD procedure that used the SRSS combination rule.

5.5.5.1. Roof displacement

The median values of bias are always larger than one, which indicates that the DBSD is biased toward overestimating the roof displacement. Two extreme values of the median

bias are 1.06 for the 6-storey building and 2.90 for the 20-storey building. For the 6-storey building many records give bias values less than one, while for the 20-storey building all records show bias larger than one. The other two buildings, 12 and 15-storey, have almost similar results. The median bias values are 1.38 and 1.34 for the 12 and 15-storey buildings, respectively, indicating that DBSD tends to overestimate the roof displacements for these buildings.

Results for 12, 15 and 20-storey buildings are significantly affected by extreme values. These buildings have bias results greater than 2 for significant number of records. On the other hand, the 6-storey building present bias values less than 2 for every record, and the results are clearly grouped within the central range of the distribution. In general, bias results for roof displacements are grouped towards values larger than one for taller buildings. The dispersion shows considerable increase as the height increases from 6 storeys to 20 storeys.

5.5.5.2. Maximum inter-storey drift ratio

The median values of the bias are larger than unity in every case, which means that the DBSD also overestimates the maximum drift response. The two extreme values of median bias come from the 6 and 20-storey buildings, with values of 1.02 and 1.59, respectively. Again, for the 20-storey building all records show a bias larger than one. The other two buildings, 12 and 15-storey, show almost similar bias, the median values being 1.18 and 1.19, respectively.

The 20-storey building is characterized by central values while other buildings have most of their results grouped on the right-hand side. There are no extreme values that may affect this response and most of the bias values are less than 2. The largest variability is seen in the 12-storey building, although the dispersion for this response is small. In general, results are grouped within bias values larger than one for taller buildings and mostly concentrated within a range of 1.0 and 2.0.

5.5.5.3. Base shear

Median bias values are similar for all buildings. The 6 and 15-storey building have median bias values larger than one, being 1.06 in both cases. The 12-storey building has a bias value of 0.98; the 20-storey building has the most unconservative result with a bias of 0.92.

In all cases the results are concentrated within the region of the unbiased values, i.e. close to one. Dispersion is comparatively small in this response; the largest range being for the 6-storey building.

5.5.5.4. Base plastic rotation

Median bias value is larger than one in every case. The minimum median bias is 1.24 for the 6-storey building and the maximum is 2.25 for the 20-storey building. The 12 and 15-storey buildings have median bias values of 1.69 and 1.89, respectively. These median values indicate that the DBSD overestimates the base plastic rotation in each case.

Results of the bias are very much affected by extreme values. These extreme values indicate that the structures behave almost elastically, with small plastic deformations for some of the input ground motions. This fact also increases the dispersion, the largest range being for the 20-storey building.

5.6. Comments on results

The results of comparison between DBSD and nonlinear RHA for each building show that the ABSSUM rule considerably overestimates the responses, the most conservative results being for the shear forces. The shear forces are larger than the 84th percentile response when the ABSSUM rule is used. The inter-storey drift ratios are also considerably conservative when this combination rule is used. The ABSSUM values are always close to or larger than the 84th percentile drift ratios. Displacements obtained from the ABSSUM rule also overestimate the displacements, particularly for taller buildings, but this is also the case when the response is obtained from the SRSS rule.

The SRSS rule always overestimates the drift ratio and displacement responses when compared to the median response. The most interesting results are seen in the analysis of the 20-storey building which is a very flexible structure that develops very small plastic deformations under many records. This behavior, in which the response is almost elastic, affects the overall results obtained from nonlinear RHA leading to an overestimation of the response. Thus, drifts and displacements for the 20-storey building obtained from DBSD are quite conservative when compared to those obtained from nonlinear RHA. The

shear response for every building is always well estimated by DBSD using the SRSS rule. One plausible reason of these contradictory results between displacements and force responses is the contribution of higher modes to the response. According to the MPA, the higher modes make substantial contribution to the shear response while the displacement and drift responses are governed only by the first mode. For the flexible buildings the first mode period is fairly long and the spectral accelerations corresponding to such long periods may be quite small for some of the records.

The higher mode effect on the shear response is clearly indicated by the nonlinear RHA. The number of modes that should be included in DBSD is related to the number of storeys in the building. According to the results from Chapter 4 and this study, including 3 modes in the response gave fairly good results for the 6 and 12-storey building. For the 15 and 20-storey buildings, inclusion of 4 and 5 modes in the total response provided reasonable results.

Most of the median responses obtained from the nonlinear RHA are less than those obtained from the DBSD. The roof displacement and maximum drift ratio obtained from DBSD are in most cases higher than the median response and only for few records the response is underestimated. The base shear obtained from DBSD is very close to the median response for each building. However, in most cases the base shears obtained from RHA are smaller than those obtained from DBSD. The plastic rotation at the base has a median response that is always smaller than that obtained from DBSD and the difference increases for taller buildings.

The dispersion in responses does not vary much among the different buildings. However, the dispersion is very different depending on the type of response. The minimum dispersion is seen in the shear responses and the maximum in the displacement responses. The dispersions for plastic rotation responses are quite large. In many cases, the structure remains almost elastic or has small plastic deformations which gives very extreme values in the statistical process. These extremes values clearly affect the dispersion of the result.

In conclusion, it can be stated on the basis of results presented here that the suggested DBSD procedure provides a reliable and simple approach to design of shear structures. The estimates of displacements and inter-storey drifts provided by DBSD are always higher than the median values obtained from nonlinear RHA of the structure for a suite of UHS compatible ground motions. The shears and forces obtained from DBSD are near the median of RHA values.

Table 5.1: Rayleigh damping coefficients for 6, 12, 15 and 20-storey buildings

| Number of storeys | First mode Period $\xi=5\%$ | Fourth mode Period $\xi=5\%$ | Mass Proportional Coefficient | Stiffness Proportional Coefficient |
|-------------------|-----------------------------|------------------------------|-------------------------------|-------------------------------------|
| N ^o | T ₁ (s) | T _m (s) | a ₀ | a ₁ (x10 ⁻³) |
| 6 | 2.337 | 0.0751 | 0.260486 | 1.15804 |
| 12 | 3.730 | 0.1160 | 0.163369 | 1.79051 |
| 15 | 4.744 | 0.1436 | 0.128554 | 2.21832 |
| 20 | 6.144 | 0.1821 | 0.099322 | 2.81479 |

Table 5.2: Final selection of 20 ground motions for the city of Vancouver

| Number of Record | Earthquake | Record | Scaling Factor | Time Step | Number of Points |
|------------------|--------------------|--------|----------------|----------------|------------------|
| N ^o | Name (year) | Name | α_{sm} | Δt (s) | N ^o |
| 1 | Tokachi Oki (2003) | VAN01a | 0.99 | 0.010 | 15709 |
| 2 | Tokachi Oki (2003) | VAN01b | 0.99 | 0.010 | 15709 |
| 3 | Olympia (1949) | VAN03a | 1.65 | 0.020 | 4454 |
| 4 | Olympia (1949) | VAN03b | 1.65 | 0.020 | 4454 |
| 5 | Tokachi Oki (2003) | VAN04A | 1.67 | 0.010 | 18509 |
| 6 | Tokachi Oki (2003) | VAN04B | 1.67 | 0.010 | 18509 |
| 7 | Nisqually (2001) | VAN09A | 3.32 | 0.010 | 17900 |
| 8 | Nisqually (2001) | VAN09B | 3.32 | 0.010 | 17900 |
| 9 | Nisqually (2001) | VAN12A | 3.88 | 0.010 | 20600 |
| 10 | Nisqually (2001) | VAN12B | 3.88 | 0.010 | 20600 |
| 11 | Nisqually (2001) | VAN15A | 4.19 | 0.010 | 20500 |
| 12 | Nisqually (2001) | VAN15B | 4.19 | 0.010 | 20500 |
| 13 | Nisqually (2001) | VAN16A | 4.47 | 0.010 | 48001 |
| 14 | Nisqually (2001) | VAN16B | 4.47 | 0.010 | 48001 |
| 15 | Nisqually (2001) | VAN19A | 4.68 | 0.010 | 94800 |
| 16 | Nisqually (2001) | VAN19B | 4.68 | 0.010 | 94800 |
| 17 | Puget Sound (1965) | VAN23a | 4.75 | 0.020 | 3706 |
| 18 | Puget Sound (1965) | VAN23b | 4.75 | 0.020 | 3706 |
| 19 | Nisqually (2001) | VAN25A | 4.83 | 0.010 | 48001 |
| 20 | Nisqually (2001) | VAN25B | 4.83 | 0.010 | 48000 |

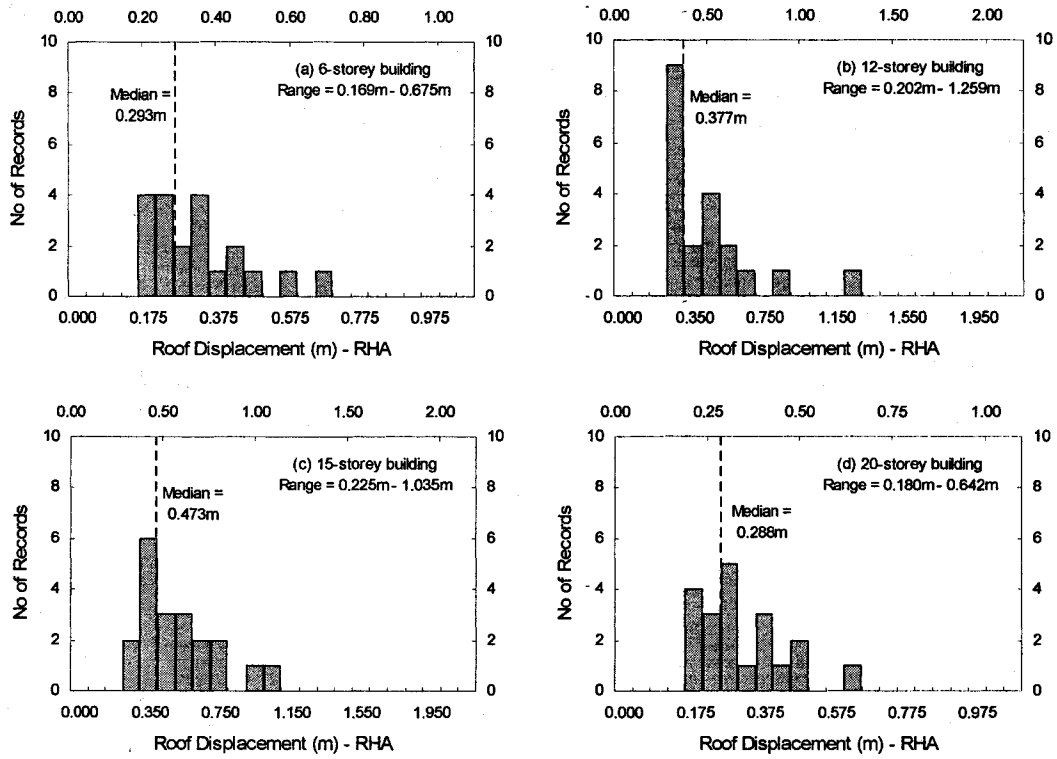


Figure 5.1: Histograms of the roof displacements obtained from nonlinear RHA of the 6, 12, 15, 20-storey buildings

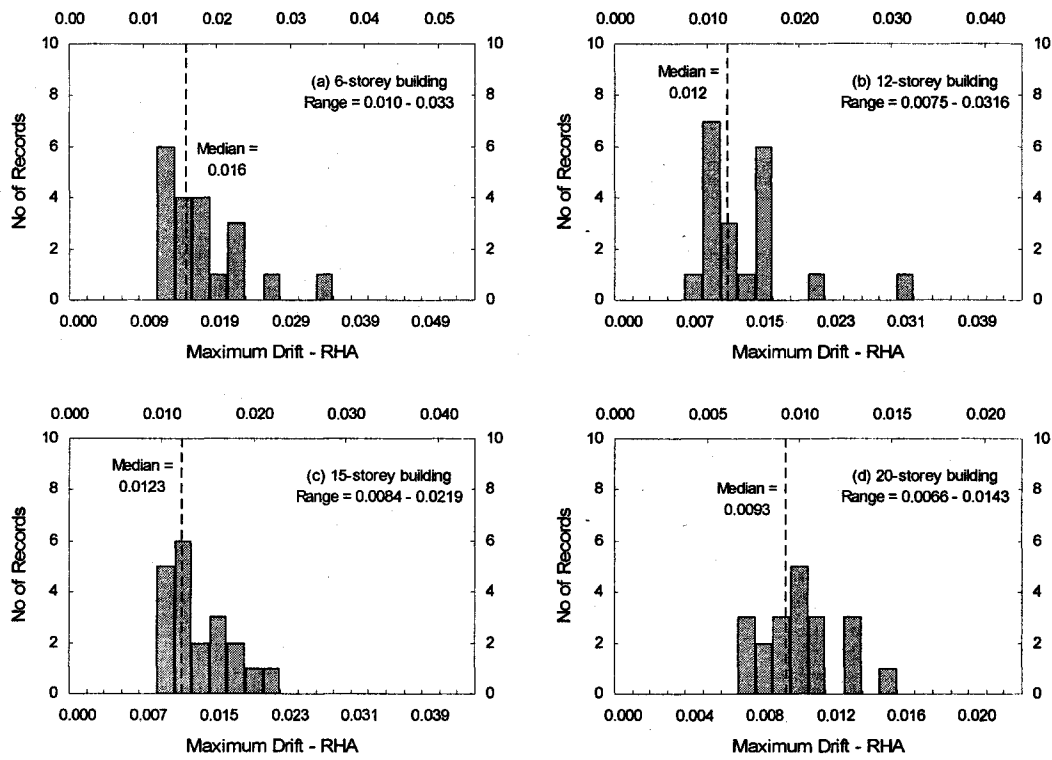


Figure 5.2: Histograms of the maximum inter-storey drift ratios obtained from nonlinear RHA of the 6, 12, 15, 20-storey buildings

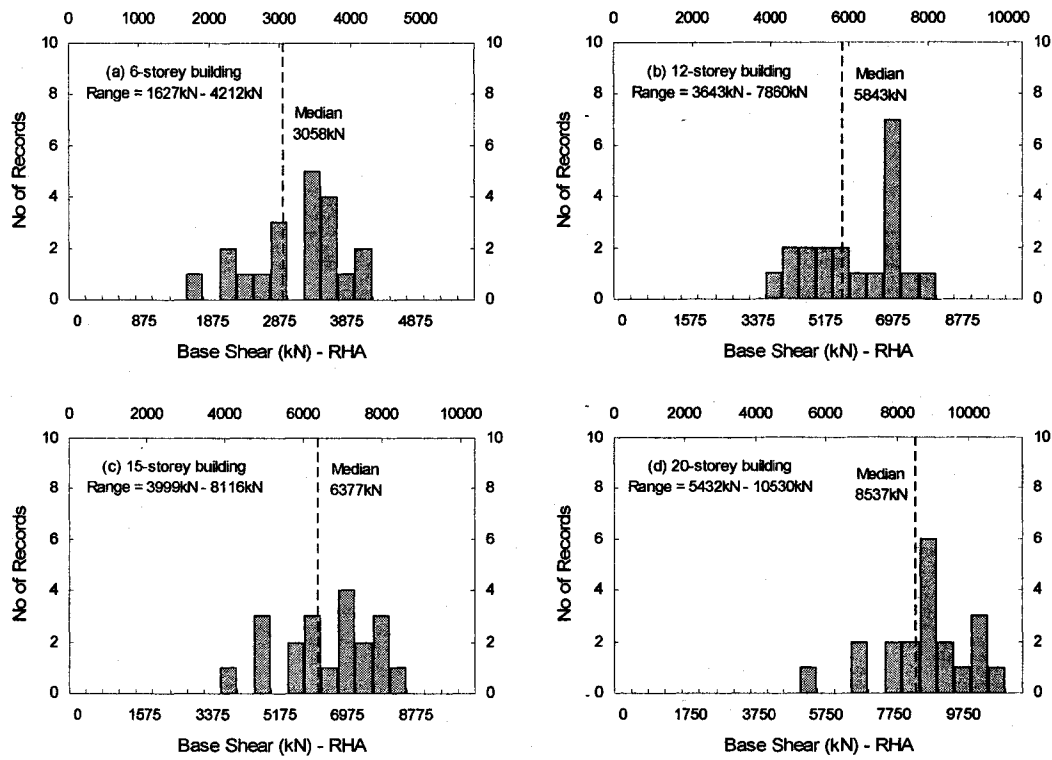


Figure 5.3: Histograms of the base shears obtained from nonlinear RHA of the 6, 12, 15, 20-storey buildings

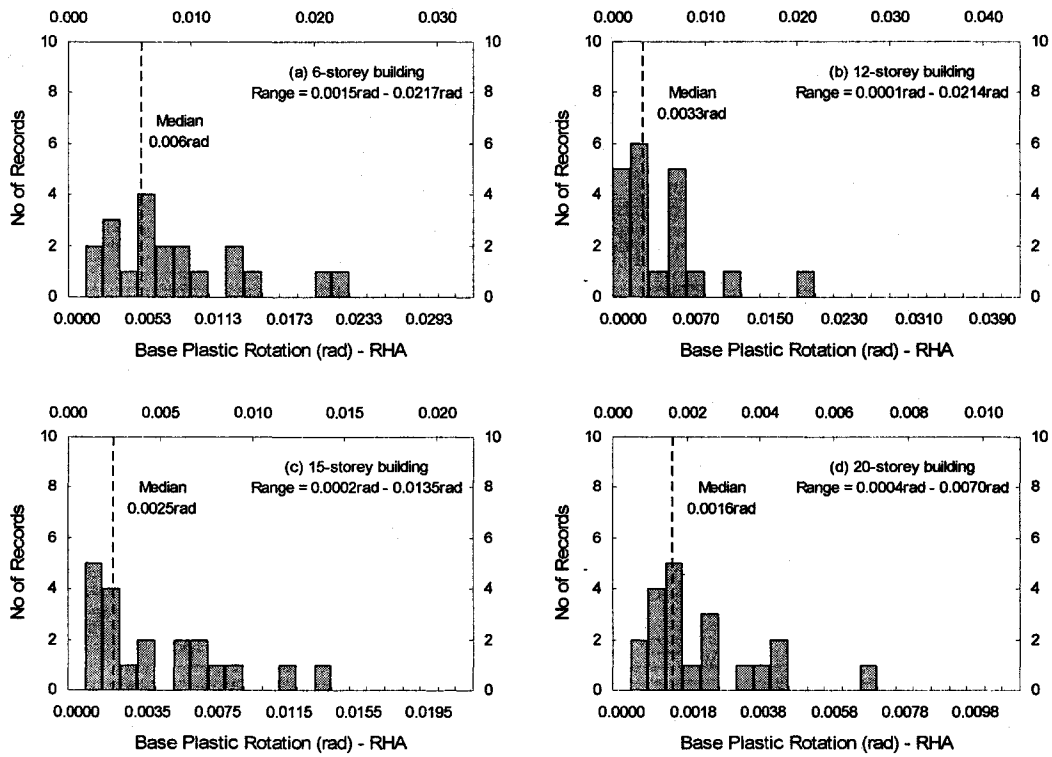


Figure 5.4: Histograms of the base plastic rotations obtained from nonlinear RHA of the 6, 12, 15, 20-storey buildings

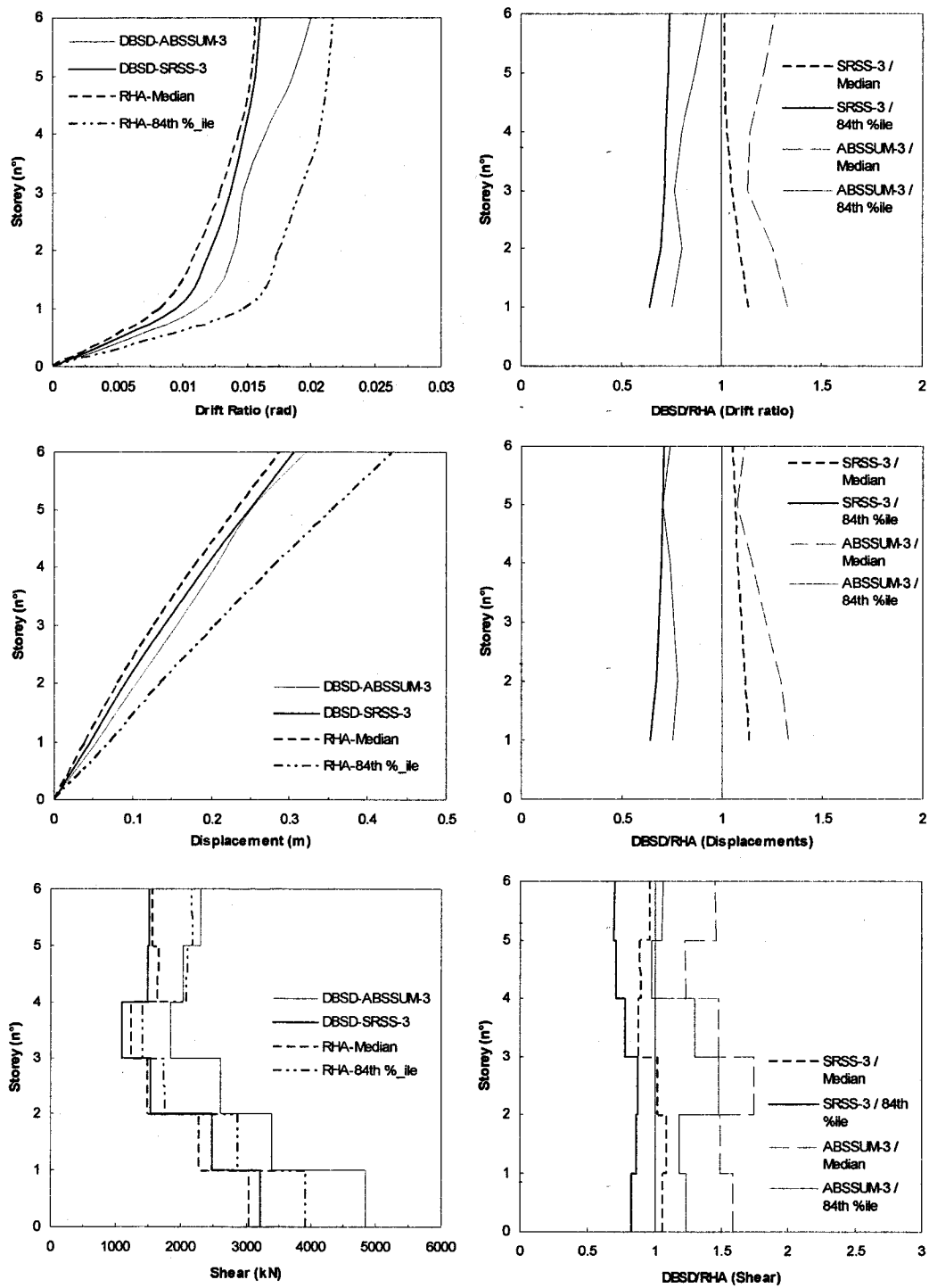


Figure 5.5: Nonlinear RHA results and DBSD/RHA ratio for story drift ratios (top), displacements (middle), and shear forces (bottom) in the 6-storey building

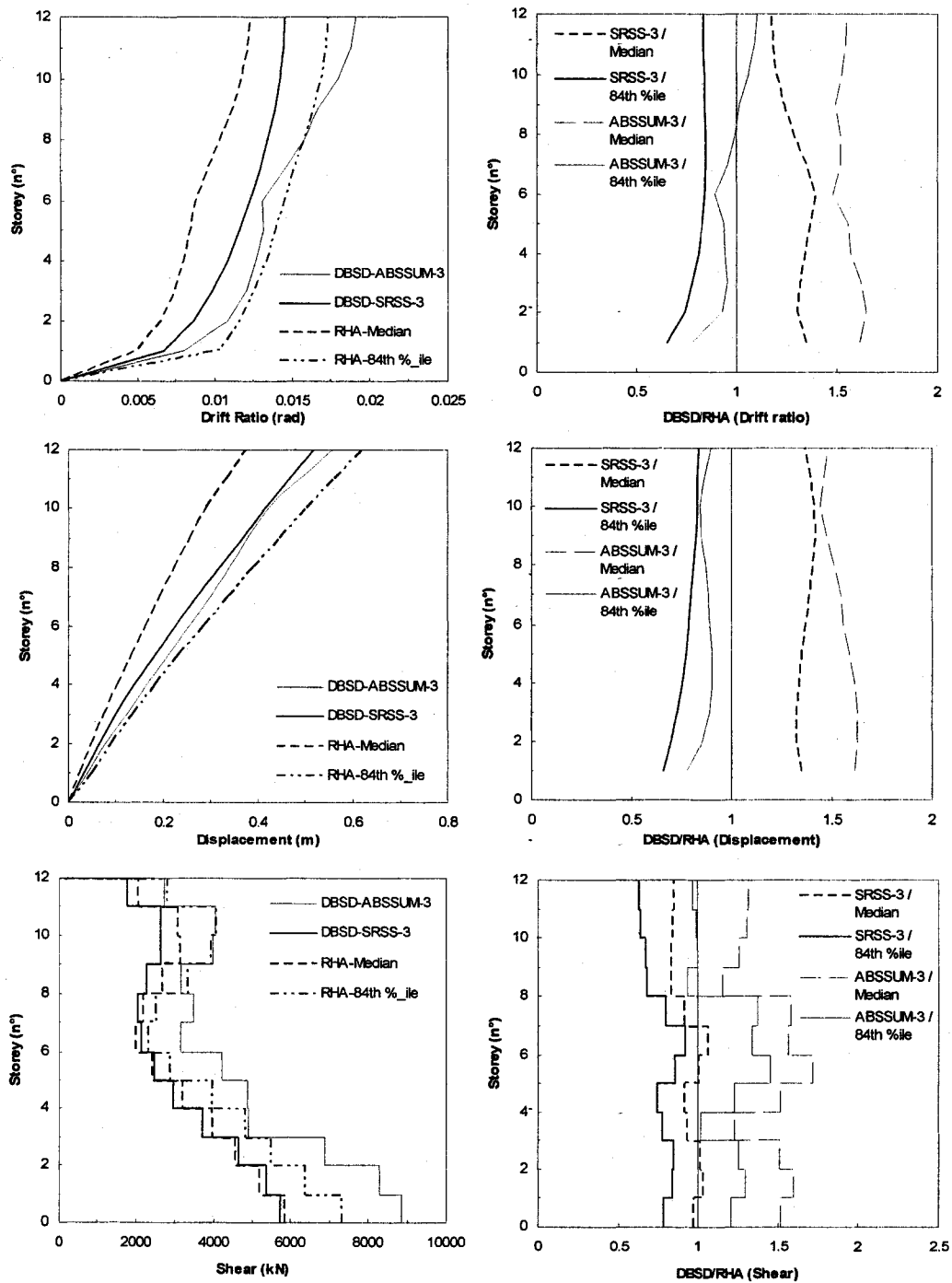


Figure 5.6: Nonlinear RHA results and DBSD/RHA ratios for story drift ratios (top), displacements (middle), and shear forces (bottom) in the 12-storey building

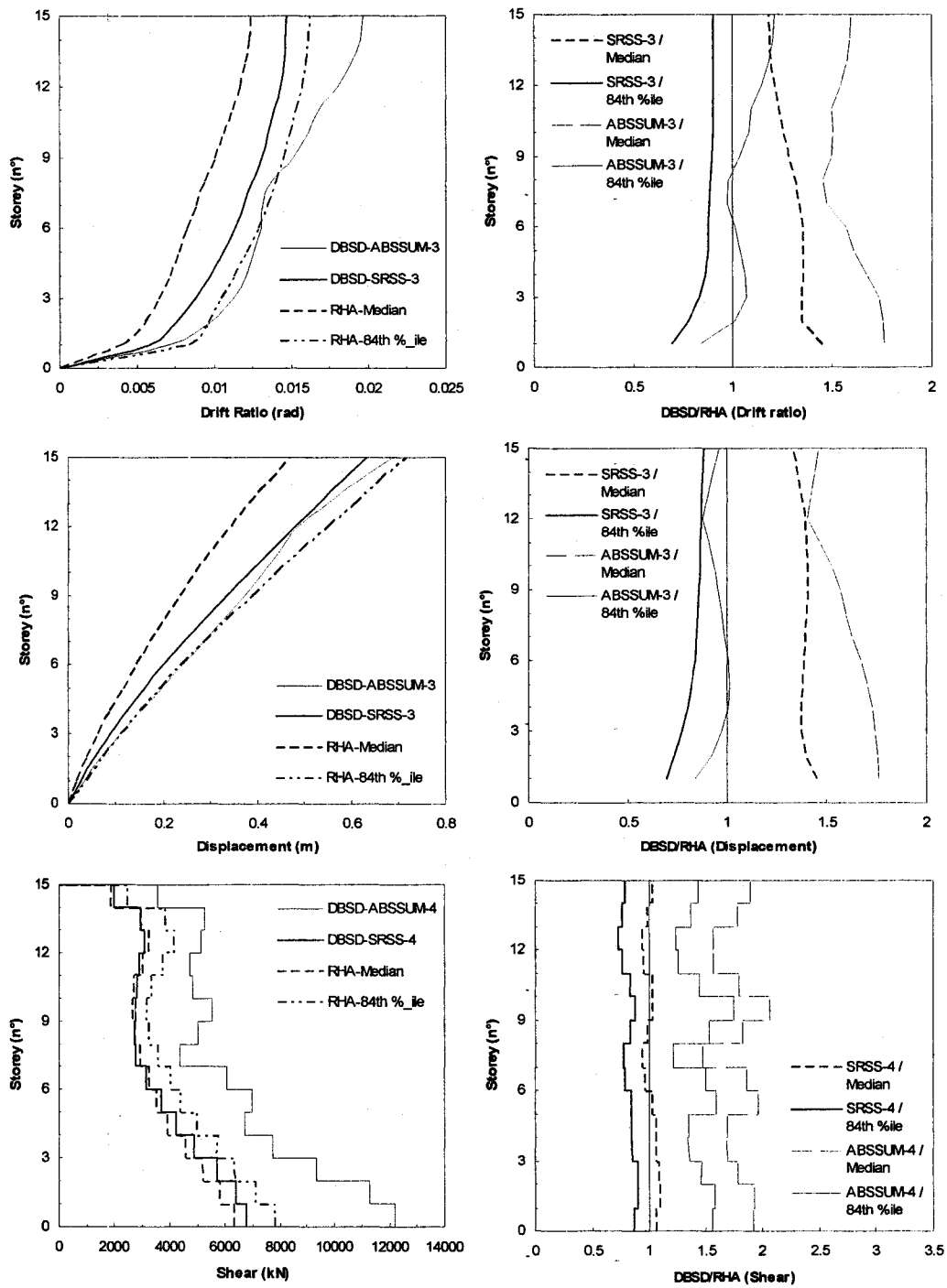


Figure 5.7: Nonlinear RHA results and DBSD/RHA ratios for story drift ratios (top), displacements (middle), and shear forces (bottom) in the 15-storey building

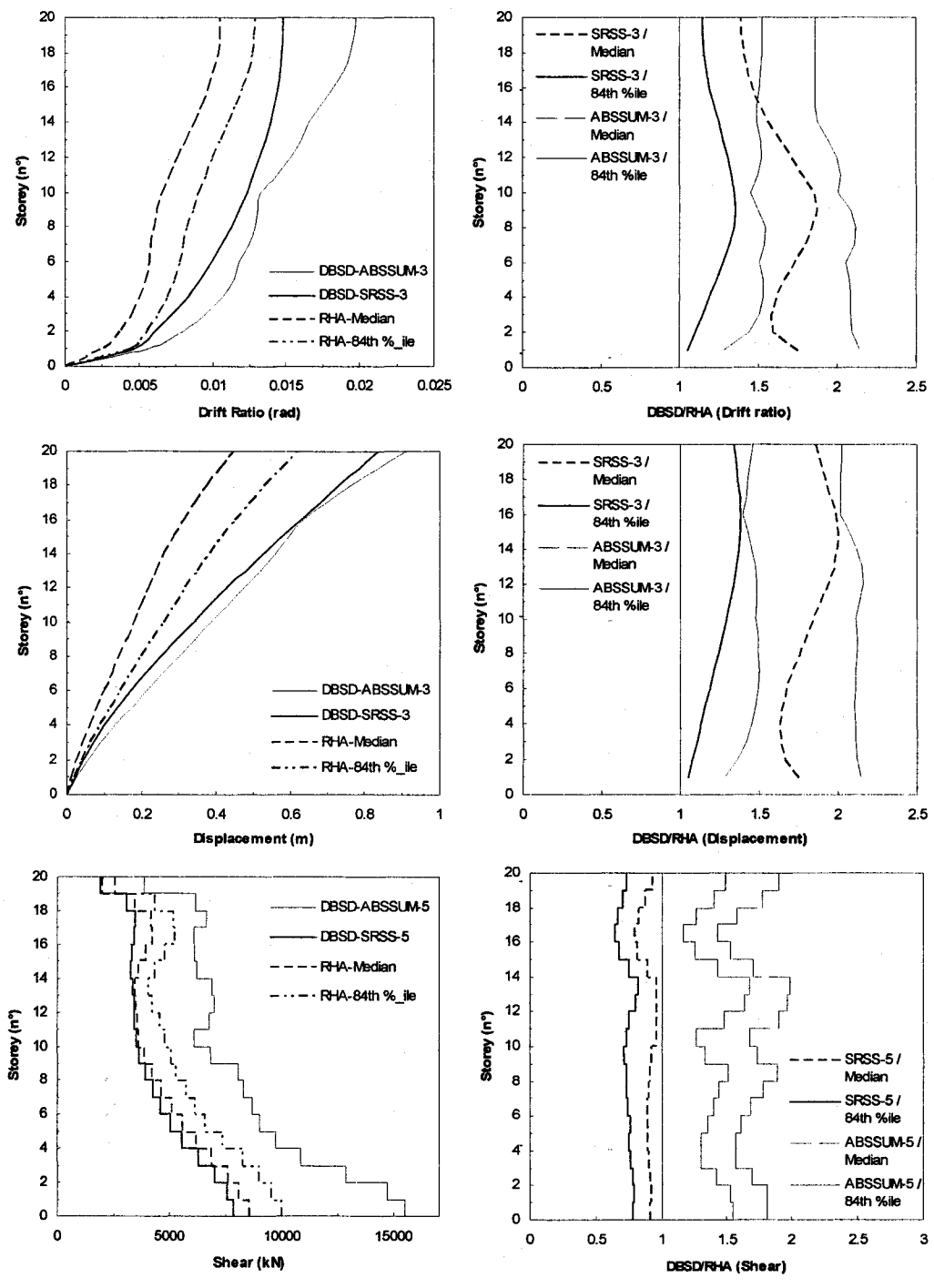


Figure 5.8: Nonlinear RHA results and DBSD/RHA ratios for story drift ratios (top), displacements (middle), and shear forces (bottom) in the 20-storey building

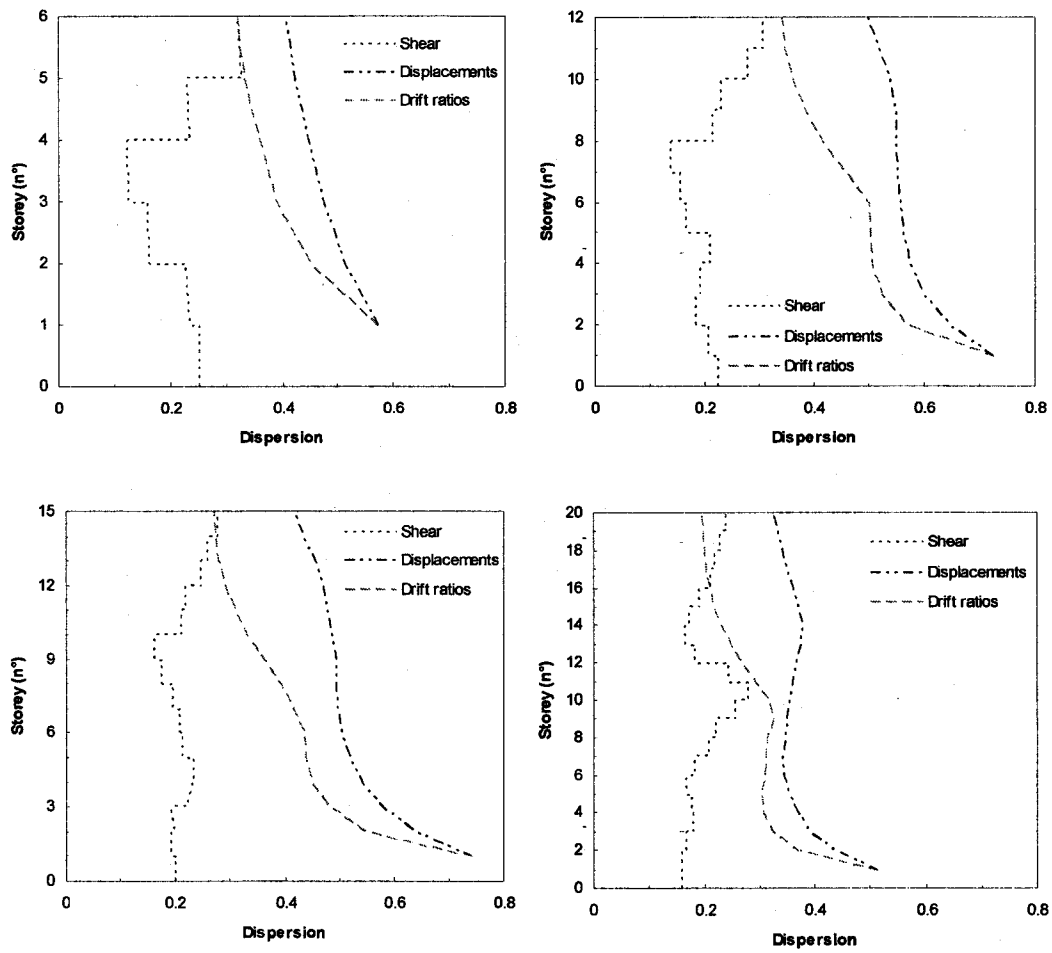


Figure 5.9: Dispersion of story drift ratios, displacements and shear forces obtained from the nonlinear RHA for the 6, 12, 15 and 20-storey buildings

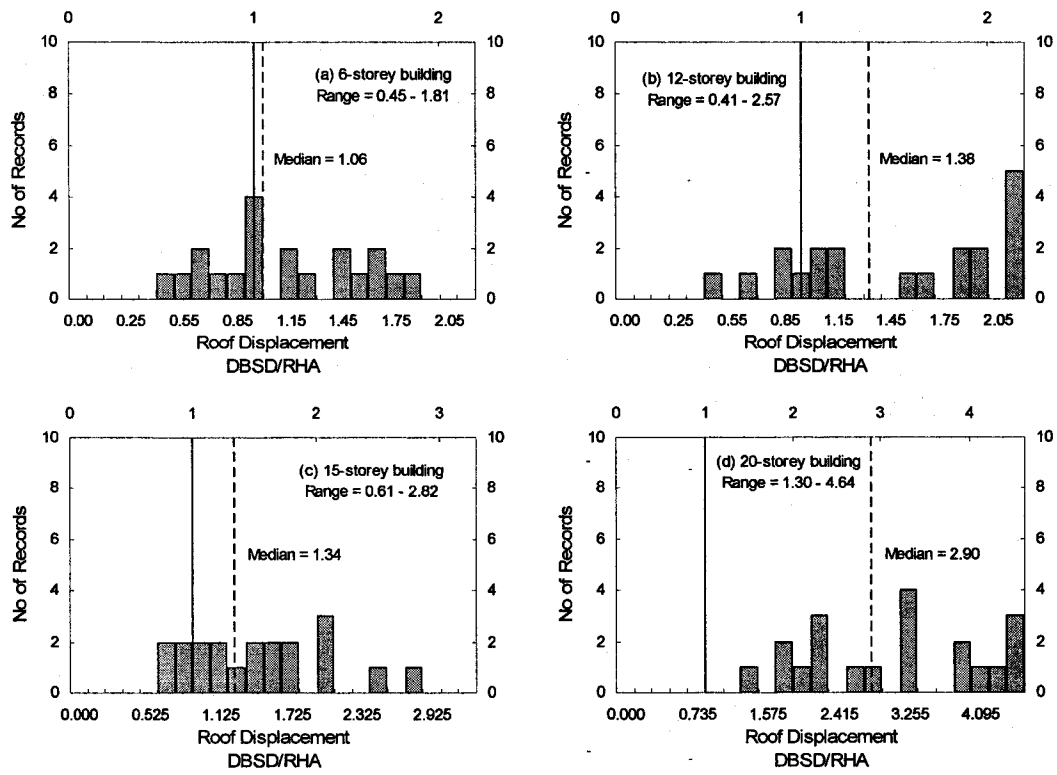


Figure 5.10: Histograms of the ratio between the roof displacements obtained from DBSD and nonlinear RHA of the 6, 12, 15, 20-storey buildings

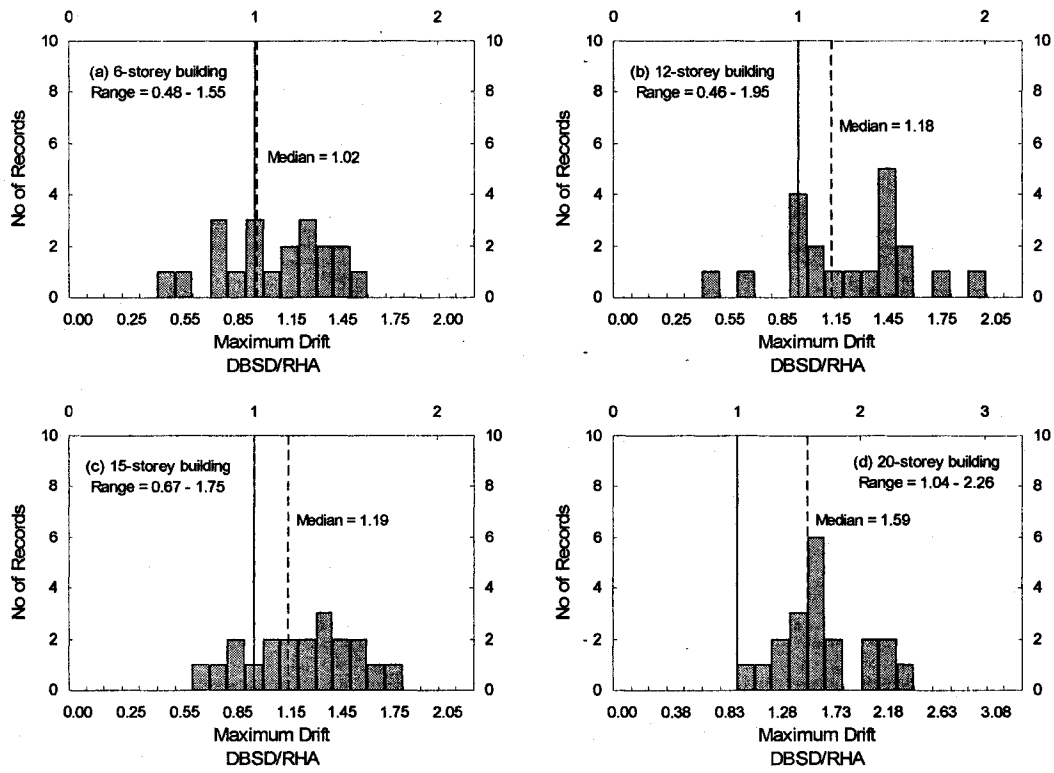


Figure 5.11: Histograms of the ratio between the maximum inter-storey drift ratios obtained from DBSD and nonlinear RHA of the 6, 12, 15, 20-storey buildings

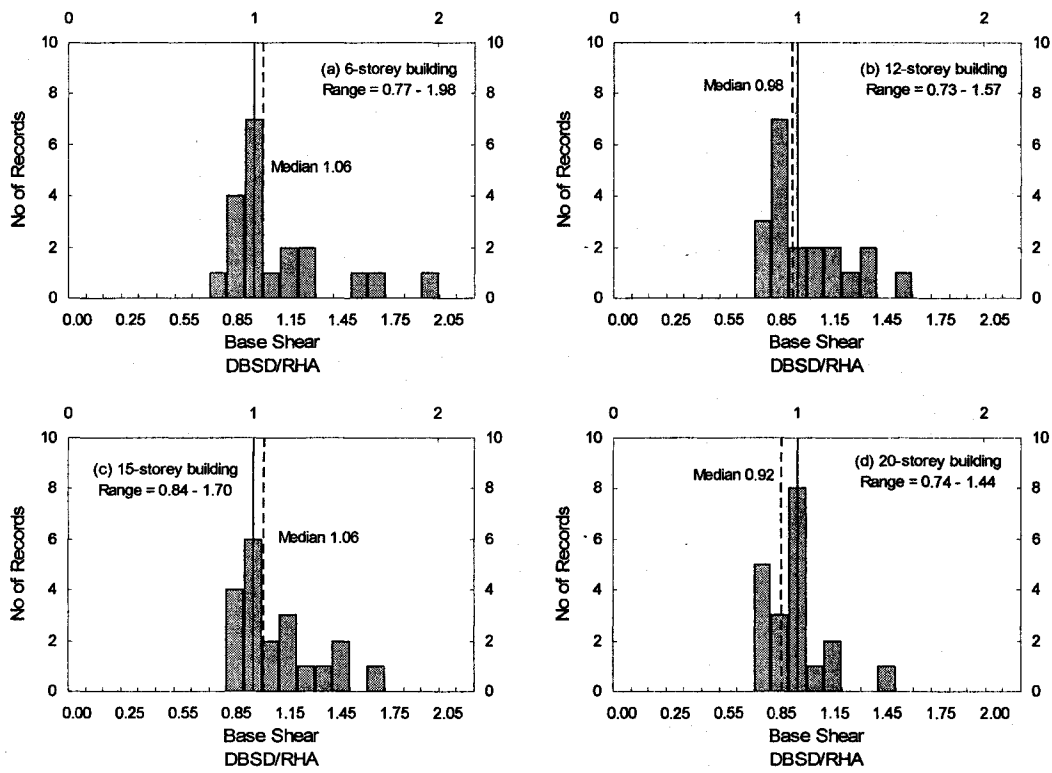


Figure 5.12: Histograms of the ratio between the base shears obtained from DBSD and nonlinear RHA of the 6, 12, 15, 20-storey buildings

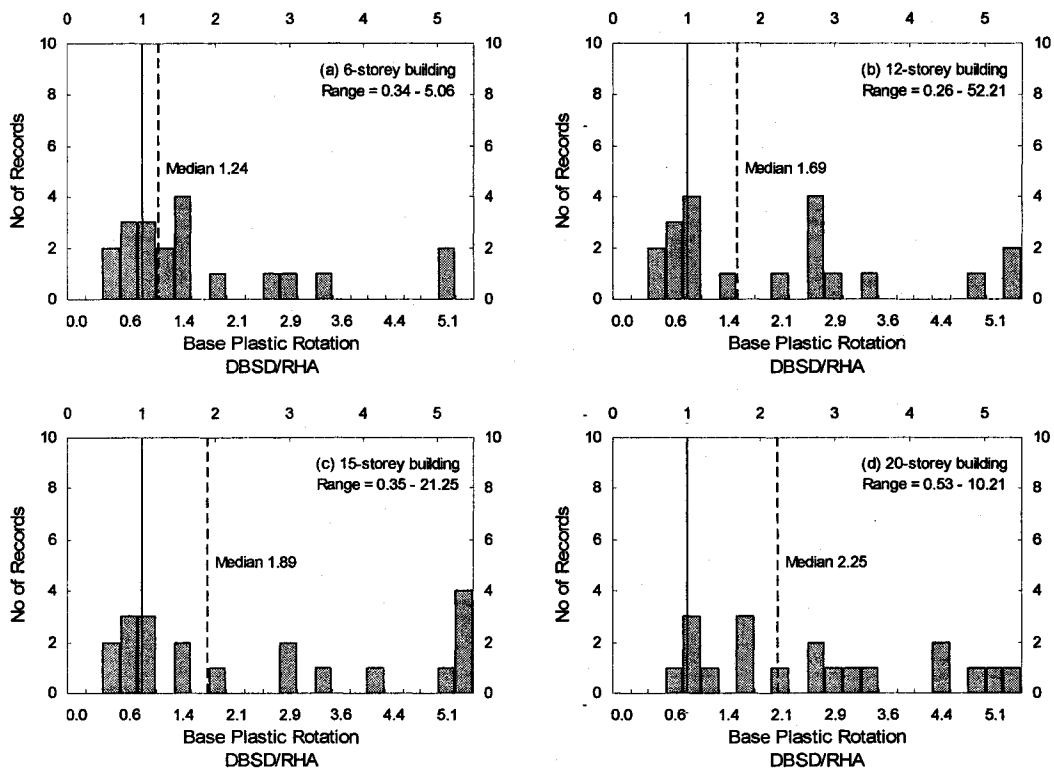


Figure 5.13: Histograms of the ratio between the base plastic rotation obtained from DBSD and nonlinear RHA of the 6, 12, 15, 20-storey buildings

Chapter 6

Summary, Conclusions and Recommendations

6.1. Introduction

The thesis presents a new procedure for the seismic design of shear wall buildings based on controlling the displacements. The proposed seismic design method is an alternative to the traditional seismic design method based on forces and is an essential step in the broader concepts of performance based design. In the context of performance-based seismic design, previous research has identified the shortcomings and conceptual problems in the force-based seismic design. One conclusion of such research is that the performance of the structure is better measured by displacements or strains than by forces or strengths. Considering that the research community, designers and professionals all consider performance-based seismic design as a desirable goal, the design procedures based on displacement are going to modify or replace the traditional force-based design. This work therefore represents a timely contribution to the new philosophy of performance-based design and a step in the direction of furthering that methodology.

The displacement-based seismic design method presented in Chapter 3 is a simple but comprehensive approach for the design of shear wall buildings having symmetric plan configuration. For a preliminary design, the DBSD is based on estimated yield and

ultimate displacements obtained from empirical equations. An iterative process involving modal and pushover analysis is used in the successive steps to obtain better estimates of the displacements. At each step in the design process a capacity-demand diagram is employed to determine the design base shear. The new procedure includes a modal analysis, and a modal pushover analysis (MPA) for the final design. Such analyses permit the consideration of contribution from higher modes in the response. The DBSD is applied to several different buildings, a 6, 12, 15, and 20 storeys in height. Results obtained from DBSD are compared with those obtained from nonlinear response history analyses (RHA). The input ground motions used in such analyses are selected and scaled so as to be compatible to the UHS for the city of Vancouver. The process of selection and scaling of the ground motions is presented in Chapter 2. The evaluation of DBSD is carried out through comparison with the nonlinear RHA results. Details of the evaluation are presented in Chapter 5.

In the present chapter, conclusions obtained from the study and recommendations for future work are presented. Conclusions obtained from Chapter 2 deal with the selection and modification of recorded ground motions. Conclusions related to the basic concepts, assumptions, and applicability of the DBSD as well as the higher mode effect follow from material presented in Chapters 3 and 4. Comments regarding validity and limitations of the proposed DBSD are based on the results of evaluation contained in Chapter 5.

6.2. Selection of ground motions

The selection of a set of ground motions that are compatible to a particular target spectrum must be carried out so as to satisfy several criteria. In this work, more than 300 records were selected, from which 20 were chosen as being compatible with the UHS for the city of Vancouver (NBCC 2005). This initial selection was from ground motions recorded in regions with tectonic settings, seismic hazard, and site conditions similar to the city of Vancouver. From the selection process used the following conclusions can be drawn:

1. Although the criteria of selecting records from similar seismic regions appears straightforward, the selection of record using these criteria is not an easy task. There exist many different regions from which ground motions that are similar to those for Vancouver can be selected because of the presence of three possible sources of seismic hazard in the city: crustal, subcrustal, and subduction earthquakes. All these types of source zones are included in the initial selection of records for this work. This data base of records may therefore prove to be useful when selecting records for a different location.
2. Although there exist many records obtained from regions with seismic hazard similar to Vancouver, it is often necessary to process such records before they are actually used in the analysis. First, most of the records need to be baseline corrected, since without such correction they may give unrealistic response. Second, the data must be

high and low-pass filtered. Most available records are filtered only to limit the high frequency to say 20 Hz, but they are not filtered for lower frequencies, which arise because of noise. Using a low-pass filter, say 0.05 Hz, will remove such frequencies and will at the same time lead to baseline correction.

6.3. Modification of ground motions

According to the literature reviewed in Chapter 2, the modification of ground motions by scaling with a single factor is the simplest approach to developing spectrum compatible ground motions and allows the retention of the characteristics of the original record. Two different scaling factors have been described in this thesis. The first scale factor matches the ground motion spectrum with the target spectrum at the first mode period of the structure (Shome *et al.* 1998), while the second minimizes the weighted sum of squared error between the selected ground motion spectrum and the target spectrum at 4 different periods, 0.3, 1, 2, and 4 seconds (Somerville *et al.* 1997). Based on the results obtained with the use of such scale factors the following conclusions can be drawn:

1. Use of either of the two scaling factors referred above, may result in large spectral values at short periods amplifying the higher mode response and leading to unrealistic overall response. It is recommended that before making a final selection the spectrum of the modified ground motion be compared with the target spectrum to verify that the match between the two is reasonable across the entire range of the periods of interest.

2. The scaling factor proposed by Somerville *et al.* (1997) present a more comprehensive and simpler approach to the modification of ground motions than the factor proposed by Shome *et al.* (1998). Shome's scaling factor requires a knowledge of the fundamental period of the structure, which is a clear disadvantage in defining a suite of ground motions for use with different structures. Moreover, the Shome's factor is only based on the first mode period and does not take into account higher mode periods. These two considerations led to the selection of Somerville's factor in the present work. In selecting the ground motions, the choice was restricted to those ground motions for which Somerville's scaling factor was less than or equal to 5.

Following the criteria described in Chapter 2, 26 pairs of records were finally selected; they are considered to be compatible with the UHS of Vancouver. During the process of selection two conclusions are reached:

1. Tokashi Oki earthquake (2003) provides very good match with the UHS of Vancouver, giving minimum values for the scaling factors. It must be mentioned that Tokashi Oki earthquake (2003) is a subduction earthquake; it was considered in the selection because of its similarity with the Cascadia region near Vancouver. It may be noted that the subduction earthquakes for Vancouver were considered in a deterministic analysis of hazard (Adams and Halchuk 2003) and provided spectral values that were lower than the UHS values given in NBCC 2005. The UHS values were obtained from a probabilistic analysis of the crustal and subcrustal earthquakes. In spite of the difference in the governing earthquake source the Tokashi Oki

earthquake (2003) records are selected because of the observed similarities between this two regions and the seismic hazard, and because of the good match in the scaled Tokashi Oki spectra and the Vancouver UHS.

2. Nisqually earthquake (2001) gave the largest number of records that were compatible with the UHS of Vancouver based on the criteria adopted in this research. The Nisqually earthquake is a subcrustal earthquake that was recorded directly in the city of Vancouver but with low levels of hazard: Therefore, the numerous ground motions selected from this earthquake clearly satisfy the selection criteria adopted in this work.

6.4. Displacement based seismic design

From the procedure presented in Chapter 3, the following conclusions can be drawn:

1. The DBSD presented in this work is both easy to follow and simple to implement. This is a real advantage in the context of performance-based design of structures that are not unusual or irregular. When multiple performance criteria need to be satisfied, several DBSD steps must be carried out, which will increase the complexity of the design process and time required. In such a situation, a simple procedure, such as the one described here, presents a clear advantage.
2. A preliminary design based on estimates of yield and ultimate displacements, and assuming a triangular shape for the first mode proved to be a good initial step in the

iterative procedure of the DBSD. It may be concluded that (a) the empirical equation proposed for yield curvature by Priestley (1998) and (b) the assumed depth of $0.3lw$ to obtain the ultimate curvature are good estimates for design purposes. The first conclusion also reinforces the concept that the yield curvature is practically independent of strength, which is the basis of the equation proposed by Priestley (1998).

3. The limit on concrete strain of 0.004 controlled the ultimate displacement for each building studied in this research, and the inter-storey drift limit of 0.025, defined by NBCC (2005), did not govern.
4. It was shown in this work that as long as there was no instability, the P- Δ effect did not cause any significant change in the inelastic response spectrum and the spectra based on an elasto-plastic force displacement relationship were still applicable.
5. The DBSD includes a nonlinear static analysis, or pushover analysis, to describe the nonlinear response of the buildings. The pushover analysis is a simple procedure that has been implemented in numerous commercial and non-commercial computer software. Some commercial programs even perform pushover analysis for a lateral force distribution that follows any given mode shape. This feature of computer software implies that the modal pushover analysis (MPA) can be easily carried out without the need to modify an existing computer program or to develop a new program.

One of the limits that defines the displacement demand is established by the need to avoid instability in the structure due to the P- Δ effect. In cantilever shear walls, if this limit is defined as the point at which the base shear versus roof displacement relationship, or the pushover curve, enters the region of negative slope, it will imply that instability in the structure may be caused as soon as the structure yields and the structure should be designed to remain elastic. Nevertheless, it was proposed in this research that incursion into the zone of negative slope be allowed and that other limits, such as those based on maximum material strains and the code-specified drift limits be used to define the displacement demand, provided the incursion into the negative slope region was not too large. It was found here that

1. The ratio between the ultimate base shear and yield base shear did not vary much and range between 0.87 and 0.90, even when the criterion of no yielding was relaxed.
2. Nonlinear analyses for the selected suite of records rarely showed instability due to P- Δ effect.

6.5. Responses from displacement-based seismic design

According to the results obtained from Chapter 4, the following conclusions can be drawn:

1. Ductility demands obtained from DBSD are very different from those specified by the design codes. In the present study the maximum ductility was found to be 2.26 for the

6-storey building and 1.47 for the 20-storey building. This points to the fact that the ductilities specified in the codes can rarely be mobilized without exceeding the code-specified drift limits or the strain limit allowed in reinforced concrete. The NBCC 2005, for example, defines a ductility of 3.5 for shear walls, which is more than twice that mobilized in the 12-storey building studied here.

2. The difference between ductility demands for individual buildings also shows that the ductility factor is not a good indicator of damage. It must be mentioned that all of the buildings studied here were designed to experience the same level of structural damage, which was defined by the limit of 0.004 in the compression concrete strain.
3. In this study, the modal responses obtained from the modal pushover analysis are combined by using two different combination rules: the square root of the sum of squares (SRSS) and the absolute sum (ABSSUM). As would be expected, more conservative results are obtained by ABSSUM. The SRSS has been adopted in the present work. This procedure, although simple, has some justification in the probability theory, particularly since the natural frequencies of the buildings studied here are well separated.
4. Modal pushover analyses confirm that displacements and inter-storey drift ratios are not affected by higher modes. However, the shear response is highly influenced by higher modes. The main contribution to the total shear response is obtained from the

second mode. The contribution from higher modes in the shear response increases for taller buildings.

6.6. Evaluation of displacement-based seismic design

The evaluation of DBSD was performed by a statistical analysis of the responses obtained from nonlinear response history analyses (RHA). Twenty ground motions were selected from the 52 records presented in Chapter 2. From the results obtained from this evaluation, the following conclusions are drawn:

1. The distribution of some response parameters in buildings subjected to the 20 ground motions showed that a lognormal distribution was appropriate to represent the variation of such parameters. However, there is still a great dispersion which may indicate that even 20 may not be an “adequate” number of records for nonlinear RHA. Further study is required in this direction.
2. In the present study, the responses obtained from the use of SRSS rule in association with DBSD gave better estimates of the median responses obtained from the nonlinear RHA. Therefore, the SRSS can be considered as being appropriate for obtaining the total response from a modal pushover analysis for structures of the type studied in this work.
3. The contribution of higher modes to the shear response increased for taller buildings. The use of 3 modes for the 6 and 12-storey building, 4 modes for the 15-storey

building, and 5 modes for the 20-storey building provided good estimates of the median response obtained from the nonlinear RHA. It is recommended that for taller buildings, say more than 15 storeys, more than 4 modes be included to calculate the shear response.

4. The new DBSD procedure introduced in this work is seen to be a reliable and simple approach to the design of shear wall buildings. The estimates of displacements and inter-storey drifts provided by DBSD are always higher than the median values obtained from nonlinear RHA of the structure for a suite of UHS compatible ground motions. The shears and forces obtained from DBSD are near the median of nonlinear RHA values.

6.7. Recommendations for future work

1. Shome's factor was also calculated in the present study to add more information related to the ground motion candidates. An arbitrary first mode period of 1 s was used to obtain the Shome's factor. In a future research, the two factors presented here, Shome's and Somerville's, can be compared by reviewing the inelastic responses of several structures characterized by different fundamental periods.
2. In Chapter 2, a parameter that measures the "severeness" of the ground motions was presented. The "severeness" is given by a modified spectral intensity proposed by Lestuzzi *et al.* (2004) and is used for helping in the selection of ground motions for nonlinear response history analyses. However, this parameters also depends on the

value of the first mode period which makes it impractical to use it in the selection of ground motions for response analyses of a variety of structures. In the present study, the modified spectral intensity based on an arbitrary first mode period of 1 s was used. In selecting the ground motions an upper limit of 20 % was set on the difference between the modified spectral intensities of the UHS and of the ground motion. The ground motions that showed a difference less than 20% were selected. Since an arbitrary definition is used in the selection of the period range for calculating the spectral intensity, it is recommended that this criterion be evaluated using different periods and limits in order to improve the selection of records.

3. There is a need for a discussion or/and study of the design demand originating from subduction events, such as the Tokashi Oki earthquake (2003) included in this work.
4. It is recommended that the P- Δ effect be evaluated in an elasto-plastic force displacement relationship with the selected ground motions presented in this thesis and for several ductility factor values.
5. For the shear wall structures used as examples in this work, the DBSD procedure required spectral values from the UHS for longer periods, longer than 4 seconds, for a performance-level of near collapse. However, in the NBCC the UHS is defined only upto a period value of 4 seconds, therefore extrapolation had to be used for longer periods. It will be useful to have UHS values for periods longer than 4 s as well as to

have UHS defined for parameters other than acceleration, such as velocity and displacements.

6. In a performance-based design UHS are required for several different return periods. In this work, an estimate of the UHS for 50 %/50 year probability was obtained on the basis of several assumptions. A detailed study must be conducted to define UHS for different earthquake design levels.
7. Further research must be carried out on the selection of the “correct” combination rule for a multi-modal analysis. The combination rules presented here and in the literature are only approximations to the total response and are intended to be used with the responses obtained from elastic analyses.

References

1. Abrahamson N., 2005. Additional remarks and settings the stage for the session. Presentation in the COSMOS annual meeting, *Pacific Engineering Research Center*, Richmond, CA, viewed April 11, 2006,
<www.cosmos-eq.org/presentations/TS2005/Abrahamson.pdf>
2. Abrahamson N.A., 1993. Non-stationary spectral matching program RSPMATCH. *PG&E*, Internal report, February.
3. Adams J. and Halchuk S., 2003. Fourth generation seismic hazard maps of Canada: values for over 650 Canadian localities intended for the 2005 National Building Code of Canada. *Geological Survey of Canada*, Ottawa, ON, Open file 4459, viewed April 06, 2006
<http://earthquakescanada.nrcan.gc.ca/hazard/OF4459/index_e.php>
4. Adams, J. and Halchuk S., 2000. Knowledge of in-slab earthquakes needed to improve seismic hazard estimates for southwestern British Columbia. *U.S. Geological Survey*, Reston, VA, Open file report: Intraslab Earthquakes, viewed April 6, 2006
<<http://earthquakescanada.nrcan.gc.ca/hazard/inslab2000/inslab2000.pdf>>
5. Adebar P., Mutrie J. and DeVall R., 2005. Ductility of concrete walls: the Canadian seismic design provisions 1984 to 2004. *Canadian Journal of Civil Engineering*, **32**, 1124-1137.

6. Antoniou S. and Pinho R., 2004. Development and verification of a displacement-based adaptive pushover procedure. *Journal of Earthquake Engineering*, **8**(5), 643-661.
7. Applied Technology Council, 1996. *Seismic evaluation and retrofit of concrete buildings*, Vol. 1, ATC 40, Applied Technology Council, Redwood City, CA.
8. Atkinson G.M. and Boore D.M., 2003. Empirical Ground-Motion Relations for Subduction-Zone Earthquakes and Their Application to Cascadia and Other Regions. *Bulletin of the Seismological Society of America*, **93**(4), 1703–1729.
9. Benjamin J.R. and Cornell C.A., 1970. *Probability, statistics and decision for civil engineers*, McGraw-Hill, Inc., New York, NY.
10. Bertero R.D. and Bertero V.V., 2002. Performance-based seismic engineering: the need for a reliable conceptual comprehensive approach. *Earthquake Engineering and Structural Dynamics*, **31**, 627-652.
11. Boore D.M., 2004. Estimating $V_s(30)$ (or NHERP site classes) from shallow velocity models (depth $\leq 30\text{m}$). *Bulletin of the Seismological Society of America*, **94**(2), 591-597.

12. Bracci J.M., Kunnath S.K. and Reinhorn A.M., 1997. Seismic performance and retrofit evaluation for reinforced concrete structures, *Journal of Structural Engineering*, ASCE, **123**(1), 3-10.
13. Calvi G.M. and Kingsley G.R., 1995. Displacement-based seismic design of multi-degree-of-freedom bridge structures. *Earthquake Engineering and Structural Dynamics*, **24**, 1247-1266.
14. Canadian Commission on Building and Fire Codes, 2005. *National Building Code of Canada 2005*, National Research Council of Canada, Ottawa, ON.
15. Celebi. M., 1988. Processed Chile earthquake records of 3 March 1985 and aftershocks, *U.S. Geological Survey*, Reston, VA, Open-file report 87-195 (Revised October 1988).
16. Chopra A.K. and Goel K.G., 1999. Capacity-Demand-Diagram Methods based on Inelastic Design Spectrum. *Earthquake Spectra*, **15**(4), 637-656.
17. Chopra A.K. and Goel K.G., 2001. Direct displacement-based design: use of inelastic vs. elastic design spectra. *Earthquake Spectra*, **17**(1), 47-65.
18. Chopra A.K. and Goel, R.K., 2002. A modal pushover analysis procedure for estimating seismic demands for buildings, *Earthquake Engineering and Structural Dynamics*. **31**(3), 561-582.

19. Chopra A.K. and Goel, R.K., 2004a. Evaluation of Modal and FEMA pushover analyses: SAC buildings. *Earthquake Spectra*. **20**(1), 225-254.
20. Chopra A.K., 2004b. *Dynamics of Structures: Theory and Applications to Earthquake Engineering*, 2nd Edition, Prentice Hall, India.
21. Computer and Structures, Inc., 2002. *SAP2000: Static and Dynamic Finite Element Analysis of Structures Nonlinear, version 8*. Computers and Structures, Inc., Berkeley, CA.
22. COSMOS Virtual data center, copyright 1999-2006, *The Regents of the University of California*, viewed 17 March 2006, < <http://db.cosmos-eq.org/scripts/default.plx> >
23. CSA, 1984. *Design of concrete structures. Standard CAN A23.3-M84*. Canadian Standards Association, Rexdale, ON.
24. CSA, 1994. *Design of concrete structures. Standard CSA A23.3-94*. Canadian Standards Association, Rexdale, ON.
25. DeVall R. 2003. Background information for some of the proposed earthquake design provisions for the 2005 edition of the National Building Code of Canada. *Canadian Journal of Civil Engineering*, **30**, 279-286.

26. Dussom K., Hadj-Hamou T. and Bakeer R., 1991. QUAKE: An expert system for the selection of design earthquake accelerogram. *Computers and Structures*, **40**(1), 161-167.
27. Fajfar P., 2000. A nonlinear analysis method for performance based seismic design. *Earthquake Spectra*, **16**(3), 573-592.
28. Federal Emergency Management Agency, 1997. *NEHRP guidelines for the seismic rehabilitation of buildings*, FEMA 273, and *NEHRP Commentary on the guidelines for the seismic rehabilitation of buildings*, FEMA 274, Federal Emergency Management Agency, Washington, D.C.
29. Federal Emergency Management Agency, 1998. *NEHRP recommended provisions for seismic regulation for new buildings and other structures. Part 2-Comentaries*, FEMA 303, Federal Emergency Management Agency, Washington, D.C.
30. Federal Emergency Management Agency, 2000. *Prestandard and Commentary for the Seismic Rehabilitation of Buildings*, FEMA 356, Federal Emergency Management Agency, Washington, D.C.
31. Ferrito J., 1992. Optimized earthquake time history and response spectra, User's guide. *Naval Civil Engineering Laboratory*, Port Huenueme, CA, Report UG-0025.

32. Freeman S.A., 1998. Development and use of capacity spectrum method. *Proceedings of the 6th U.S. National Conference on Earthquake Engineering*, Seattle, WA.
33. Freeman S.A., Nicoletti J.P. and Tyrell J.V., 1975. Evaluations of existing buildings for seismic risk – A case study of Puget Sound Naval Shipyard, Bremeton, Washington. *Proceedings of 1st U.S. National Conference on Earthquake Engineering*, EERI, Berkeley, CA, 113-122.
34. Ghorbanie M., 2005. *Performance-based seismic design of building structures*. Doctoral thesis proposal, Department of Civil and Environmental Engineering, Carleton University, Ottawa, ON.
35. GSC: Current earthquake information for British Columbia and western Canada, copyright date 21 November 2005, *Geological Survey of Canada*, Sidney Subdivision, BC, viewed 17 March 17, 2006,
< <http://www.pgc.nrcan.gc.ca/seismo/table.htm> >
36. Gupta B. and Kunnath S.K., 2000. Adaptive spectra-based pushover procedure for seismic evaluation of structures. *Earthquake Spectra*, 16(2), 367-392.
37. Halchuk S. and Adams J., 2004. Deaggregation of seismic hazard for selected Canadian cities. *Proceedings of the 13th world conference on earthquake engineering*, Vancouver, BC, Canada, paper 2470.

38. Humar J. and Ghorbanie M., 2005. A new displacement-based design method for building. *Proceeding of the 33rd Annual General Conference of the Canadian Society for Civil Engineering*, Toronto, ON, GC-136, 1-10.
39. Kik-net (Kiband-Kyoshin network) Digital strong-motion seismograph network, 2006, *National Research Institute for Earth Science and Disaster Prevention*, Japan, viewed 17 March 2006, < <http://www.kik.bosai.go.jp/> >
40. Kowalsky M.J., 2001. RC structural walls designed according to UBC and displacement-based methods. *Journal of Structural Engineering*, ASCE, **127**(5), 506-516.
41. Kowalsky M.J., Priestley M.J.N. and MacRae G.A., 1995. Displacement-based design of RC bridge columns in seismic regions. *Earthquake Engineering and Structural Dynamics*, **24**(12), 1623-1643.
42. Kramer S., 1996. *Geotechnical Earthquake Engineering*. 1st edition, Pearson Education, Singapore.
43. Krawinkler H. and Nassar A.A., 1992. Seismic design based on ductility and cumulative damage demands and capacities. *In Nonlinear Seismic Analysis and Design of Reinforced Concrete Buildings (Editors: H. Krawinkler and P. Fajfar)*. Elsevier Applied Science, UK, 95-104.

44. Krawinkler H. and Seneviratna G.D.P.K., 1998. Pros and cons of a pushover analysis of seismic performance evaluation. *Engineering Structures*, **20**(4-6), 452-464.
45. Krawinkler H., 1999. Challenges and progress in performance-based earthquake engineering. *International Seminar on Seismic Engineering for Tomorrow – In Honor of Professor Hiroshi Akiyama*, Tokyo, Japan.
46. Krinitzky E. and Chang F., 1979. State-of-the-art for assessing earthquake hazards in the United States: specifying peak motions for design earthquakes. *U.S. Army Corps of Engineers Waterways Experiment Station*, Vicksburg, MS, miscellaneous paper S-73-1, report 7,
47. Lestuzzi P., Schwab P., Koller M. and Lacave C., 2004. How to choose earthquake recordings for non-linear seismic analysis of structures. *Proceedings of the 13th world conference on earthquake engineering*, Vancouver, BC, Canada, paper 1241.
48. Mahgoub M.A., 2004. *A study of some issues related to seismic design provisions of National Building Code of Canada*. Ph.D. thesis, Department of Civil and Environmental Engineering, Carleton University, Ottawa, ON.
49. Naeim F. and Marshal L., 1995. On the use of design-spectrum compatible time histories. *Earthquake Spectra*, **11**(1), 111-127.

50. Naumosky N., 1998. Program SYNTH-theoretical background. *McMaster Earthquake Engineering Software Library*, Department of Civil Engineering, McMaster University, Hamilton, ON.
51. Naumosky N., Saatcioglu M. and Amiri-Hormozaki K., 2004. Effects of scaling of earthquake excitations on the dynamic response of reinforced concrete frame buildings. *Proceedings of the 13th world conference on earthquake engineering*, Vancouver, BC, Canada, paper 2917.
52. Newmark N.M. and Hall W.J., 1982. *Earthquake Spectra and Design*. Earthquake Engineering Research Institute, Berkeley, CA.
53. Onur T., Cassidy J. and Rogers G., 2005. Selection and compilation of strong motion records for earthquake engineering use in Canada: Preliminary steps. *Seismological Society of America Annual Meeting*, Lake Tahoe, NV.
54. Paulay T., 2001. Seismic response of structural walls: recent developments. *Canadian Journal of Civil Engineering*, **28**, 922-937.
55. Paulay T. and Priestley M.J.N., 1992. *Seismic design of reinforced concrete and masonry buildings*. John Wiley & Sons, Inc., New York, NY.

56. PNSN Strong motion network, 2003, *University of Washington, Department of Earth and Space Science*, viewed 17 March 2006,
<<http://www.pnsn.org/SMO/STA/welcome.html>>
57. Prakash V., Powell G.H. and Campbell S., 1993. DRAIN-2DX Base program description and user guide: version 1.10. *Department of Civil Engineering, University of California*, Berkeley, CA, report No UCB/SEMM-93/17
58. Priestley M.J.N. and Calvi G.M., 1997. Concepts and procedures for direct displacement-based seismic design and assessment. Proceedings of the International Workshop on *Seismic Design Methodologies for the Next Generation of Codes*, (Editors: P. Fajfar and H. Krawinkler), Bled, Slovenia, 24-27 June 1997, 171-181.
59. Priestley M.J.N. and Kowalsky M.J., 2000. Direct displacement-based seismic design of concrete buildings. *Bulletin of the New Zealand Society for Earthquake Engineering*, **33**(4), 421-444.
60. Priestley M.J.N. and Kowalsky M.J., 1998. Direct displacement-based seismic design of concrete buildings. *Bulletin of the New Zealand National Society for Earthquake Engineering*, **31**(6), 73-85.
61. Priestley M.J.N., 1998. Brief comments on elastic flexibility of reinforced concrete frames. *Bulletin of the New Zealand National Society for Earthquake Engineering*, **31**(4), 246-259.

62. Priestley M.J.N., 2000. Performance based seismic design. *Bulletin of the New Zealand National Society for Earthquake Engineering*, **33**(3), 325-346.
63. Priestley M.J.N., 2003. Does Capacity Design Do the Job? An examination of higher mode effects in cantilever walls. *Bulletin of the New Zealand Society for Earthquake Engineering*, **36**(4).
64. Scholl R. and Thiel, Jr. C., 1986. The Chile Earthquake of March 3, 1985. *Earthquake Spectra*, **2**.
65. SEAOC Blue Book, 1999. *Recommended Lateral Force Requirements and Commentary*. Structural Engineers Association of California, Sacramento, CA.
66. SEAOC Vision 2000 Committee, 1995. *Performance-based seismic engineering*. Report prepared by Structural Engineers Association of California, Sacramento, CA.
67. Shibata A. and Sozen M.A., 1976. Substitute-structure method for seismic design in R/C. *Journal of the Structural Division, ASCE*, **102**(1), 1-18.
68. Shome N., Cornell C.A., M. EERI, Bazzurro P. and Carballo J.E., 1998. Earthquake, records, and nonlinear responses. *Earthquake Spectra*, **14**(3), 469-498.
69. Somerville P., Smith N., Punyamurthula S. and Sun J., 1997. Development of ground motion time histories for phase 2 of FEMA/SAC steel project. *SAC joint venture*, Sacramento, CA, report SAC/BD-07/04.

70. SSN-UNAM National Seismological Service (Servicio Seismológico Nacional, in spanish), 2006, *Institute of Geophysic* (Instituto de Geofísica, in spanish), *Universidad Autónoma de México*, México, viewed 17 Mar 2006, < <http://www.ssn.unam.mx/> >
71. The Mathworks, Inc., 2002. *MATLAB: The language of technical computing, Version 6.5, Release 13*, The Mathworks, Inc., Natick, MA.
72. UCA, 2001. Strong motion data from the January-February 2001 earthquakes in El Salvador. *Universidad Centro-Americana*, San Salvador, El Salvador.
73. UNR: The Guerrero Accelerograph Network, 2006, *Seismological Laboratory, UNR*, and *Instituto de Ingeniería, UNAM*, viewed 17 March 2006, <<http://www.seismo.unr.edu/guerrero/description.html> >
74. USGS Earthquake hazard program, 2006, U.S. Department of the Interior, *U.S. Geological Survey*, viewed 17 March 2006, < <http://earthquake.usgs.gov/index.php> >
75. Vanmarcke E., 1979. State-of-the-art for assessing earthquake hazards in the United States: Representation of earthquake ground motion: scaled accelerograms and equivalent response spectra. *U.S. Army Corps of Engineers Waterways Experiment Station*, Vicksburg, MS, miscellaneous paper S-73-1, Report 7.

76. Vidic T., Fajfar P. and Fishinger M., 1994. Consistent inelastic design spectra: strength and displacement. *Earthquake Engineering and Structural Dynamics*, **23**(5), 507-521.
77. Williams R.A., Stephenson W.J., Frankel A.D., Odum J.K., 1999a. Surface seismic measurements of near-surface P- and S-wave seismic velocities at earthquake recording stations, Seattle, Washington. *Earthquake Spectra*, **15**(3), 20.
78. Williams R.A., Stephenson W.J., Odum J.K., and Worley D.M., 1999b. S-wave velocities for specific near-surface deposit in Seattle, Washington. Poster presented at 1999 Spring meeting of the SSA. *Seismological Research Letters*, **70**(2), 257.
79. Wilson E., 1998. *Three Dimensional Static and Dynamic Analysis of Structures: A physical approach with emphasis on earthquake engineering*. Computers and Structures, Inc., Berkeley, CA.
80. Yavari S., 2001. *Design of Concrete Shear Wall Buildings for Earthquake Induced Torsion*. Master of Applied Science thesis, Department of Civil and Environmental Engineering, Carleton University, Ottawa, ON.

Appendix A

A.1. DBSD of a 12-storey building

A.1.1. General Calculation

Floor dead load, q_f

| | |
|---------------------------------|--|
| Slab | $q_{\text{slab}} = t h_s \times \gamma_{\text{rc}} = 0.2 \times 24 = 4.8 \text{ kN/m}^2$ |
| Partition | $q_p = 0.5 \text{ kN/m}^2$ |
| Electrical, mechanical, ceiling | $q_{\text{EMC}} = 0.5 \text{ kN/m}^2$ |
| Total | $q_f = q_{\text{slab}} + q_p + q_{\text{EMC}} = 5.8 \text{ kN/m}^2$ |

The roof dead load is also 5.8 kN/m^2 since partition load is replaced by the same amount of load due to insulation and roofing.

Load due to self weight

Upper floor columns

$$q_{\text{fc}} = \frac{n_c \times A_{\text{col}} \times \gamma_{\text{rc}} \times 3.65\text{m}}{A_{\text{plan}}} = \frac{18 \times 0.5 \times 0.5 \times 24 \times 3.65}{24 \times 36} = 0.456 \text{ kN/m}^2$$

1st level columns

$$q_{1c} = \frac{n_c \times A_{col} \times \gamma_{rc} \left(\frac{3.65 + 4.85}{2} \right)}{A_{plan}} = \frac{18 \times 0.5 \times 0.5 \times 24 \times 4.25}{24 \times 36} = 0.531 \text{ kN/m}^2$$

Roof level columns

$$q_{roofc} = \frac{n_c \times A_{col} \times \gamma_{rc} \left(\frac{3.65}{2} \right)}{A_{plan}} = \frac{18 \times 0.5 \times 0.5 \times 24 \times 1.825}{24 \times 36} = 0.228 \text{ kN/m}^2$$

Upper floor walls

$$q_{fsw} = \frac{4 \times l_w \times th_w \times \gamma_{rc} \times 3.65m}{A_{plan}} = \frac{4 \times 7.5 \times 0.4 \times 24 \times 3.65}{24 \times 36} = 1.217 \text{ kN/m}^2$$

1st level walls

$$q_{1sw} = \frac{4 \times l_w \times th_w \times \gamma_{rc} \left(\frac{3.65 + 4.85}{2} \right)}{A_{plan}} = \frac{4 \times 7.5 \times 0.4 \times 24 \times 4.25}{24 \times 36} = 1.417 \text{ kN/m}^2$$

Roof level walls

$$q_{roofsw} = \frac{4 \times l_w \times th_w \times \gamma_{rc} \left(\frac{3.65}{2} \right)}{A_{plan}} = \frac{4 \times 7.5 \times 0.4 \times 24 \times 1.825}{24 \times 36} = 0.608 \text{ kN/m}^2$$

Total dead load and mass

Floor

$$q_{fDL} = q_f + q_{fc} + q_{fsw} = 5.8 + 0.456 + 1.217 = 7.473 \text{ kN/m}^2$$

1st level

$$q_{1DL} = q_f + q_{lc} + q_{lsw} = 5.8 + 0.531 + 1.417 = 7.748 \text{ kN/m}^2$$

Roof (including 25% of snow load)

$$\begin{aligned} q_{rDL} &= 0.25q_s + q_f + q_{roofc} + q_{roofsw} \\ &= 0.25 \times 2.2 + 5.8 + 0.228 + 0.608 = 7.186 \text{ kN/m}^2 \end{aligned}$$

Considering a tributary area of 432 m² (half of the plan area), the distribution of dead loads and masses for each wall and floor is presented on Table A.1.

A.1.2. Gravity loads

The gravity loads are divided in two types: design axial load, and axial load for P-Δ effect. The design load or maximum axial load is computed at the shear wall base and will be used in the moment-curvature analysis. Another load is calculated assuming that the two shear walls together resist the P-Δ effect produced by the entire gravity load.

A.1.2.1. Design axial load, P_b

The gravity loads on the shear wall will be obtained from the floor loads acting on a tributary area of 94.5 m² (15.75 m x 6 m) plus the self weight. These loads are calculated as follows:

Upper floor level self weight, P_{wf}

$$P_{wf} = 3.65 \times l_w \times t_h \times \gamma_{rc} = 3.65 \times 7.5 \times 0.4 \times 24 = 262.80 \text{ kN}$$

1st level self weight, P_{w1}

$$P_{w1} = 4.85 \times l_w \times th_w \times \gamma_{rc} = 4.85 \times 7.5 \times 0.4 \times 24 = 349.20 \text{ kN}$$

Bottom of top storey, P_{top}

Snow load, $P_s = 0.25 \times q_s \times A_{trib} = 0.25 \times 2.2 \times 94.5 = 51.98 \text{ kN}$

Roof load, $P_r = q_r \times A_{trib} = 5.8 \times 94.5 = 548.1 \text{ kN}$

Total $P_{top} = P_{wf} + P_s + P_r = 862.88 \text{ kN}$

Bottom of typical storey, P_{ts}

Floor load, $P_f = q_f \times A_{trib} = 5.8 \times 94.5 = 548.1 \text{ kN}$

Total $P_{ts} = P_{wf} + P_f = 810.90 \text{ kN}$

Bottom of first storey, P_1 $P_1 = P_{w1} + P_f = 897.30 \text{ kN}$

The live load is included according to the NBCC 2005 requirements. This load is reduced by the live load reduction factor, LLRF, which is given by:

$$LLRF = 0.3 + \sqrt{\frac{9.8}{CA_{trib}}} \quad (A.1)$$

where CA_{trib} is the cumulative tributary area in m^2 . The calculations are presented in Table A.2.

Finally, the factored dead and live loads are combined using two load combination rules:

$1.25 D + 1.50 L$ and $1.0D + 0.5 L$, where L is the reduced live load. The results are

presented in Table A.3. The design gravity load in the presence of earthquake loads is obtained from the combination $D + 0.5 L$ and is seen to be 10,364.5 kN.

A.1.2.2. Axial load for P- Δ effect

In this case, the tributary area will be assumed to be half of the total plan area, 432 m². The live loads are computed using the same procedure as the previous section and the results are shown on Table A.4. The factored dead load and reduced live loads are finally combined using the rule: $1.0 D + 0.5 L$ and the results for each wall and floor are shown in Table A.5.

A.1.3. DBSD

The calculations presented bellow follow the steps presented in the summary Chapter 3.

1. The yield displacement and rotation are given by Equations (3.2) and (3.3) where

$$\epsilon_y = \frac{f_y \times \phi_s}{E_s} = \frac{400 \times 0.85}{200000} = 0.0017$$

is the factored yield steel strain. The yield curvature is given by Equation (3.4)

$$\phi_y = \frac{2.0 \epsilon_y}{l_w} = \frac{2 \times 0.0017}{7500} = 4.533 \times 10^{-7} \text{ 1/mm}$$

Hence the yield rotation is

$$\theta_y = \frac{\phi_y H}{2} = \frac{4.533 \times 10^{-7} \times 45000}{2} = 0.0102 \text{ rad}$$

and the yield displacement is

$$\Delta_y = \frac{\phi_y H^2}{3} = \frac{4.533 \times 10^{-7} \times 45000^2}{3} = 306.00 \text{ mm}$$

2. The ultimate rotation and displacement are defined by Equations (3.5) and (3.7), and together provide the required local ductility. The ultimate curvature is given by

$$\phi_u = \frac{\epsilon_{cu}}{0.3l_w} = \frac{0.004}{0.3 \times 7500} = 1.78 \times 10^{-6} \text{ 1/mm.}$$

Assuming a plastic hinge length of $0.5l_w$ the plastic rotation and displacement are obtained from Equations (3.6) and (3.8) as follows:

$$\theta_p = (\phi_u - \phi_y) L_p = (17.8 - 4.533) \times 10^{-7} \times 0.5 \times 7500 = 0.00497 \text{ rad}$$

$$\Delta_p = \theta_p (H - 0.5L_p) = 0.00497 \times (45000 - 0.5 \times 3750) = 214.19 \text{ mm.}$$

Finally, the ultimate rotation is given by

$$\theta_u = \theta_y + \theta_p = 0.0102 + 0.00497 = 0.01517 \text{ rad}$$

and the ultimate displacement is

$$\Delta_u = \Delta_y + \Delta_p = 306.0 + 214.2 = 520.2 \text{ mm.}$$

Note that by using the drift limit establish by the NBCC 2005, the ultimate displacement is given by (Equation (3.9))

$$\Delta_u = 306 + (45000 - 0.5 \times 3750) \cdot \left(0.025 - \frac{4.533 \times 10^{-7} \times 45000}{2} \right) = 944.3 \text{ mm}$$

which is larger than that obtained from limiting the concrete strain to 0.004.

Therefore, the ultimate displacement is set at 520.2 mm and the ductility capacity is

given by

$$\mu = \frac{\Delta_u}{\Delta_y} = \frac{520.2}{306.0} = 1.70$$

3. The mass distribution is shown in Table A.1 and the displacement shape assumed to be in the form of an inverted triangle is obtained from the following

$$\phi^T = \frac{h}{H} =$$

$$\frac{\{4.85 \quad 8.5 \quad 12.15 \quad 15.8 \quad 19.45 \quad 23.1 \quad 26.75 \quad 30.4 \quad 34.05 \quad 37.7 \quad 41.35 \quad 45\}}{45}$$

$$= \{0.11 \quad 0.19 \quad 0.27 \quad 0.35 \quad 0.43 \quad 0.51 \quad 0.59 \quad 0.68 \quad 0.76 \quad 0.84 \quad 0.92 \quad 1\}$$

The modal participation factor and effective modal mass are now calculated from Equations (3.10) and (3.11), respectively

$$\Gamma = \frac{(\phi^T \mathbf{M} \mathbf{1})}{(\phi^T \mathbf{M} \phi)} = 1.442$$

$$M^* = \frac{(\phi^T \mathbf{M} \mathbf{1})^2}{(\phi^T \mathbf{M} \phi)} = 3138.5 \text{ tonne}$$

4. The yield and ultimate displacements for the equivalent SDOF system are thus given by

$$\delta y = \frac{\Delta_y}{\Gamma \phi^T} = \frac{306.0}{1.442 \times 1} = 212.15 \text{ mm}$$

$$\delta u = \frac{\Delta_u}{\Gamma \phi^T} = \frac{520.2}{1.442 \times 1} = 360.65 \text{ mm}$$

5. From the capacity-demand method (Figure A.1) and using δy , δu and μ , the inelastic pseudo-acceleration, A , is

$$A = 0.0513 \text{ g}$$

6. The corresponding base design shear is

$$V_b = A \cdot M^* = 0.0513 \times 9.81 \times 3138.5 = 1580.57 \text{ kN}$$

7. The base shear is distributed according to the distribution product of the floor weights and the floor height shown in Table A.1:

$$F^T = V_b \times \frac{W \cdot h}{\sum W \cdot h} = \left\{ \begin{array}{cccccc} 26.71 & 45.15 & 64.54 & 83.93 & 103.32 & 122.7 & 142.09 \\ 161.48 & 180.87 & 200.26 & 219.65 & 229.87 \end{array} \right\} \text{ kN}$$

The base moment is then given by

$$M_b = \sum [F(h_{i+1} - h_i)] = 49312.6 \text{ kN} \cdot \text{m}$$

8. The structure is now designed to resist P_b , V_b and M_b . The minimum requirements are taken from the CSA A23.3-94.

The minimum area of concentrated reinforcement is given by

$$A_{s_{\min}} = 0.002 \cdot t h_w \cdot l_w = 0.002 \times 400 \times 7500 = 6000 \text{ mm}^2.$$

The minimum distributed reinforcement is obtained from

$$A_{s_{d\min}} = 0.0025 \cdot t h_w = 0.0025 \times 400 = 1000 \text{ mm}^2 / \text{m}$$

and is provided by 2 layers of #10 at 200 mm spacing.

The required vertical concentrated reinforcement is calculated by following the simplified method presented on Chapter 3. The depth of the compression zone is

given by

$$c = \frac{P_b + A_d \phi_s f_y l_w}{\alpha_1 \phi_c f_c \beta_1 b_w + 2A_d \phi_s f_y}$$

$$= \frac{10364.5 + 1000 \times 0.85 \times 400 \times 7500}{0.805 \times 0.6 \times 30 \times 0.895 \times 400 + 2 \times 1000 \times 0.85 \times 400} = 2201.06 \text{ mm}$$

The concrete resistant moment is obtained from

$$M_c = \alpha_1 \phi_c f_c c^2 \beta_1 b_w (1 - 0.5\beta_1)$$

$$= 0.805 \times 0.6 \times 30 \times 2201.06^2 \times 0.895 \times 400 \times (1 - 0.5 \times 0.895) = 13885 \text{ kN} \cdot \text{m}$$

The resistant moment provided by the distributed reinforcement is give by

$$M_{Ad} = A_d \phi_s f_y c^2 \left[1 + \left(\frac{l_w}{c} - 1 \right)^2 - \frac{2}{3} \left(\frac{\epsilon_y}{\epsilon_{cu}} \right)^2 \right] =$$

$$1000 \times 0.85 \times 400 \times 2201.06^2 \left[1 + \left(\frac{7500}{2201.06} - 1 \right)^2 - \frac{2}{3} \left(\frac{0.002}{0.0035} \right)^2 \right] = 5417.7 \text{ kN} \cdot \text{m}$$

The restoring moment provided by the axial load is obtained from

$$M_p = P_b \cdot \left(\frac{l_w}{2} - c \right) = 10364.5 \left(\frac{7500}{2} - 2201.06 \right) = 16054.06 \text{ kN} \cdot \text{m}$$

Thus, the resistant moment to be contributed by the concentrated reinforcement is obtained from

$$M_{cr} = M_b - M_c - M_{Ad} - M_p$$

$$= 49312.6 - (13885 + 5417.7 + 16054.06) = 13955.9 \text{ kN} \cdot \text{m}$$

and the corresponding steel area is given by

$$A_{cr} = \frac{M_{cr}}{\phi_s f_y (l_w - 2h_m)} = \frac{13955.9}{0.85 \times 400 \times (7500 - 2 \times 205)} = 5789.37 \text{ mm}^2$$

This area is smaller than the minimum area required by the code, $A_{s_{min}} = 6000 \text{ mm}^2$.

Therefore, an arrangement of 9 bars #30 is adopted which gives an area of 6300 mm². The value of h_m was obtained by assuming a spacing of 150 mm plus a cover of 40 mm, and half of the steel section diameter, 15 mm (see Figure A.2). Using this reinforcement, the moment-curvature analysis gives the curve shown in Figure A.3. From the idealized curve shown with a dotted line, the following results are obtained

| | |
|--|----------------------------|
| Moment capacity, M_c | 50528 kN·m |
| Yield curvature, ϕ_y | 4.55×10^{-7} 1/mm |
| Ultimate curvature, ϕ_u | 1.98×10^{-6} 1/mm |
| Ratio of effective moment of inertia to the gross moment of inertia, I_r | 0.3223 |

From these results the refined plastic rotation and roof displacement can be computed as follows

$$\theta_p = (\phi_u - \phi_y) L_p = (19.8 - 4.55) \times 10^{-6} \times 3750 = 0.00571 \text{ rad}$$

$$\Delta_p = 0.00571(45000 - 0.5 \times 3750) = 246.33 \text{ mm}$$

Also from these results, the stability of this shear wall can be checked by obtaining the critical thickness according to Equation (3.18) as follows

$$b_c = 0.017 \cdot l_w \cdot \sqrt{\mu_\phi} = 0.017 \times 7500 \times \sqrt{\frac{19.8}{4.45}} = 265.85 \cdot \text{mm}$$

Thus the 400 mm thickness will avoid any instability problem.

9. The modal analysis including the P- Δ effect gives the following properties related to the first mode

| | |
|--------------------------------|---------------|
| Period of vibration, T1 | 3.73 s |
| Mode shape at roof, ϕ^r | 0.0293 |
| Participation factor, Γ | 1.489 |
| Effective modal mass, M^* | 2587.05 tonne |

10. Distributing the forces according to Equation (3.26) a first mode pushover analysis is carried out. The roof displacement versus base shear relationship obtained is shown in Figure A.4. The important result from this curve is the yield point which is given by

| | |
|-------------------------------------|-----------|
| Yield base shear, V_{by} | 1336.2 kN |
| Yield roof displacement, Δ_y | 271 mm |

From this displacement and the moment-curvature analysis, the new target ultimate displacement is defined as follows

$$\Delta_u = \Delta_y + \Delta_p = 271 + 246.33 = 517.33 \text{ mm}$$

That gives a new ductility demand of

$$\mu = \frac{\Delta_u}{\Delta_y} = 1.909$$

11. The yield and ultimate displacement for the equivalent SDOF system are now given by

$$\delta y = \frac{\Delta_y}{\Gamma \phi^r} = \frac{271}{1.489 \times 0.0293} = 182.04 \text{ mm}$$

$$\delta u = \frac{\Delta_u}{\Gamma \phi^r} = \frac{517.33}{1.489 \times 0.0293} = 347.50 \text{ mm}$$

The inelastic acceleration, A , is obtained by using δy , δu , and μ in the capacity-demand method (Figure A.5)

$$A = 0.0523 \text{ g.}$$

Finally, the new base shear is

$$V_{y_{\text{new}}} = M^* A = 2787.05 \times 0.0523 \times 9.81 = 1326.9 \text{ kN}$$

12. The difference between the two successive estimates is

$$\text{diff}_{V_y} = \frac{V_y - V_{y_{\text{new}}}}{V_y} = 0.701 \text{ \%}.$$

This first try immediately converges and another try is not necessary. It must be mentioned that 3 tries were carried out before for a length of 8 m. This previous wall converged to a less capacity than the minimum requirements. Therefore, a new length was defined and shown on this section with only one try. The final design gives a ratio of the ultimate base shear to yield shear $V_u/V_y = 0.878$, which is a measure of the excursion into the unstable part of the pushover curve

13. The method was seen to converge on the first attempt. It may be noted that all of the preceding computations were based on the first mode. The moment estimate obtained from the first mode is expected to be reasonable. However, in a shear wall structure the higher modes make significant contribution to the base shear. Hence two higher modes, 2nd and 3rd are included and analysis is repeated with these modes following the procedure presented in Section 3.11 of modal pushover analysis. The modal analysis results are shown in Table A.6 for three modes. The pushover curves obtained by using distribution of forces according to the second

and third mode shapes are shown in Figure A.6. These curves are transformed into equivalent SDOF systems and then plotted on the capacity-demand diagrams presented in Figure A.7. That figure, as well as the data summarized in Table A.7, show that the performance points do not lie in the inelastic zone of the capacity diagram, which means that both responses remain elastic. The responses in the first, second and third modes are combined according to the SRSS and ABSSUM rules and the results are shown in Figure A.8 for the inter-storey drifts and displacements and in Figure A.9 for shear forces. As examples, three particular results are obtained as follows:

Roof displacement

$$\Delta_{\text{roof}} = \sqrt{\Delta_{u1}^2 + \Delta_{u2}^2 + \Delta_{u3}^2} = \sqrt{517.3^2 + 36.7^2 + 4.0^2} = 518.6 \text{ mm}$$

Maximum drift ratio

$$\theta_{\text{max}} = \sqrt{\theta_{\text{max}1}^2 + \theta_{\text{max}2}^2 + \theta_{\text{max}3}^2} = \sqrt{0.014^2 + 0.004^2 + 0.001^2} = 0.015$$

Base shear

$$V_b = \sqrt{V_{b1}^2 + V_{b2}^2 + V_{b3}^2} = \sqrt{1336^2 + 4824^2 + 1336^2} = 5618 \text{ kN}$$

where the numeric subscript indicates the mode number.

Assuming a horizontal reinforcement of #15 at 200 mm and an effective depth of $d = 0.8l_w$, the simplified method gives a shear capacity of (Clause 11.3 of the CSA 1994):

$$V_{\text{capacity}} = 0.2\phi_c \sqrt{f_c} \cdot t h_w d_v + \phi_s \frac{A_v f_y}{s} d =$$

$$0.2 \times 0.6 \times \sqrt{30} \times 400 \times 0.8 \times 7500 + 0.85 \frac{400 \times 400}{200 \times 1000} 0.8 \times 7500 = 5929.4 \text{ kN}$$

Thus, the provided horizontal reinforcement will ensure sufficient capacity to resist the shear demand of 5,618 kN.

14. The design spectrum corresponding to 50%/50 year probability is obtained by scaling down the UHS corresponding to 2%/50 year probability by the ratio obtained in Section 3.12.1, that is, 0.325. The spectral acceleration from the UHS corresponding to 2%/50 year probability at $T_1 = 3.73$ s is 0.102 g. Thus, the demand acceleration for the operational level is $0.102 \times 0.325 = 0.024$ g. Considering the equivalent modal mass for the final design $M1^* = 2787.05$ tonne, the demand base shear, V_{bOP} , is given by

$$V_{bOP} = 2787.05 \times 9.81 \times 0.024 = 657.7 \text{ kN}$$

15. From the pushover curve shown in Figure A.4, the roof displacement is 133.4 mm for the calculated base shear, V_{bOP} . From pushover analysis data base, the maximum drift ratio at this roof displacement is 0.5 %. Therefore, the design is satisfactory for the operational performance level.

Table A.1: Floor dead loads and masses tributary to each wall in the 12-storey building

| Storey Number | Accumulated height (m) | Dead Load (kN) | Mass (tonne) |
|------------------|------------------------------|-------------------|-----------------|
| 1 | 4.85 | 3347.1 | 341.19 |
| 2 | 8.50 | 3228.3 | 329.08 |
| 3 | 12.15 | 3228.3 | 329.08 |
| 4 | 15.80 | 3228.3 | 329.08 |
| 5 | 19.45 | 3228.3 | 329.08 |
| 6 | 23.10 | 3228.3 | 329.08 |
| 7 | 26.75 | 3228.3 | 329.08 |
| 8 | 30.40 | 3228.3 | 329.08 |
| 9 | 34.05 | 3228.3 | 329.08 |
| 10 | 37.70 | 3228.3 | 329.08 |
| 11 | 41.35 | 3228.3 | 329.08 |
| 12 | 45.00 | 3104.6 | 316.47 |

Table A.2: Reduced live load calculations for each wall of the 12-storey building

| Storey N° | Live Load LL (kN) | Cumulative Live Load CLL (kN) | Cumulative Tributary Area CA_{trib} (m ²) | Live Load Reduction Factor LLRF | Reduced Cumulative Live Load RCLL (kN) |
|--------------|----------------------------|--|---|--|--|
| 1 | 226.8 | 2494.8 | 1039.5 | 0.397 | 990.7 |
| 2 | 226.8 | 2268.0 | 945.0 | 0.402 | 911.4 |
| 3 | 226.8 | 2041.2 | 850.5 | 0.407 | 831.5 |
| 4 | 226.8 | 1814.4 | 756.0 | 0.414 | 750.9 |
| 5 | 226.8 | 1587.6 | 661.5 | 0.422 | 669.5 |
| 6 | 226.8 | 1360.8 | 567.0 | 0.431 | 587.1 |
| 7 | 226.8 | 1134.0 | 472.5 | 0.444 | 503.5 |
| 8 | 226.8 | 907.2 | 378.0 | 0.461 | 418.2 |
| 9 | 226.8 | 680.4 | 283.5 | 0.486 | 330.6 |
| 10 | 226.8 | 453.6 | 189.0 | 0.528 | 239.4 |
| 11 | 226.8 | 226.8 | 94.5 | 0.622 | 141.1 |
| 12 | 0 | 0 | 0 | 0 | 0 |

Table A.3: Gravity load combinations for each wall of the 12-storey building

| Storey | Dead Load | Cumulative Dead Load | Reduced Cumulative Live Load | Cumulative 1.25D+1.5L | Cumulative 1.0D+0.5L |
|--------|-----------|----------------------|------------------------------|-----------------------|----------------------|
| n | DL (kN) | CDL (kN) | RCLL (kN) | (kN) | (kN) |
| 1 | 897.3 | 9869.2 | 990.7 | 13822.5 | 10364.5 |
| 2 | 810.9 | 8971.9 | 911.4 | 12581.9 | 9427.6 |
| 3 | 810.9 | 8161.0 | 831.5 | 11448.4 | 8576.7 |
| 4 | 810.9 | 7350.1 | 750.9 | 10313.9 | 7725.5 |
| 5 | 810.9 | 6539.2 | 669.5 | 9178.2 | 6873.9 |
| 6 | 810.9 | 5728.3 | 587.1 | 8041.1 | 6021.9 |
| 7 | 810.9 | 4917.4 | 503.5 | 6902.0 | 5169.1 |
| 8 | 810.9 | 4106.5 | 418.2 | 5760.4 | 4315.6 |
| 9 | 810.9 | 3295.6 | 330.6 | 4615.4 | 3460.9 |
| 10 | 810.9 | 2484.7 | 239.4 | 3464.9 | 2604.4 |
| 11 | 810.9 | 1673.8 | 141.1 | 2303.8 | 1744.3 |
| 12 | 862.9 | 862.9 | 0 | 1078.6 | 862.9 |

Table A.4: Reduced tributary live loads for calculating the P- Δ effect for each wall of the 12-storey building

| Storey | Live Load | Cumulative Live Load | Cumulative Tributary Area | Live Load Reduction Factor | Reduced Cumulative Live Load | Reduced Live Load |
|--------|-----------|----------------------|--------------------------------------|----------------------------|------------------------------|-------------------|
| n | LL (kN) | CLL (kN) | CA _{trib} (m ²) | LLRF | RCLL (kN) | RLL (kN) |
| 1 | 1036.8 | 11404.8 | 9504 | 0.332 | 3787.7 | 328.08 |
| 2 | 1036.8 | 10368.0 | 8640 | 0.334 | 3459.6 | 328.96 |
| 3 | 1036.8 | 9331.2 | 7776 | 0.336 | 3130.6 | 329.99 |
| 4 | 1036.8 | 8294.4 | 6912 | 0.338 | 2800.6 | 331.21 |
| 5 | 1036.8 | 7257.6 | 6048 | 0.340 | 2469.4 | 332.71 |
| 6 | 1036.8 | 6220.8 | 5184 | 0.343 | 2136.7 | 334.61 |
| 7 | 1036.8 | 5184.0 | 4320 | 0.348 | 1802.1 | 337.11 |
| 8 | 1036.8 | 4147.2 | 3456 | 0.353 | 1465.0 | 340.63 |
| 9 | 1036.8 | 3110.4 | 2592 | 0.361 | 1124.4 | 346.14 |
| 10 | 1036.8 | 2073.6 | 1728 | 0.375 | 778.2 | 356.78 |
| 11 | 1036.8 | 1036.8 | 864 | 0.407 | 421.5 | 421.46 |
| 12 | 0 | | 0 | 0 | 0 | 0 |

Table A.5: Floor gravity loads tributary to each wall for calculating the P- Δ effect in the 12-storey building.

| Storey | Dead Load | Reduced Live Load | Combined Load |
|--------|-----------|-------------------|----------------|
| n | CDL (kN) | RCLL (kN) | 1.0D+0.5L (kN) |
| 1 | 3347.1 | 328.08 | 3511.1 |
| 2 | 3228.3 | 328.96 | 3392.8 |
| 3 | 3228.3 | 329.99 | 3393.3 |
| 4 | 3228.3 | 331.21 | 3393.9 |
| 5 | 3228.3 | 332.71 | 3394.7 |
| 6 | 3228.3 | 334.61 | 3395.6 |
| 7 | 3228.3 | 337.11 | 3396.9 |
| 8 | 3228.3 | 340.63 | 3398.6 |
| 9 | 3228.3 | 346.14 | 3401.4 |
| 10 | 3228.3 | 356.78 | 3406.7 |
| 11 | 3228.3 | 421.46 | 3439.0 |
| 12 | 3104.6 | 0 | 3104.6 |

Table A.6: Modal analysis results for the 1st design iteration on a 12-storey building

| Mode | Period | Participation factor | Modal mass participation | Effective modal mass |
|----------------|--------------------|----------------------|--------------------------|----------------------|
| N ^o | T _n (s) | Γ | (%) | M* (tonne) |
| 1 | 3.73 | 1.489 | 65.52 | 2587.05 |
| 2 | 0.58 | 0.720 | 20.48 | 808.65 |
| 3 | 0.22 | 0.367 | 6.987 | 275.88 |

Table A.7: Results from modal pushover analyses in the 1st design iteration on a 12-storey building

| Mode | Yield base shear | Yield Roof Displ. | Yield PSA | Elastic PSA | Reduction Factor | Ultimate Roof Displ. | Ultimate Base Shear |
|----------------|----------------------|-------------------|-----------|-------------|------------------|----------------------|---------------------|
| N ^o | V _{by} (kN) | Δ_y (mm) | A (g) | PSA (g) | R _y | Δ_u (mm) | V _y (kN) |
| 2 | 5188.7 | 39.5 | 0.654 | 0.608 | 0.93 | 36.73 | 4824.4 |
| 3 | 8759.4 | 13.7 | 3.237 | 0.942 | 0.29 | 3.97 | 2549.4 |

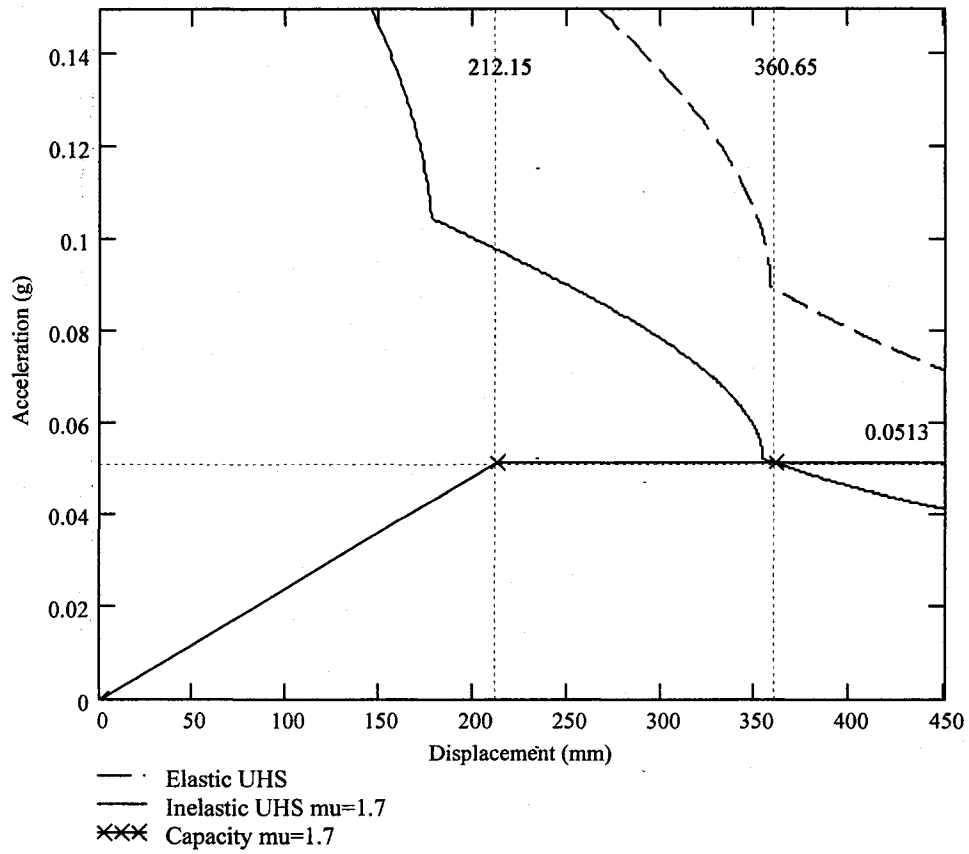


Figure A.1: Capacity-demand diagram for the preliminary design of shear walls for a 12-storey shear wall

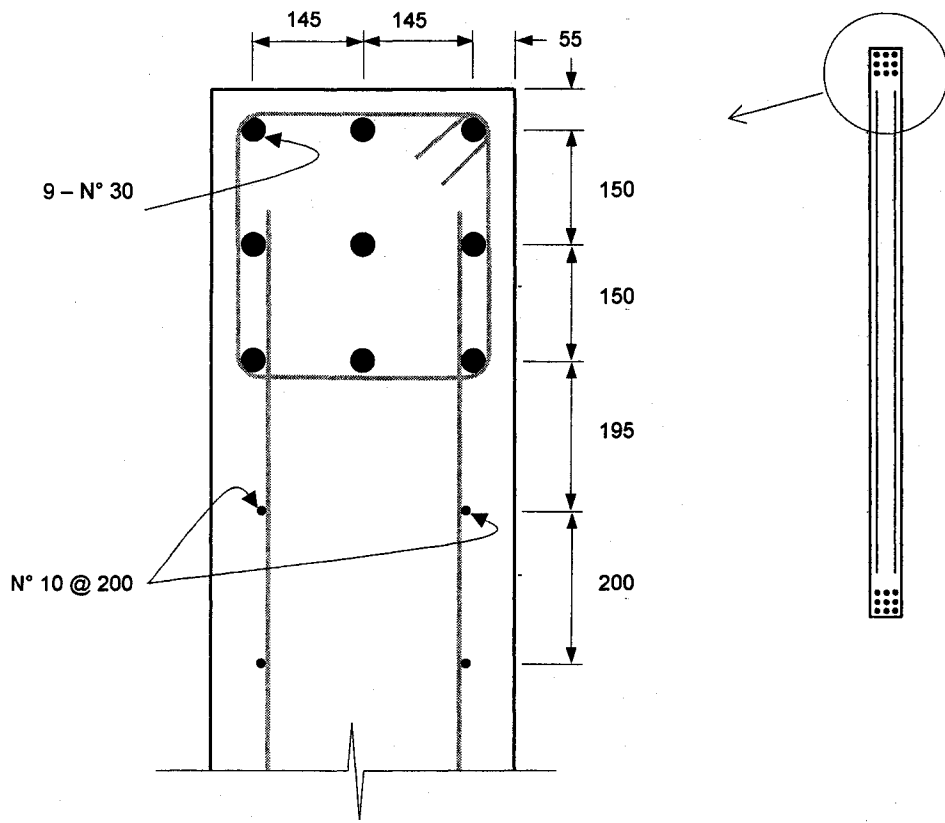


Figure A.2: Detail of reinforcement for the preliminary design of shear walls for a 12-storey building

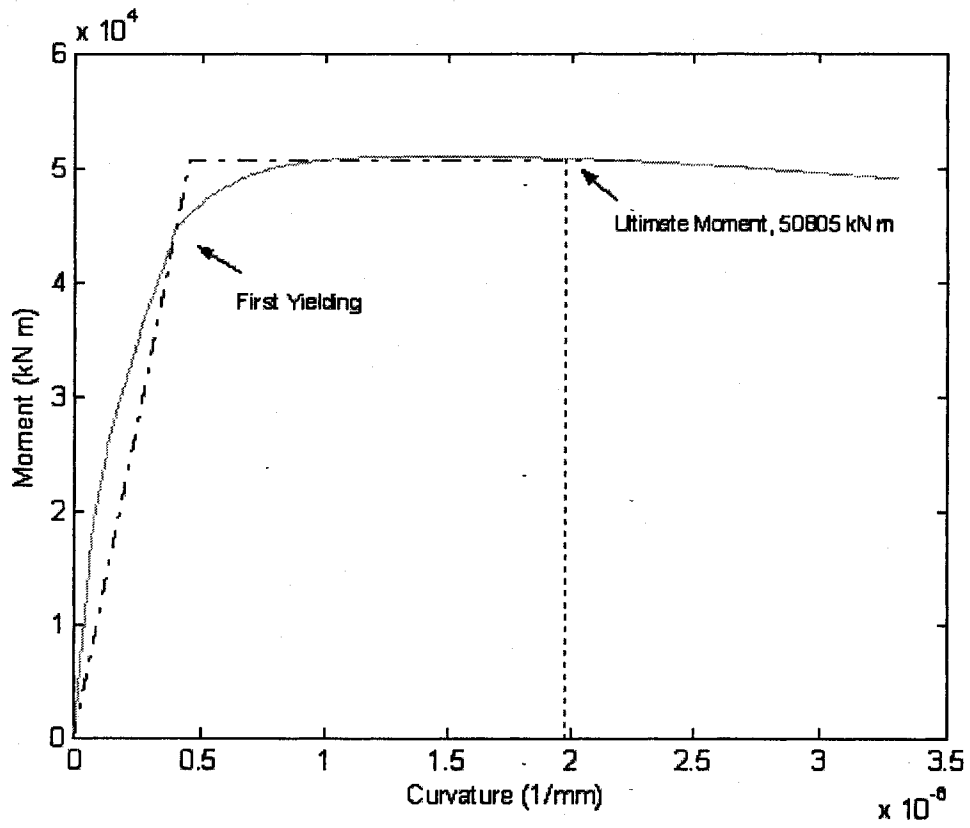


Figure A.3: Moment-curvature relationship for the preliminary design of shear walls for a 12-storey building

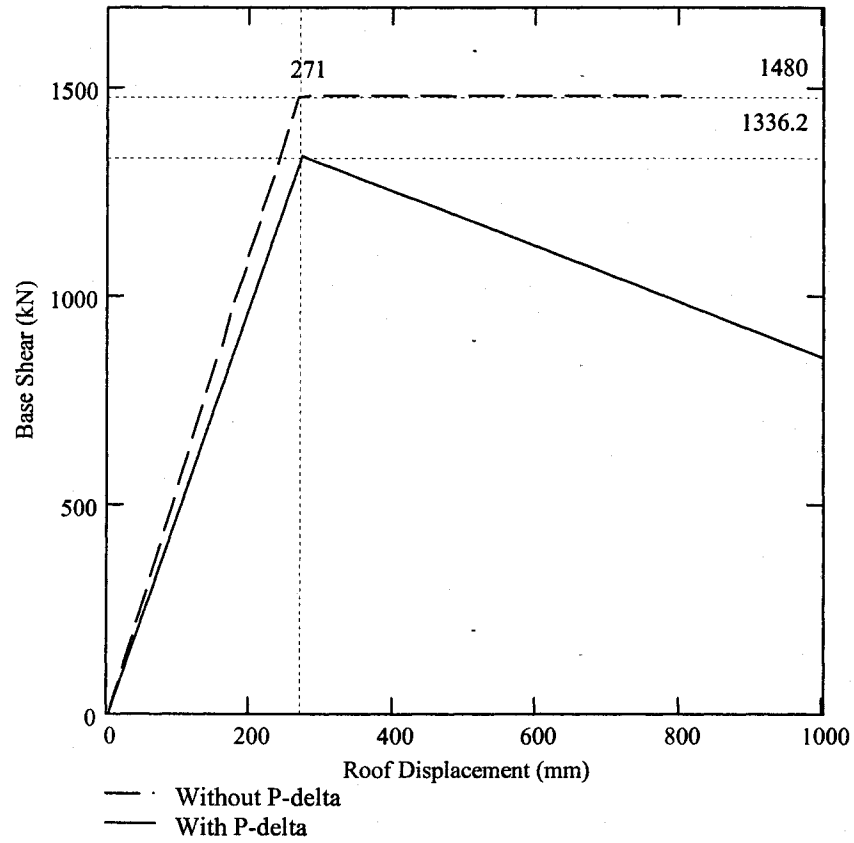


Figure A.4: Pushover curves with and without P- Δ effect for the preliminary design of shear walls for a 12-storey building

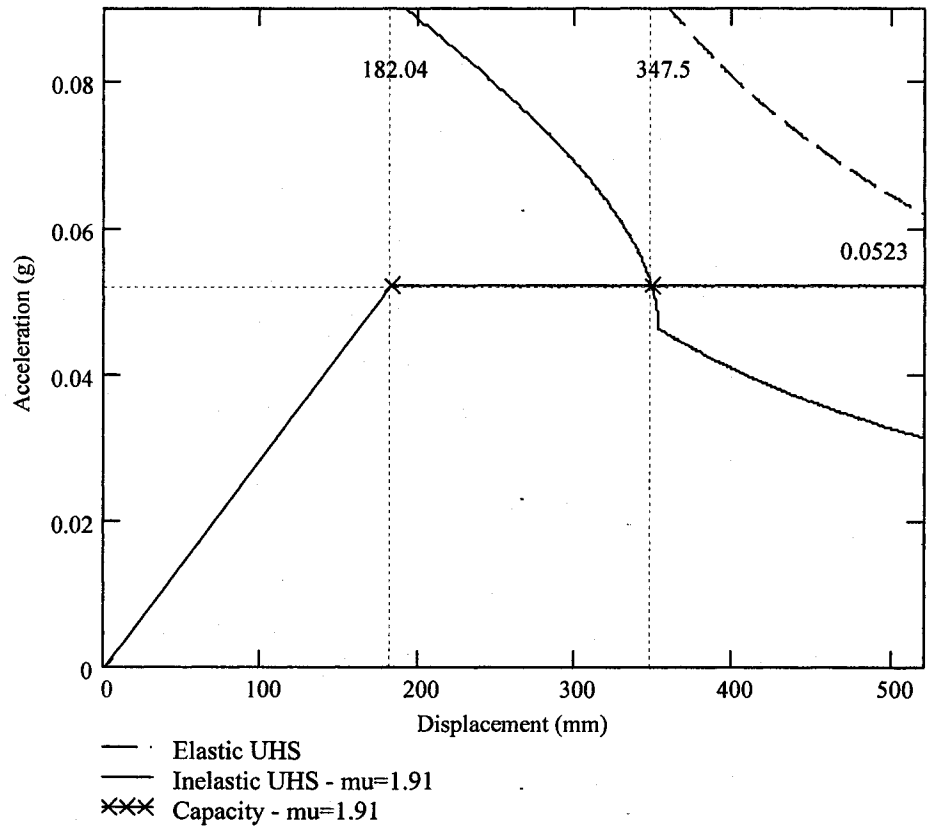


Figure A.5: Capacity-demand diagram for the first design iteration on a 12-storey building

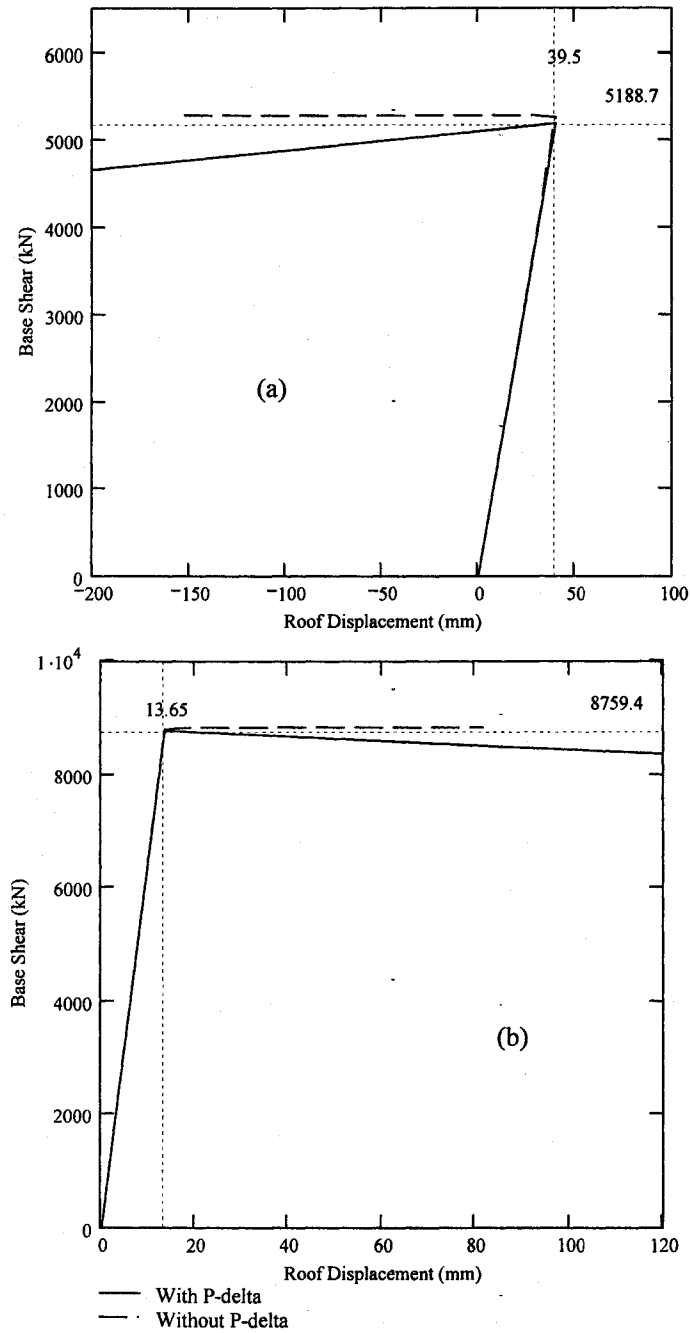


Figure A.6: Pushover curves with and without P- Δ effect for the final design of shear walls for a 12-storey building obtained by distributing the lateral forces according to

(a) the second mode shape, and (b) the third mode shape

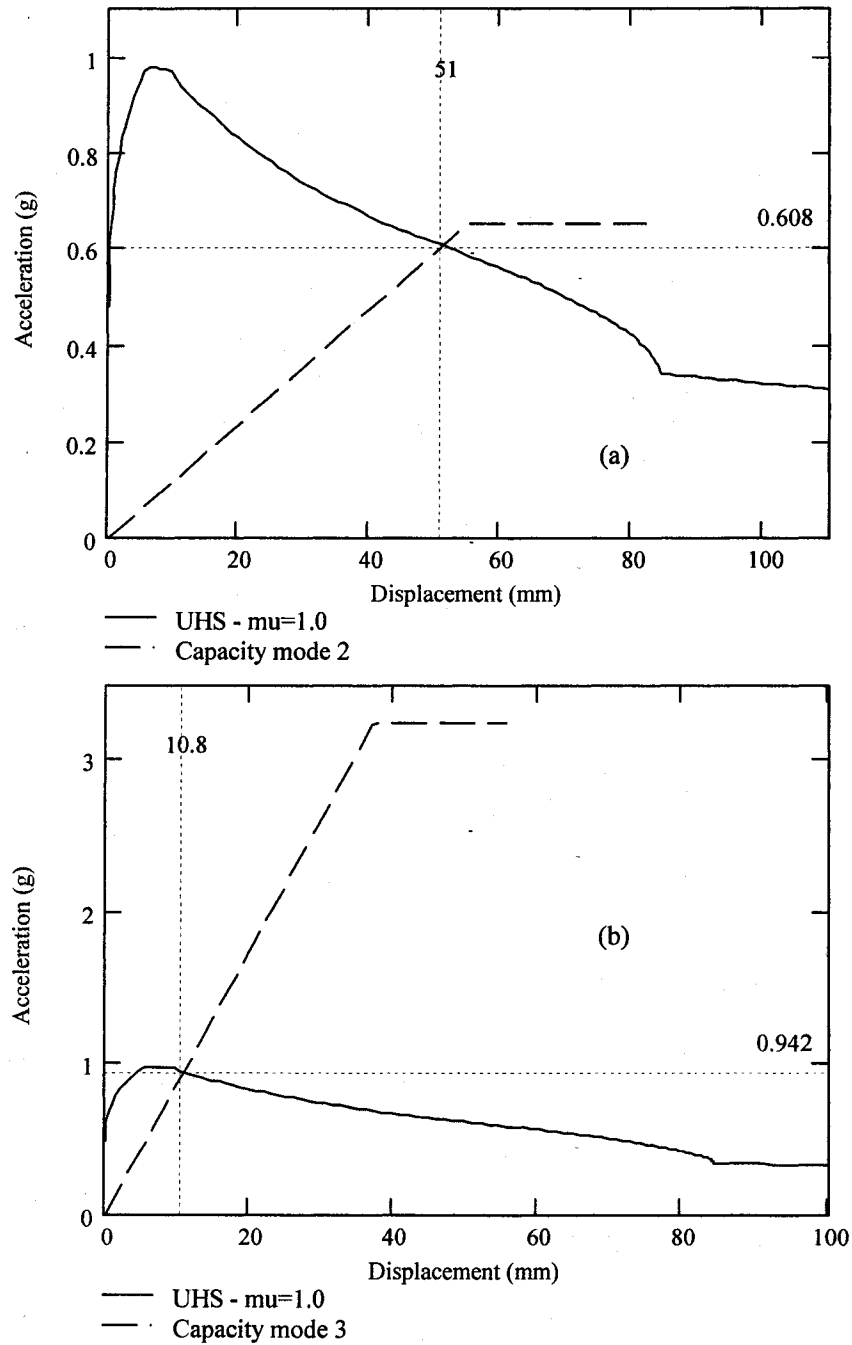


Figure A.7: Capacity-demand diagrams for the final design of shear walls for a 12-storey building obtained by distributing the lateral forces according to (a) the second mode shape, and (b) the third mode shape

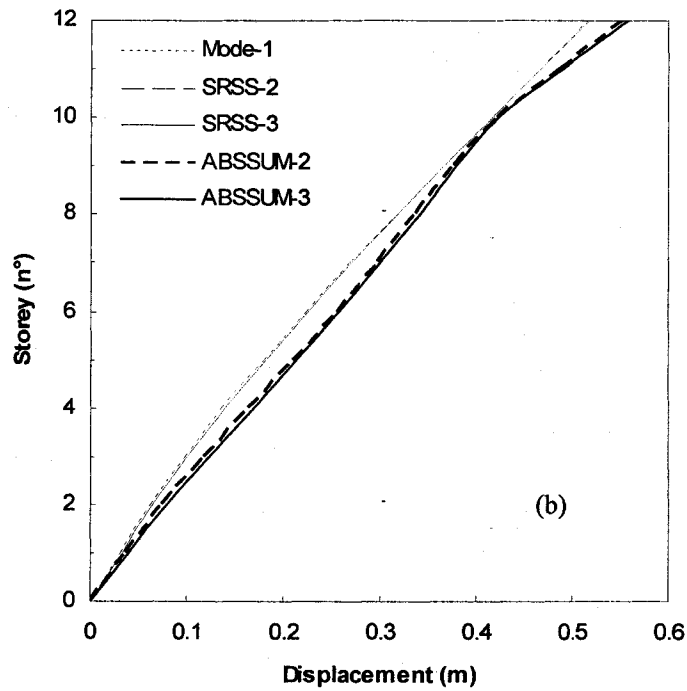
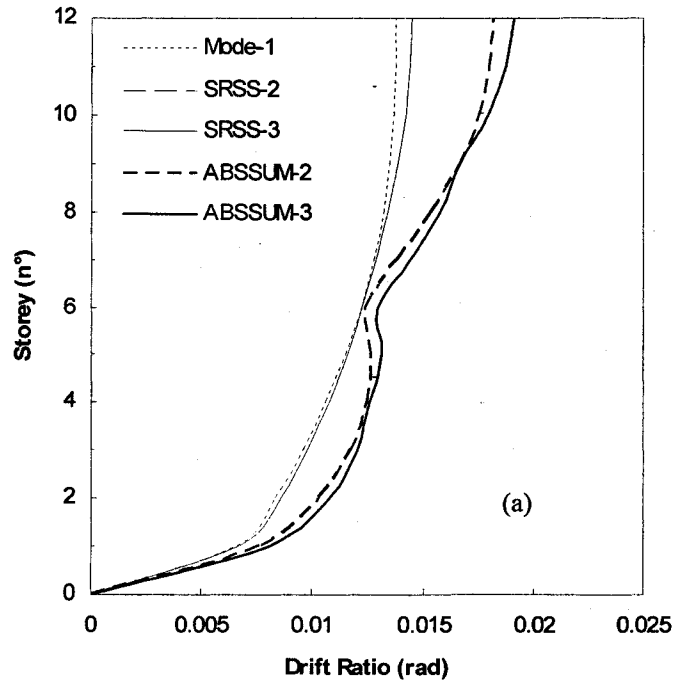


Figure A.8: (a) Inter-storey drifts ratios and (b) displacements for a 12-storey building

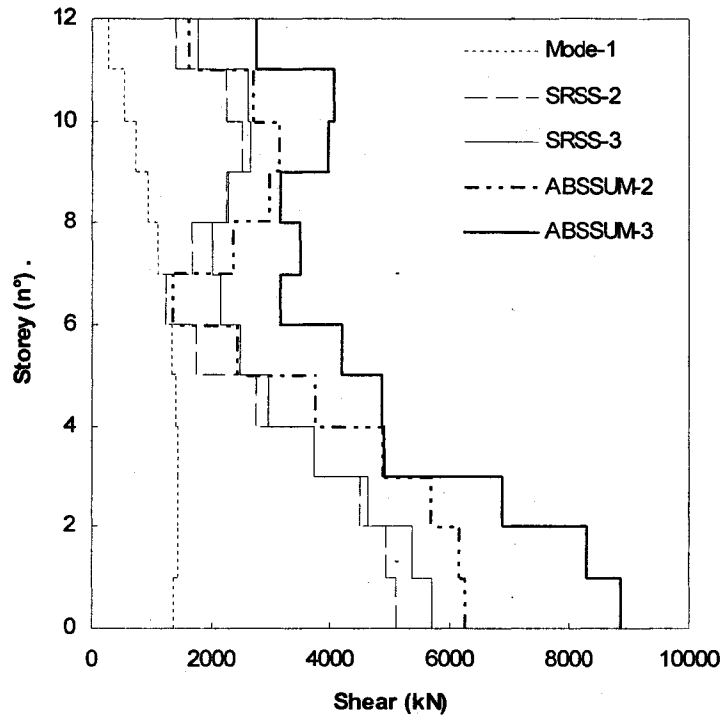


Figure A.9: Shear forces for a 12-storey building

Appendix B

B.1. DBSD of a 15-storey building

B.1.1. General Calculation

Floor dead load, q_f

| | |
|---------------------------------|--|
| Slab | $q_{\text{slab}} = t h_s \times \gamma_{\text{rc}} = 0.2 \times 24 = 4.8 \text{ kN/m}^2$ |
| Partition | $q_p = 0.5 \text{ kN/m}^2$ |
| Electrical, mechanical, ceiling | $q_{\text{EMC}} = 0.5 \text{ kN/m}^2$ |
| Total | $q_f = q_{\text{slab}} + q_p + q_{\text{EMC}} = 5.8 \text{ kN/m}^2$ |

The roof dead load is also 5.8 kN/m^2 since partition load is replaced by the same amount of load due to insulation and roofing.

Load due to self weight

Upper floor columns

$$q_{\text{fc}} = \frac{n_c \times A_{\text{col}} \times \gamma_{\text{rc}} \times 3.65\text{m}}{A_{\text{plan}}} = \frac{18 \times 0.6 \times 0.6 \times 24 \times 3.65}{24 \times 36} = 0.657 \text{ kN/m}^2$$

1st level columns

$$q_{1c} = \frac{n_c \times A_{col} \times \gamma_{rc} \left(\frac{3.65 + 4.85}{2} \right)}{A_{plan}} = \frac{18 \times 0.6 \times 0.6 \times 24 \times 4.25}{24 \times 36} = 0.765 \text{ kN/m}^2$$

Roof level columns

$$q_{roofc} = \frac{n_c \times A_{col} \times \gamma_{rc} \left(\frac{3.65}{2} \right)}{A_{plan}} = \frac{18 \times 0.6 \times 0.6 \times 24 \times 1.825}{24 \times 36} = 0.328 \text{ kN/m}^2$$

Upper floor walls

$$q_{fsw} = \frac{4 \times l_w \times th_w \times \gamma_{rc} \times 3.65m}{A_{plan}} = \frac{4 \times 8.5 \times 0.4 \times 24 \times 3.65}{24 \times 36} = 1.379 \text{ kN/m}^2$$

1st level walls

$$q_{1sw} = \frac{4 \times l_w \times th_w \times \gamma_{rc} \left(\frac{3.65 + 4.85}{2} \right)}{A_{plan}} = \frac{4 \times 8.5 \times 0.4 \times 24 \times 4.25}{24 \times 36} = 1.606 \text{ kN/m}^2$$

Roof level walls

$$q_{roofsw} = \frac{4 \times l_w \times th_w \times \gamma_{rc} \left(\frac{3.65}{2} \right)}{A_{plan}} = \frac{4 \times 8.5 \times 0.4 \times 24 \times 1.825}{24 \times 36} = 0.689 \text{ kN/m}^2$$

Total dead load and mass

Floor

$$q_{DL} = q_f + q_{fc} + q_{fsw} = 5.8 + 0.657 + 1.379 = 7.836 \text{ kN/m}^2$$

1st level

$$q_{IDL} = q_f + q_{ic} + q_{lsw} = 5.8 + 0.765 + 1.606 = 8.171 \text{ kN/m}^2$$

Roof (including 25% of snow load)

$$\begin{aligned} q_{rDL} &= 0.25q_s + q_f + q_{roofc} + q_{roofsw} \\ &= 0.25 \times 2.2 + 5.8 + 0.328 + 0.689 = 7.368 \text{ kN/m}^2 \end{aligned}$$

Considering a tributary area of 432 m² (half of the plan area), the distribution of dead loads and masses for each wall and floor is presented on Table B.1.

B.1.2. Gravity loads

The gravity loads are divided in two types: design axial load, and axial load for P-Δ effect. The design load or maximum axial load is computed at the shear wall base and will be used in the moment-curvature analysis. Another load is calculated assuming that the two shear walls together resist the P-Δ effect produced by the entire gravity load.

B.1.2.1. Design axial load, P_b

The gravity loads on the shear wall will be obtained from the floor loads acting on a tributary area of 97.5 m² (16.25 m × 6 m) plus the self weight. These loads are calculated as follows:

Upper floor level self weight, P_{wf}

$$P_{wf} = 3.65 \times l_w \times t_h \times \gamma_{rc} = 3.65 \times 8.5 \times 0.4 \times 24 = 297.84 \text{ kN}$$

1st level self weight, P_{w1}

$$P_{w1} = 4.85 \times l_w \times th_w \times \gamma_{rc} = 4.85 \times 8.5 \times 0.4 \times 24 = 395.76 \text{ kN}$$

Bottom of top storey, P_{top}

$$\text{Snow load, } P_s = 0.25 \times q_s \times A_{trib} = 0.25 \times 2.2 \times 97.5 = 53.6 \text{ kN}$$

$$\text{Roof load, } P_r = q_r \times A_{trib} = 5.8 \times 97.5 = 565.5 \text{ kN}$$

$$\text{Total } P_{top} = P_{wf} + P_s + P_r = 916.97 \text{ kN}$$

Bottom of typical storey, P_{ts}

$$\text{Floor load, } P_f = q_f \times A_{trib} = 5.8 \times 97.5 = 565.5 \text{ kN}$$

$$\text{Total } P_{ts} = P_{wf} + P_f = 863.34 \text{ kN}$$

$$\text{Bottom of first storey, } P_1 \quad P_1 = P_{w1} + P_f = 961.26 \text{ kN}$$

The live load is included according to the NBCC 2005 requirements. This load is reduced by the live load reduction factor, LLRF, which is given by:

$$LLRF = 0.3 + \sqrt{\frac{9.8}{CA_{trib}}} \quad (B.1)$$

where CA_{trib} is the cumulative tributary area in m^2 . The calculations are presented in Table B.2.

Finally, the factored dead and live loads are combined using two load combination rules: $1.25 D + 1.50 L$ and $1.0D + 0.5 L$, where L is the reduced live load. The results are

presented in Table B.3. The design gravity load in the presence of earthquake loads is obtained from the combination $D + 0.5 L$ and is seen to be 13,731.84 kN.

B.1.2.2. Axial load for P- Δ effect

In this case, the tributary area will be assumed to be half of the total plan area, 432 m². The live loads are computed using the same procedure as the previous section and the results are shown on Table B.4. The factored dead load and reduced live loads are finally combined using the rule: $1.0 D + 0.5 L$ and the results for each wall and floor are shown in Table B.5.

B.1.3. DBSD

The calculations presented bellow follow the steps presented in the summary Chapter 3.

1. The yield displacement and rotation are given by Equations (3.2) and (3.3) where

$$\epsilon_y = \frac{f_y \times \phi_s}{E_s} = \frac{400 \times 0.85}{200000} = 0.0017$$

is the factored yield steel strain. The yield curvature is given by Equation (3.4)

$$\phi_y = \frac{2.0\epsilon_y}{l_w} = \frac{2 \times 0.0017}{8500} = 4.0 \times 10^{-7} \text{ 1/mm}$$

Hence the yield rotation is

$$\theta_y = \frac{\phi_y H}{2} = \frac{4.0 \times 10^{-7} \times 55950}{2} = 0.0112 \text{ rad}$$

and the yield displacement is

$$\Delta_y = \frac{\phi_y H^2}{3} = \frac{4.0 \times 10^{-7} \times 55950^2}{3} = 417.39 \text{ mm}$$

2. The ultimate rotation and displacement are defined by Equations (3.5) and (3.7), and together provide the required local ductility. The ultimate curvature is given by

$$\phi_u = \frac{\epsilon_{cu}}{0.3l_w} = \frac{0.004}{0.3 \times 8500} = 1.57 \times 10^{-6} \text{ 1/mm.}$$

Assuming a plastic hinge length of $0.5l_w$ the plastic rotation and displacement are obtained from Equations (3.6) and (3.8) as follows:

$$\theta_p = (\phi_u - \phi_y) L_p = (15.7 - 4.0) \times 10^{-7} \times 0.5 \times 8500 = 0.00497 \text{ rad}$$

$$\Delta_p = \theta_p (H - 0.5L_p) = 0.00497 \times (55950 - 0.5 \times 4250) = 267.33 \text{ mm.}$$

Finally, the ultimate rotation is given by

$$\theta_u = \theta_y + \theta_p = 0.0102 + 0.00497 = 0.01616 \text{ rad}$$

and the ultimate displacement is

$$\Delta_u = \Delta_y + \Delta_p = 417.4 + 267.3 = 684.7 \text{ mm.}$$

Note that by using the drift limit establish by the NBCC 2005, the ultimate displacement is given by (Equation (3.9))

$$\Delta_u = 417.4 + (55950 - 0.5 \times 4250) \cdot \left(0.025 - \frac{4.0 \times 10^{-7} \times 55950}{2} \right) = 1160.7 \text{ mm}$$

which is larger than that obtained from limiting the concrete strain to 0.004.

Therefore, the ultimate displacement is set at 684.7 mm and the ductility capacity is

given by

$$\mu = \frac{\Delta_u}{\Delta_y} = \frac{684.7}{417.4} = 1.64$$

3. The mass distribution is shown in Table B.1 and the displacement shape assumed to be in the form of an inverted triangle is obtained from the following

$$\phi^T = \frac{h}{H} = \{0.087 \quad 0.152 \quad 0.217 \quad 0.282 \quad 0.348 \quad 0.413 \quad 0.478 \\ 0.543 \quad 0.609 \quad 0.674 \quad 0.739 \quad 0.804 \quad 0.87 \quad 0.935 \quad 1\}$$

The modal participation factor and effective modal mass are now calculated from Equations (3.10) and (3.11), respectively

$$\Gamma = \frac{(\phi^T \mathbf{M} \mathbf{1})}{(\phi^T \mathbf{M} \phi)} = 1.456$$

$$M^* = \frac{(\phi^T \mathbf{M} \mathbf{1})^2}{(\phi^T \mathbf{M} \phi)} = 4065.6 \text{ tonne}$$

4. The yield and ultimate displacements for the equivalent SDOF system are thus given by

$$\delta y = \frac{\Delta_y}{\Gamma \phi^r} = \frac{417.39}{1.456 \times 1} = 286.74 \text{ mm}$$

$$\delta u = \frac{\Delta_u}{\Gamma \phi^r} = \frac{684.7}{1.456 \times 1} = 470.39 \text{ mm}$$

5. From the capacity-demand method (Figure B.1) and using δy , δu and μ , the inelastic pseudo-acceleration, A , is

$$A = 0.041 \text{ g}$$

6. The corresponding base design shear is

$$V_b = A \cdot M^* = 0.041 \times 9.81 \times 4065.6 = 1636.4 \text{ kN}$$

7. The base shear is distributed according to the product of the floor weights and the floor height shown in Table B.1

$$F^T = V_b \times \frac{W \cdot h}{\sum W \cdot h} = \{18.27 \quad 30.71 \quad 43.90 \quad 57.09 \quad 70.28 \quad 83.47 \quad 96.66 \\ 109.85 \quad 123.04 \quad 136.23 \quad 149.42 \quad 162.61 \quad 175.80 \quad 188.99 \quad 190.10\} \text{ kN}$$

The base moment is then given by

$$M_b = \sum [F(h_{i+1} - h_i)] = 62899.6 \text{ kN} \cdot \text{m}$$

8. The structure is now designed to resist P_b , V_b and M_b . The minimum requirements are taken from the CSA A23.3-94.

The minimum area of concentrated reinforcement is given by

$$A_{s_{\min}} = 0.002 \cdot t_h \cdot l_w = 0.002 \times 400 \times 8500 = 6800 \text{ mm}^2$$

The minimum distributed reinforcement is obtained from

$$A_{s_{d\min}} = 0.0025 \cdot t_h = 0.0025 \times 400 = 1000 \text{ mm}^2 / \text{m}$$

and is provided by 2 layers of #10 at 200 mm spacing.

The required vertical concentrated reinforcement is calculated by following the simplified method presented on Chapter 3. The depth of the compression zone is given by

$$c = \frac{P_b + A_d \phi_s f_y l_w}{\alpha_1 \phi_c f_c \beta_1 b_w + 2A_d \phi_s f_y}$$

$$= \frac{13731.8 + 1000 \times 0.85 \times 400 \times 8500}{0.805 \times 0.6 \times 30 \times 0.895 \times 400 + 2 \times 1000 \times 0.85 \times 400} = 2832.9 \text{ mm}$$

The concrete resistant moment is obtained from

$$M_c = \alpha_1 \phi_c f_c c^2 \beta_1 b_w (1 - 0.5\beta_1)$$

$$= 0.805 \times 0.6 \times 30 \times 2832.9^2 \times 0.895 \times 400 \times (1 - 0.5 \times 0.895) = 23001 \text{ kN} \cdot \text{m}$$

The resistant moment provided by the distributed reinforcement is give by

$$M_{Ad} = A_d \phi_s f_y c^2 \left[1 + \left(\frac{l_w}{c} - 1 \right)^2 - \frac{2}{3} \left(\frac{\epsilon_y}{\epsilon_{cu}} \right)^2 \right] =$$

$$1000 \times 0.85 \times 400 \times 2832.9^2 \left[1 + \left(\frac{8500}{2832.9} - 1 \right)^2 - \frac{2}{3} \left(\frac{0.002}{0.0035} \right)^2 \right] = 6527 \text{ kN} \cdot \text{m}$$

The restoring moment provided by the axial load is obtained from

$$M_p = P_b \cdot \left(\frac{l_w}{2} - c \right) = 13731.8 \left(\frac{8500}{2} - 2832.9 \right) = 19459.3 \text{ kN} \cdot \text{m}$$

Thus, the resistant moment to be contributed by the concentrated reinforcement is obtained from

$$M_{cr} = M_b - M_c - M_{Ad} - M_p$$

$$= 62899.6 - (23001 + 6527 + 19459.3) = 13912.2 \text{ kN} \cdot \text{m}$$

and the corresponding steel area is given by

$$A_{cr} = \frac{M_{cr}}{\phi_s f_y (l_w - 2h_m)} = \frac{13912.2}{0.85 \times 400 \times (8500 - 2 \times 217.5)} = 5268 \text{ mm}^2 < A_{s_{min}}$$

This area is smaller than the minimum area required by the code, $A_{s_{min}} = 6800 \text{ mm}^2$.

Therefore, an arrangement of 4 bars #35 and 4 bars #30 is adopted which gives an

area of 6800 mm^2 . The value of h_m was obtained by assuming a spacing of 160 mm plus a cover of 40 mm, and half of the steel section diameter, 15 mm (see Figure B.2). Using this reinforcement, the moment-curvature analysis gives the curve shown in Figure B.3. From the idealized curve shown with a dotted line, the following results

| | |
|--|------------------------------------|
| Moment capacity, M_c | 67349 kNm |
| Yield curvature, ϕ_y | $4.07 \times 10^{-7} \text{ 1/mm}$ |
| Ultimate curvature, ϕ_u | $1.54 \times 10^{-6} \text{ 1/mm}$ |
| Ratio of effective moment of inertia to the gross moment of inertia, I_r | 0.3301 |

From these results the refined plastic rotation and roof displacement can be computed as follows

$$\theta_p = (\phi_u - \phi_y) L_p = (15.4 - 4.07) \times 10^{-6} \times 4250 = 0.00483 \text{ rad}$$

$$\Delta_p = 0.00483(55950 - 0.5 \times 4250) = 259.87 \text{ mm}$$

Also from these results, the stability of this shear wall can be checked by obtaining the critical thickness according to Equation (3.18) as follows

$$b_c = 0.017 \cdot l_w \cdot \sqrt{\mu_\phi} = 0.017 \times 8500 \times \sqrt{\frac{15.4}{4.07}} = 281.35 \text{ mm}$$

Thus the 400 mm thickness will avoid any instability problem.

- The modal analysis including the P- Δ effect gives the following properties related to the first mode

| | |
|-------------------------|--------|
| Period of vibration, T1 | 4.85 s |
|-------------------------|--------|

| | |
|--------------------------------|--------------|
| Mode shape at roof, ϕ^T | 0.0261 |
| Participation factor, Γ | 1.506 |
| Effective modal mass, M^* | 3340.9 tonne |

10. Distributing the forces according to Equation (3.26) a first mode pushover analysis is carried out. The roof displacement versus base shear relationship obtained is shown in Figure B.4. The important result from this curve is the yield point which is given by

| | |
|-------------------------------------|-----------|
| Yield base shear, V_{by} | 1393.9 kN |
| Yield roof displacement, Δ_y | 374 mm |

From this displacement and the moment-curvature analysis, the new target ultimate displacement is defined as follows

$$\Delta_u = \Delta_y + \Delta_p = 374 + 259.87 = 633.87 \text{ mm}$$

That gives a new ductility demand of

$$\mu = \frac{\Delta_u}{\Delta_y} = 1.695$$

11. The yield and ultimate displacement for the equivalent SDOF system are now given by

$$\delta_y = \frac{\Delta_y}{\Gamma \phi^T} = \frac{374}{1.506 \times 0.0261} = 248.4 \text{ mm}$$

$$\delta_u = \frac{\Delta_u}{\Gamma \phi^T} = \frac{633.87}{1.506 \times 0.0261} = 421.0 \text{ mm}$$

The inelastic acceleration, A , is obtained by using δ_y , δ_u , and μ in the capacity-

demand method (Figure B.5)

$$A = 0.044 \text{ g}$$

Finally, the new base shear is

$$V_{y_{\text{new}}} = M^* A = 3340.9 \times 0.044 \times 9.81 = 1449.2 \text{ kN}$$

12. The difference between the two successive estimates is

$$\text{diff}_{V_y} = \frac{V_y - V_{y_{\text{new}}}}{V_y} = -3.97 \%$$

Therefore, a new design will be carried out. The new base design moment is obtained from

$$M_b = M_c (1 - \text{error}_{V_y}) = 67349 \times (1 + 0.0211) = 68767.4 \text{ kN} \cdot \text{m}$$

The computations presented in Steps 8 through 12 are repeated; results of the moment-curvature analysis, modal analysis, and pushover analysis are shown in Table B.6, Table B.7, and Table B.8 for another try, including the results from the first try. Two tries were needed to find an error less than 1 %. From the last column of Table B.8 it is possible to see how the procedure immediately converges. The results obtained from the last attempt are shown in Figure B.6 through Figure B.9. This design gives an ultimate base shear of $V_u = 1278 \text{ kN}$, the corresponding ratio of the ultimate base shear to yield shear $V_u / V_y = 0.878$, which is a measure of the excursion into the unstable part of the pushover curve.

13. The method was seen to converge on the second attempt. It may be noted that all of the preceding computations were based on the first mode. The moment estimate obtained from the first mode is expected to be reasonable. However, in a shear wall

structure the higher modes make significant contribution to the base shear. Hence four higher modes, 2nd, 3rd, and 4th are included and analysis is repeated with these modes following the procedure presented in Section 3.11 of modal pushover analysis. The modal analysis results are shown in Table B.9 for four modes. The pushover curves obtained by using distribution of forces according to the second, third, and fourth mode shapes are shown in Figure B.10. These curves are transformed into equivalent SDOF systems and then plotted on the capacity-demand diagrams presented in Figure B.11. That figure, as well as the data summarized in Table B.10, show that the performance points do not lie in the inelastic zone of the capacity diagram, which means that responses remain elastic. The responses in the four modes are combined according to the SRSS and ABSSUM rules and the results are shown Figure B.12 for the inter-storey drifts and displacements and in Figure B.13 for shear forces. As examples, three particular results are obtained as follows:

Roof displacement

$$\begin{aligned}\Delta_{\text{roof}} &= \sqrt{\Delta_{u1}^2 + \Delta_{u2}^2 + \Delta_{u3}^2 + \Delta_{u4}^2} \\ &= \sqrt{632.2^2 + 50.9^2 + 6.2^2 + 1.2^2} = 634.3 \text{ mm}\end{aligned}$$

Maximum drift ratio

$$\begin{aligned}\theta_{\text{max}} &= \sqrt{\theta_{\text{max}1}^2 + \theta_{\text{max}2}^2 + \theta_{\text{max}3}^2 + \theta_{\text{max}4}^2} \\ &= \sqrt{0.0139^2 + 0.0048^2 + 0.0011^2 + 0.0004^2} = 0.0147\end{aligned}$$

Base shear

$$\begin{aligned}V_b &= \sqrt{V_{b1}^2 + V_{b2}^2 + V_{b3}^2 + V_{b4}^2} \\ &= \sqrt{1458^2 + 5288^2 + 3115^2 + 1695^2} = 6531 \text{ kN}\end{aligned}$$

where the numeric subscript indicates the mode number.

Assuming a horizontal reinforcement of #15 at 150 mm and an effective depth of $d = 0.8lw$, the simplified method gives a shear capacity of (Clause 11.3 of the CSA 1994):

$$V_{\text{capacity}} = 0.2\phi_c \sqrt{f_c} \cdot t h_w d_v + \phi_s \frac{A_v f_y}{s} d =$$

$$0.2 \times 0.6 \times \sqrt{30} \times 400 \times 0.8 \times 8500 + 0.85 \frac{400 \times 400}{150 \times 1000} 0.8 \times 8500 = 7590.4 \text{ kN}$$

Thus, the provided horizontal reinforcement will ensure sufficient capacity to resist the shear demand of 6,531 kN.

14. The design spectrum corresponding to 50%/50 year probability is obtained by scaling down the UHS corresponding to 2%/50 year probability by the ratio obtained in Section 3.12.1, that is, 0.325. The spectral acceleration from the UHS corresponding to 2%/50 year probability at $T_1 = 4.744$ s is 0.076 g. Thus, the demand acceleration for the operational level is $0.076 \times 0.325 = 0.018$ g. Considering the equivalent modal mass for the final design $M1^* = 3340.9$ tonne, the demand base shear, V_{bOP} , is given by

$$V_{\text{bOP}} = 3340.9 \times 9.81 \times 0.018 = 587.46 \text{ kN}$$

15. From the pushover curve shown in Figure B.8, the roof displacement is 150.9 mm for the calculated base shear, V_{bOP} . From pushover analysis data base, the maximum drift ratio at this roof displacement is 0.46 %. Therefore, the design is satisfactory for the operational performance level.

Table B.1: Floor dead loads and masses tributary to each wall in the 15-storey building

| Storey Number | Accumulated height (m) | Dead Load (kN) | Mass (tonne) |
|--------------------------|---------------------------------------|---------------------------|-------------------------|
| 1 | 4.85 | 3529.68 | 359.80 |
| 2 | 8.50 | 3385.10 | 345.07 |
| 3 | 12.15 | 3385.10 | 345.07 |
| 4 | 15.80 | 3385.10 | 345.07 |
| 5 | 19.45 | 3385.10 | 345.07 |
| 6 | 23.10 | 3385.10 | 345.07 |
| 7 | 26.75 | 3385.10 | 345.07 |
| 8 | 30.40 | 3385.10 | 345.07 |
| 9 | 34.05 | 3385.10 | 345.07 |
| 10 | 37.70 | 3385.10 | 345.07 |
| 11 | 41.35 | 3385.10 | 345.07 |
| 12 | 45.00 | 3385.10 | 345.07 |
| 13 | 48.65 | 3385.10 | 345.07 |
| 14 | 52.30 | 3385.10 | 345.07 |
| 15 | 55.95 | 3182.95 | 324.46 |

Table B.2: Reduced live load calculations for each wall of the 15-storey building

| Storey | Live Load | Cumulative Live Load | Cumulative Tributary Area | Live Load Reduction Factor | Reduced Cumulative Live Load |
|---------------|------------------|-----------------------------|--|-----------------------------------|-------------------------------------|
| N° | LL (kN) | CLL (kN) | CA_{trib} (m²) | LLRF | RCLL (kN) |
| 1 | 234 | 3276 | 1365.0 | 0.385 | 1260.38 |
| 2 | 234 | 3042 | 1267.5 | 0.388 | 1180.08 |
| 3 | 234 | 2808 | 1170.0 | 0.392 | 1099.39 |
| 4 | 234 | 2574 | 1072.5 | 0.396 | 1018.25 |
| 5 | 234 | 2340 | 975.0 | 0.400 | 936.60 |
| 6 | 234 | 2106 | 877.5 | 0.406 | 854.36 |
| 7 | 234 | 1872 | 780.0 | 0.412 | 771.43 |
| 8 | 234 | 1638 | 682.5 | 0.420 | 687.68 |
| 9 | 234 | 1404 | 585.0 | 0.429 | 602.92 |
| 10 | 234 | 1170 | 487.5 | 0.442 | 516.89 |
| 11 | 234 | 936 | 390.0 | 0.459 | 429.17 |
| 12 | 234 | 702 | 292.5 | 0.483 | 339.10 |
| 13 | 234 | 468 | 195.0 | 0.524 | 245.32 |
| 14 | 234 | 234 | 97.5 | 0.617 | 144.39 |
| 15 | 0 | 0 | 0 | 0 | 0 |

Table B.3: Gravity load combinations for each wall of the 15-storey building

| Storey | Dead Load | Cumulative Dead Load | Reduced Cumulative Live Load | Cumulative 1.25D+1.5L | Cumulative 1.0D+0.5L |
|---------------|------------------|-----------------------------|-------------------------------------|------------------------------|-----------------------------|
| n | DL (kN) | CDL (kN) | RCLL (kN) | (kN) | (kN) |
| 1 | 961.26 | 13101.645 | 1260.38 | 18267.63 | 13731.84 |
| 2 | 863.34 | 12140.385 | 1180.08 | 16945.61 | 12730.43 |
| 3 | 863.34 | 11277.045 | 1099.39 | 15745.39 | 11826.74 |
| 4 | 863.34 | 10413.705 | 1018.25 | 14544.51 | 10922.83 |
| 5 | 863.34 | 9550.365 | 936.60 | 13342.86 | 10018.67 |
| 6 | 863.34 | 8687.025 | 854.36 | 12140.32 | 9114.21 |
| 7 | 863.34 | 7823.685 | 771.43 | 10936.75 | 8209.40 |
| 8 | 863.34 | 6960.345 | 687.68 | 9731.95 | 7304.19 |
| 9 | 863.34 | 6097.005 | 602.92 | 8525.64 | 6398.47 |
| 10 | 863.34 | 5233.665 | 516.89 | 7317.41 | 5492.11 |
| 11 | 863.34 | 4370.325 | 429.17 | 6106.67 | 4584.91 |
| 12 | 863.34 | 3506.985 | 339.10 | 4892.37 | 3676.53 |
| 13 | 863.34 | 2643.645 | 245.32 | 3672.53 | 2766.30 |
| 14 | 863.34 | 1780.305 | 144.39 | 2441.96 | 1852.50 |
| 15 | 916.97 | 916.965 | 0 | 1146.21 | 916.97 |

Table B.4: Reduced tributary live loads for calculating the P- Δ effect for each wall of the
15-storey building

| Storey | Live Load | Cumulative Live Load | Cumulative Tributary Area | Live Load Reduction Factor | Reduced Cumulative Live Load | Reduced Live Load |
|--------|-----------|----------------------|--------------------------------------|----------------------------|------------------------------|-------------------|
| n | LL (kN) | CLL (kN) | CA _{trib} (m ²) | LLRF | RCLL (kN) | RLL (kN) |
| 1 | 1036.8 | 14515.2 | 12096 | 0.328 | 4767.72 | 326.07 |
| 2 | 1036.8 | 13478.4 | 11232 | 0.330 | 4441.65 | 326.66 |
| 3 | 1036.8 | 12441.6 | 10368 | 0.331 | 4114.99 | 327.33 |
| 4 | 1036.8 | 11404.8 | 9504 | 0.332 | 3787.67 | 328.08 |
| 5 | 1036.8 | 10368.0 | 8640 | 0.334 | 3459.58 | 328.96 |
| 6 | 1036.8 | 9331.2 | 7776 | 0.336 | 3130.62 | 329.99 |
| 7 | 1036.8 | 8294.4 | 6912 | 0.338 | 2800.64 | 331.21 |
| 8 | 1036.8 | 7257.6 | 6048 | 0.340 | 2469.43 | 332.71 |
| 9 | 1036.8 | 6220.8 | 5184 | 0.343 | 2136.72 | 334.61 |
| 10 | 1036.8 | 5184.0 | 4320 | 0.348 | 1802.11 | 337.11 |
| 11 | 1036.8 | 4147.2 | 3456 | 0.353 | 1465.00 | 340.63 |
| 12 | 1036.8 | 3110.4 | 2592 | 0.361 | 1124.38 | 346.14 |
| 13 | 1036.8 | 2073.6 | 1728 | 0.375 | 778.24 | 356.78 |
| 14 | 1036.8 | 1036.8 | 864 | 0.407 | 421.46 | 421.46 |
| 15 | 0 | 0 | 0 | 0 | 0 | 0 |

Table B.5: Floor gravity loads tributary to each wall for calculating the P- Δ effect in the
15-storey building

| Storey | Dead Load | Reduced Live Load | Combined Load |
|--------|-----------|-------------------|----------------|
| n | CDL (kN) | RCLL (kN) | 1.0D+0.5L (kN) |
| 1 | 3529.68 | 326.07 | 3692.71 |
| 2 | 3385.10 | 326.66 | 3548.43 |
| 3 | 3385.10 | 327.32 | 3548.77 |
| 4 | 3385.10 | 328.08 | 3549.15 |
| 5 | 3385.10 | 328.96 | 3549.58 |
| 6 | 3385.10 | 329.99 | 3550.10 |
| 7 | 3385.10 | 331.21 | 3550.71 |
| 8 | 3385.10 | 332.71 | 3551.46 |
| 9 | 3385.10 | 334.61 | 3552.41 |
| 10 | 3385.10 | 337.11 | 3553.66 |
| 11 | 3385.10 | 340.63 | 3555.42 |
| 12 | 3385.10 | 346.14 | 3558.17 |
| 13 | 3385.10 | 356.78 | 3563.49 |
| 14 | 3385.10 | 421.46 | 3595.83 |
| 15 | 3182.95 | 0 | 3182.95 |

Table B.6: Results of moment-curvature analysis in the 2 iterations in the design of a
15-storey building

| Iteration | Moment Capacity | Yield curvature | Ultimate curvature | Moment of Inertia ratio | Plastic rotation |
|-----------|-----------------|-----------------|--------------------|-------------------------|-----------------------------|
| Number | M_c (kN m) | ϕ_y (1/mm) | ϕ_u (1/mm) | I_r | θ_p (10^{-2} rad) |
| 1 | 67349 | 4.07E-07 | 1.54E-06 | 0.330 | 0.497 |
| 2 | 70094 | 4.08E-07 | 1.54E-06 | 0.343 | 0.483 |

Table B.7: First mode analysis results for the 2 design iterations on a 15-storey building

| Iteration | First mode period | Participation factor | Modal mass participation | Effective modal mass |
|-----------|-------------------|----------------------|--------------------------|----------------------|
| Number | T_1 (s) | Γ | (%) | M^* (tonne) |
| 1 | 4.848 | 1.506 | 64.62 | 3340.9 |
| 2 | 4.744 | 1.506 | 64.63 | 3341.5 |

Table B.8: Results from pushover analysis for the 2 design iterations on a 15-storey building

| Iteration | Yield base shear | Yield Roof Displ. | Ultimate Roof Displ. | Ductility Factor | Reduction Factor | Inelastic PSA | New Yield Shear | Base Shear Error |
|-----------|------------------|-------------------|----------------------|------------------|------------------|---------------|-----------------|------------------|
| Number | V_{by} (kN) | Δ_v (mm) | Δ_u (mm) | μ | R_y | A(g) | V_y (kN) | (%) |
| 1 | 1393.9 | 374.0 | 633.87 | 1.695 | 1.712 | 0.044 | 1449.16 | -3.97 |
| 2 | 1458.1 | 374.5 | 632.24 | 1.688 | 1.705 | 0.045 | 1459.28 | -0.08 |

Table B.9: Modal analysis results for the 2nd design iteration on a 15-storey building

| Mode | Period | Participation factor | Modal mass Participation | Effective modal mass |
|----------------|-----------|----------------------|--------------------------|----------------------|
| N ^o | T_n (s) | Γ | (%) | M^* (tonne) |
| 1 | 4.744 | 1.506 | 64.63 | 3341.5 |
| 2 | 0.727 | 0.752 | 20.26 | 1047.5 |
| 3 | 0.268 | 0.397 | 6.99 | 361.3 |
| 4 | 0.144 | 0.251 | 3.51 | 181.4 |

Table B.10: Results from modal pushover analyses in the 2nd design iteration on a
15-storey building

| Mode | Yield base shear | Yield Roof Displ. | Yield PSA | Elastic PSA | Reduction Factor | Ultimate Roof Displ. | Ultimate Base Shear |
|-------------|---------------------------------|----------------------------------|----------------------|------------------------|-----------------------------|-------------------------------------|------------------------------------|
| N° | V_{by}(kN) | Δ_y(mm) | A (g) | PSA (g) | R_y | Δ_u(mm) | V_y (kN) |
| 2 | 5771.1 | 55.5 | 0.562 | 0.515 | 0.916 | 50.852 | 5287.8 |
| 3 | 9758.7 | 19.5 | 2.753 | 0.879 | 0.319 | 6.224 | 3114.6 |
| 4 | 14208.5 | 10.3 | 7.983 | 0.952 | 0.119 | 1.228 | 1694.6 |

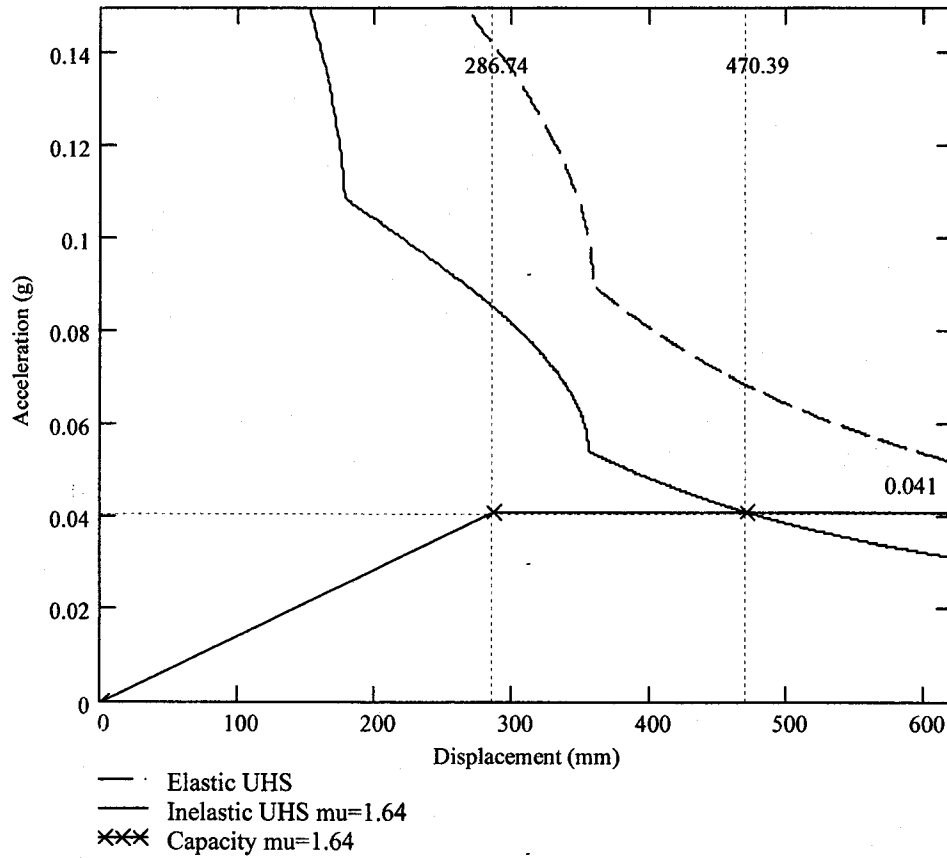


Figure B.1: Capacity-demand diagram for the preliminary design of shear walls for a 15-storey building

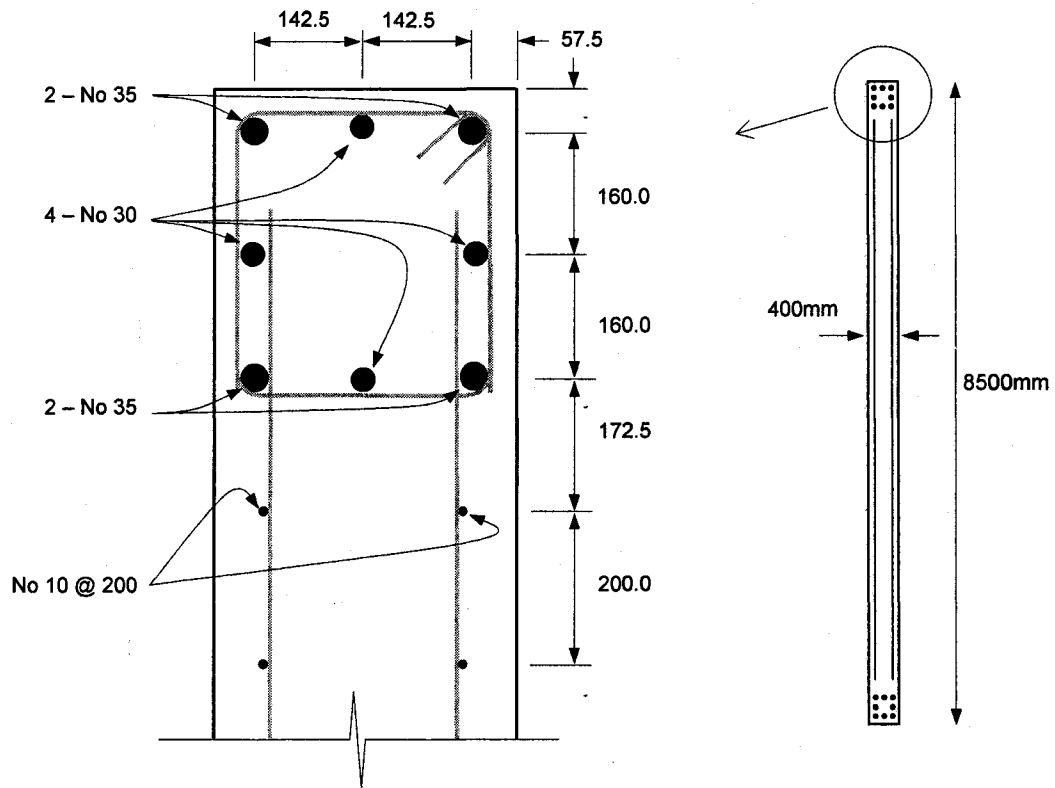


Figure B.2: Detail of reinforcement for the preliminary design of shear walls for a 15-storey building

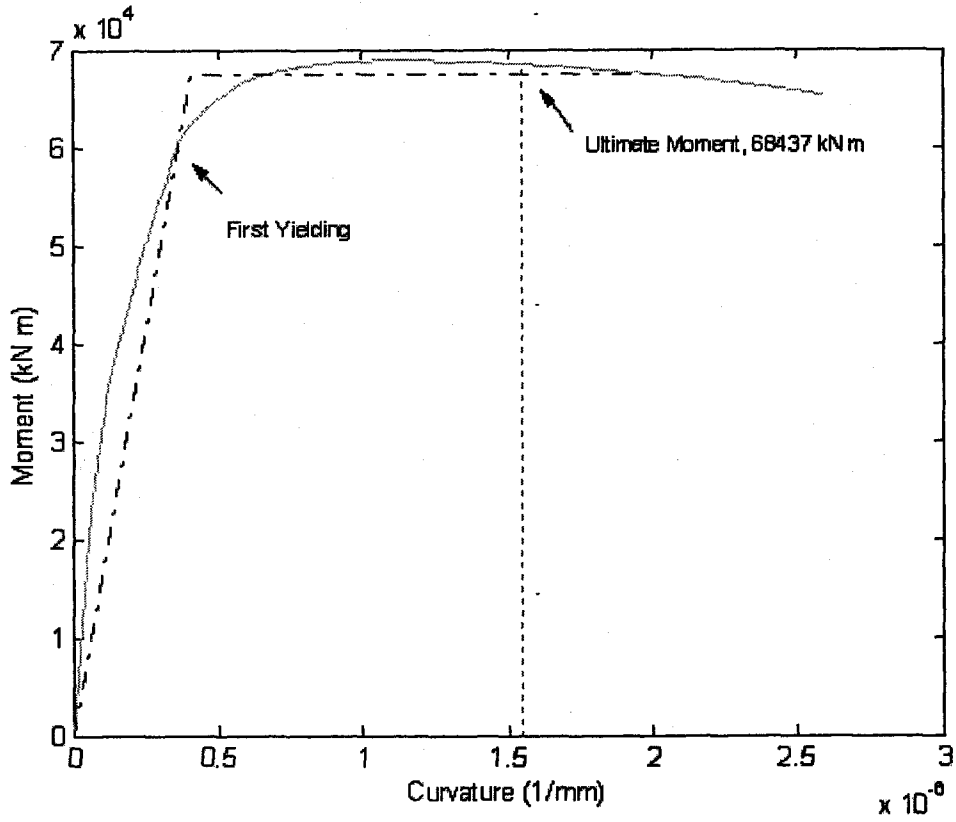


Figure B.3: Moment-curvature relationship for the preliminary design of shear walls for a 15-storey building

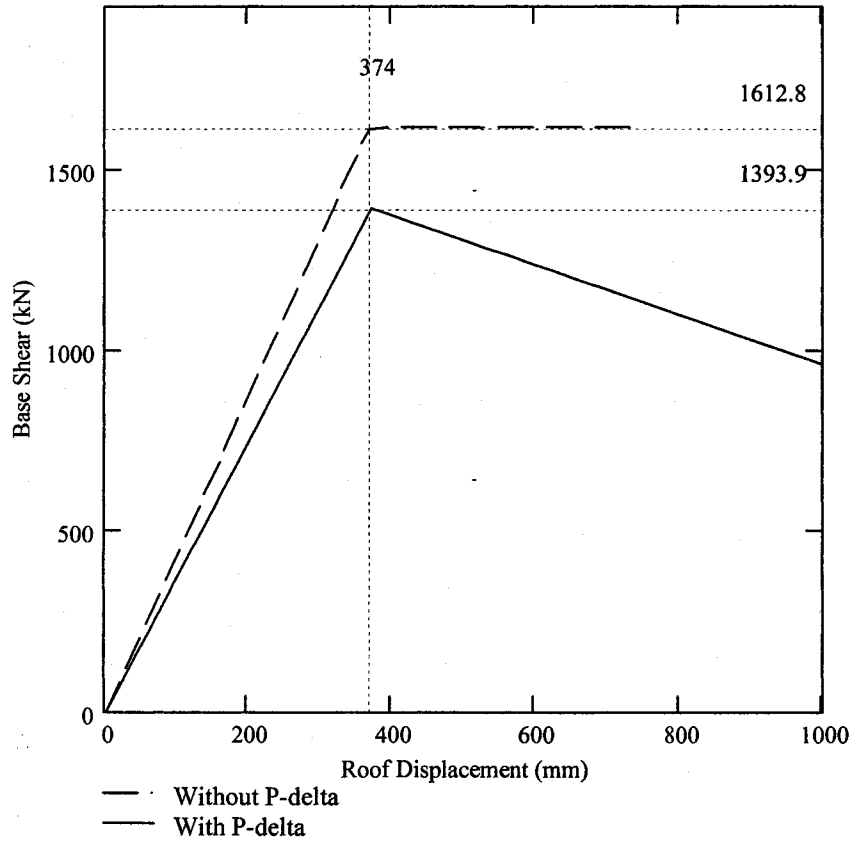


Figure B.4: Pushover curves with and without P- Δ effect for the preliminary design of shear walls for a 15-storey building

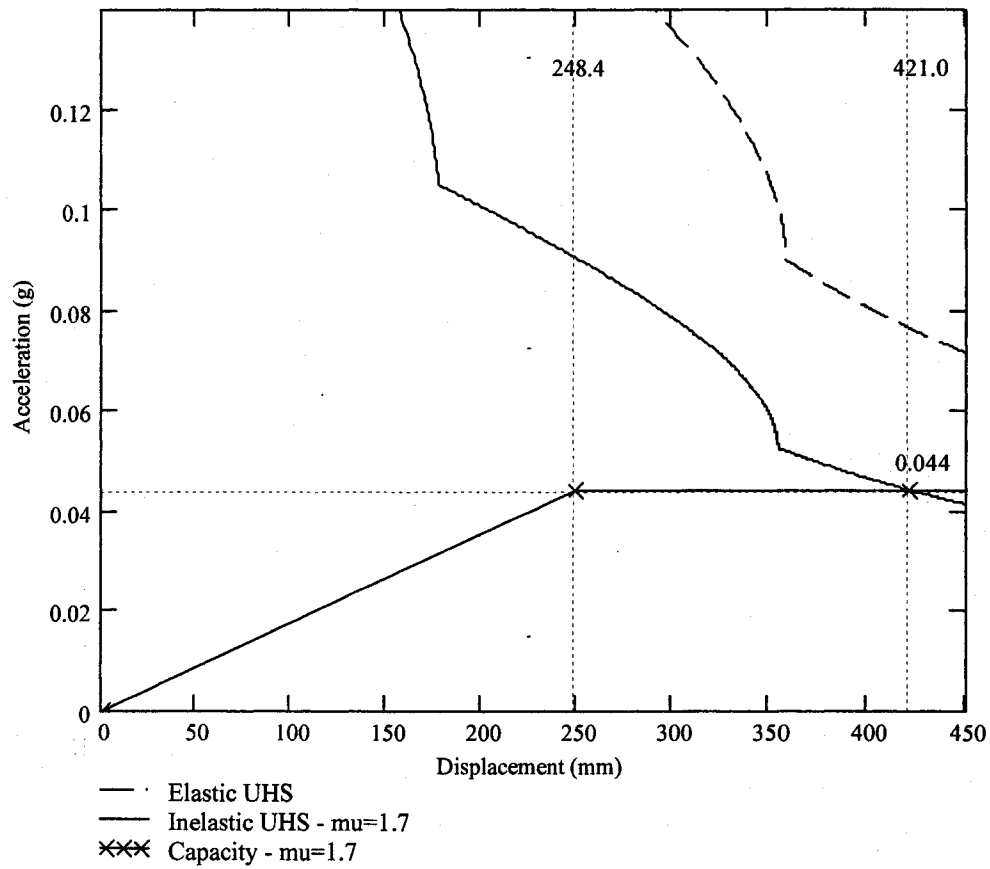


Figure B.5: Capacity-demand diagram for the first design iteration on a 15-storey building

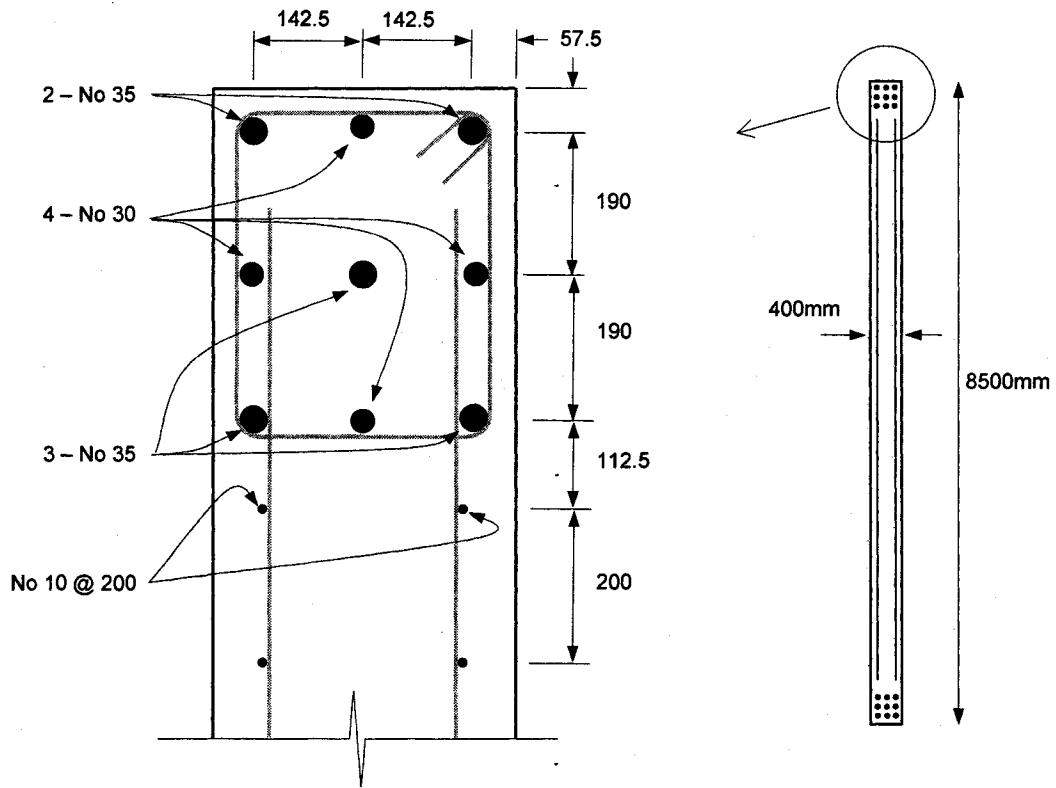


Figure B.6: Detail of reinforcement for the final design of shear walls for a 15-storey building

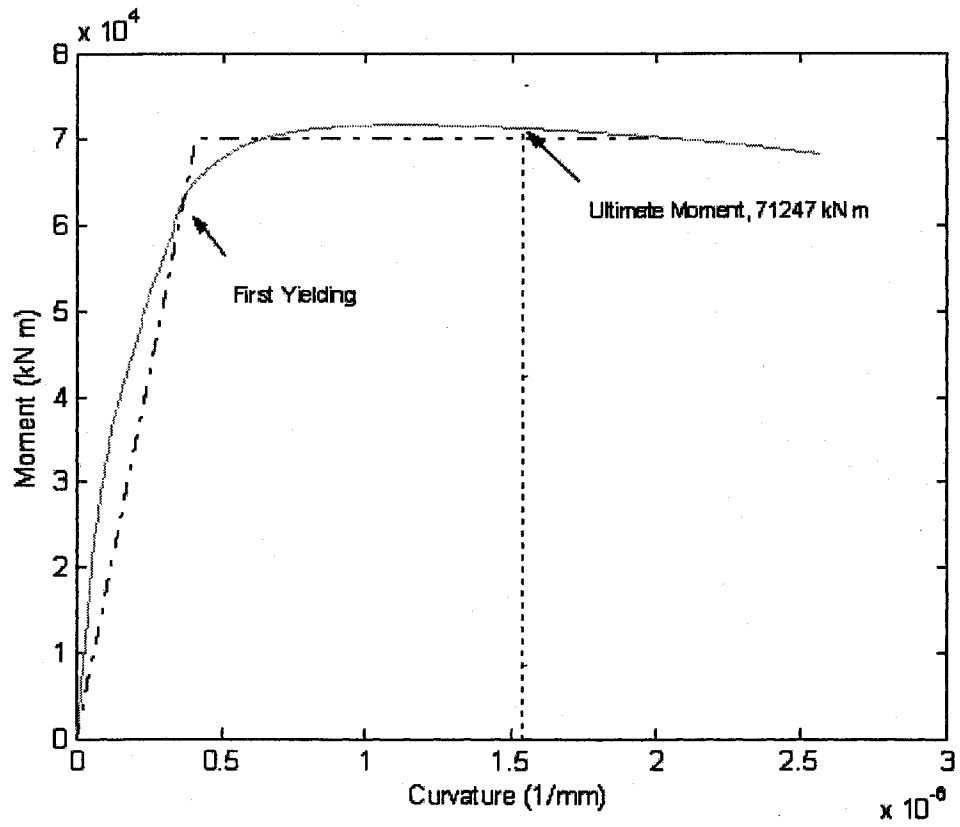


Figure B.7: Moment-curvature relationship for the final design of shear walls for a 15-storey building

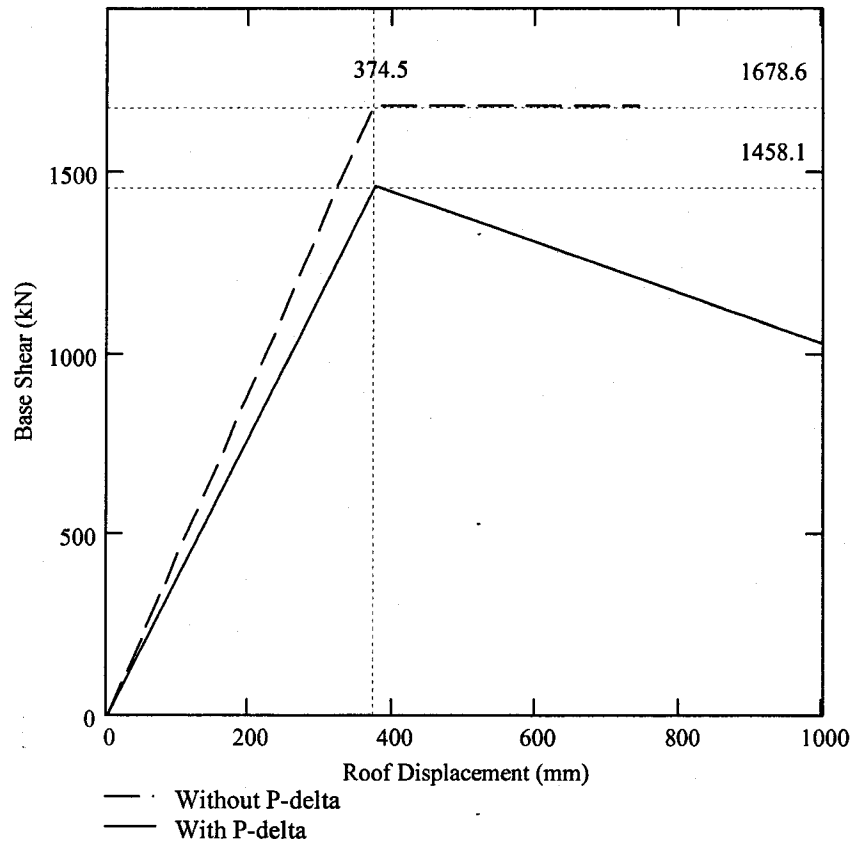


Figure B.8: Pushover curves with and without P- Δ effect for the final design of shear walls for a 15-storey building

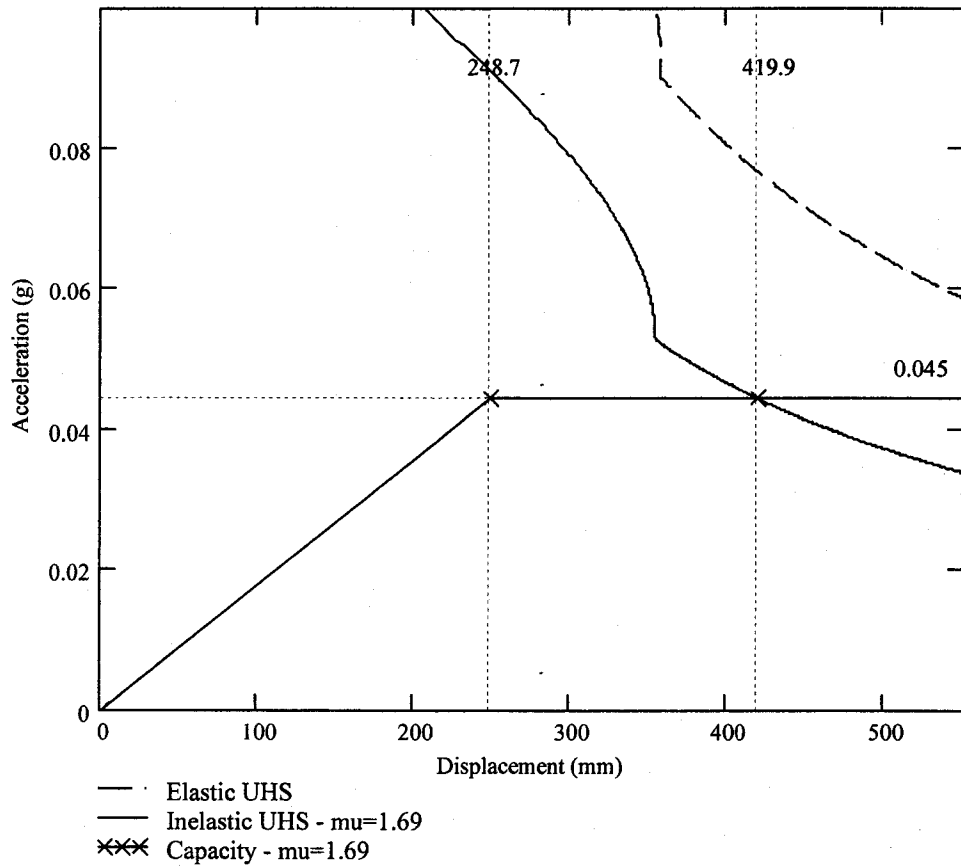


Figure B.9: Capacity-demand diagram for the final design of shear walls for a 15-storey building

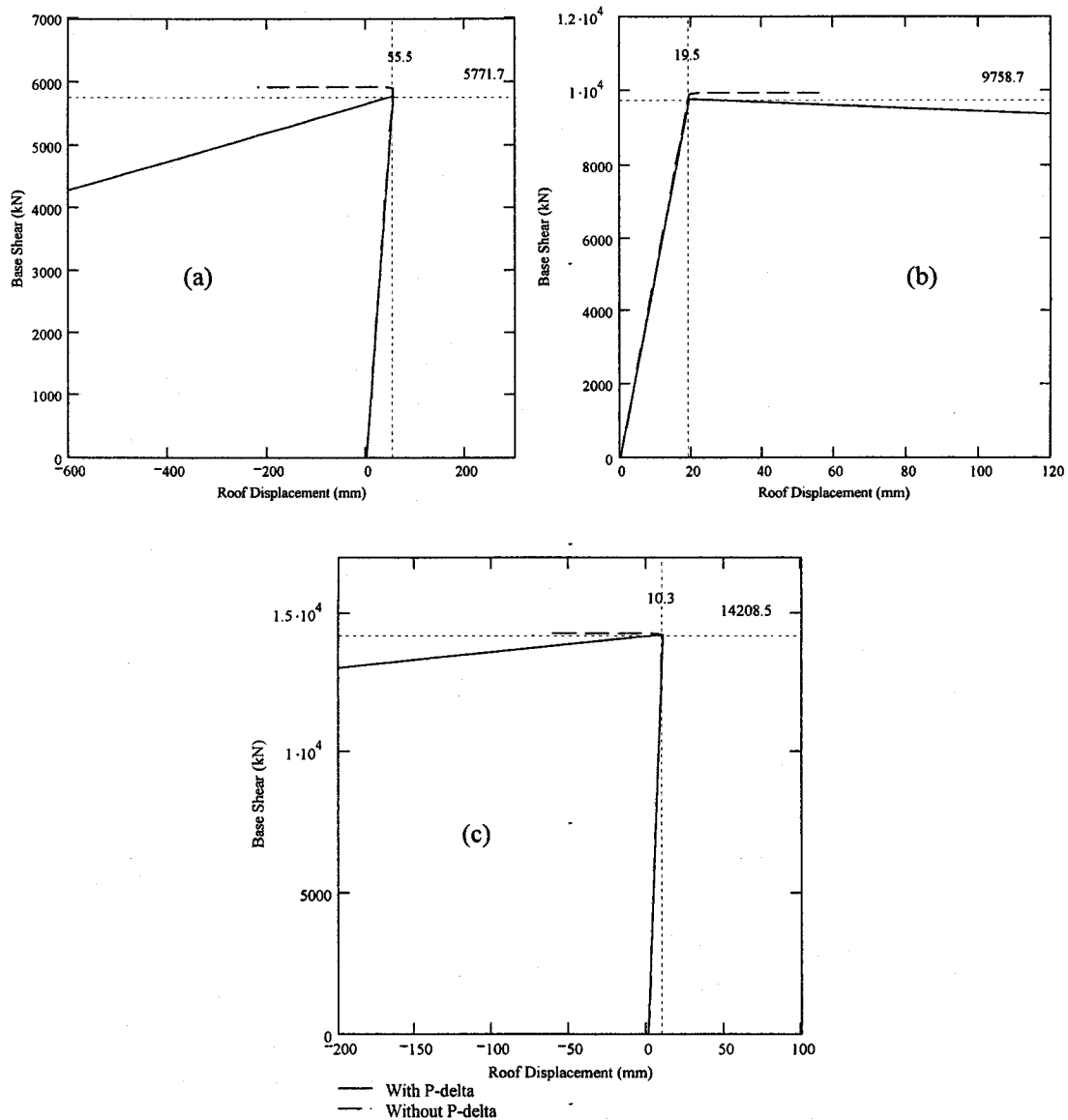


Figure B.10: Pushover curves with and without P- Δ effect for the final design of shear walls for a 15-storey building obtained by distributing the lateral forces according to (a) the second mode shape, (b) the third mode shape, and (c) the fourth mode shape

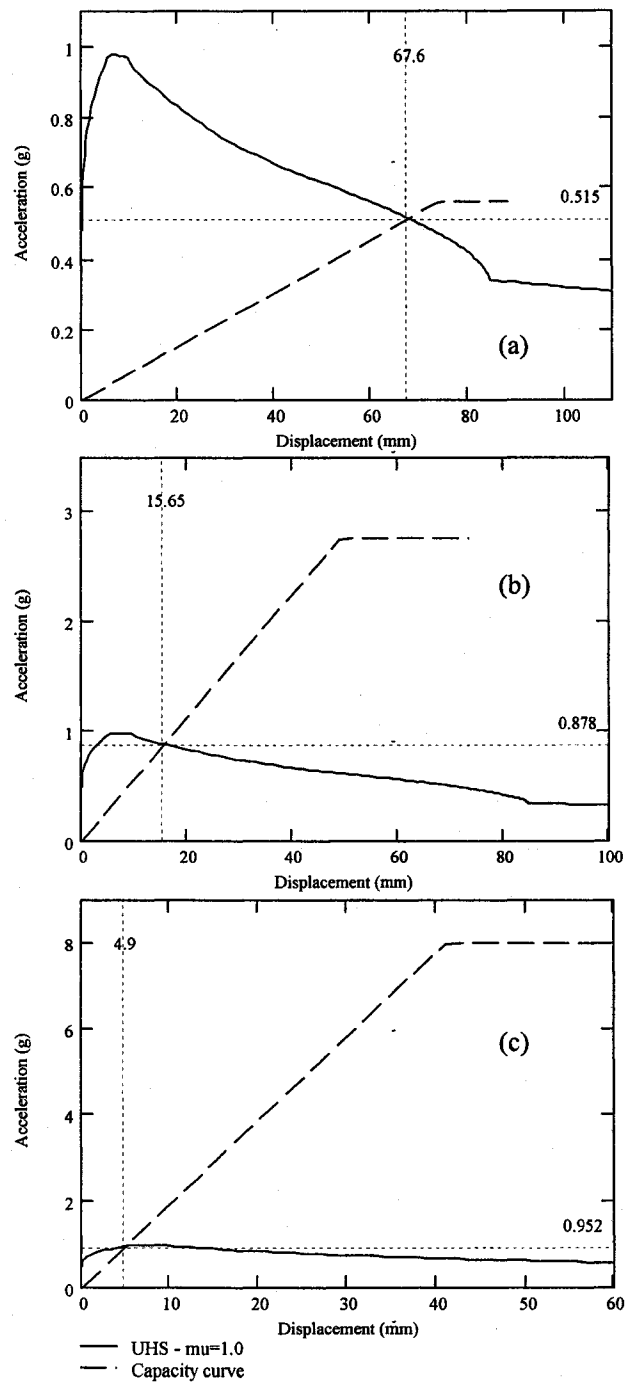


Figure B.11: Capacity-demand diagrams for the final design of shear walls for a 15-storey building obtained by distributing the lateral forces according to (a) the second mode shape, (b) the third mode shape, and (c) the fourth mode shape.

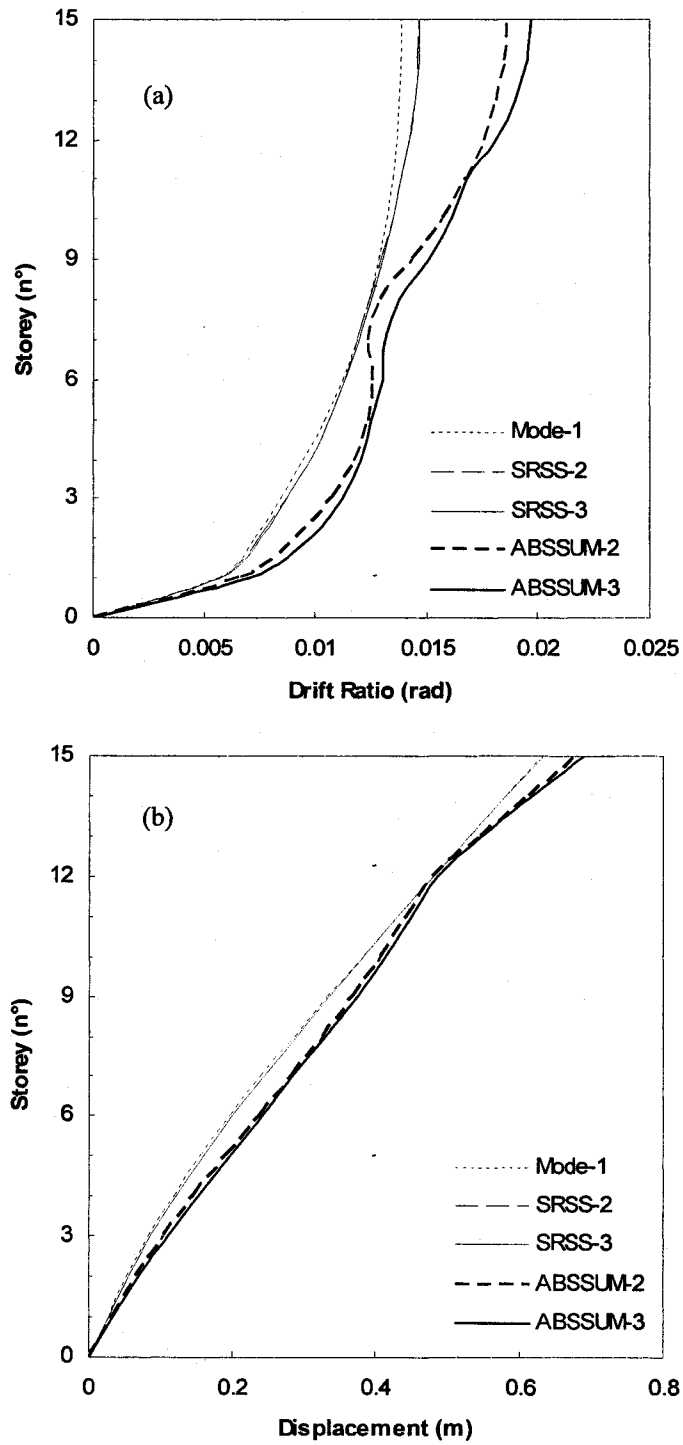


Figure B.12: (a) Inter-storey drifts ratios and (b) displacements for a 15-storey building

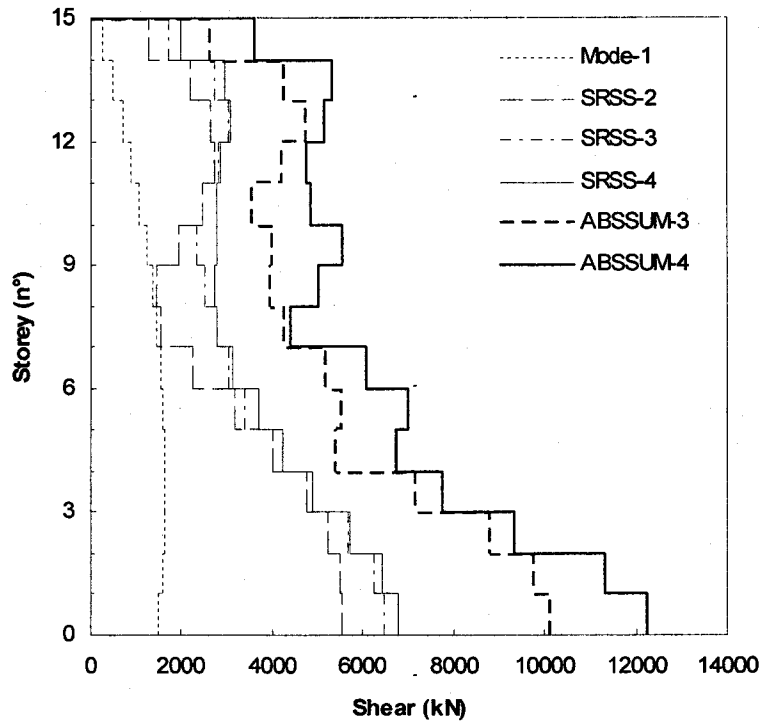


Figure B.13: Shear forces for a 15-storey building

Appendix C

C.1. DBSD of a 20-storey building

C.1.1. General Calculation

Floor dead load, q_f

| | |
|---------------------------------|--|
| Slab | $q_{\text{slab}} = t h_s \times \gamma_{\text{rc}} = 0.2 \times 24 = 4.8 \text{ kN/m}^2$ |
| Partition | $q_P = 0.5 \text{ kN/m}^2$ |
| Electrical, mechanical, ceiling | $q_{\text{EMC}} = 0.5 \text{ kN/m}^2$ |
| Total | $q_f = q_{\text{slab}} + q_P + q_{\text{EMC}} = 5.8 \text{ kN/m}^2$ |

The roof dead load is also 5.8 kN/m^2 since partition load is replaced by the same amount of load due to insulation and roofing.

Load due to self weight

Upper floor columns

$$q_{fc} = \frac{n_c \times A_{\text{col}} \times \gamma_{\text{rc}} \times 3.65\text{m}}{A_{\text{plan}}} = \frac{18 \times 0.7 \times 0.7 \times 24 \times 3.65}{24 \times 36} = 0.894 \text{ kN/m}^2$$

1st level columns

$$q_{1c} = \frac{n_c \times A_{col} \times \gamma_{rc}}{A_{plan}} \left(\frac{3.65 + 4.85}{2} \right) = \frac{18 \times 0.7 \times 0.7 \times 24 \times 4.25}{24 \times 36} = 1.041 \text{ kN/m}^2$$

Roof level columns

$$q_{roofc} = \frac{n_c \times A_{col} \times \gamma_{rc}}{A_{plan}} \left(\frac{3.65}{2} \right) = \frac{18 \times 0.7 \times 0.7 \times 24 \times 1.825}{24 \times 36} = 0.447 \text{ kN/m}^2$$

Upper floor walls

$$q_{fsw} = \frac{4 \times l_w \times th_w \times \gamma_{rc} \times 3.65m}{A_{plan}} = \frac{4 \times 10 \times 0.4 \times 24 \times 3.65}{24 \times 36} = 1.622 \text{ kN/m}^2$$

1st level walls

$$q_{1sw} = \frac{4 \times l_w \times th_w \times \gamma_{rc}}{A_{plan}} \left(\frac{3.65 + 4.85}{2} \right) = \frac{4 \times 10 \times 0.4 \times 24 \times 4.25}{24 \times 36} = 1.889 \text{ kN/m}^2$$

Roof level walls

$$q_{roofsw} = \frac{4 \times l_w \times th_w \times \gamma_{rc}}{A_{plan}} \left(\frac{3.65}{2} \right) = \frac{4 \times 10 \times 0.4 \times 24 \times 1.825}{24 \times 36} = 0.811 \text{ kN/m}^2$$

Total dead load and mass

Floor

$$q_{DL} = q_f + q_{fc} + q_{fsw} = 5.8 + 0.894 + 1.622 = 8.316 \text{ kN/m}^2$$

1st level

$$q_{IDL} = q_f + q_{lc} + q_{lsw} = 5.8 + 1.041 + 1.889 = 8.73 \text{ kN/m}^2$$

Roof (including 25 % of snow load)

$$\begin{aligned} q_{rDL} &= 0.25q_s + q_f + q_{roofc} + q_{roofsw} \\ &= 0.25 \times 2.2 + 5.8 + 0.447 + 0.811 = 7.608 \text{ kN/m}^2 \end{aligned}$$

Considering a tributary area of 432 m² (half of the plan area), the distribution of dead loads and masses for each wall and floor is presented on Table C.1.

C.1.2. Gravity loads

The gravity loads are divided in two types: design axial load, and axial load for P-Δ effect. The design load or maximum axial load is computed at the shear wall base and will be used in the moment-curvature analysis. Another load is calculated assuming that the two shear walls together resist the P-Δ effect produced by the entire gravity load.

C.1.2.1. Design axial load, P_b

The gravity loads on the shear wall will be obtained from the floor loads acting on a tributary area of 102 m² (17 m × 6 m) plus the self weight. These loads are calculated as follows:

Upper floor level self weight, P_{wf}

$$P_{wf} = 3.65 \times l_w \times t_h \times \gamma_{rc} = 3.65 \times 10 \times 0.4 \times 24 = 350.4 \text{ kN}$$

1st level self weight, P_{w1}

$$P_{w1} = 4.85 \times l_w \times th_w \times \gamma_{rc} = 4.85 \times 10 \times 0.4 \times 24 = 465.6 \text{ kN}$$

Bottom of top storey, P_{top}

$$\text{Snow load, } P_s = 0.25 \times q_s \times A_{trib} = 0.25 \times 2.2 \times 102 = 56.1 \text{ kN}$$

$$\text{Roof load, } P_r = q_r \times A_{trib} = 5.8 \times 102 = 591.6 \text{ kN}$$

$$\text{Total } P_{top} = P_{wf} + P_s + P_r = 998.1 \text{ kN}$$

Bottom of typical storey, P_{ts}

$$\text{Floor load, } P_f = q_f \times A_{trib} = 5.8 \times 102 = 591.6 \text{ kN}$$

$$\text{Total } P_{ts} = P_{wf} + P_f = 942 \text{ kN}$$

$$\text{Bottom of first storey, } P_1 = P_{w1} + P_f = 1057.2 \text{ kN}$$

The live load is included according to the NBCC 2005 requirements. This load is reduced by the live load reduction factor, LLRF, which is given by:

$$LLRF = 0.3 + \sqrt{\frac{9.8}{CA_{trib}}} \quad (C.1)$$

where CA_{trib} is the cumulative tributary area in m^2 . The calculations are presented in Table C.2.

Finally, the factored dead and live loads are combined using two load combination rules: $1.25 D + 1.50 L$ and $1.0D + 0.5 L$, where L is the reduced live load. The results are

presented in Table C.3. The design gravity load in the presence of earthquake loads is obtained from the combination $D + 0.5 L$ and is seen to be 19,874.4 kN.

C.1.2.2. Axial load for P-delta effect

In this case, the tributary area will be assumed to be half of the total plan area, 432 m². The live loads are computed using the same procedure as the previous section and the results are shown on Table C.4. The factored dead load and reduced live loads are finally combined using the rule: $1.0 D + 0.5 L$ and the results for each wall and floor are shown in Table C.5.

C.1.3. DBSD

The calculations presented bellow follow the steps presented in the summary Chapter 3.

1. The yield displacement and rotation are given by Equations (3.2) and (3.3) where

$$\epsilon_y = \frac{f_y \times \phi_s}{E_s} = \frac{400 \times 0.85}{200000} = 0.0017$$

is the factored yield steel strain. The yield curvature is given by Equation (3.4)

$$\phi_y = \frac{2.0 \epsilon_y}{l_w} = \frac{2 \times 0.0017}{10000} = 3.4 \times 10^{-7} \text{ 1/mm}$$

Hence the yield rotation is

$$\theta_y = \frac{\phi_y H}{2} = \frac{3.4 \times 10^{-7} \times 74200}{2} = 0.01261 \text{ rad}$$

and the yield displacement is

$$\Delta_y = \frac{\phi_y H^2}{3} = \frac{3.4 \times 10^{-7} \times 74200^2}{3} = 623.97 \text{ mm}$$

2. The ultimate rotation and displacement are defined by Equations (3.5) and (3.7), and together provide the required local ductility. The ultimate curvature is given by

$$\phi_u = \frac{\varepsilon_{cu}}{0.3l_w} = \frac{0.004}{0.3 \times 10000} = 1.33 \times 10^{-6} \text{ 1/mm,}$$

Assuming a plastic hinge length of $0.5l_w$ the plastic rotation and displacement are obtained from Equations (3.6) and (3.8) as follows:

$$\theta_p = (\phi_u - \phi_y)L_p = (13.3 - 3.4) \times 10^{-7} \times 0.5 \times 10000 = 0.00497 \text{ rad}$$

$$\Delta_p = \theta_p (H - 0.5L_p) = 0.00497 \times (74200 - 0.5 \times 5000) = 356.11 \text{ mm.}$$

Finally, the ultimate rotation is

$$\theta_u = \theta_y + \theta_p = 0.0126 + 0.00497 = 0.01758 \text{ rad}$$

and the ultimate displacement is

$$\Delta_u = \Delta_y + \Delta_p = 623.97 + 356.11 = 980.08 \text{ mm.}$$

Note that by using the drift limit establish by the NBCC 2005, the ultimate displacement is given by (Equation (3.9))

$$\Delta_u = 623.97 + (74200 - 0.5 \times 5000) \cdot \left(0.025 - \frac{3.4 \times 10^{-7} \times 74200}{2} \right) = 1512.1 \text{ mm}$$

which is larger than that obtained from limiting the concrete strain to 0.004.

Therefore, the ultimate displacement is set at 980.08 mm and the ductility capacity

is given by

$$\mu = \frac{\Delta_u}{\Delta_y} = \frac{980.08}{623.97} = 1.57$$

3. The mass distribution is shown in Table C.1 and the displacement shape assumed to be in the form of an inverted triangle is obtained from the following

$$\phi^T = \frac{h}{H} = \{0.065 \quad 0.115 \quad 0.164 \quad 0.213 \quad 0.262 \quad 0.311 \quad 0.361 \quad 0.41 \quad 0.459 \\ 0.508 \quad 0.557 \quad 0.606 \quad 0.656 \quad 0.705 \quad 0.754 \quad 0.803 \quad 0.852 \quad 0.902 \quad 0.951 \quad 1\}$$

The modal participation factor and effective modal mass are now calculated from Equations (3.10) and (3.11), respectively .

$$\Gamma = \frac{(\phi^T \mathbf{M} \mathbf{1})}{(\phi^T \mathbf{M} \phi)} = 1.468$$

$$M^* = \frac{(\phi^T \mathbf{M} \mathbf{1})^2}{(\phi^T \mathbf{M} \phi)} = 5685.4 \text{ tonne}$$

4. The yield and ultimate displacements for the equivalent SDOF system are thus given by

$$\delta y = \frac{\Delta_y}{\Gamma \phi^T} = \frac{623.97}{1.468 \times 1} = 424.92 \text{ mm}$$

$$\delta u = \frac{\Delta_u}{\Gamma \phi^T} = \frac{980.08}{1.468 \times 1} = 667.42 \text{ mm}$$

5. From the capacity-demand method (Figure C.1) and using δy , δu and μ , the inelastic pseudo-acceleration, A , is

$$A = 0.0304 \text{ g}$$

6. The corresponding base design shear is

$$V_b = A \cdot M^* = 0.0304 \times 9.81 \times 5685.4 = 1694.5 \text{ kN}$$

7. The base shear is distributed according to the product between the floor weights and the floor height shown in Table C.1

$$F^T = V_b \times \frac{W \cdot h}{\sum W \cdot h} = \left\{ \begin{array}{cccccccc} 11.00 & 18.36 & 26.25 & 34.13 & 42.02 & 49.90 & 57.79 \\ 65.67 & 73.56 & 81.44 & 89.33 & 97.21 & 105.10 & 112.98 \\ 120.86 & 128.75 & 136.63 & 144.52 & 152.40 & 146.64 \end{array} \right\} \text{ kN}$$

The base moment is then given by

$$M_b = \sum [F(h_{i+1} - h_i)] = 85623.5 \text{ kN} \cdot \text{m}$$

8. The structure is now designed to resist P_b , V_b and M_b . The minimum requirements are taken from the CSA A23.3-94.

The minimum area of concentrated reinforcement is given by

$$A_{s_{\min}} = 0.002 \cdot t h_w \cdot l_w = 0.002 \times 400 \times 10000 = 8000 \text{ mm}^2$$

The minimum distributed reinforcement is obtained from

$$A_{s_{d\min}} = 0.0025 \cdot t h_w = 0.0025 \times 400 = 1000 \text{ mm}^2 / \text{m}$$

and is provided by 2 layers of #10 at 200 mm spacing.

The required vertical concentrated reinforcement is calculated by following the simplified method presented on Chapter 3. The depth of the compression zone is given by

$$c = \frac{P_b + A_d \phi_s f_y l_w}{\alpha_1 \phi_c f_c \beta_1 b_w + 2A_d \phi_s f_y}$$

$$= \frac{19874.4 + 1000 \times 0.85 \times 400 \times 10000}{0.805 \times 0.6 \times 30 \times 0.895 \times 400 + 2 \times 1000 \times 0.85 \times 400} = 3966.7 \text{ mm}$$

The concrete resistant moment is obtained from

$$M_c = \alpha_1 \phi_c f_c c^2 \beta_1 b_w (1 - 0.5\beta_1)$$

$$= 0.805 \times 0.6 \times 30 \times 3966.7^2 \times 0.895 \times 400 \times (1 - 0.5 \times 0.895) = 45096.7 \text{ kN} \cdot \text{m}$$

The resistant moment provided by the distributed reinforcement is give by

$$M_{Ad} = A_d \phi_s f_y c^2 \left[1 + \left(\frac{l_w}{c} - 1 \right)^2 - \frac{2}{3} \left(\frac{\epsilon_y}{\epsilon_{cu}} \right)^2 \right] =$$

$$1000 \times 0.85 \times 400 \times 3966.7^2 \left[1 + \left(\frac{10000}{3966.7} - 1 \right)^2 - \frac{2}{3} \left(\frac{0.002}{0.0035} \right)^2 \right] = 8280.7 \text{ kN} \cdot \text{m}$$

The restoring moment provided by the axial load is obtained from

$$M_p = P_b \cdot \left(\frac{l_w}{2} - c \right) = 19874.4 \left(\frac{10000}{2} - 3966.7 \right) = 20536 \text{ kN} \cdot \text{m}$$

Thus, the resistant moment to be contributed by the concentrated reinforcement is obtained from

$$M_{cr} = M_b - M_c - M_{Ad} - M_p$$

$$= 85623.5 - (45096.7 + 8280.7 + 20536) = 11710.2 \text{ kN} \cdot \text{m}$$

and the corresponding steel area is given by

$$A_{cr} = \frac{M_{cr}}{\phi_s f_y (l_w - 2h_m)} = \frac{11710.2}{0.85 \times 400 \times (10000 - 2 \times 252.5)} = 3627 \text{ mm}^2 < A_{s_{min}}$$

This area is smaller than the minimum area required by the code, $A_{s_{min}} = 8000 \text{ mm}^2$.

Therefore, an arrangement of 8 bars #35 is adopted which gives an area of

8000 mm². The value of h_m was obtained by assuming a spacing of 195 mm plus a cover of 40 mm, and half of the steel section diameter, 15 mm (see Figure C.2).

Using this reinforcement, the moment-curvature analysis gives the curve shown in Figure C.3. From the idealized curve shown with a dotted line, the following results

| | |
|--|-----------------------------|
| Moment capacity, M_c | 100830 kNm |
| Yield curvature, ϕ_y | 3.46×10^{-7} 1/mm |
| Ultimate curvature, ϕ_u | 1.102×10^{-6} 1/mm |
| Ratio of effective moment of inertia to the gross moment of inertia, I_r | 0.3564 |

From these results the refined plastic rotation and roof displacement can be computed as follows

$$\theta_p = (\phi_u - \phi_y) L_p = (11.02 - 3.46) \times 10^{-6} \times 5000 = 0.00378 \text{ rad}$$

$$\Delta_p = 0.00378(74200 - 0.5 \times 5000) = 270.9 \text{ mm}$$

Also from these results, the stability of this shear wall can be checked by obtaining the critical thickness according to Equation (3.18) as follows

$$b_c = 0.017 \cdot 1_w \cdot \sqrt{\mu_\phi} = 0.017 \times 10000 \times \sqrt{\frac{11.02}{3.46}} = 303.34 \text{ mm}$$

Thus the 400 mm thickness will avoid any instability problem.

9. The modal analysis including the P- Δ effect gives the following properties related to the first mode

| | |
|------------------------------|---------|
| Period of vibration, T1 | 6.728 s |
| Mode shape at roof, ϕ^T | 0.0223 |

| | |
|--------------------------------|------------|
| Participation factor, Γ | 1.522 |
| Effective modal mass, M^* | 4659 tonne |

10. Distributing the forces according to Equation (3.26) a first mode pushover analysis is carried out. The roof displacement versus base shear relationship obtained is shown in Figure C.4. The important result from this curve is the yield point which is given by

| | |
|----------------------------|-----------|
| Yield base shear, V_{by} | 1496.1 kN |
|----------------------------|-----------|

| | |
|-------------------------------------|----------|
| Yield roof displacement, Δ_y | 560.5 mm |
|-------------------------------------|----------|

From this displacement and the moment-curvature analysis, the new target ultimate displacement is defined as follows

$$\Delta_u = \Delta_y + \Delta_p = 560.5 + 270.9 = 831.4 \text{ mm}$$

That gives a new ductility demand of

$$\mu = \frac{\Delta_u}{\Delta_y} = 1.483$$

11. The yield and ultimate displacement for the equivalent SDOF system are now given by

$$\delta y = \frac{\Delta_y}{\Gamma \phi^r} = \frac{560.5}{1.522 \times 0.0223} = 368.2 \text{ mm}$$

$$\delta u = \frac{\Delta_u}{\Gamma \phi^r} = \frac{831.4}{1.522 \times 0.0223} = 546.2 \text{ mm}$$

The inelastic acceleration, A , is obtained by using δy , δu , and μ in the capacity-demand method (Figure C.5)

$$A = 0.039 \text{ g}$$

Finally, the new base shear is

$$V_{y_{\text{new}}} = M^* A = 4659 \times 0.039 \times 9.81 = 1798.8 \text{ kN}$$

12. The difference between the two successive estimates is

$$\text{diff}_{V_y} = \frac{V_y - V_{y_{\text{new}}}}{V_y} = -20.23 \cdot \%$$

Therefore, a new design will be carried out. The new base design moment is obtained from

$$M_b = M_c (1 - \text{diff}_{V_y}) = 100830 \times (1 + 0.2023) = 121228.5 \text{ kN} \cdot \text{m}$$

The computations presented in Steps 8 through 12 are repeated; results of the moment-curvature analysis, modal analysis, and pushover analysis are shown in Table C.6, Table C.7, and Table C.8 for 3 tries, including the results from the first try. Three tries were needed to find an error less than 1%. From the last column of Table C.8, it is possible to see how the procedure converges. The results obtained from the last attempt are shown in Figure C.6 through Figure C.9. This design gives an ultimate base shear of $V_u = 1618 \text{ kN}$, the corresponding ratio of the ultimate base shear to yield shear $V_u / V_y = 0.893$, which is a measure of the excursion into the unstable part of the pushover curve.

13. The method was seen to converge on the third attempt. It may be noted that all of the preceding computations were based on the first mode. The moment estimate obtained from the first mode is expected to be reasonable. However, in a shear wall structure the higher modes make significant contribution to the base shear. Hence

five higher modes, 2nd, 3rd, 4th, and 5th are included and analysis is repeated with these modes following the procedure presented in Section 3.11 of modal pushover analysis. The modal analysis results are shown in Table C.9 for five modes. The pushover curves obtained by using distribution of forces according to the second, third, fourth, and fifth mode shapes are shown in Figure C.10. These curves are transformed into equivalent SDOF systems and then plotted in the capacity-demand diagrams presented in Figure C.11. That figure, as well as the data summarized in Table C.10, show that the performance points do not lie in the inelastic zone of the capacity diagram, which means that responses remain elastic. The responses in the four modes are combined according to the SRSS and ABSSUM rules and the results are shown in Figure C.12 for the inter-storey drifts and displacements and in Figure C.13 for shear forces. As examples, three particular results are obtained as follows:

Roof displacement

$$\begin{aligned}\Delta_{\text{roof}} &= \sqrt{\Delta_{u1}^2 + \Delta_{u2}^2 + \Delta_{u3}^2 + \Delta_{u4}^2 + \Delta_{u5}^2} \\ &= \sqrt{833.6^2 + 64.7^2 + 9.8^2 + 2.3^2 + 0.6^2} = 836.2 \text{ mm}\end{aligned}$$

Maximum drift ratio

$$\begin{aligned}\theta_{\text{max}} &= \sqrt{\theta_{\text{max}1}^2 + \theta_{\text{max}2}^2 + \theta_{\text{max}3}^2 + \theta_{\text{max}4}^2 + \theta_{\text{max}5}^2} \\ &= \sqrt{0.0141^2 + 0.0045^2 + 0.0012^2 + 0.0004^2 + 0.0001^2} = 0.0148\end{aligned}$$

Base shear

$$\begin{aligned}V_b &= \sqrt{V_{b1}^2 + V_{b2}^2 + V_{b3}^2 + V_{b4}^2} \\ &= \sqrt{1813^2 + 5562^2 + 3992^2 + 2494^2 + 1321^2} = 7624 \text{ kN}\end{aligned}$$

where the numeric subscript indicates the mode number.

Assuming a horizontal reinforcement of #15 at 150 mm and an effective depth of $d = 0.81w$, the simplified method gives a shear capacity of (Clause 11.3 of the CSA 1994):

$$V_{\text{capacity}} = 0.2\phi_c \sqrt{f_c} \cdot t h_w d_v + \phi_s \frac{A_v f_y}{s} d =$$

$$0.2 \times 0.6 \times \sqrt{30} \times 400 \times 0.8 \times 10000 + 0.85 \frac{400 \times 400}{150 \times 1000} \times 0.8 \times 10000 = 7906 \text{ kN}$$

Thus, the provided horizontal reinforcement will ensure sufficient capacity to resist the shear demand of 7,624 kN.

14. The design spectrum corresponding to .50%/50 year probability is obtained by scaling down the UHS corresponding to 2%/50 year probability by the ratio obtained in Section 3.12.1, that is, 0.325. The spectral acceleration from the UHS corresponding to 2%/50 year probability at $T_1 = 6.144$ s is 0.059 g. Thus, the demand acceleration for the operational level is $0.059 \times 0.325 = 0.014$ g. Considering the equivalent modal mass for the final design $M1^* = 4659$ tonne, the demand base shear, V_{bOP} , is given by

$$V_{\text{bOP}} = 4659 \times 9.81 \times 0.014 = 636.0 \text{ kN}$$

15. From the pushover curve shown in Figure C.8, the roof displacement is 198.6 mm for the calculated base shear, V_{bOP} . From pushover analysis data base, the maximum drift ratio at this roof displacement is 0.46 %. Therefore, the design is satisfactory for the operational performance level.

Table C.1: Floor dead loads and masses tributary to each wall in the 20-storey building

| Storey Number | Accumulated height (m) | Dead Load (kN) | Mass (tonne) |
|--------------------------|---------------------------------------|---------------------------|-------------------------|
| 1 | 4.85 | 3771.42 | 384.45 |
| 2 | 8.50 | 3592.72 | 366.23 |
| 3 | 12.15 | 3592.72 | 366.23 |
| 4 | 15.80 | 3592.72 | 366.23 |
| 5 | 19.45 | 3592.72 | 366.23 |
| 6 | 23.10 | 3592.72 | 366.23 |
| 7 | 26.75 | 3592.72 | 366.23 |
| 8 | 30.40 | 3592.72 | 366.23 |
| 9 | 34.05 | 3592.72 | 366.23 |
| 10 | 37.70 | 3592.72 | 366.23 |
| 11 | 41.35 | 3592.72 | 366.23 |
| 12 | 45.00 | 3592.72 | 366.23 |
| 13 | 48.65 | 3592.72 | 366.23 |
| 14 | 52.30 | 3592.72 | 366.23 |
| 15 | 55.95 | 3592.72 | 366.23 |
| 16 | 59.60 | 3592.72 | 366.23 |
| 17 | 63.25 | 3592.72 | 366.23 |
| 18 | 66.90 | 3592.72 | 366.23 |
| 19 | 70.55 | 3592.72 | 366.23 |
| 20 | 74.20 | 3286.76 | 335.04 |

Table C.2: Reduced live load calculations for each wall of the 20-storey building

| Storey | Live Load | Cumulative Live Load | Cumulative Tributary Area | Live Load Reduction Factor | Reduced Cumulative Live Load |
|---------------|------------------|-----------------------------|--|-----------------------------------|-------------------------------------|
| N° | LL (kN) | CLL (kN) | CA_{trib} (m²) | LLRF | RCLL (kN) |
| 1 | 244.8 | 4651.2 | 1938 | 0.371 | 1726.11 |
| 2 | 244.8 | 4406.4 | 1836 | 0.373 | 1643.85 |
| 3 | 244.8 | 4161.6 | 1734 | 0.375 | 1561.34 |
| 4 | 244.8 | 3916.8 | 1632 | 0.377 | 1478.56 |
| 5 | 244.8 | 3672.0 | 1530 | 0.380 | 1395.48 |
| 6 | 244.8 | 3427.2 | 1428 | 0.383 | 1312.08 |
| 7 | 244.8 | 3182.4 | 1326 | 0.386 | 1228.31 |
| 8 | 244.8 | 2937.6 | 1224 | 0.389 | 1144.14 |
| 9 | 244.8 | 2692.8 | 1122 | 0.393 | 1059.50 |
| 10 | 244.8 | 2448.0 | 1020 | 0.398 | 974.35 |
| 11 | 244.8 | 2203.2 | 918 | 0.403 | 888.60 |
| 12 | 244.8 | 1958.4 | 816 | 0.410 | 802.14 |
| 13 | 244.8 | 1713.6 | 714 | 0.417 | 714.84 |
| 14 | 244.8 | 1468.8 | 612 | 0.427 | 626.51 |
| 15 | 244.8 | 1224.0 | 510 | 0.439 | 536.87 |
| 16 | 244.8 | 979.2 | 408 | 0.455 | 445.52 |
| 17 | 244.8 | 734.4 | 306 | 0.479 | 351.75 |
| 18 | 244.8 | 489.6 | 204 | 0.519 | 254.19 |
| 19 | 244.8 | 244.8 | 102 | 0.610 | 149.32 |
| 20 | 0 | 0 | 0 | 0 | 0 |

Table C.3: Gravity load combinations for each wall of the 20-storey building

| Storey | Dead Load | Cumulative Dead Load | Reduced Cumulative Live Load | Cumulative 1.25D+1.5L | Cumulative 1.0D+0.5L |
|---------------|------------------|-----------------------------|-------------------------------------|------------------------------|-----------------------------|
| n | DL (kN) | CDL (kN) | RCLL (kN) | (kN) | (kN) |
| 1 | 1057.2 | 19011.3 | 1726.11 | 26353.29 | 19874.36 |
| 2 | 942.0 | 17954.1 | 1643.85 | 24908.40 | 18776.03 |
| 3 | 942.0 | 17012.1 | 1561.34 | 23607.13 | 17792.77 |
| 4 | 942.0 | 16070.1 | 1478.56 | 22305.46 | 16809.38 |
| 5 | 942.0 | 15128.1 | 1395.48 | 21003.35 | 15825.84 |
| 6 | 942.0 | 14186.1 | 1312.08 | 19700.74 | 14842.14 |
| 7 | 942.0 | 13244.1 | 1228.31 | 18397.59 | 13858.25 |
| 8 | 942.0 | 12302.1 | 1144.14 | 17093.83 | 12874.17 |
| 9 | 942.0 | 11360.1 | 1059.50 | 15789.38 | 11889.85 |
| 10 | 942.0 | 10418.1 | 974.35 | 14484.15 | 10905.28 |
| 11 | 942.0 | 9476.1 | 888.60 | 13178.02 | 9920.40 |
| 12 | 942.0 | 8534.1 | 802.14 | 11870.83 | 8935.17 |
| 13 | 942.0 | 7592.1 | 714.84 | 10562.38 | 7949.52 |
| 14 | 942.0 | 6650.1 | 626.51 | 9252.38 | 6963.35 |
| 15 | 942.0 | 5708.1 | 536.87 | 7940.43 | 5976.54 |
| 16 | 942.0 | 4766.1 | 445.52 | 6625.90 | 4988.86 |
| 17 | 942.0 | 3824.1 | 351.75 | 5307.75 | 3999.97 |
| 18 | 942.0 | 2882.1 | 254.19 | 3983.91 | 3009.20 |
| 19 | 942.0 | 1940.1 | 149.32 | 2649.10 | 2014.76 |
| 20 | 998.1 | 998.1 | 0 | 1247.63 | 998.10 |

Table C.4: Reduced tributary live loads for calculating the P- Δ effect for each wall of the
20-storey building

| Storey | Live Load | Cumulative Tributary Area | Live Load Reduction Factor | Reduced Live Load | Dead Load |
|--------|-----------|--------------------------------------|----------------------------|-------------------|-----------|
| n | LL (kN) | CA _{trib} (m ²) | LLRF | RLL (kN) | DL (kN) |
| 1 | 1036.8 | 19699.2 | 16416 | 0.324 | 6391.07 |
| 2 | 1036.8 | 18662.4 | 15552 | 0.325 | 6067.20 |
| 3 | 1036.8 | 17625.6 | 14688 | 0.326 | 5742.96 |
| 4 | 1036.8 | 16588.8 | 13824 | 0.327 | 5418.32 |
| 5 | 1036.8 | 15552.0 | 12960 | 0.327 | 5093.26 |
| 6 | 1036.8 | 14515.2 | 12096 | 0.328 | 4767.72 |
| 7 | 1036.8 | 13478.4 | 11232 | 0.330 | 4441.65 |
| 8 | 1036.8 | 12441.6 | 10368 | 0.331 | 4114.99 |
| 9 | 1036.8 | 11404.8 | 9504 | 0.332 | 3787.67 |
| 10 | 1036.8 | 10368.0 | 8640 | 0.334 | 3459.58 |
| 11 | 1036.8 | 9331.2 | 7776 | 0.336 | 3130.62 |
| 12 | 1036.8 | 8294.4 | 6912 | 0.338 | 2800.64 |
| 13 | 1036.8 | 7257.6 | 6048 | 0.340 | 2469.43 |
| 14 | 1036.8 | 6220.8 | 5184 | 0.343 | 2136.72 |
| 15 | 1036.8 | 5184.0 | 4320 | 0.348 | 1802.11 |
| 16 | 1036.8 | 4147.2 | 3456 | 0.353 | 1465.00 |
| 17 | 1036.8 | 3110.4 | 2592 | 0.361 | 1124.38 |
| 18 | 1036.8 | 2073.6 | 1728 | 0.375 | 778.24 |
| 19 | 1036.8 | 1036.8 | 864 | 0.407 | 421.46 |
| 20 | 0 | 0 | 0 | 0 | 0 |

Table C.5: Floor gravity loads tributary to each wall for calculating the P- Δ effect in the
15-storey building

| Storey | Dead Load | Reduced Live Load | Combined Load 1.0D+0.5L |
|--------|-----------|-------------------|----------------------------|
| n | CDL (kN) | RCLL (kN) | (kN) |
| 1 | 3771.42 | 323.88 | 3933.36 |
| 2 | 3592.72 | 324.24 | 3754.84 |
| 3 | 3592.72 | 324.63 | 3755.03 |
| 4 | 3592.72 | 325.07 | 3755.25 |
| 5 | 3592.72 | 325.54 | 3755.49 |
| 6 | 3592.72 | 326.07 | 3755.75 |
| 7 | 3592.72 | 326.66 | 3756.05 |
| 8 | 3592.72 | 327.32 | 3756.38 |
| 9 | 3592.72 | 328.08 | 3756.76 |
| 10 | 3592.72 | 328.96 | 3757.20 |
| 11 | 3592.72 | 329.99 | 3757.71 |
| 12 | 3592.72 | 331.21 | 3758.32 |
| 13 | 3592.72 | 332.71 | 3759.07 |
| 14 | 3592.72 | 334.61 | 3760.02 |
| 15 | 3592.72 | 337.11 | 3761.27 |
| 16 | 3592.72 | 340.63 | 3763.03 |
| 17 | 3592.72 | 346.14 | 3765.78 |
| 18 | 3592.72 | 356.78 | 3771.10 |
| 19 | 3592.72 | 421.46 | 3803.45 |
| 20 | 3286.76 | 0 | 3286.76 |

Table C.6: Results of moment-curvature analysis in the 3 design iterations of a 20-storey
building

| Try | Moment Capacity | Yield curvature | Ultimate curvature | Moment of Inertia ratio | Plastic rotation |
|--------|-----------------|-----------------|--------------------|-------------------------|-----------------------------|
| Number | M_c (kNm) | ϕ_y (1/mm) | ϕ_u (1/mm) | I_r | θ_p (10^{-2} rad) |
| 1 | 100830 | 3.46E-07 | 1.10E-06 | 0.356 | 0.497 |
| 2 | 117200 | 3.51E-07 | 1.10E-06 | 0.408 | 0.378 |
| 3 | 118530 | 3.51E-07 | 1.10E-06 | 0.414 | 0.373 |

Table C.7: First mode analysis results for the 3 design iterations on a 20-storey building

| Try | First mode period | Participation factor | Modal mass participation | Effective modal mass |
|--------|-------------------|----------------------|--------------------------|----------------------|
| Number | T_1 (s) | Γ | (%) | M^* (tonne) |
| 1 | 6.728 | 1.522 | 63.72 | 4658.97 |
| 2 | 6.194 | 1.522 | 63.76 | 4661.89 |
| 3 | 6.144 | 1.522 | 63.77 | 4662.63 |

Table C.8: Results from pushover analyses for the 3 design iterations on a 20-storey building

| Try | Yield base shear | Yield Roof Displ. | Ultimate Roof Displ. | Ductility Factor | Reduction Factor | Inelastic PSA | New Yield Shear | Base Shear Error |
|--------|------------------|-------------------|----------------------|------------------|------------------|---------------|-----------------|------------------|
| Number | V_{by} (kN) | Δ_y (mm) | Δ_u (mm) | μ | R_y | A(g) | V_y (kN) | (%) |
| 1 | 1496.1 | 560.5 | 831.38 | 1.483 | 1.491 | 0.039 | 1798.77 | -20.23 |
| 2 | 1788.6 | 552.7 | 820.36 | 1.484 | 1.492 | 0.040 | 1822.38 | -1.89 |
| 3 | 1812.7 | 566.0 | 833.62 | 1.473 | 1.480 | 0.040 | 1808.53 | 0.23 |

Table C.9: Modal analysis results for the 3rd design iteration on a 20-storey building

| Mode | Period | Participation factor | Modal mass Participation | Effective modal mass |
|------|-----------|----------------------|--------------------------|----------------------|
| N° | T_n (s) | Γ | (%) | M^* (tonne) |
| 1 | 6.144 | 1.522 | 63.77 | 4662.63 |
| 2 | 0.927 | 0.784 | 20.04 | 1465.25 |
| 3 | 0.340 | 0.427 | 6.96 | 508.89 |
| 4 | 0.182 | 0.281 | 3.57 | 261.17 |
| 5 | 0.117 | 0.198 | 2.10 | 153.54 |

**Table C.10: Results from modal pushover analysis in the 3rd design iteration on a
20-storey building**

| Mode | Yield base shear | Yield Roof Displ. | Yield Acc_n | Elastic Acc_n | Reduction Factor | Ultimate Roof Displ. | Ultimate Base Shear |
|-------------|---------------------------------|----------------------------------|------------------------|--------------------------|-----------------------------|-------------------------------------|------------------------------------|
| N° | V_{by}(kN) | Δ_y(mm) | A (g) | PSA (g) | R_y | Δ_u(mm) | V_{bu} (kN) |
| 2 | 7393.9 | 86.0 | 0.514 | 0.387 | 0.752 | 64.698 | 5562.43 |
| 3 | 12573.2 | 31.0 | 2.519 | 0.800 | 0.317 | 9.842 | 3991.77 |
| 4 | 18241.8 | 16.5 | 7.120 | 0.974 | 0.137 | 2.256 | 2494.40 |
| 5 | 24524.5 | 10.9 | 16.282 | 0.877 | 0.054 | 0.587 | 1320.64 |

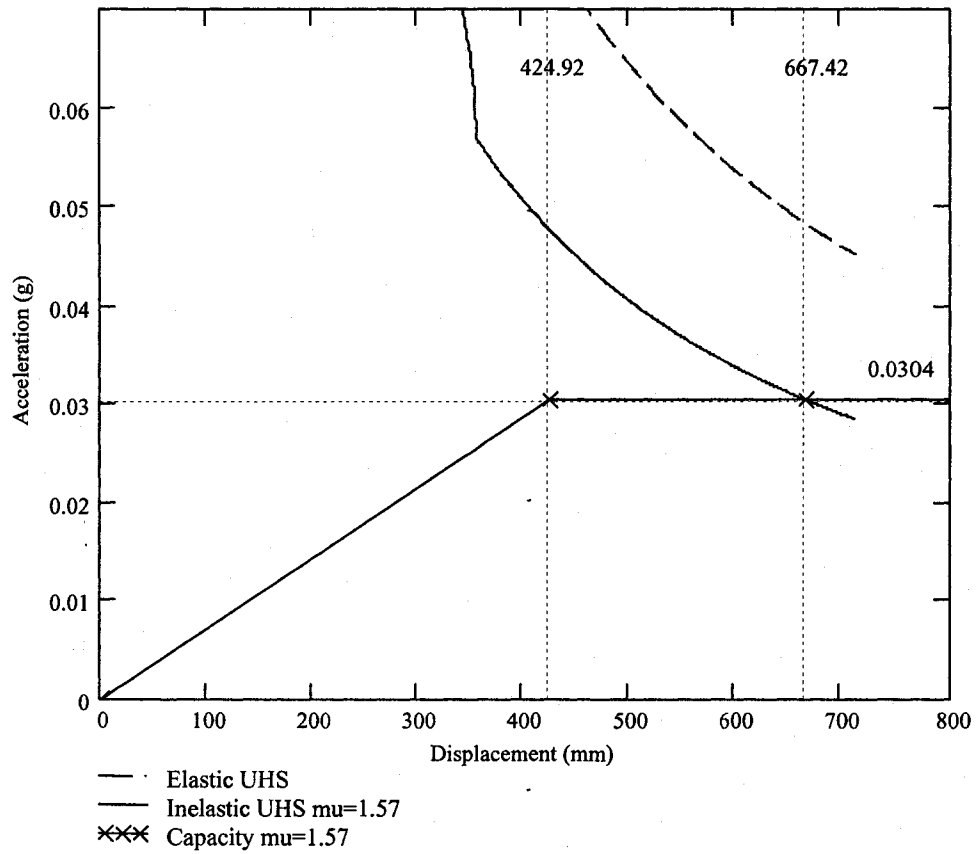


Figure C.1: Capacity-demand diagram for the preliminary design of shear walls for a 20-storey building

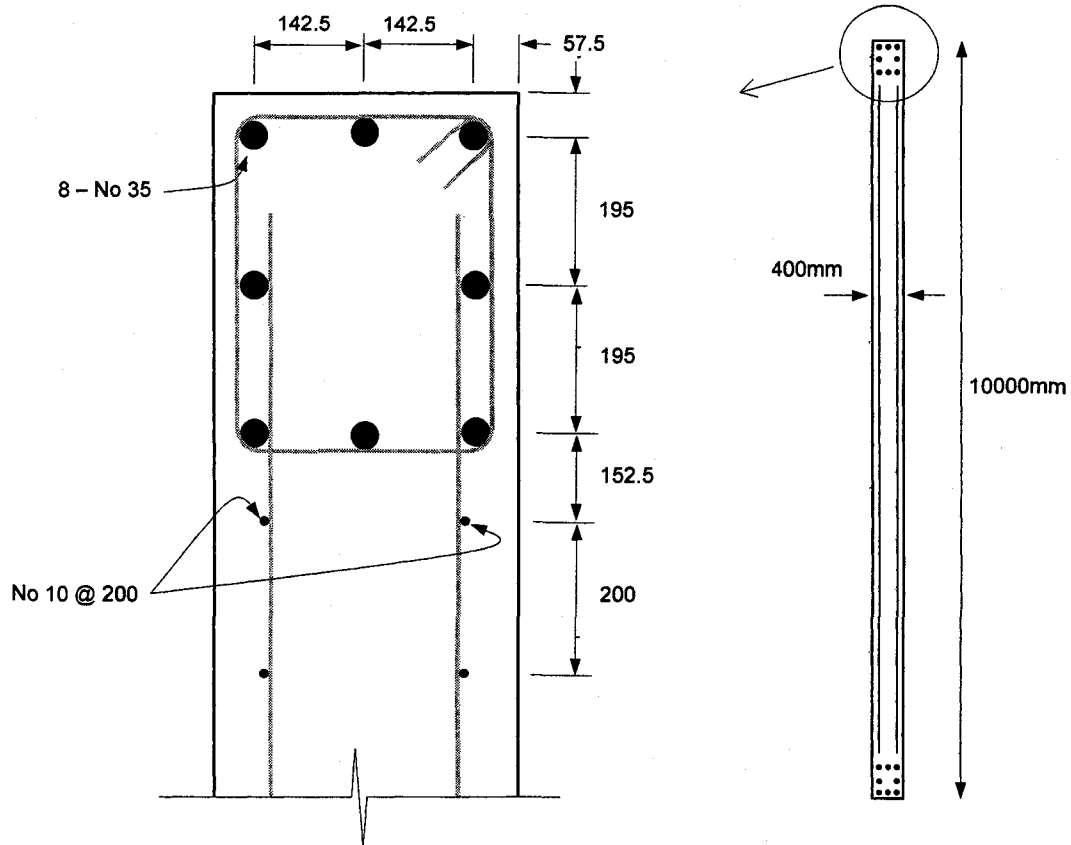


Figure C.2: Detail of reinforcement of the first design of shear walls for a 20-storey building

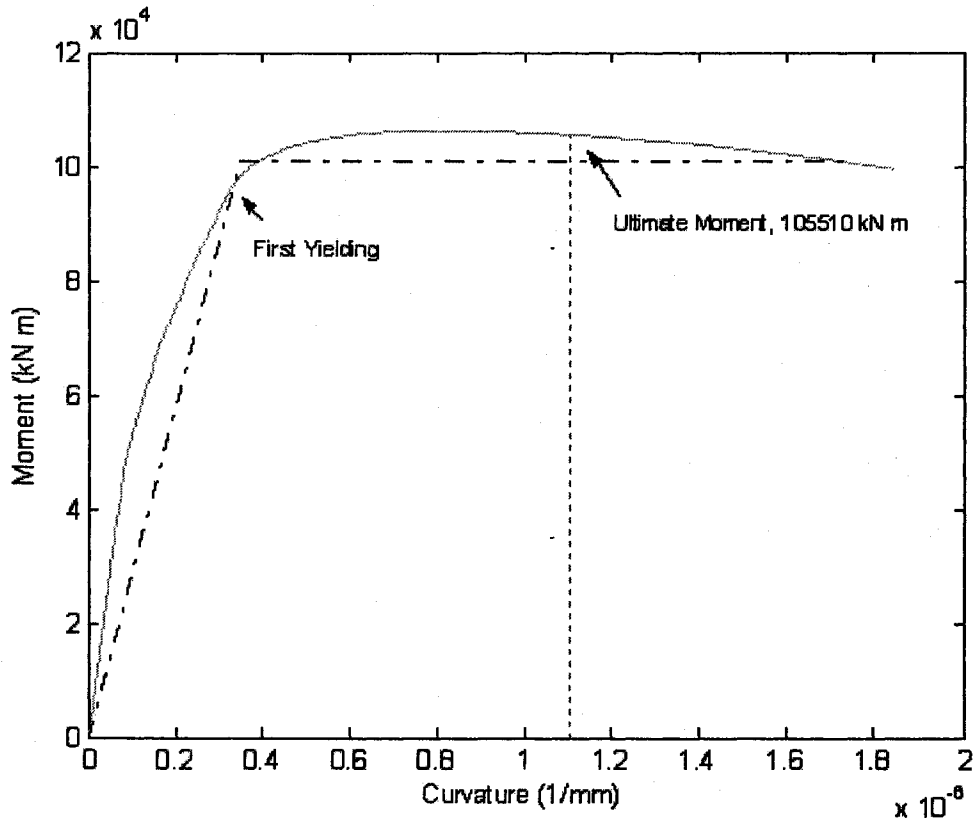


Figure C.3: Moment-curvature relationship for the preliminary design of shear walls for a 20-storey building

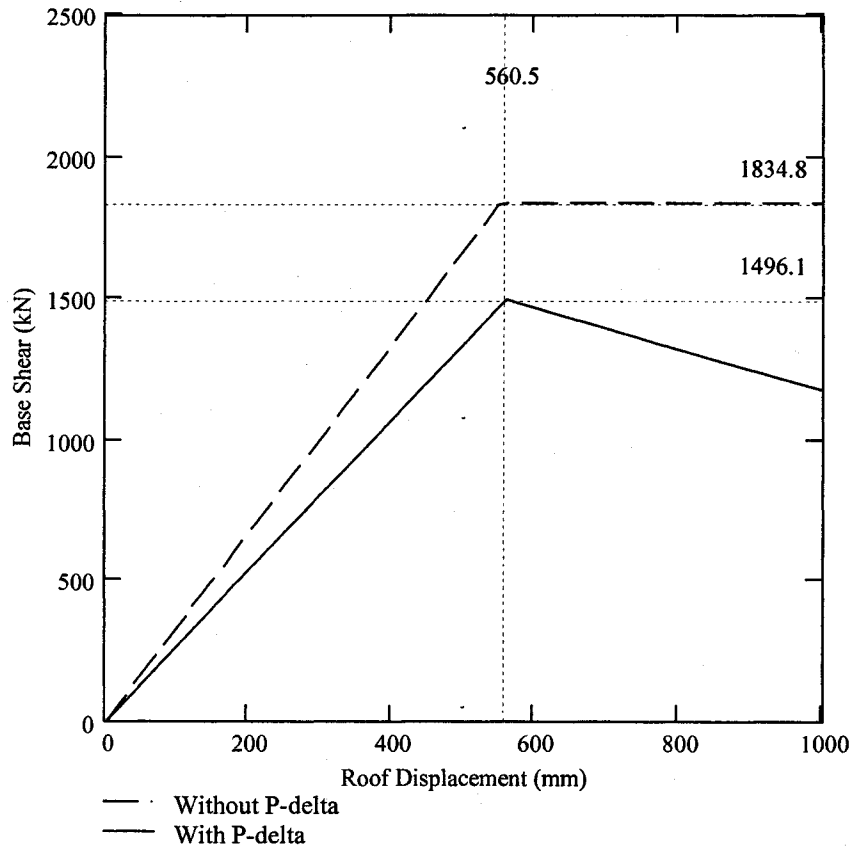


Figure C.4: Pushover curves with and without P- Δ effect for the preliminary design of shear walls for a 20-storey building

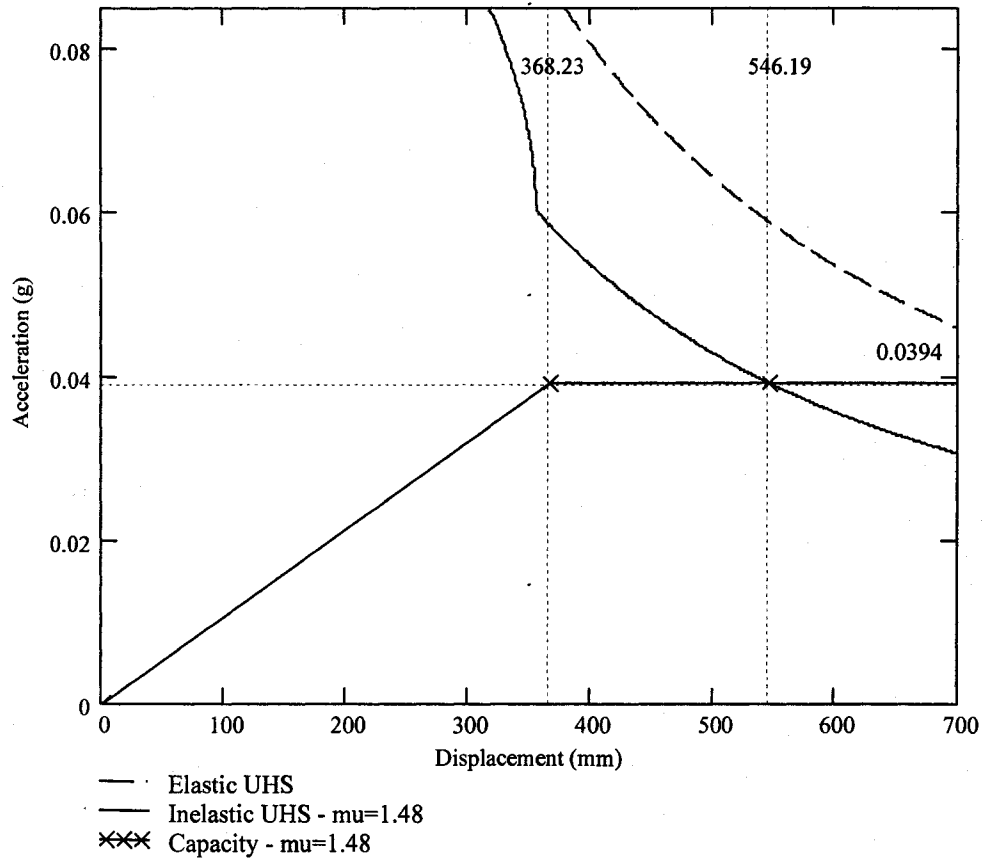


Figure C.5: Capacity-demand diagram for the first design iteration on a 20-storey building

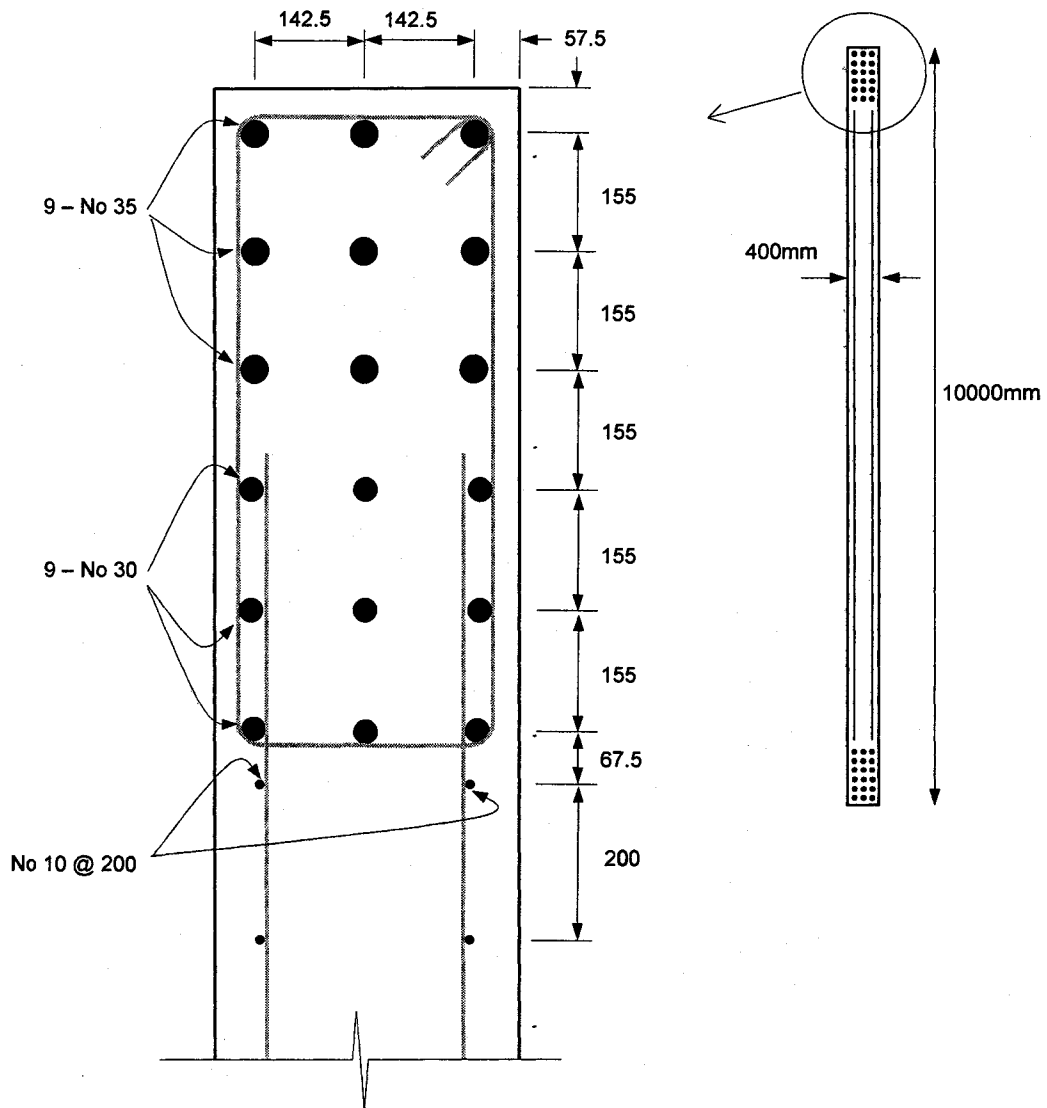


Figure C.6: Detail of reinforcement for the final design of shear walls for a 20-storey building

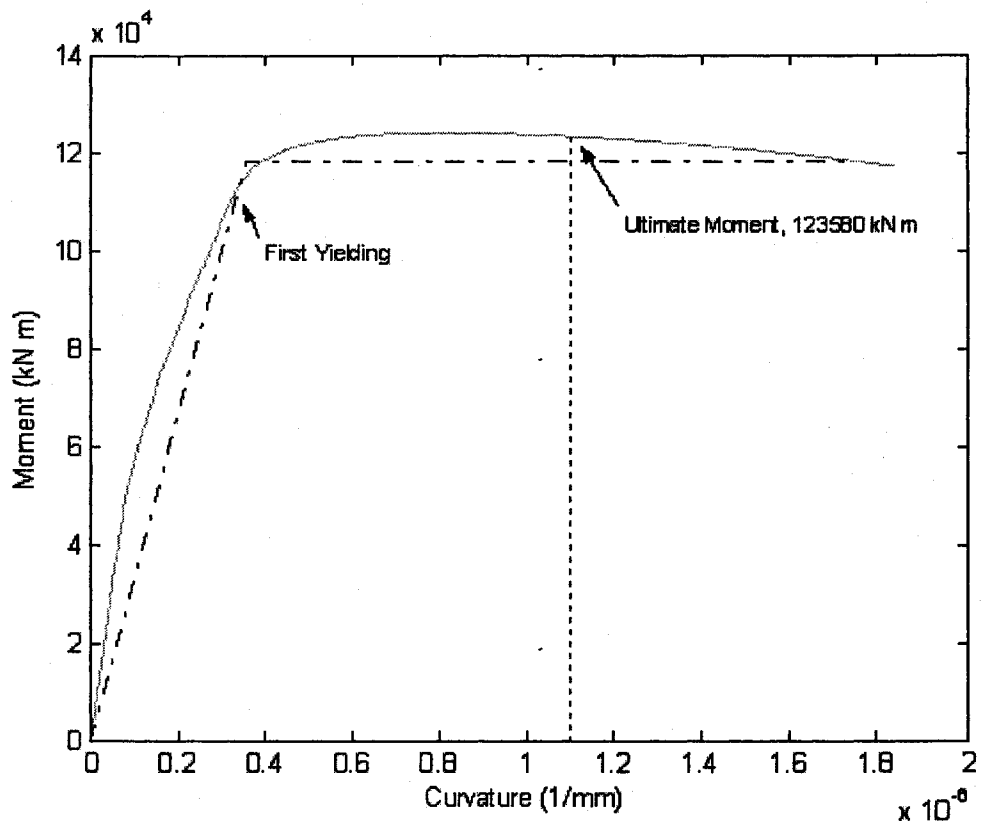


Figure C.7: Moment-curvature relationship for the final design of shear walls for a 20-storey building

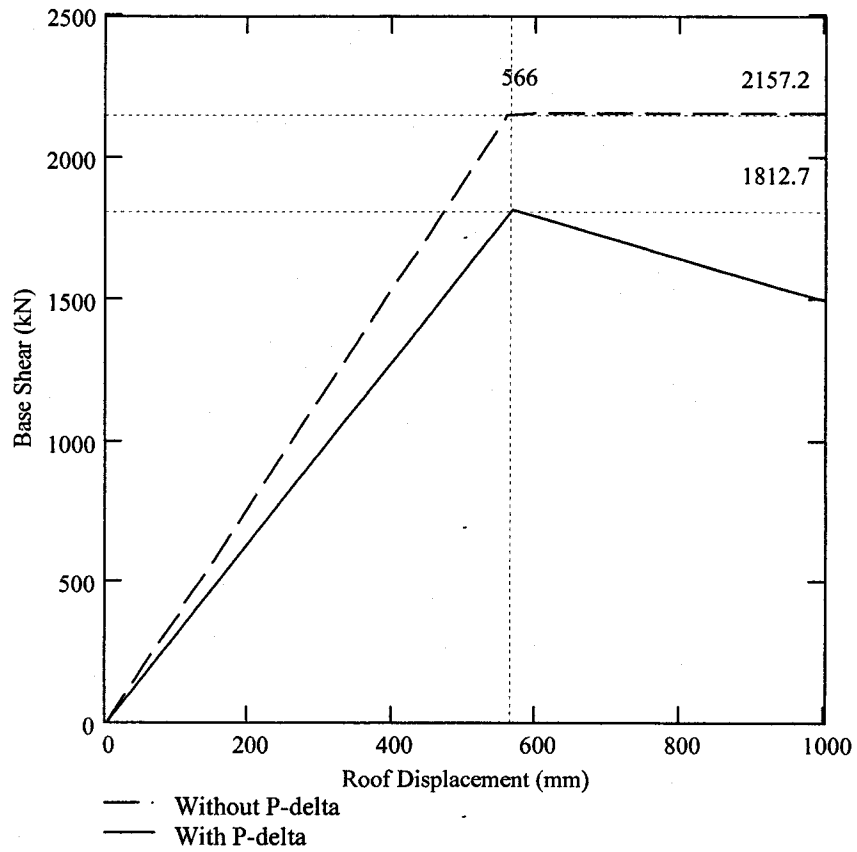


Figure C.8: Pushover curves with and without P- Δ effect for the final design of shear walls for a 20-storey building

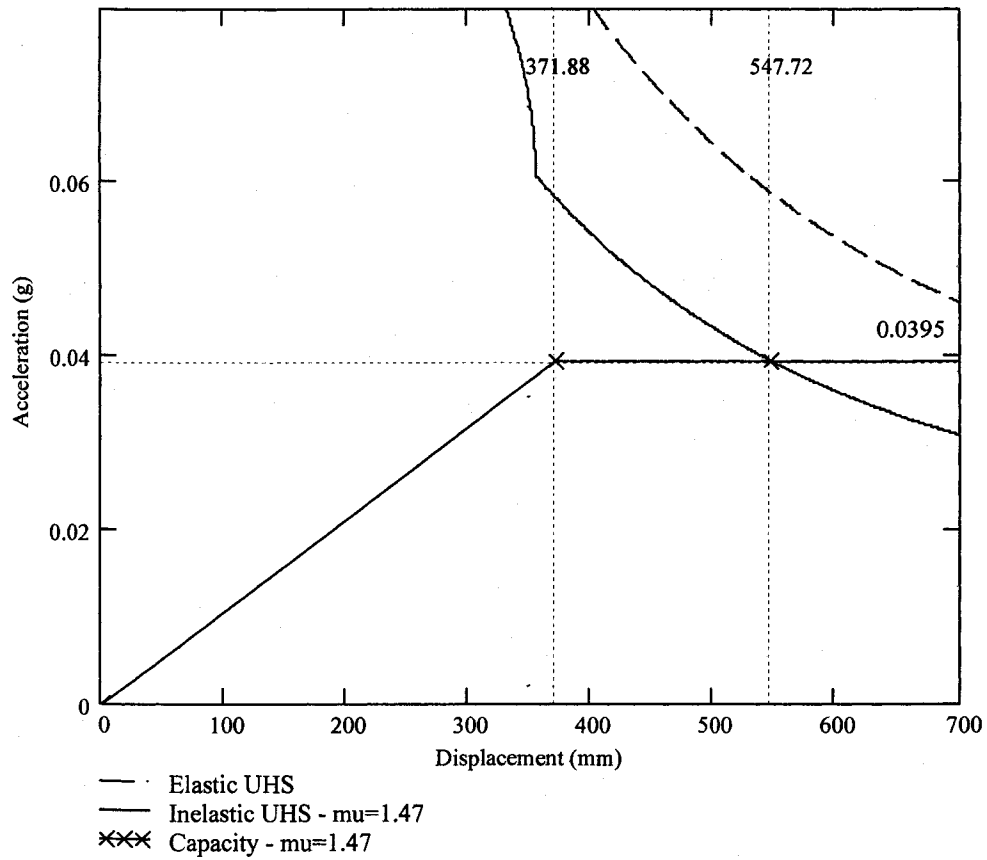


Figure C.9: Capacity-demand diagram for the final design of shear walls for a 20-storey building

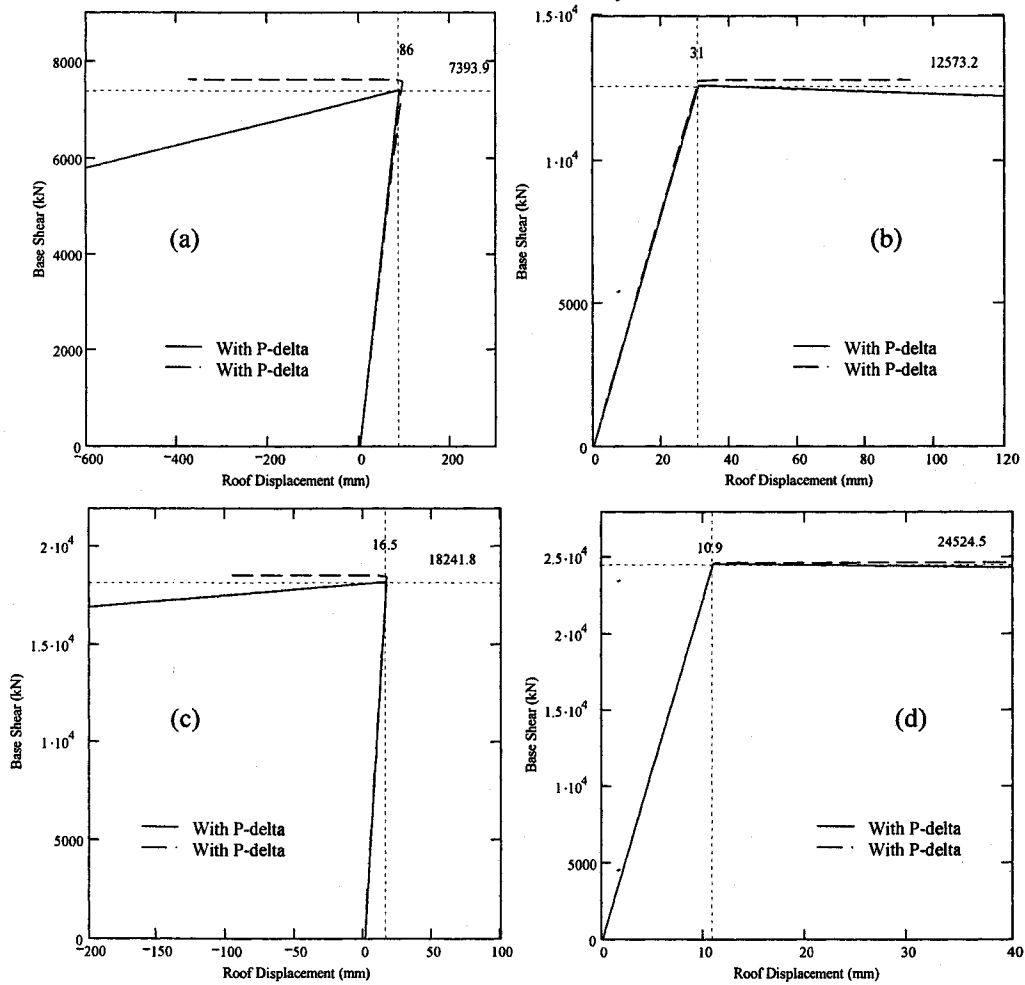


Figure C.10: Pushover curves with and without P- Δ effect for the final design of shear walls for a 20-storey building obtained by distributing the lateral forces according to (a) the second mode shape, (b) the third mode shape, (c) the fourth mode shape, and (d) the fifth mode shape.

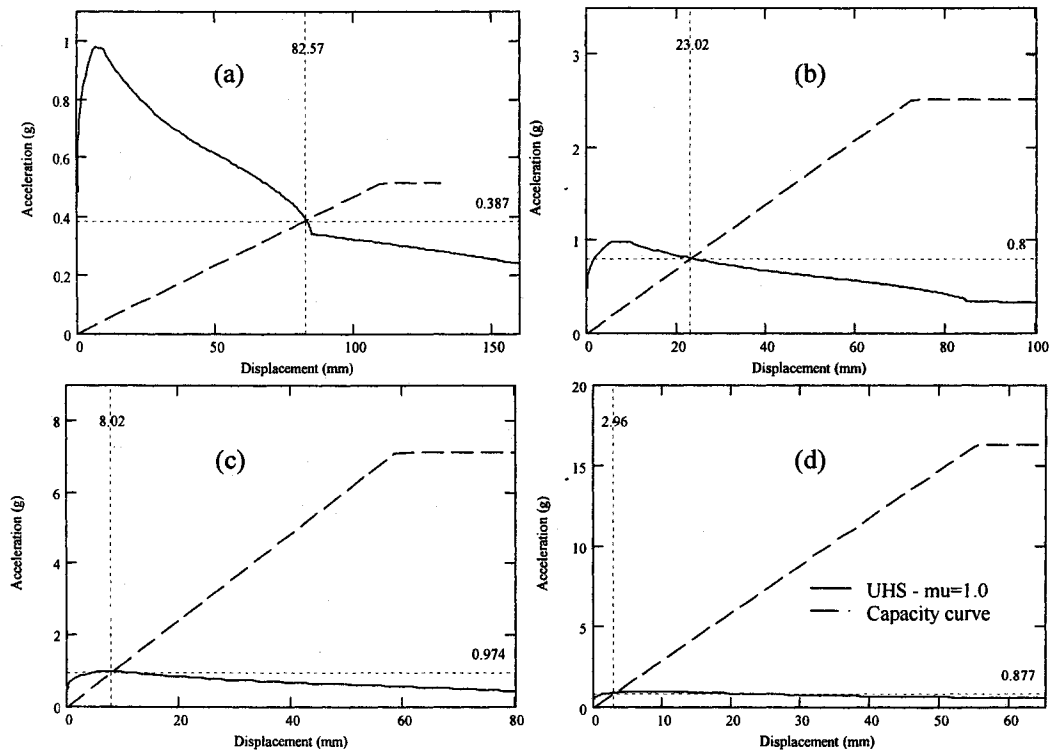


Figure C.11: Capacity-demand diagrams for the final design of shear walls for a 20-storey building obtained by distributing the lateral forces according to (a) the second mode shape, (b) the third mode shape, (c) the fourth mode shape, and (d) the fifth mode shape

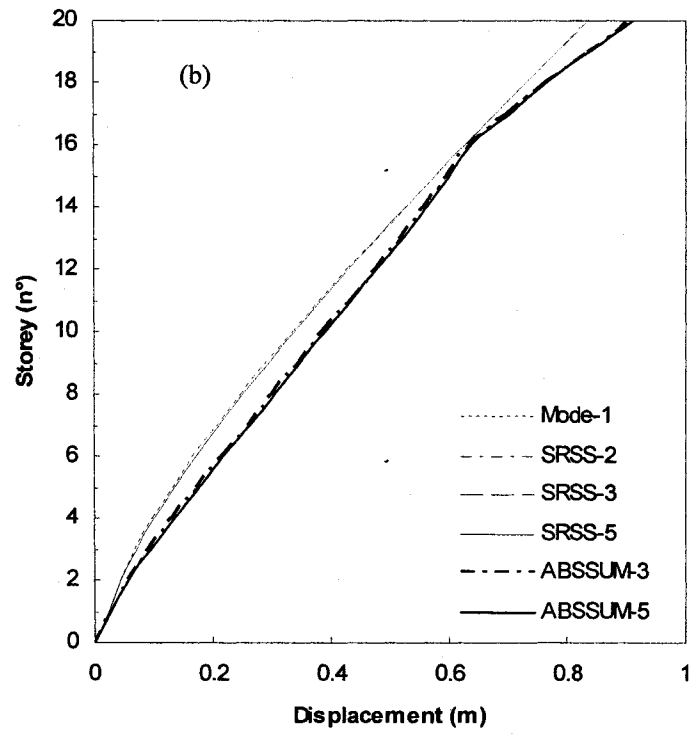
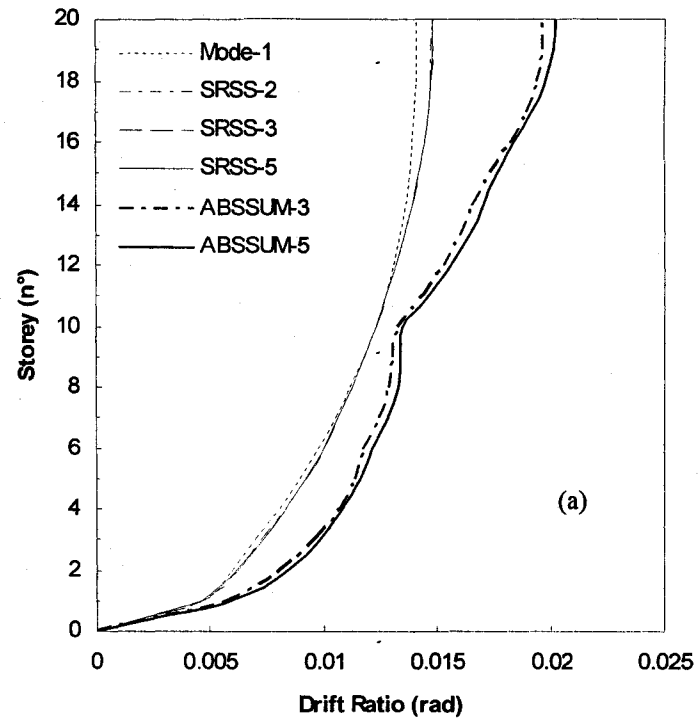


Figure C.12: (a) Inter-storey drifts ratios and (b) displacements for a 20-storey building

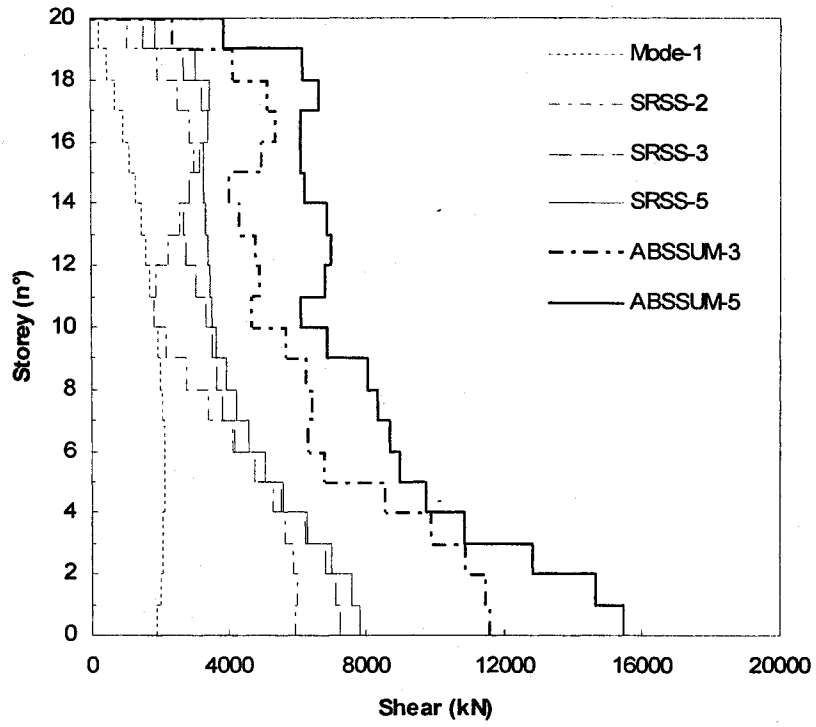


Figure C.13: Shear forces for a 20-storey building